Adaptations of autophagy and lysosomal systems upon membrane damage and pathogenic invasion

Dissertation
zur Erlangung des Doktorgrades der Naturwissenschaften

vorgelegt beim
Fachbereich Biochemie, Chemie und Pharmazie (FB14)
der Johann Wolfgang Goethe -Universität
in Frankfurt am Main

von Anshu Bhattacharya aus West Bengal, India

Frankfurt am Main 2023
(D 30)

vom Fachbereich 14 der

Johann Wolfgang Goethe - Universität als Dissertation angenommen.

Dekan: Prof. Dr. Clemens Glaubitz

Gutachter: Prof. Dr. Volker Dötsch, Prof. Dr. Ivan Dikic

Datum der Disputation: 24.4.23

Zusammenfassung

Autophagie ist ein konservierter zellulärer Prozess, welcher sich aus dem griechischen Wort „*autóphagos*“, der für selbst-verdauend steht, ableitet. In vereinfachter Form entspricht dies dem Prozess bei welchem ungebräuchlichen Material, z.B.: beschädigte Organelle oder Proteinaggregate, durch Lysosomen abgebaut wird. Lysosomen sind hierbei der Endpunkt dieses Signalwegs und sind dafür zuständig empfangene Fracht abzubauen. Aktuell gibt es drei verschiedene Arten von Autophagie Signalwegen, welche sich darin unterscheiden wie das abzubauende Material zu den Lysosomen transportiert wird. Diese drei Arten werden als Makroautophagie, Mikroautophagie und Chaperonen-abhängige Autophagie bezeichnet. Im Falle von Makroautophagie werden zum Abbau bestimmte Frachten in speziellen vesikulären Strukturen namens Autophagosomen verpackt. Normalerweise sind Autophagosomen nicht sehr zahlreich in der Zelle vertreten, sondern werden unter Konditionen von zellulärem Stress durch eine komplexe Kaskade von molekularen Signalen gebildet. Gefüllte Autophagosomen verschmelzen dann mit Lysosomen zu Autolysosomen und übertragen damit ihren Inhalt, welcher durch lysosomale Hydrolasen zu essentiellen molekularen Bausteinen degradiert und zur Wiederaufnahme ins Zytosol freigesetzt wird. Hierbei funktionieren Lysosomen also als Recycling Einheit und bestimmen dabei die metabolische Zusammensetzung der Zelle. Im Vergleich zur Makroautophagie, ist Mikroautophagie nicht mit der Formation von Autophagosomen verbunden. Stattdessen können Lysosomen die Fracht direkt durch Membraneinstülpung einnehmen. Bei der dritten Art, der Chaperonen- abhängigen Autophagie oder CAA werden zytosolische Proteine mit einem speziellen Aminosäurenmotiv (KFERQ) identifiziert und durch Kooperation von HSPA80 und LAMP2A für den lysosomalen Abbau vorbestimmt. Autophagie spielt eine essentielle Rolle bei der Erhaltung der zellulären Homöostase und kann sich selbst verschiedenen Situationen anpassen, die von der Zerstörung von beschädigten Organellen bis hin zu Beseitigung von intrazellulären Pathogenen reichen können. Aufgrund der essentiellen zellulären Schutzfunktion dieses Prozesses ist es von fundamentaler Bedeutung diesen Prozess und die damit verbundenen Mechanismen im genauen Detail zu untersuchen um zu verstehen wie er zur Pathogenese verschiedener Krankheiten beiträgt (Elazar and Dikic 2018, Levine and Kroemer 2019).

Proteine sind die Hauptarbeitskräfte der Zelle und deren Funktion wird and verschiedenen Kontrollpunkten reguliert um die ordnungsgemäße Funktion sicher zu stellen. Eine Art dies zu

garantieren sind posttranslationale Modifikationen (PTM) von Proteinen, welche zelluläre Prozesse modulieren. Eine dieser posttranslationalen Modifikationen ist Ubquitinierung, die das zelluläre Proteom auf verschiedene Weise beeinflusst. Eine der Hauptfunktionen von Ubiquitinierung, neben funktioneller Modulierung, ist die Regulierung des Abbaus des modifizierten Proteins. Aus diesem Grund ist Ubiquitinierung einer der zentralen Signale die das autophagisch lysosomale System diktieren. Ubquitinierung geschieht über spezielle Signalmechanismen welche aus drei verschiedenen Enzymklassen bestehen; das Ubquitin aktivierende Enzyme E1, das konjugierende Enzym E2 und das Ubiquitin Ligase Enzym E3. Ubiquitin Moleküle können darüber hinaus selbst als Substrat für Ubiquitinierung dienen und diese komplexen Verlinkungen von Ubiquitinketten tragen zu der Diversität der Ubiquitin-Kodierung bei. In den meisten Fällen dient die Aminosäure Lysin an den Positionen K6, K11, K48, K63 vom Ubiquitin Molekül als Ankerpunkt für die Entstehung von Ubiquitin Ketten, bei denen jedes einzelne Ubiquitin wiederum durch dasselbe oder unterschiedlich positionierte Lysine verlinkt werden können. K48 Verlinkung führt zum proteosomalen, während K63 Verlinkung zum lysosomalen Abbau des Zielproteins führt. Die anderen Arten von Verlinkungen führen nicht zum Abbau, sondern ändern die Funktion der Proteine.
Abgesehen von den oben genannten klassischen Ubiquitinierungsprozessen, wo Proteine als Substrate fungieren, wurden in den letzten Jahren auch atypische Ubiquitinierungen identifiziert. Auch Lipide und Zucker können z.B. ubiquitiniert werden und während der Invasion von Pathogenen wurde eine unkonventionelle Ubiquitinierung über eine Phosphoribosylbrücke am R42 des Ubiquitin Moleküls entdeckt. Wenn wir diese Ubiqutinierungsprozesse als Addierung von Molekülen betrachten, existieren in der Zelle auch Prozesse um diesen Vorgang umzukehren. Moleküle die diese Prozesse durchführen werden als Deubiquitinasen oder DUB bezeichnet. Durch die delikate Balance von Ubquitinierung und Deubiquitinierung werden eine Diversität an zellulären Prozessen reguliert, darunter hauptsächlich das autophagisch lysosomale System (Dikic and Schulman 2022).

Wie bereits erwähnt, agieren Lysosomen als terminale Zentren für den Autophagiesignalweg und tragen zur Kontrolle von zellulären Signalwegen bei. Christian de Duve war der Erste der Lysosomen entdeckt hat und sie wurden vor allem durch ihre Fähigkeit biologische Makromoleküle abzubauen, bekannt. In den letzten Jahren weisen allerdings viele Entdeckungen darauf hin, dass sie auch eine wichtige Rolle in der Aufrechterhaltung von der zellulären Homöostase spielen. Verschiedene Krankheiten sind mit nicht-funktionellen Lysosomen assoziiert und durch die zentrale Rolle von Lysosomen in der Autophagie und dem endosomalen

Signalweg ist es von äußerster Notwendigkeit diese Organelle im Detail zu erforschen. Die Abbaukapazität von Lysosomen stammt von den Enzymen die in den Lysosomen eingeschlossen sind und das saure Milieu, das deren Funktion sicherstellt. Diese von einer einzigen Membran umgebenen Organelle sind sehr mobil und können ihre Verteilung abhängig vom Zustand der Zelle verändern. Lysosomen können zudem auch Kontakte mit verschiedenen anderen Organellen herstellen und agieren als Plattform um diese molekularen Signalwege zu koordinieren. Lysosomale Biogenese ist bei induzierter Autophagie hoch reguliert und dies wird vor allem durch TFEB/TFE3, zwei bekannte Transkriptionsfaktoren lysosomaler Gene, reguliert. Es gibt unterschiedliche Ionenkanäle die an der limitierenden lysosomalen Membran liegen und dabei helfen die nötige Ionenkonzentration im lysosomalen Lumen zu erhalten. Einige dieser Gene sind dafür bekannt lysosomale Aufbewahrungsstörungen zu verursachen. Die Membranproteine der Lysosomen bestehen aus einer Hauptgruppe von bona fide lysosomalen Membranproteinen, die in der Regel eine oder mehrere Transmembrandomänen aufweisen, und einer zweiten Kategorie von lysosomal assoziierten Proteinen, die sich je nach Zellzustand mit den Lysosomen verbinden können. Der mTOR-Komplex, eine Kinase, ist eines der Beispiele für die zweite Art von Lysosom-assoziierten Komplexen, die an der Lysosomen Membran lokalisiert sind und unter nährstoffreichen Bedingungen aktiv bleiben; die Induktion der Autophagie bewirkt seine Dissoziation von der Lysosomen Membran, wodurch er inaktiv wird, und induziert anschließend die lysosomale Genexpression. mTOR ist bekanntlich das Stoffwechselzentrum der Zellen und spielt nachweislich eine wichtige Rolle bei verschiedenen Krankheiten, insbesondere Krebs. Da Lysosomen ein Konvergenzpunkt von mindestens zwei wichtigen zellulären Stoffwechselwegen sind, wie Autophagie und Endozytose, und diese Organellen auch dafür bekannt sind, dass sie auf Veränderungen in benachbarten Organellen reagieren, weisen viele wichtige Krankheiten veränderte lysosomale Signale und Funktionen auf. Es gibt eine bestimmte Klasse von genetischen Störungen, die durch Mutationen in lysosomalen Genen verursacht werden, und diese Gruppe von Krankheiten ist als lysosomale Speicherkrankheiten (LSK) bekannt. In den letzten Jahren wurden jedoch auch mehrere andere Krankheiten mit dysfunktionalen Lysosomen in Verbindung gebracht, z. B. neurodegenerative Erkrankungen, Krebs und andere Stoffwechselstörungen wie Fettleibigkeit und Diabetes. Es ist auch bekannt, dass viele Krankheitserreger die autophagischen Lysosomensignalwege verändern, um in den Zellen zu überleben. Nach dem Eindringen von Krankheitserregern aktivieren die Zellen die Autophagie, um die Erreger abzubauen, so dass fast alle Krankheitserreger Mittel und Wege entwickelt haben, diese zu umgehen. So können beispielsweise Legionellen die Autophagie deaktivieren, um den Abbau zu vermeiden, während Salmonellen in sauren Lysosomen wachsen können, ohne abgebaut

zu werden. Wie alle anderen Organellen sind auch Lysosomen nicht immun gegen verschiedene Bedrohungen und können geschädigt werden. Lysosomenschäden sind ein ernstes Problem, da die ausgetretenen Kathepsine die Apoptose aktivieren können und eine insgesamt gestörte Autophagie zu einer Anhäufung von nicht abgebautem Material in den Zellen führen kann. Zellen haben verschiedene Wege entwickelt, um mit lysosomalen Schäden fertig zu werden, und obwohl die Wahrscheinlichkeit größer ist, dass diese Wege zusammenarbeiten, erfordert das Ausmaß der lysosomalen Schäden die verstärkte Beteiligung des einen oder anderen Weges (Ballabio und Bonifacino 2019).

Während meiner Doktorarbeit habe ich untersucht, wie sich autophagisch lysosomale Wege als Reaktion auf verschiedene Stimuli anpassen. Meine Arbeit lässt sich in zwei Hauptkapitel unterteilen, von denen sich das eine mit der Reaktion auf lysosomale Schäden befasst und das andere beschreibt, wie Legionellen verschiedene Autophagie-Schritte modifizieren können, um dem lysosomalen Abbau zu entgehen und gleichzeitig das Wachstum von legionellenhaltigen Vakuolen (LCV) zu fördern.
Was die Reaktion auf lysosomale Schäden betrifft, so möchte ich verstehen, wie Zellen mit akuten lysosomalen Schäden umgehen. Wenn Zellen über längere Zeit lysosomotropen Stoffen ausgesetzt sind, die eine Membranschädigung verursachen, scheint es als sei die lysosomale Membran Integrität über mehrere Stunden verloren und Autophagie wird aktiviert. Seit langem ist man auf dem Gebiet der Autophagie der Ansicht, dass diese stark geschädigten Lysosomen durch selektive Autophagie entfernt werden können, wobei die geschädigten Lysosomen in Autophagosomen verpackt werden und dann mit aktiven funktionellen Lysosomen zu deren Abbau verschmolzen werden. Dieser Prozess wird als Lysophagie bezeichnet (Maejima et al. 2013). Nach einer akuten Schädigung kam es jedoch zu einem starken Rückgang funktioneller Lysosomen in den Zellen, was die Frage nach der Wirksamkeit der Beseitigung dieser geschädigten Organellen durch die kanonische Autophagosom-Lysosom-Fusion aufwarf, da die Zellen fast 90 % funktioneller Lysosomen verloren hatte. Interessanterweise konnten kurz nach der Entfernung der schädigenden Substanzen funktionale Lysosomen entdeckt werden, und fast 50 % der lysosomalen Aktivität wurde innerhalb der ersten zwei Stunden der Erholungsphase wiederhergestellt. Da diese funktionellen Lysosomen in einem relativ kurzen Zeitraum wieder auftauchten, war es unwahrscheinlich, dass diese Lysosomen ein Produkt der lysosomalen Biogenese waren. Um zu verstehen, wie Zellen in dieser kurzen Zeit funktionale Lysosomen reproduzieren können, habe ich verschiedene massenspektrometrische, zellbiologische und

biochemische Techniken eingesetzt und die Existenz eines lysosomalen Regenerationsweges entschlüsselt, der für diese schnelle lysosomale Regeneration während der Erholungsphase verantwortlich ist. Proximity Labelling und regelmäßige massenspektrometrische Analysen auf der Grundlage des Interaktoms zeigten die Rekrutierung eines Proteins an spezifisch geschädigten Stellen, die sonst zytosolisch bleiben. Bei diesem Protein, TBC1D15, handelt es sich um eine bekannte GTPase für Rab7, die sich normalerweise für einen sehr kurzen Zeitraum in Lysosomen ansiedelt, um dort ihre GAP-Aktivität auszuüben, die die lysosomalen Fusions- und Spaltungsvorgänge reguliert. Nach einer akuten Schädigung rekrutiert sich dieses Protein stabil an die geschädigten Lysosomen und trägt zur Regeneration der Lysosomen bei. Die Abwesenheit von TBC1D15 blockierte den Verlauf des Lysophagie-Flusses vollständig, was auf seine Bedeutung für den Prozess hinweist. Durch verschiedene Experimente habe ich ein echtes lysosomales Membranprotein LIMP2 (*SCARB2*) identifiziert, das als Lysophagie-Rezeptor fungiert, da es sein LIR-Motiv zur Bindung mit ATG8-Proteinen auf beschädigten Lysosomen nutzt. Es wurde festgestellt, dass TBC1D15 mit diesem Komplex interagiert, was die direkte und stabile Rekrutierung dieses Proteins nur an beschädigte Organellen erklären kann. TBC1D15 besitzt auch ein LIR-Motiv, das zur Interaktion mit ATG8-Proteinen an Ort und Stelle genutzt wird. Sowohl das LIR-Motiv als auch das GAP-Motiv von TBC1D15 sind für den fortschreitenden Lysophagie-Fluss wichtig, obwohl die tatsächliche Beteiligung des GAP-Motivs schwer zu fassen ist. Nachdem TB1D15 an geschädigte Lysosomen rekrutiert wurde, kann es durch direkte und indirekte Interaktionen andere Proteine rekrutieren, die für regenerierte Lysosomen benötigt werden. Einige Proteine wie Clathrin schwere Kette 1 (CLTC) und Dynamin 2 (DNM2) interagieren physisch mit TBC1D15 an beschädigten Stellen. Clathrine bilden einen Mantel auf diesen Membranen, die sowohl lysosomale als auch autophagosomale Membranen enthielten, und dann kann man sehen, wie sich lysosomale Tubuli bilden, vermutlich durch das Herausziehen dieser beschichteten Membranteile durch KIF5B. Wir konnten KIF5B durch Proximity Labelling von TBC1D15 nachweisen, aber dieses Protein interagiert nicht direkt mit TBC1D15. Schließlich entstanden durch die DMN2-vermittelte Spaltung dieser Tubuli neue Lysosomen, die nicht nur sauer, sondern auch aktiv für die Signatur lysosomaler Hydrolase-Aktivität waren. Wir haben diesen Prozess als lysosomale Regeneration nach einer Schädigung bezeichnet, und die Zellen könnten dies als unmittelbare Reaktion auf eine akute Schädigung der Lysosomen nutzen und so den Lysophagie-Fluss aktiv halten, bis neue Lysosomen nach der Biogenese hinzukommen.

Im nächsten Teil meiner Dissertation untersuchte ich die Auswirkungen der Phosphoribosyl-verknüpften Serin-Ubiquitinierung auf den endolysosomalen Stoffwechselweg während der

Infektion mit Legionella pneumophila. Dabei handelt es sich um eine nicht-kanonische Ubiquitinierung, die nur von den SidE-Effektorproteinen von Legionella katalysiert wird. Zwei Autophagie-Proteine - Syntaxin17 (STX17) und SNAP29 - werden in den ersten zwei Stunden nach der Infektion durch Serin-Ubiquitinierung verändert. Diese Proteine gehören zur SNARE-Familie, die für die Vesikelfusion unerlässlich ist. STX17 befindet sich auf der autophagosomalen Membran, während SNAP29 ein zytosolisches SNARE ist. Die SNARE-Domänen dieser beiden Proteine interagieren mit dem lysosomalen Membran-SNARE VAMP8 und bilden ein Vier-Helix-Bündel, das als autophagosomaler SNARE-Komplex bezeichnet wird. Die Bildung des autophagosomalen SNARE-Komplexes ist für die Autophagosom-Lysosom-Fusion erforderlich. Ich habe die Serinreste auf STX17 und SNAP29 identifiziert, die durch Phosphoribosyl-Ubiquitinierung modifiziert wurden, und durch biochemische und zellbiologische Assays gezeigt, wie die Modifizierung von STX17 und SNAP29 innerhalb der Qa- bzw. Qb-SNARE-Domänen die Bildung des autophagosomalen SNARE-Komplexes sterisch blockiert. In mit Legionellen infizierten Zellen sezernieren die Bakterien einen weiteren Effektor namens RavZ, der die Bildung von Autophagosomen blockiert, indem er die Delipidierung von ATG8-Proteinen bewirkt. In Abwesenheit von lipidkonjugiertem LC3 bildet das serinubiquitinierte STX17 autophagosomartige Vesikel, die von den Bakterien als replikative Vakuolen genutzt werden. Diese STX17-positiven Vakuolen verschmelzen aufgrund der Serin-Ubiquitinierung von SNAP29 nicht mit den Lysosomen. Ich fand auch heraus, dass die Serin-Ubiquitinierung von STX17 für die bakterielle Replikation in A549-Zellen wichtig ist. Das Vorhandensein von RavZ und SidE ist notwendig, um die selektive Autophagie intrazellulärer Bakterien (Xenophagie) zu vermeiden. Die Serin-Ubiquitinierung trägt zur Bildung von Autophagosom-ähnlichen bakteriellen Vakuolen bei, die nicht mit dem Lysosom verschmelzen, während RavZ die Bildung von herkömmlichen ATG8-positiven Autophagosomen hemmt. Stämme, denen eines der Effektorproteine fehlt, haben ein geringeres Replikationspotenzial als die WT-Bakterien, während der Stamm, dem beide Effektoren fehlen, am anfälligsten für Xenophagie ist.

CHAPTER 2

Abstract

Lysosomes are major degradative organelles that contain enzymes capable of breaking down proteins, nucleic acids, carbohydrates, and lipids. In the last decade, new discoveries have traced also important roles for lysosomes as signalling hubs, affecting metabolism, autophagy and pathogenic infections. Therefore, maintenance of a healthy lysosome population is of utmost importance to the cell to respond to both stress conditions and also homeostatic signalling. For example, for minor perturbations to the lysosomal membrane, the cell activates repair processes which seal membrane nicks. For more extensive damage, autophagy is activated to remove damaged organelles from the cell. on the other hand, during pathogen invasion host cells have also evolved mechanisms to hijack the endolysosomal pathway to facilitate their own growth and replication in host cells.

The first part of the thesis work focuses on a lysosomal regeneration program which is activated under conditions where the entire lysosomal pool of the cell is damaged. Upon extensive membrane damage induced by the lysosomotropic drug LLOMe, the cell activates a regeneration pathway which helps in the formation of new functional lysosomes by recycling damaged membranes. I have identified the molecules important for this novel pathway of lysosomal regeneration and showed how the protein TBC1D15 orchestrates this process to regenerate functional organelles from completely damaged membrane masses in the first 2 hours following lysosomal membrane damage. This process resembles the process of auto-lysosomal reformation (ALR)- involving the formation of lysosomal tubules which are extended along microtubules and cleaved in a dynamin2 dependent manner to form proto-lysosomes which develop into fully functional mature lysosomes. These lysosomal tubules are closely associated with ATG8 positive autophagosomal membranes and require ATG8 proteins to bind to the lysophagy receptor LIMP2 on damaged membranes. This process is physiologically important under conditions of crystal nephropathy where calcium oxalate crystals induce damage to lysosomal membranes in nephrons in kidney disease.

The second part of the thesis shows how the endolysosomal system of the cell is hijacked by the bacteria *Legionella pneumophila*. During Legionella infection the formation of conventional ATG8 positive autophagosomes are blocked due to the protease activity of the bacterial effector protein RavZ which cleaves lipidated ATG8 proteins from autophagosomal membranes. The SidE effectors of Legionella modify STX17 and SNAP29 by the process of non-canonical ubiquitination called phosphoribose-linked serine ubiquitination (PR-Ub). These proteins are essential for the formation of the autophagosomal SNARE complex which is used for fusion of the autophagosome with the lysosome. Upon Legionella infection, PR-UB of STX17 aids in formation of autophagosome-like replication vacuoles. These vacuoles do not fuse with the lysosome because SNAP29 is also PR-Ub modified. PR-Ub of STX17 and SNAP29 sterically blocks the formation of the autophagosomal-SNARE complex thereby preventing fusion of the autophagosome with the lysosome. As a result, Legionella can replicate in autophagosome-like vacuoles which do not undergo lysosomal degradation. In absence of PR-Ub modified STX17, bacterial replication is compromised when measured by bacterial replication assays in lung epithelial (A549) cells.

Taken together, this thesis highlights two important aspects of the autophagy-lysosomal system- how it responds to extensive membrane damage and its importance in Legionella pneumophila infection. Extensive damage to lysosomal membranes triggers a rapid regeneration process to partially restore lysosomal function before the effects of TFEB dependent lysosomal biogenesis becomes apparent. On the other hand, Legionella pneumophila infection segregates the lysosomes from the rest of the endo-lysosomal system by blocking autophagosome-lysosome fusion. Though lysosomes remain active, they are incapable of degrading pathogens since pathogen containing vacuoles do not fuse with the lysosome.

CHAPTER 3
Abbreviations

ABC	Ammonium bi carbonate
ADP	Adenosine di phosphate
AGC	Automatic gain control
ALR	Autophagic lysosomal reformation
ATP	Adenosine tri phosphate
Aβ	Amyloid beta
BLAST	Basic local alignment search tool
CCCP	Carbonyl Cyanide Chlorophenylhydrazone
CFU	Colony forming units
cGAS	Cyclic GMP-AMP synthase
CLEAR	Coordinated lysosomal expression and regulation
CMA	Chaperone mediated autophagy
DAPI	4′,6-diamidino-2-phenylindole
DMEM	Dulbecco´s modified Eagle medium
DUB	De-ubiqtuitinase
DUP	Deubiquitinase for Pr-Ubquitination
EBSS	Earle´s balanced salt solution
ELDR	Endo-lysosomal damage response
ER	Endoplasmic reticulum
ERGIC	ER-Golgi intermediate compartment
ESCRT	Endosomal sorting complexes required for transport machinery
ETD	Electron transfer dissociation
FA	Formic acid
FBS	Fetal bovine serum
FDR	False discovery rate
GAP	GTP-ase activating protein
GDP	Guanosine di-phosphate
GEF	Guanine nucleotide exchange factor
GFP	Green fluorescent protein
GO	Gene ontology
GST	Glutathione S-transferases
GTP	Guanosine tri-phosphate
HA	Human influenza hemagglutinin
HCV	Hepatitis C virus
HEK	Human Embryonic kidney
HIV	Human immunodeficiency virus
HOPS	Mammalian homotypic fusion and vacuole protein sorting.
ILV	Intralumenal vesicles
IPTG	Isopropyl β-d-1-thiogalactopyranoside
LAP	LC3 assisted phagocytosis

LCV	Legionella containing vacoules
LD	Legionaries' diseases
LIR	LC3 interacting region
LLOMe	L-leucyl-leucine methyl ester
LMP	Lysosomal membrane permiabilisation
LSD	Lysosomal storage disorder
M6PR	Mannose 6 phosphate receptor
MAM	Mitochondria associated membrane
mART	Mono ADP-Ribosyl transferase
MHC	Major histocompatibility complex
MOI	Multiplicity of infection
MOM	Mitochondrial outer membrane
MS	Mass spectrometry
MVB	Multi vesicular bodies
OD	Optical density
PBS	Phosphate buffered saline
PDE	Phospho-di esterase
PFA	Paraformaldehyde
PR-Ub	Phosphoribosylated ubiquitin
PTEC	Proximal tubular endothelial cells
PVDF	Polyvinylidene difluoride
RFP	Red fluorescent protein
RILP	Rab interacting lysosomal protein
ROS	Reactive oxygen species
SCV	Salmonella containing vacoules
SDS-PAGE	Sodium dodecyl-sulfate polyacrylamide gel electrophoresis
SEM	Standard error of mean
SNARE	Soluble N-ethylmaleimide-sensitive factor activating protein receptor
STED	Stimulated emission depletion microscopy
TEM	Transmission electron microscopy
TGN	Trans Golgi network
TLR	Toll like receptor
TM	Transmembrane
TMT	Tandem mass tag
Ub	Ubiquitin
WT	Wild type

CHAPTER 4
Introduction

4.1 Lysosomes

Lysosomes, also known as the suicidal bag of cells, was first discovered by Christian de Duve in the 1950s (Duve et al 1955). These intracellular organelles contain a single membrane which harbours several hydrolases which are responsible for the degradation of a variety of biological macromolecules. These includes proteins, lipids, carbohydrates, nucleic acids as well as damaged organelles and even invading pathogens. There are different routes present within the cells which deliver these macromolecular cargoes to the lysosomes. These routes are known as the endocytic, phagocytic and autophagic pathways. Upon reaching the lysosomes, these cargoes are degraded within the lysosomal lumen with the help of more than 60 acid hydrolases for subsequent reutilization by the metabolic processes of the cell. Other than the luminal hydrolases, the lysosomal integrity depends on several integral membrane proteins which are usually heavily glycosylated in order to prevent degradation by the luminal hydrolases. Apart from there are several lysosome-associated proteins that dynamically interact with the lysosomal surface under certain conditions in order to carry out several important cellular signalling events

(Bonifacino and Ballabio 2020; Klumperman and Saftig 2009; Hesketh et al 2018) (Fig 4.1).

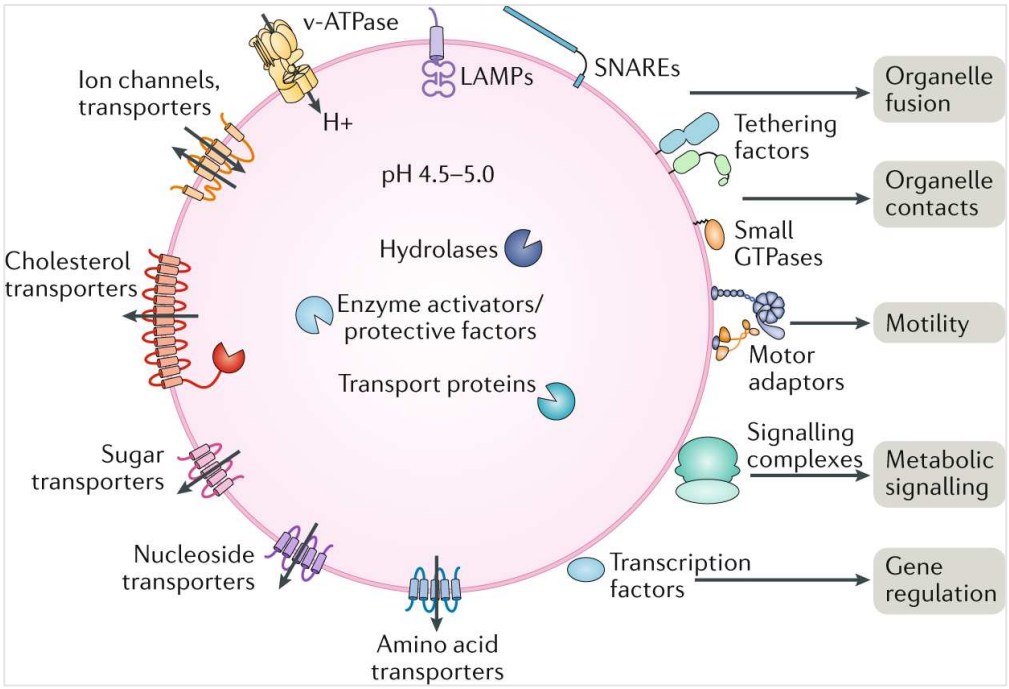

Figure 4.1: Schematic of lysosome outlining its major functions. (Adapted from Bonifacino and Ballabio 2019)

There are at around 50-1000 lysosomes present in each mammalian cells which are usually distributed throughout the cytoplasm. Since lysosomes are the terminal organelle of the

autophagy pathway, for a long time they have been regarded as the "disposal bags" of the cells serving as 'housekeeping' organelles that perform their degradative function. Also, for long time, these organelles have been thought of as static organelles and functions in isolation form other cellular organelles. Moreover, instances of lysosomal dysfunction, caused by impaired degradation of lysosomal substrates, has been historically associated with some rare diseases also known as lysosomal storage disorders (LSDs). Due to these factors, the study of lysosomal signalling and homeostasis remained quite a narrow field with little connection to overall cellular signalling and organismal physiology. During the last decade, several important discoveries have been made regarding lysosomal homeostasis to change this view and it is sufficed to say that lysosomes are one of the major signalling hubs of mammalian cells performing several important functions and it has also been reported to be involved in various diseases scenarios. As for example, besides degradation, lysosomal function could be attributed to be involved in metabolic signalling, immunity gene regulation, cell adhesion, plasma membrane repair and migration. Lysosomes have been shown to differ in contents and functionality as well as in distribution according to cell types and cellular need. While it was thought that lysosomes work in isolation, several reports have shown that lysosomal membrane proteins can form several membrane contacts sites with other organelles which can serve as signalling. Lysosomes have also been observed to be quite dynamic in terms of their positioning in the cytosol and they often change their shape and size by undergoing fission and fusion events. Finally, altered lysosomal function have been implicated in the pathogenesis of common diseases such as neurodegenerative diseases, several metabolic disorders, pathogenic invasion as well as cancer (Lawrence et al 2019). Some major aspects of lysosomal signalling are described below:

4.1 Lysosomal biogenesis

In response to diverse environmental cues, cellular metabolism adapts itself over the course of any changes and as lysosomes serves as a major metabolic signalling hub, it was important to identify how lysosomes adapted to these changes. Through an in-silico based approach, a transcriptional gene network was identified which includes genes involved in different aspects of lysosomal function and autophagy. This network is also known as 'CLEAR' (for 'coordinated lysosomal expression and regulation'). After that a specific transcription factor, known as TFEB, was identified to be the master regulator of this CLEAR gene network. Combining both the activities of TFEB and CLEAR network, lysosomal function is controlled in different scenarios (Sardiello et al 2009; Settembre et al 2011). As a member of the MiT-

TFe family of helix–loop–helix leucine zipper transcription factors, TFEB regulates lysosomal function by controlling several aspects of autophagy and lysosomal pathways such as autophagosomal biogenesis, autophagosome lysosome fusion, lysosomal Ca^{2+} homeostasis, lysosomal positioning and lysosomal acidification (Sardiello et al 2009; Palmieri et al 2011; Willet,R et al 2017). Apart from TFEB, there are also other transcriptional factors that belong to the MiT-TFe family such as MITF and TFE3 (Hemesath, T.J et al 1994). Other than TFEB, TFE3 has also been shown to modulate lysosome and autophagy (Martina et al 2014). Overexpressing TFEB and in some specific cases TFE3 has been reported to promote clearance of intracellular cargoes and also to rescue different phenotypic abnormalities in a variety of cellular and mouse models where accumulation of autophagic/lysosomal substrates are hallmark. Some examples of these instances include diseases like LSD, metabolic disorders and common neurodegenerative diseases (Rega et al 2016; Spampanato et al 2013; Chauhan et al 2015; Decressac et al 2013; Polito et al 2013; Xiao et al 2015). Considering all these evidences, it could be concluded that MiT-TFe directed CLEAR network has a broad implication in several physiologically relevant scenarios. Studies have shown that although under steady state or nutrient rich conditions, TFEB is usually locate in the cytosol, upon serum starvation it re-localises to nucleus in order induce lysosome related gene translation (Settembre et al 2011). Phosphorylation of specific serine residues by lysosome associated kinase mTORC1 has been attributed to its cytosolic retention as well as that of the other MiT-TFE factors (Settembre et al 2011; Peña-Llopis et al 2011; Martina et al 2012; Roczniak-Ferguson et al 2012; Settembre et al 2012; Vega-Rubin-de-Celis et al 2017). Interestingly, MiT-TFE can also promote the lysosomal recruitment of mTORC1 by the transcriptional induction of RAGD and RAGC (Di Malta et al 2017) thus providing a balance between anabolism and catabolism within the cell. Yet another important player has also been identified which plays a key for the nuclear translocation of TFEB named Calcineurin. This Ca^{2+} dependent phosphatase can de-phosphorylate under serum starved condition prompting its shuttling to nucleus (Medina et al 2015). These indicates the presence of a sophisticated signalling network within the cell which regulates lysosomal function depending on environmental cues.

4.2 Lysosome as a signalling hub

Like many other organelles, lysosomal membrane protein complexes participate in several important molecular signalling and organellar contact processes. mTORC1 or mechanistic target of rapamycin complex 1 is one of these major macro-molecular

complexes which serve as a control centre for cellular anabolism and catabolism (Saxton et al 2017). Amino acid dependent activation of heterodimeric RAG GTPases and their subsequent interaction with Ragulator complex is needed for the recruitment of mTORC1 to lysosomal surface (Lawrence et al 2019; Sancak et al 2010). The cholesterol-binding protein Niemann–Pick type C1 or (NPC1) has also been identified to help the RAG-dependent recruitment of mTORC1 to the lysosomal surface (Castellano et al 2017). While on lysosomal surface, active mTORC1 can inhibit autophagy and thus it maintains a crucial balance between cellular anabolic and catabolic states. Another important signalling even tis cellular Ca^{2+} signalling which also involves lysosomal participation. Lysosomal Ca^{2+} release is important for its fusion with other subcellular structures such as endosomes and autophagosomes (Morgan et al 2011; Li, P et al 2011). Ca^{2+} release form lysosomes have also been to be important for marinating its contact with ER where the Ca^{2+} store of lysosomes could be replenished and this is quite crucial for maintaining the acidic environment within the lumen of lysosomes ensuring the hydrolytic activities of the proteases (Wang et al 2017). Three major categories of lysosomal calcium channels have been identified so far namely mucolipin family, two pore channels and the trimeric Ca^{2+} two-transmembrane channel $P2X_4$ (Morgan et al 2011; Li, P et al 2019). Among these, Mucolipin1 or TRPML1 has been the best characterised so far and a mutation within this gene have been identified to be associated with mucolipidosis type IV, a lysosomal storage disorder diseases which is characterized by early onset and progressive neurodegeneration (Bassi et al 2000; Bargal et al 2000). TRPML1 has also been shown to be involved in the nuclear translocation of TFEB prompting the intracellular clearance of accumulating substrates which can be seen in different LSDs (Medina et al 2011). Apart from metabolites and nutrients, lysosomes can also sense nucleic acids by the activity of Toll like receptor family of proteins or also known as TLRs. These proteins are highly expressed in macrophages and in dendritic cells (Matz et al 2019; Vidya et al 2018). TLRs are an integral part of the innate immune response. They can recognize pathogen-associated molecular patterns. Amongst the 13 members of the TLR family, three of them (TLR3, TLR7/8 and TLR9) signal from endolysosomes. Microbial nucleic acids can activate these receptors and in turn they can stimulate the production of inflammatory cytokines and/or interferons through different signalling cascades. Since endocytosis is one of the most common mechanisms for pathogen entry into host cells, the strategic localisation of TLRs can elicit an efficient host response for pathogenic invasion (Majer et al 2017). Lysosomes also play a crucial role for cellular lipid homeostasis and phosphoinositide has been shown to be an integral part of lysosomal biology. This lipid maintains several aspects of lysosomal homeostasis such as

fusion with autophagosomes, biogenesis and even lipid transfer through membrane contact sites (Thelen et al 2017; Ebner et al 2019).

4.3 Interaction with other organelles

Like other cellular organelles, lysosomal fusion events can also be broadly categorised as homotypic fusions such as with other lysosomes or heterotypic fusion events such as with autophagosomes, macropinosomes, endosomes and with plasma membrane. Most of these fusion events are carried out by SNARE complexes comprising of R-SNARE and Q-SNAREs. Ca^{2+} has also been observed to play a very crucial role in these events (Ebner et al 2019). Lysosomes serve as the end point of endocytosis pathway and are capable of fusing with endosomes. Several molecular machineries have been identified over the past few years which are important for this process such as small GTPase ARL8 and its effectors, tethering complex HOPS: Additionally, PLEKHM1 has also been identified to be interacting with this complex (Garg et al 2011; McEwan et al 2015; Marwaha et al 2017). Lysosome lysosome homotypic fusion also utilises the similar machinery but VAMP8 plays a crucial role in this event (Antonin et al 2000). Over the past few years contact sites involving lysosomes and several other organelles such as ER, mitochondria, peroxisome have been discovered (Wu, H et al 2018). ER-lysosome contact sites can serve several different purposes including calcium transfer and most importantly transportation of cholesterol. Hydrolysis of cholesterol ester in the lysosomal lumen generates free cholesterol which are then exported out by NPC1 and NPC2. Subsequent transfer of free cholesterol into the ER occurs at membrane contact sites and this is mediated by lipid-transfer proteins such as ORP5 and ORP1L, and ER-resident proteins such as VAPA and VAPB (Luo et al 2017). Lysosomes are also able to transfer free cholesterol to peroxisome via membrane contact sites through the activity of lysosomal synaptogamin 7 and peroxisomal PtdIns(4,5)P_2 (Chu, B. et al 2015). Lysosomes and mitochondria contact sites are regulated by Rab7 and TBC1D15. TBC1D15 interacts with mitochondrial outer membrane protein FIS1 to convert Rab7-GTP to Rab7-GDP and thus releases the contact which also serves as a spot for mitochondrial fission (Wong et al 2018). This event helps in maintaining both lysosomal and mitochondrial dynamics. Another important aspect of lysosomal interaction with other organelle is the fusion of autophagosome and lysosome. We will discuss more about it in the next chapter. Since lysosomes are the terminal points where many of our cellular processes merge, I will now discuss some of those pathways in this next section. One of these cellular pathways is the endolysosomal system.

4.4 Endolysosomal system

The endosomal system is a complex vesicular trafficking pathway that exists within our cells. It comprises of distinct yet interdependent vesicles that interact and fuse with each other in order to decide the fate of materials that are being trafficked from within the cells or from outside. Endocytosis is a process where cells engulf foreign material through plasma membrane invagination. This mechanism can often vary depending on the molecules involved, such as clathrin, Cdc42 etc (Cesar-silva et al 2022). After successful membrane invagination, these newly generated vesicles then fuse with early endosomes. These early endosomes are often found to be mildly acidic having a pH from within 5.9 to 6.8. Usually, materials which are to be recycled or are destined to be digested are sorted into these early endosomes. Following fusion of incoming vesicles with endosomes, several ligands get dissociated from the receptors which starts the subsequent signalling process. Early endosomes are rich in vacuolar sorting domains and tubular recycling domains which helps endosomes to accurately deliver the material to the next destination. Materials to be digested gets delivered to late endosomes using the sorting domains whereas recycling domains containing endosomes deliver cargos to other membrane compartments of the cell such as plasma membrane, trans Golgi network or to recycling endosomes. Different molecules get distinctly enriched in subdomains to endosomes in order to achieve correct sorting. Some examples of these molecules are Rab5, Rab7, Rab11, retromer, ARF/COPI etc (Ward et al 2005; Huotari et al 2011; Yuan et al 2020). The Rab proteins belong to the Ras superfamily of proteins and these are very crucial for proper vesicle fusion and targeting events. For example, Rab4 and Rab11 are involved with recycling endosomes and are often involved in events where materials are trafficked to the plasma membrane. In contrast to that Rab7 are associated with lysosomal trafficking and fusion events and therefore are often highly enriched in lysosomes. Rab5 however is a component of the early endosome and is often lost in the process of maturation of early endosomes to late endosomes (Wandinger-Ness et al 2014; Li, H et al 2008; Balderhaar et al 2013). The membrane fusion evets are coordinated by proper interactions of Rab proteins, SNAREs, ESCRT machineries and HOPS complex. ESCRT is a multiprotein complex which drives membrane remodelling. There are four main complexes are known, such as ESCRT 0, I, II and III. HOPS complexes are consisting of VPS proteins and they also act as membrane tethering complex mostly between lysosomes and other vesicles (Balderhaar et al 2013; Solinger et al 2013; Van der Kant et al 2015). SNARE family of proteins also interacts between different members of SNARE families and drives membrane fusion. I will discuss more about SNARE in a later section. Early endosomes are also often reported to

interact with trans-golgi network to receive acid hydrolases. These hydrolases either get secreted out of the cells and then sometimes can also be taken up via a M6PR dependent manner. So, it is sufficed to say that accurate interactions between vesicles must happen in an orderly fashion for a successful maturation of early endosomes to late endosomes. Late endosomes are usually more acidic than the rest of the pathway lysosomes being the most acidic of the lot. The maturation form early to late endosomes starts with small membrane invaginations which are directed inwards. These structures are also known as ILVs or Intra luminal vesicles. As maturation progresses, these ILVs accumulates and gives rise to MVBs or multi vesicular bodies which then in turn can fuse with lysosomes or secret the ILVs out as exosomes (Huotari et al 2011). The different vesicles belonging to the endo lysosomal pathway is depicted in the next diagram (Fig 4.2).

4.5 Autophagic-lysosomal system:

The autophagic-lysosomal system is another arm of cellular signalling which also merges with lysosomes at a later stage. Autophagy is also known as the catabolic pathway of the cells. This pathway is used in a plethora of situations ranging from degradation of damaged organelles and materials to clearance of intracellular pathogens. All autophagic cargo are destined to get degraded into lysosomes hence these two pathways work in a very orchestrated manner. There are three major types of autophagy pathway active in eukaryotes; macroautophagy, microautophagy and chaperone-mediated autophagy. While macroautophagy delivers cytoplasmic material to lysosomes via the double-membraned autophagosome, chaperone-mediated autophagy and microautophagy, occur directly on the lysosome. Lysosomes not only serve as the degradation destination for these different arms of autophagy, it can also regulate autophagy via some feedback mechanism and also can become a substrate of autophagy when severely damaged. During the course of progression

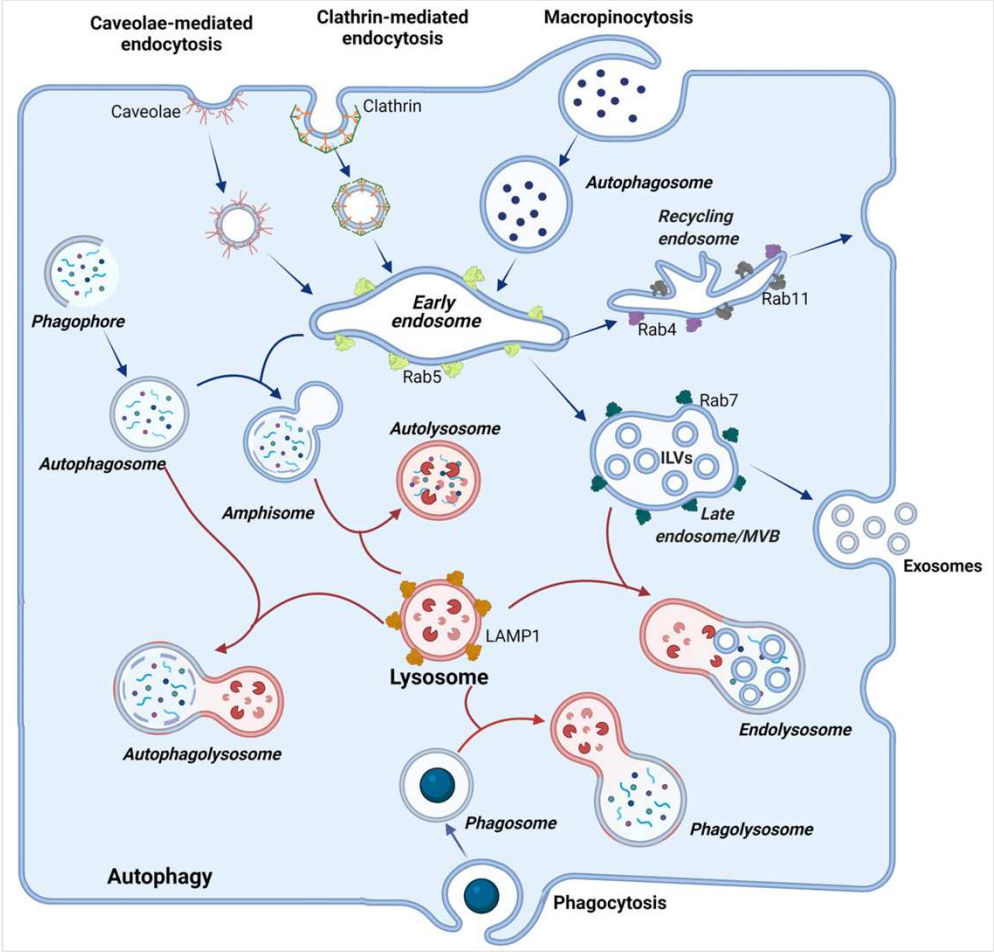

Figure 4.2: Different arms of endolysosomal pathways. (Adapted from Cesar-Silva et al 2022)

of autophagy, lysosomes show some distinctive changes in their acidity and cellular positioning.

4.6 Types of autophagy

A) Macroautophagy

Amongst the three main arms of autophagy, macroautophagy is the most well studied and it was first discovered in mammalian system back in 1960 (Nakatogawa et al 2020). While the most fundamental role of autophagy is realised by its ability to supply nutrients in times of need, such as starvation; autophagy also helps to maintain cellular homeostasis by clearing debri, damaged organelles even invading pathogens. This housekeeping function of autophagy becomes more important for really long living cells such as neurons (Schuck et al 2020; Mizushima et al 2011; Levine et al 2019; Mejlvang et al 2018). We will now discuss some important steps of macroautophagy,

(i) Initiation of macroautophagy:

The ULK complex is the major initiation factor of macroautophagy. This complex is made up with FIP200, ATG3, ATG101 and the serine/threonine kinases ULK1/ULK2. mTORC1 gets inactivated when cells face starvation and this leads to the recruitment of the ULK complex in the vicinity of ER where it then recruits downstream autophagy related proteins, or also known as ATGs, to initiate the formation of autophagosomes. Apart from starvation, ULK1 assembly can also be driven by autophagy cargos. This situation is quite common in case of selective autophagy pathway when some intracellular organelles are damaged and then some membrane proteins get ubiquitinated which in turn recruit autophagy adapters like SQSTM or p62. This autophagy adaptors then drives the local assembly of the autophagosome formation complex through interacting with FIP200 (Turco et al 2019). Some other examples of autophagy adapters are NDP52, TAX1BP1 and CCPG1 which are also capable of assembling the autophagosome initiation complex by interacting with FIP200 (Vargas et al 2019; Ravenhill et al 2019Turco et al 2021; Smith et al 2018; Zhou et al 2021). Upon activation, ULK1 recruits ATG9 vesicles via the interaction between HORMA domain of ATG13-ATG101 subcomplex and the C terminal of ATG9A (Sawa-Makarska et al 2020). In case of organellophagy, ATG9vesicles get recruited through their interaction with adapter proteins, such as OPTN in case of mitophagy (Yamano et al 2020).

(ii) Membrane elongation:

Following the assembly of the ULK complex, it engages the PI3KC3-C1 complex (Class III phosphatidylinositol 3-kinase complex 1) which produces PI(3)P to elongate the autophagic membrane. This PI3KC3-C1 comprises of VPS34, VPS15, BECN1, ATG14 and NRBF2 (Hurley et al 2017). After that PI(3)P effectors are recruited such as WIPI2 which then recruits ATG2. ATG2 transfer lipids from ER to the growing phagophore via its hydrophobic cavity (Maeda et al 2019; Osawa et al 2019). WIPIs are a part of PROPPIN family of proteins and there are four types such as WIPI1-4. But WIPI2 is the predominant one driving autophagy since its absence can significantly block autophagy (Dooley et al 2014; Bakula et al 2017). WIPI2 can bind with ATG16L1 which is a part of a complex comprising of ATG12-ATG5-ATG16L1. This complex works in concert and has an E3 activity which drives the lipidation of ATG8 family of proteins. After ATG2 transfers lipids, ATG9 scrambles the lipids on autophagosomal membrane. There are also two additional scrambles present at ER namely VMP1 and TMEM41B. The job of the scrambles is to properly distribute lipids hence maintaining the proper density (Meda et al 2020; Matoba et al 2020; Li et al 2021; Huang et al 2021).

(iii) Closure of autophagosome:

Autophagosomal membrane closure is achieved by the activity of ESCRT proteins however the exact mechanism is not known for mammals. Closure is achieved by membrane scission at both the inner and outer leaflet and is topologically similar to vesicular budding from MVBs or virus entry via plasma membrane (Takahasi et al 2018; Zhou et al 2019; Zhen et al 2020).

(iv) Fusion with lysosomes:

When the autophagosome is closed, it fuses with lysosomes to degrade the cargos and this is achieved by the function of SNARE proteins. Autophagosomal SNARE STX17 and YKT6 is recruited to only closed autophagosome and then subsequently interact with cytosolic SNARE SNAP29. Next step is the recruitment of lysosomal SNAREs VAMP7/VAMP8 and STX7. This multimolecular assembly then drives the fusion between these two vesicles. There are other tethering factors involved in this process such as HOPS, PLEKHM1 and EPG5 (Itakura et al 2012; Matsui et al 2018; McEwan et al 2015). PLEKHM1 and EPG5 can also directly interact with ATG8 proteins via their LIR motifs. Upon fusion, lysosomal enzymes digest the inner membrane of the autophagosome and this concludes the process of autolysosome formation and fusion.

(v) Autophagic lysosomal reformation (ALR):

During prolonged starvation, an interesting phenomenon occurs where new lysosomes can be generated from autolysosomes. This process takes place by recycling lysosomal membranes and is triggered by mTORC1 activity. After prolonged starvation, when amino acids are being released from lysosomes, that reactivates mTORC1 and this in turn activates the lysosomal reformation events. PI(4)P 5 kinase PIP5K1A and PIP5K1B generates PI(4,5)P_2 in different microdomains of autolysosomes which are then subsequently rearranged by clathrin and adapter protein 2 (AP2). KIF5B drives tubulation events from these foci and then DNM2 make a scission to generate new protolysosomes. These protolysosomes gradually gets acidified with time and can serve as a functional lysosome (Yu et al 2010; Rong et al 2012; Du et al 2016).

All of the above-described steps are summarized in this diagram (**Fig 4.3**).

(B) Chaperone mediated autophagy (CMA)

Unlike macroautophagy, chaperone mediated autophagy works on some selected substrates which have a specific motif present within them known as KFERQ (Dice JF 1990). Almost 30% of cytosolic proteins are known to harbour this motif and can be targeted by CMA. After the activation of CMA, KFERQ motifs are recognised by heat shock 70 kDa protein 8 (HSPA8/HSC70) (Chiang H-L et al 1989). Also, other co chaperones are known to be participating in this step. HSPA8 then can deliver these substrates to the lysosomal surface

where LAMP2A comes into play. This lysosomal membrane protein acts as a receptor for CMA.

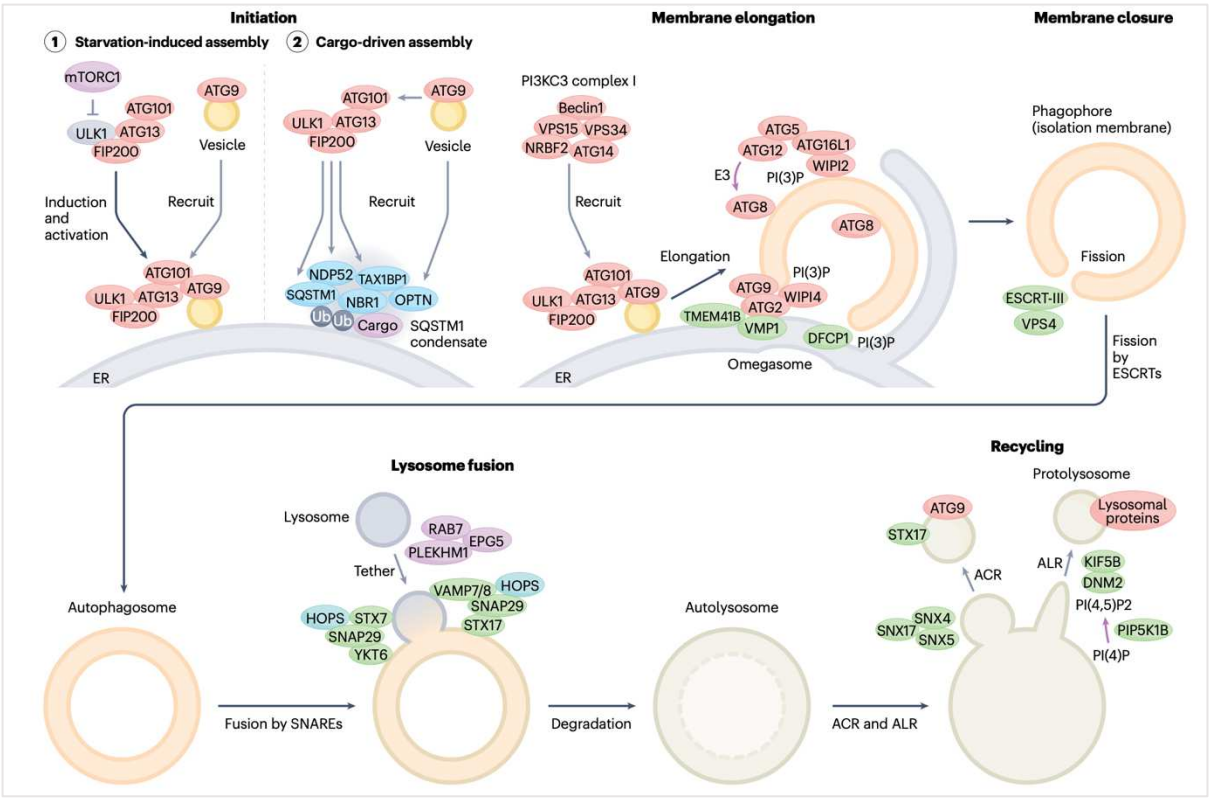

Figure 4.3: Major steps of mammalian macro autophagy. (Adapted from Yamamoto et al 2023)

Upon substrate binding, LAMP2A goes multimerization steps to form a translocation complex. The luminal side of this complex is stabilised by HSC70 whereas HSPA8 helps deliver the substrates across to the lumen. After finishing the delivery of the substrates, this whole complex dissembles and LAMP2A comes back to its original monomeric state (Bandyopadhyay et al 2008; Cuervo et al 1996). The basic steps of CMA are depicted in Fig 4.4.

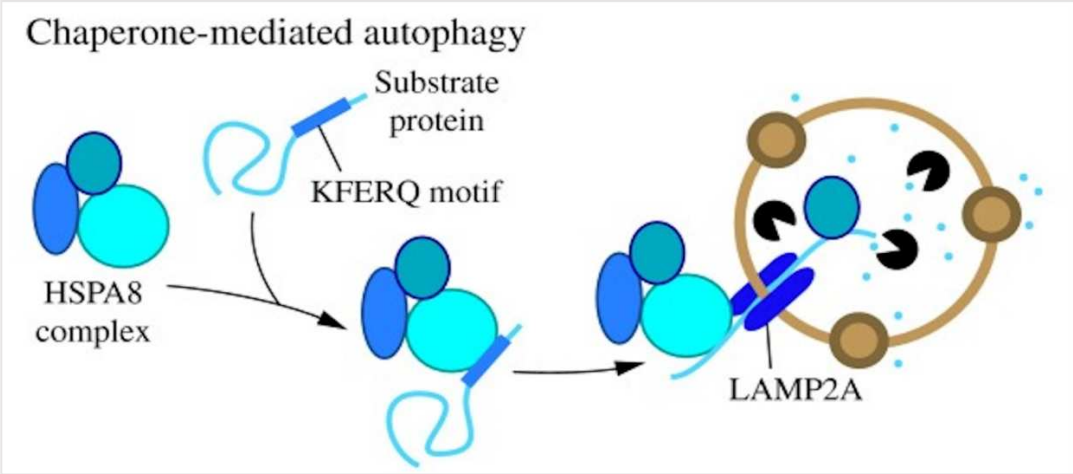

Figure 4.4: Basic outline of Chaperone mediated autophagy. (Adapted from Klionsky and Parzych 2014)

(C) Microautophagy

Microautophagy also happens in eukaryotes where cytosolic cargo gets directly engulfed into lysosomes by lysosomal membrane invagination (Marzella et al 1981; Mortimore et al 1983). This process can be both selective and non-selective. At the membrane fission steps, ESCRT machineries are known to be involved and the ATG proteins are also thought to be involved but it depends on the cargo types and induction triggers.

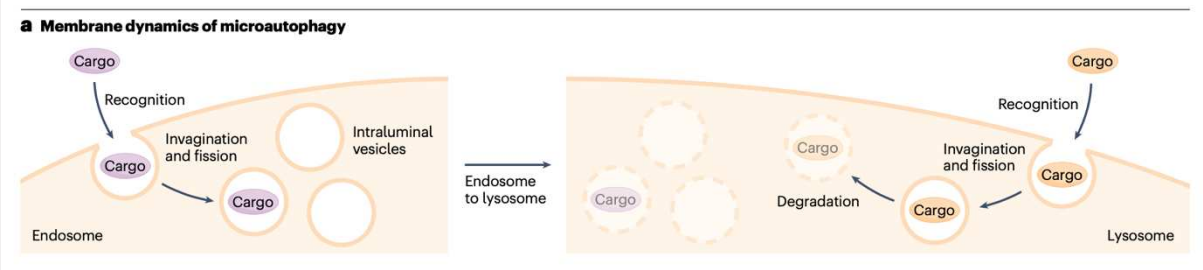

Figure 4.5: Steps involved in micro autophagy. (Adapted from Yamaoto et al 2023)

In mammals, micromitophagy and macrolipophagy does not require the involvement of ATG proteins but cGAS mediated micronucleophagy seems to engage ATG8 proteins (Bandyopadhyay et al 2008). Thus, microautophagy can be roughly divided into two processes, 1. ATG dependent and 2. ATG independent. In mammalian cells, NCOA4-ferritin condensates are subjected to endosomal microautophagy and TAX1BP1 helps in its incorporation. Although the exact mechanism of this event is not known as this is independent of ATG8 proteins (Ohshima et al 2022). Another endosomal microautophagy depends on HSC70/HSPA8 and the presence of

KFERQ motifs. Interestingly, this process requires ATG1 and ATG13 but not ATG5,7 or 12 (Sahu et al 2011).

So far, I have introduced lysosomes as an important subcellular organelle and have described different cellular pathways that merges at lysosomes. Now, I will discuss some common diseases where lysosomal function is important.

4. 8 Lysosomes and diseases

Initially, lysosomal dysfunction was primarily attributed to a rare group of inherited diseases known as Lysosomal storage disorders (LSDs). But with expanding knowledge, we can now appreciate its implications in several common diseases such as neurodegenerative diseases, cancers and metabolic disorders etc. It has been shown that with aging rapid lysosomal de-acidification happens which contribute to the pathophysiology of several diseases.

(A) Lysosomal storage disorders

In this group of diseases, mutations in lysosomal genes or proteins which modulates lysosomal functions leads to dysfunctional lysosomes which impair the recycling process. These are inherited monogenic diseases which are often associated with early onset of neurodegeneration (Platt et al 2018; Platt et al 2018; Marques et al 2019; Ballabio and Gieselmann 2009). One category of LSDs is the result of mutations in the lysosomal hydrolases and these diseases are very similar in their pathology. Another type of LSDs happens when lysosomal membrane proteins harbour the mutations and these diseases are more complex in nature. Some examples are mucolipidosis type IV and Niemann-Pick disease type C1. The first disease is caused by a mutation in the major lysosomal calcium channel TRPML1 and the second one is caused by mutation in NPC1 and is characterized by cholesterol accumulation in the lysosomes. LSDs can also result from mutations of genes which are not directly lysosomal. Some examples include, N-acetyl glucosamine-1-phosphotransferese, *SMUF1* and CLN8. In the first cases, manose-6-phaospahate receptor pathway driven delivery of lysosomal proteins are disturbed. Mutation in *SMUF1* results in the deficiency of several lysosomal sulfatases (Dierks et al 2003). CLN8 is responsible for transferring lysosomal proteins from ER to Golgi and mutation in this protein cause neuronal ceroid lipofuscinosis which is characterized by early onset of neurodegeneration and blindness (Di Ronza et al 2018). Although initially it was thought that the accumulation of substrates within lysosomal lumen is the main cause for these LSDs but now a days more and more processes are being discovered to have a link to the pathophysiology of these LSDs. For example, abnormal accumulation of cholesterol in lysosomal membrane disrupts the sorting and

recycling of SNARE proteins which in turn impairs the autolysosome formation (Fraldi et al 2010; Seranova et al 2017). Blockade in autophagy also results in accumulation in aggregate prone proteins and dysfunctional organelles which leads to further inflammation (Seranova et al 2017). mTORC1 has also been reported to be deregulated due to LSDs although this perturbation is very specific to cell type and disease type. Mucopolysaccharidosis types VI and VII and Niemann-Pick disease type C1 has been linked with increased mTORC1 activity whereas Pompe disease and Gaucher diseases results in lower mTORC1 activity (Bartolomeo et al 2017; Lim et al 2017; Kinghorn et al 2016).

(B) Neurodegenerative diseases

Other than LSDs, lysosomal dysfunction has been linked to several neurodegenerative diseases such as Alzheimer disease, Parkinson's disease and Huntingtin diseases. Alzheimer´s patients have been shown to carry mutation in presenilin 1 (*PSEN1*) gene. The underlying mechanism is thought to be impaired lysosomal acidification and defective Ca^{2+} homeostasis (Lee et al 2010; Coen et al 2012; Lee et al 2015). Altered production of amyloid-β peptide in Alzheimer's diseases is also known to be a result of disrupted endo-lysosomal transport (Nixon 2017). Similarly, a major percentage of patients suffering from Parkinson's diseases are known to have mutations in lysosome related genes. A homozygous mutation in the GBA causes an LSD known as Gaucher disease is also predisposition factor for Parkinson's (Aflaki et al 2017). Impaired autophagic lysosomal system causes accumulation within lewy bodies and neurites in neurons which are hallmark for Parkinson and related ´synucleopathies´. α-synuclein toxicity has also been shown to result in reduced lysosomal function due to more cytoplasmic retention of TFEB (Boya et al 2008). All these examples point towards the involvement of autophagic lysosomal system for the progression of different neurodegenerative diseases.

(C) Cancer

Cancer cells are known to have altered metabolism and hence they exclusively rely on autophagy and lysosomal pathway since this can act as a primary nutrient scavenging pathway. Therefore, a lot of therapeutic strategies have been tested to weaponize this cellular signalling against cancer. Initially, given lysosomes involvement in cell death pathway, lysosomes were targeted to induce apoptosis in cancer cells but in recent times, several different links have been discovered between lysosomes and cancer sub types hence the interest in therapeutic targeting is even broader now (Boya et al 2008; Appelqvist et al 2013; Kimmelman et al 2017). Since, autophagy lysosomal pathway can support proliferation, several different cancer types like renal cell carcinoma,

melanoma, pancreatic adenocarcinoma are known to induce the expression of MiT-TFE genes (Perrera et al 2015; Perrera et al 2019). In these tumour types, concomitant activation of mTORC1 mediated lysosomal biogenesis and high autophagy flux ensures the nutrient scavenging pathway to work at its highest peak to keep up with the high energy demand of cancer cells. The acidic tumour microenvironment, often lysosomes get redistributed towards the cell periphery and show enhance proliferation via increased mTORC1 and mTORC2 activity. Other than supplying with the energy demand, lysosomal exocytosis has also been shown to be hijacked by cancer cells (Bian et al 2016).

Thus, we could understand that being one of the terminal organelles of two major cellular pathways. Lysosomes can play crucial role for the progression of several diseases and hence it's a lucrative opportunity to target lysosomes in many diseases. Lysosomes themselves are also sometimes become target of damage and depending on the severity of damage, cells can either try to repair the membrane damage or even activate autophagy to clear the damaged lysosomes. In the next section, the major cellular responses for lysosomal damage will be discussed;

4.9 Cellular response to lysosomal damage

Lysosomal membrane damage can be caused by several different agents such as endocytosed silica particles, cholesterol crystals, invading pathogens or even neurotoxic aggregates such as α-synuclein, mutant huntingtin, Aβ or tau fibrils (R. Gomez-Sintes et al 2016; Papadopoulos et al 2017; Otomo et al 2017; L. Cantuti-Castelvetri et al 2018; Boyle et al 2013). Changes in lipid composition of the membrane, which is associated with aging or lysosomal storage diseases, are also able to induce lysosomal membrane permeabilization. Alteration in the membrane composition of lysosomes leads to a more fragile lysosome which can then be damaged really easily. Intra lysosomal Fenton reaction, reactive oxygen species are also known to be the major cause for lysosomal membrane permeabilization or LMP (Kirkegaard et al 2010; Peterson et al 2013; Boya et al 2008). Lysosomal damage not only results into dysfunctional lysosomes and henceforth impaired autophagy, but also the released cathepsins can cause cell death, can activate inflammation through NRLP3 inflammasome. Therefor cell have developed different strategies to deal with this membrane damage which is also known as ELDR or endolysosomal damage response. A diagrammatic representation is below,

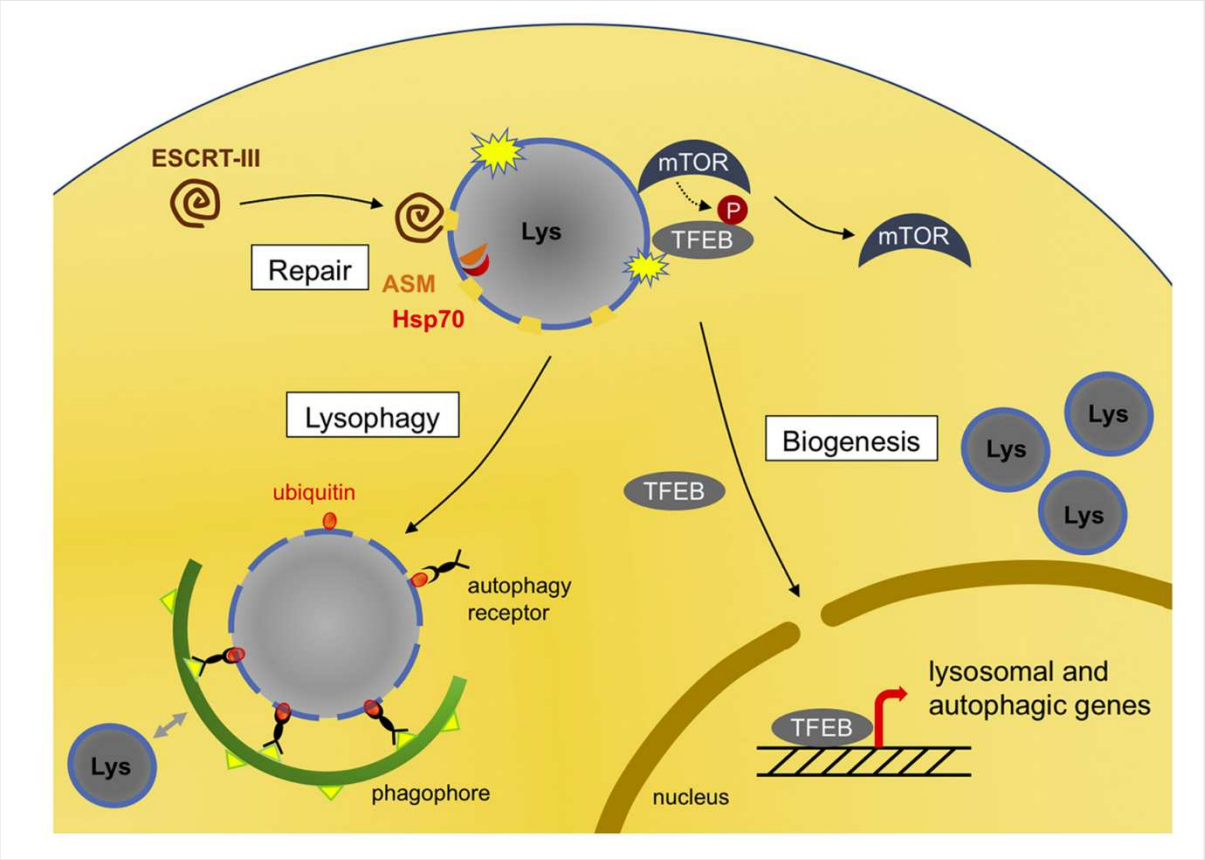

Figure 4.6: Cellular responses to lysosomal damage. (Adapted from Papadopoulos et al 2020)

One of these responses is to activate new lysosomal biogenesis via TFEB mediated biogenesis. This branch is dictated by the activity of mTORC1 (Jia et al 2018; Settembre et al 2013). The next branch is usually activated after small membrane perforation which can be closed by the action of ESCRT machineries. But in case of bigger damages which are caused by long sustained exposure, lysophagy takes over where cellular autophagy machinery gets involved into cleaning the damaged lysosomes.

(A) Repairing lysosomal membrane after small damage

In cell culture model, L-leucyl-L-leucine methyl ester or LLOMe is being regularly used for mimicking lysosomal membrane damage. This lysosomotropic agent can get accumulated inside the acidic compartments of our cell and then by the activity of cathepsin molecules, it gets cleaved to generate membranolytic peptides (Thiele et al 1990). After even a minute of exposure to LLOMe, ESCRT machinery gets recruited to lysosomes and Ca^{2+} efflux from these perforated membranes have been identified as a signal for this assembly. A specific component of the ESCRT machinery, known as ALIX, is activated through the released calcium and in turn recruit the

ESCRT III machinery at place. These “low damages” can be effectively dealt with by quick re sealing of the membrane (Skowyra et al 2018; Radulovic et al 2018; Repnik et al 2017). This mechanism also stays active in infected conditions where pathogen try to make leakage at the endolysosomal membrane in order to escape autophagy mediated degradation.

(B) Lysophagy deals with acute membrane damage

Acute lysosomal membrane damage occurs as a result of sustained damage and these lysosomes can be differentiated from other lysosomes by the recruitment of Gal3 within them. LLOMe damage for even 30 minutes does not result in the Gal3 recruitment so Gal3 positive lysosomes can be described as compartments suffering from heavier damage (Maejima et al 2013). The recruitment of Gal3 occurs by its binding to the glycosylated membrane proteins of lysosomes which normally stays inaccessible. Following recruitment of Gal3, these lysosomes also become marked by ubiquitin and also becomes positive for lapidated LC3. Amongst 600 E3 ligases present in mammalian cells, TRIM16 and FBXO27 has been identified so far as the main E3 ligases driving ubiquitination of damaged lysosomes (Chauhan et al 2016; Yoshida et al 2017). Both Lys48 and Lys63 ubiquitin chains can be detected on damaged lysosomes whereas Lys63 appears a bit earlier compared to Lys48 ubiquitin chains which peak 2-4hr of LLOMe damage. Although up to now, no specific DuB or deubiquitinases has been identified which regulates lysophagy, a recent study has identified UBE2QL1 as one of the E2 enzymes required for lysophagy (Koerver et al 2019). Amongst different receptors TAX1BP1 and P62 has been identified to act as a major receptor active during lysophagy (Papadopoulos et al 2017; Eapen et al 2021). Overall further work is needed to shed more insight on lysosomal damage responses as being one of the major regulators of the cells damaged lysosomes can have several pathological consequences.

4.10 TBC family of proteins

The TBC (Tre-2/Bub2/Cdc16) domain was originally identified among the tre-2 oncogene product and the yeast cell cycle regulators Bub2 and Cdc16. It is a conserved protein motif, and it consists of around 200 amino acids. TBC domain containing proteins in yeast has originally been identified to show GAP activity and in other species it also has been described to have certain Rab-GAP activity. In human and mice, more than 40 different TBC proteins have been identified to exist and many has been assigned for performing GAP activity for specific Rab proteins. Apart from serving as Rab-GAP, some TBC family of proteins are also known to participated in different cellular signalling related to maintenance of cellular homeostasis (Fukuda 2011). Rab small GTPases are known to be conserved family of proteins existing in eukaryotic cells and they are

mostly involved with cellular trafficking events (Pereira-Leal et al 2001). Normally Rab proteins can cycle between active and inactive states and in active state they stay bound to GTP (Guanosine triphosphate) and then by the activity of Gap protein, they can transition to GDP (Guanosine di-phosphate) bound inactive state (Grosshans et al 2006; Schwartz et al 2007; Fukuda 2008; Stenmark 2009). In the active state, several Rab directed vesicular trafficking events get promoted. Two classes of enzymes are crucial for Rab proteins to effectively cycle between GTP and GDP bound states. They are known as GEF or guanine-nuceoltide-exchange-factor, and GAP or GTPase activating protein. The first kind of proteins are required for converting from GDP bound state to GTP bound state while GAP proteins catalyse the reaction of GTP to GDP. TBC domain containing family of proteins are known for their GAP activities.

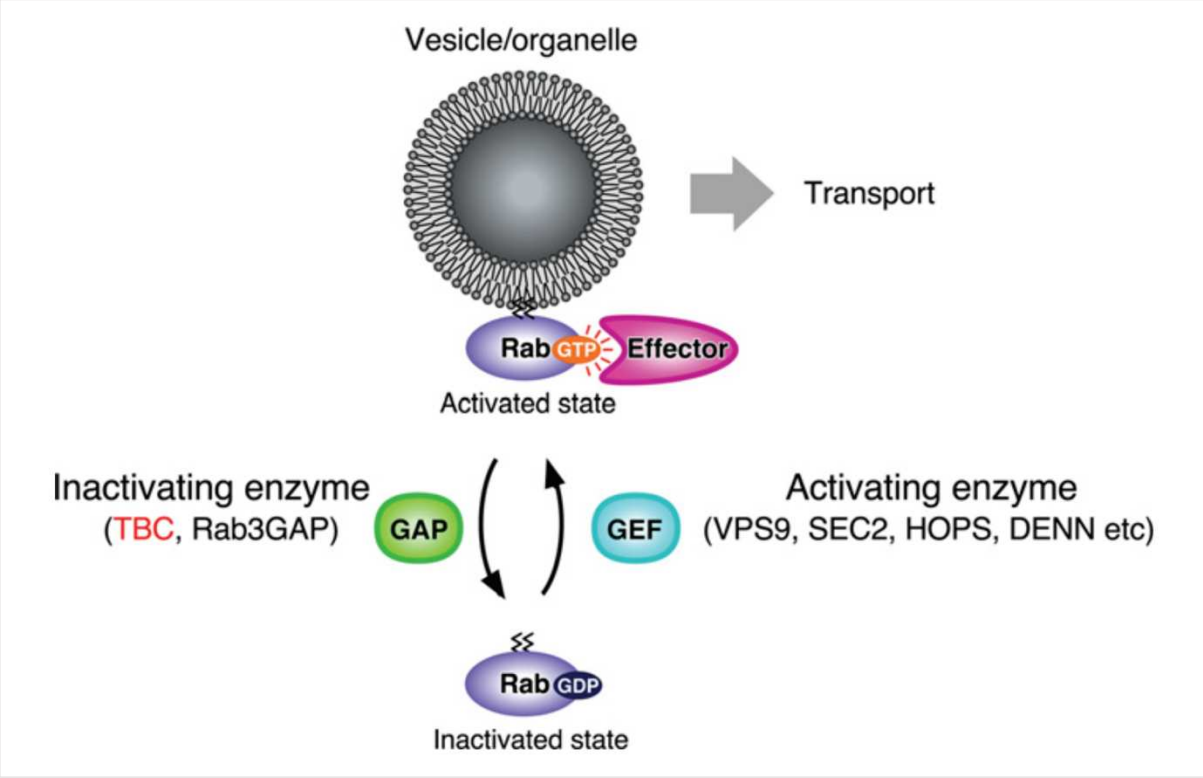

Figure 4.7: Vesicular transport depends on cycling of Rab proteins between GTP and GDP bound states. (Adapted from Fukuda 2011)

In order to identify the specific Rabs as a substrate for TBC proteins, it was thought that a specific interaction between TBC proteins and corresponding Rabs will be important (). For example, Rab5-GAP, Rab41-GAP and Rab6-GAP was shown to be directly interacting with their substrates in order to perform their GAP activities (Cuif et al 1999; Lanzetti et al 2000). These GAPs are RUTBC3, USP6NL/RN- tre and TBC1D-11 respectively. But later some genome wide screen has suggested that in order to perform their GAP activity, TBC family of proteins does not need

to directly bind their substrate Rabs (Itoh et al 2006). A different approach has also been taken to correctly identify the substrate Rabs of TBC proteins by utilising in-vitro GAP activity assay, but due to high variability of experimental methods, there seem to be certain discrepancies amongst these results (Haas et al 2007; Sklan et al 2007; Yoshimura et al 2007). Several factors can point to different directions such as if the protein purification has been done from mammalian source or bacterial and presence or absence of post translational modification also can tamper these results. Nonetheless, further investigations are important in order to correctly identify the substrates of TBC proteins. But it is really important to understand the science of TBC family of proteins as by affecting the spatiotemporal regulation of Rab proteins, TBC family of proteins participate in several important cellular signalling. Dysregulation of these controls has been shown to be involved in disease conditions as summarised in this study (Sebra et al 2002). For example, a mutation has been identified in *TBC1D1* gene in lean mouse model and in insulin resistant patients, a truncation in *TBC1D4* has been identified (Chadt et al 2008; dash et al 2009). A gene rearrangement in *TBC1D18* has been linked with Klinefelter syndrome although it is yet not determined whether it is directly involved or not (Roberti et al 2009). Rab1-GAP *TBC1D20* helps in HCV replication by interacting with an HCV protein known as NS5A (Sklan et al 2007). Additionally many TBC proteins have been shown to be linked with several cancer scenarios but the exact mechanisms are not yet known.

4.11 Vesicular rearrangement in pathogenic infection

A very common phenomenon is observed when pathogens invade cells is the rearrangement of host vesicular trafficking pathways. Usually, following infection host cells can automatically activate autophagy in order to degrade the invading pathogen and this response is known as "Xenophagy". But several if not most pathogens have been known to possess certain tactics to hijack the vesicular pathway and use these to their own advantages. *L. pneumophila*, *Brucella abortus* and *S. Typhimurium* can be considered as some model pathogen which alters vesicular trafficking very efficiently. Both legionella and brucella make utilisation of some vesicles within which they replicate efficiently and usually these vesicles get derived from the ER. Salmonella containing vacuoles or SCVs acquire early endosomal proteins just after infection and then at a later timepoint these vesicles become positive for late endosomal and lysosomal markers. But interestingly, these vesicles do not acquire cathepsins. On the other hand, *L. pneumophila*, *M. tuberculosis* and *C. trachomatis* have found ways to block the vesicular fusion between autophagosome and lysosome in order to avoid degradation and they also are often known to deacidify bacteria containing phagosomes. Whereas, *Coxiella burnetii* and *B. abortus* have

developed ways to replicate within acidic compartments. As discussed in the previous section, Rab proteins are the major regulators of cellular trafficking events and in case of several infections, pathogens target these proteins to hijack the cellular trafficking events. *S. enterica*, *C. trachomatis* and *L. pneumophila* harbours several effector proteins that regulate Rabs. For example, legionella has several E3 ligases and DUBs that regulate the function of Rab proteins. Interestingly, one effector protein of legionella named SidE can modify Rab1, Rab30 and Rab33 by unconventional serine ubiquitination and they are also known to possess certain effectors that can cleave this specific type of ubiquitination. (Mukherjee and Dikic 2022; Kitao et al 2020). The endosomal sorting complex required for transport or the ESCRT machineries are required for a variety of vesicular trafficking related events such as cytokinesis, vesicular budding processes, autophagy and endolysosomal repair processes and there are several instances where pathogens regulate the functions of ESCRT proteins towards their advantages. Some enveloped viruses such as HIV, Rous Sarcoma virus and Ebola viruses are known to utilise the late assembly domain in their Gag proteins which recruits ESCRT proteins at the site of viral budding (Meng et al 2021; Strickland et al 2021). Antigen presentation by the MHC-II molecules in antigen presenting cells is one of the primary mechanisms of cellular immunity and they also use endolysosomal system for this process. Recent studies have shown that salmonella can downregulate this process by ubiquitinating MHC-II molecules and promoting their degradation via effector protein SteD (Alix E et al 2020). Some important vesicular trafficking pathway and how they are targeted by pathogens have been described in Fig 4.8,

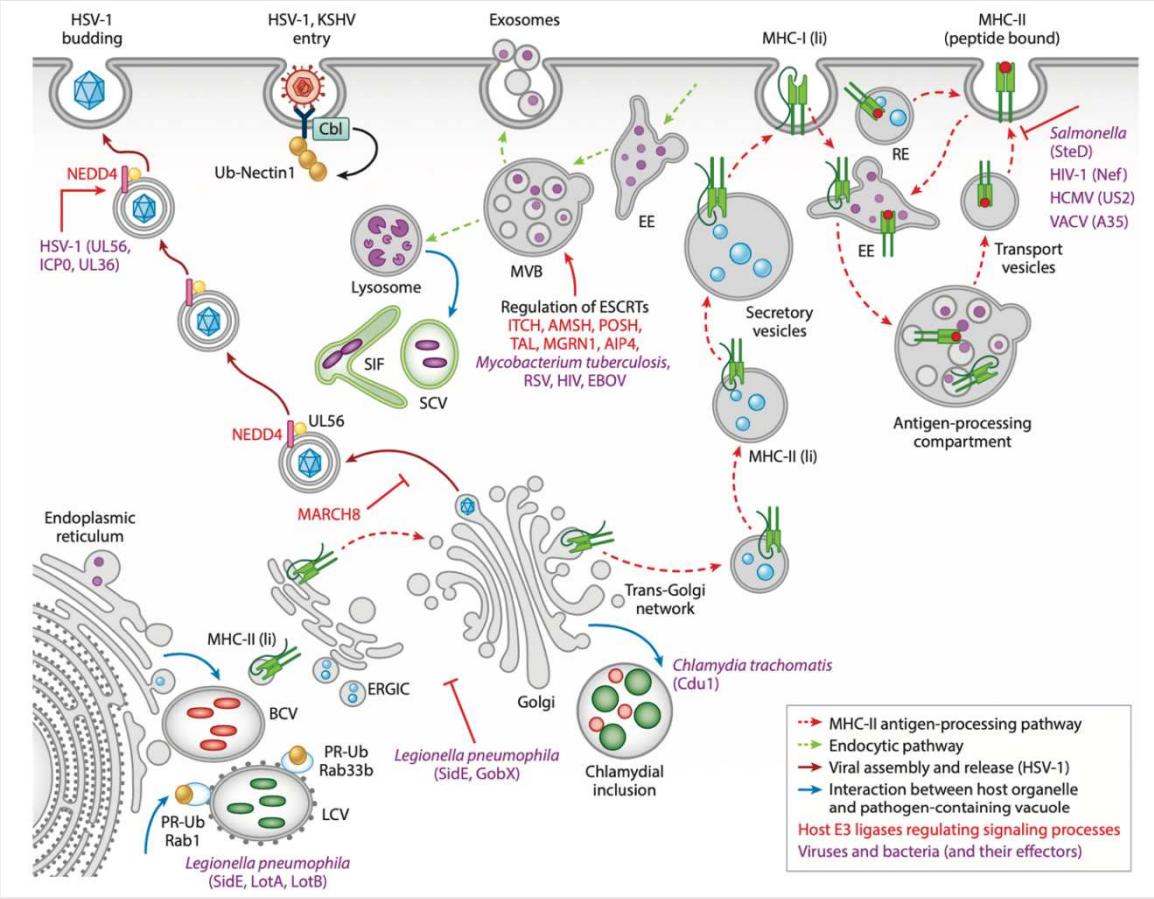

Figure 4.8: Pathogens hijacks the vesicular transport system at several points. (Adapted form Mukherjee and Dikic 2022)

(A) Cellular response to *L. pneumophila* infection

Back in 1976, due to an unknown pathogen, more than 200 participants were infected with pneumonia at the annual convention of American legion. Later, investigations by Centres for diseases control and prevention led to the identification of a gram-negative, rod-shaped intracellular bacteria as the causative agent of the diseases and this pathogen were named as *L. pneumophila.* The disease was also named as Legionnaires' disease (Brenner et al 1979; Fraser et al 1977; Macdade et al 1977). Subsequently, an influenza like fever was also associated as a result of legionella infection and this was named as Pontiac fever (Glick et al 1978). Legionella can be found in various types of aquatic and soil environments including natural water sources and built systems such as spa, pools and air conditioning devices. It has two natural hosts and can grow very effectively in biofilms and also within human host cells. Once they manage to attach themselves to the host cell surface, legionella uses type II or type IV secretion systems to release effector proteins within the host cell. The primary host for legionella is actually amoebae and other protozoa and they are also called as the natural host of legionella. Human macrophages serve as a secondary target for legionella although they can very efficiently infect and replicate within these cells (Hilbi et al 2010; Newton et al 2010). Most of the legionella infection cases are sporadic

and the recent reported outbreak was in the North of Portugal in October 2020 with a mortality rate of 12.5% (Camoes et al 2021). Aerosol inhalation and aspiration from aquatic systems are the most commonly known causes of the LD or Legionnaires' disease. Once inside the human host cells, the life cycle of legionella can be roughly divided into two different phases. One is the replicative phase and then the transmissive phase. Usually right after infection legionella secrets more than 300 effector to re-wire the cellular signalling pathways. Within cells legionella reside inside a vacuole where they replicate and this vacuole is called legionella containing vacuoles or LCV. These vacuoles are rich in nutrients but do not harbour hydrolases inside thus ensuring the safety of replicating legionella. Legionella can also escape the lysosomal degradation; we will discuss more about this mechanism in the results section. Legionella targets several host signalling pathways during the course of infection and one of the major signalling pathways that gets affected is the ubiquitin pathway. We will have a closer look to what is known so far about legionella directed modulation of host ubiquitin pathway.

(B) Legionella mediated modifications of ubiquitin pathway

Ubiquitination is an evolutionary conserved post translation modification that cell uses to modulate several cellular pathways. Some examples are DNA damage repair, immunity and vesicular trafficking (Hershko et al 1998). Legionella uses some of its many effector proteins to alter both canonical and non-canonical ubiquitination pathway. Ubiquitin is a small protein weighing around 8-9 kDa can get attached to other substrates or target proteins through forming a covalent bond between the terminal glycine residue of ubiquitin and substrates' lysine residue. Although lysine residues are the major target of canonical ubiquitination, other residues can also be modified via ubiquitin but to a much lesser extent (McClellan et al 2019). Canonical ubiquitination occurs by three enzymes known as E1, E2 and E3. Depending on their activity they are also known as ubiquitin activating enzyme, ubiquitin conjugating enzyme and ubiquitin ligase enzyme respectively. There are approximately two genes in mammalian that encodes the E1 enzymes, 30 genes for encoding E2 enzymes and around 1000 genes are there encoding for E3 ligases (Rytkonen et al 2007; Ye et al 2009). This whole ubiquitination process is ATP dependent and also reversible in nature. There are around 100 deubiquitinating enzymes present within mammalian cells that can reverse this process by hydrolysing the peptide/isopeptide bond between ubiquitin and its substrate (Clague et al 2019). SidE family of effector proteins in legionella are the first known effectors from a pathogen which can bypass this E1-E2-E3 enzyme cascade and still modify proteins with ubiquitin. During this process, legionella also modifies the ubiquitin molecule first and then transfer this modified ubiquitin to substrate proteins via effectors. The

SidE family of proteins contains four paralogues known as SidE, SdeA, SdeB and SdeC and these are needed for the full bacterial virulence (Bardill et al 2005; Luo et al 2004). These enzymes contain three domains; 1. A DUB domain at the N terminus, followed by a 2. Phosphodiesterase or PDE domain and then a 3. Mono ADP-ribosyltransferase domain at the C terminal. The whole ubiquitination process can be catalysed by this one single enzyme thus avoiding the classical E1-E2-E3 enzymatic cascade and this process is dependent on NAD^+ instead of ATP. At first step cellular ubiquitin molecules get modified by ADP-ribosylation at its arginine 42 residue through the activity of the ART domain. This domain utilizes β-nicotinamide adenine dinucleotide (NAD^+) for this particular process. Next, PDE domain process this ADPR-Ub to PR-Ub and transfer it to substrate or further hydrolysis generates free ubiquitin (Bhogaraju et al 2016). Since, this process of PR-ubiquitination can block conventional cellular ubiquitination, many ubiquitin dependent processes can be altered by this process. Interestingly, just like conventional ubiquitination, this atypical ubiquitination process can also be altered by some legionella proteins and these are called DUPs or DUB for PR-ubiquitination. In legionella two major DUPs exists, DupA and DupB. Structurally these DUPs resembles the PDE domain of SdeA but have much higher affinity towards PR-ubiquitin compared to SidE PDE domains. They can also convert ADPR-Ub to PR-ub but fails to transfer this PR-Ub to substrate proteins (Shin et al 2020). Thus, by changing the cellular ubiquitin pathway, legionella balances the cellular homeostasis in order to replicate efficiently within host cells. A depiction of the key steps citing the differences in the canonical and non-canonical ubiquitination is depicted in Fig 4.9;

(C) Effect of non-canonical serine ubiquitination on host pathways

As described above, this non canonical PR-ubiquitination plays a key part in legionella pathogenesis and alters several key cellular pathways. By using an inactive mutant of DupA (ref 180) over 200 cellular proteins were identified to be modified by this PR-Ubiquitination process. This modification happens within the first two hours of infection and the target proteins are part of ER, Golgi, Mitochondria and endo lysosomal pathways. Endoplasmic reticulum or ER is undergoing constant remodelling depending on cellular status and legionella targets several ER remodelling proteins as a site of modifications such as FAM134A, FAM134B, FAM134C, RTN3 and TEX264. As a result of these modification, severe fragmentation is noticed during infection and ER gets majorly remodelled. Interestingly many of these proteins are known to function as ER-phagy receptors and delivers subpart of damaged

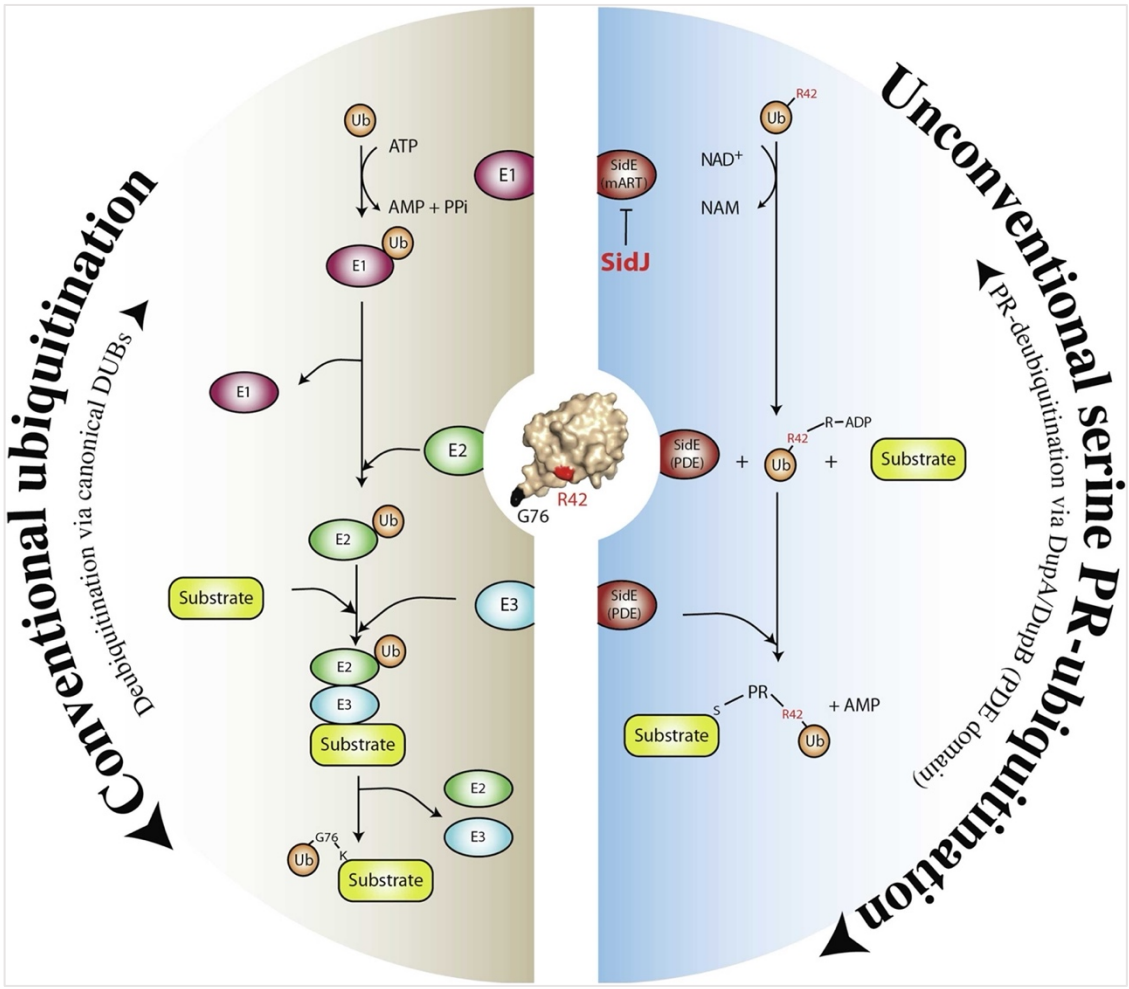

Figure 4.9: Schematic illustrating the main difference between canonical and non-canonical ubiquitination. (Adapted from Tomaskovic et al 2022)

ER to lysosomes for degradation. So, it is definitely one of the processes that get affected by PR-ubiquitination. SidE family of proteins also is known to target RTN4 or reticulon 4 during early infection to alter the tubular ER dynamics (Kotewicz et al 2017). SdeA is also known to modify several ER related Rab GTPase proteins and this alteration probably help the pathogen to derive membrane for making LCVs (Qiu et al 2016). Moreover, legionella also possess a unique effector protein RavZ which delipidates LC3 in order to block autophagy. So, it can be easily imagined that by engaging several ER structural and remodelling and ER-Phagy receptor proteins, legionella induces ER fragmentation and rearrangement but at the same time it also blocks the lysosomal degradation but rather redirect these fragmented membranes as a source of growing LCV. Although more experiments are needed to properly dissect the effect of PR-Ubiquitination and growth of LCV. Apart from targeting the ER, legionella also affects the Golgi complex by PR-ubiquitination. The Golgi complex comprises with a complex network of cisternae which can

be subdivided into three separate modules: the *cis*-, which is close to the ER and receives the ER output, *medial* and *trans*-Golgi network (TGN) that contains glycosylation enzymes and process cargo proteins and lipids. As a major part of the secretory organelle of the cells the Golgi complex helps to sort the cargos into different destinations (Huang et al 2017). PI4P has been identified as a main phosphoinositide theta controls the membrane trafficking mediated by Golgi complex and interestingly, the legionella containing vacuoles or LCV are known to acquire PI4P vesicles in order to grow in size (Weber et al 2018). Apart from this, one of the main SidE family proteins SdeA has been shown to partially localise to Golgi complex and two Golgi proteins, namely GRASP55 and GRASP65 were also identified as a substrate for PR-Ubiquitination. It has been shown that PR-Ubiquitination of these two proteins, which form trans oligomer to maintain proper Golgi stacks, results in disruption of Golgi structure and therefore opens up additional avenues for legionella to control host cell secretory pathways (Liu et al 2021). The endo lysosomal system and autophagy pathways can also be modulated via PR-Ubiquitination. As explained before, RavZ hydrolyses the amide bond between the carboxyl-terminal Gly residue and an aromatic residue in ATG8 proteins thus inactivating both LC3 and GABARAP family of proteins (Choy et al 2012). Additionally, they also modify several autophagy and lysosome related SNARE proteins like STX17, SNAP29 to modulate autophagic lysosomal degradation. But these effects are not yet studied in details. PR-ubiquitination inhibits the activity of small Rag GTPases and therefore inhibit the mTORC1 activity (De leon et al 2017). This mTORC1 inhibition is thought to increase the amount of free amino acids that helps in bacterial replication. One of the serine proteases form *Legionella*, named as Lpg1137, localize in mitochondria and MAMs in order to cleave the host STX17. This phenomenon leads to STX17 degradation, disassembly of STX17-ATG14L and inhibition of STX17-Drp1 complex, thereby inhibiting an early key step of autophagy. Furthermore, cleaving STX17 also inhibits staurosporine-induced apoptosis which in turn ensures bacterial safety. Some other studies have also revealed that the effector protein LpSpl exhibits sphingosine-1-phosphate lyase activity during infection which results in disruption of the sphingolipid metabolism and thus decreases autophagic flux (Arasaki et al 2017; Banga et al 2007; Blatt et al 1993). A depiction of host pathways those are being modified by legionella are shown below,

4.12 SNARE proteins and their role in cellular trafficking and autophagy

Membrane trafficking comprises of wide variety of processes that are related to the movement of cargo using transport vesicles which are often membrane bound. Some of these membrane trafficking events includes, vesicle budding, transport, tethering, and fusion. SNARE proteins

usually take part in mediating membrane fusion. And as a result they work together with coats, tethers, and Rabs. Depending on their functionality, SNAREs can be broadly classified into two types, such as v-SNAREs and t-SNAREs. V-SNAREs are usually associated with vesicles or other forms of transport intermediate and t-SNAREs are associated with the target compartments. A v-SNARE interacts with the cognate t-SNARE to form trans-SNARE complexes and this happens at the interface of the transport vesicle and the target compartment. Tethering factors also play a crucial part to facilitate this interaction. The interaction between
v- and t-SNAREs is required to bring the two different membranes close enough together to facilitate fusion process. After the fusion is complete, the ATPase NSF unravels both the v- and t-SNAREs. The v-SNAREs are then recycled to the starting membrane compartment. SNAREs (soluble N-ethylmaleimide-sensitive factor attachment protein receptors) are generally accepted to be the major players in the final stage of the docking and the subsequent fusion of diverse vesicle-mediated transport events and this process is conserved evolutionally from yeast to human. They are also similar in nature in terms of mechanistically and structurally across almost all different transport events in eukaryotic cells. Amongst all these different processes mediated by SNARE proteins, one central process is the autolysosome formation. This is the final step of autophagy where an autophagosome fuse with lysosome to form an autolysosome and thus degrading the contents within. But not only SNAREs but also activity of several other small GTPases and tethering factors are needed to proper completion
of this step (Zhao et al 2019). But amongst the SNARE proteins, autophagosomal SNARE STX17, cytosolic SNAP29 and lysosome localised VAMP7 or VAMP8 are known to be of utmost importance. Although a very recent report has shown that Ykt6 can also function in concert with SNAP29 to help this process independent of STX17 (Matsui et al 2018). Amongst different Rab proteins, RAB7A, RAB2A and AB33B have been reported to be important for autolysosome formation. A Rab7 effector PLEKHM1 is also known to be recruiting the HOPS complex to promote fusion between the two membranes. HOPS complex is reported to interact with the SNARE complex to regulate the assembly of the said complex (Gutierrez et al 2004; Itoh et al 2011; Ding et al 2019; Takats et al 2014; Jiang et al 2014).

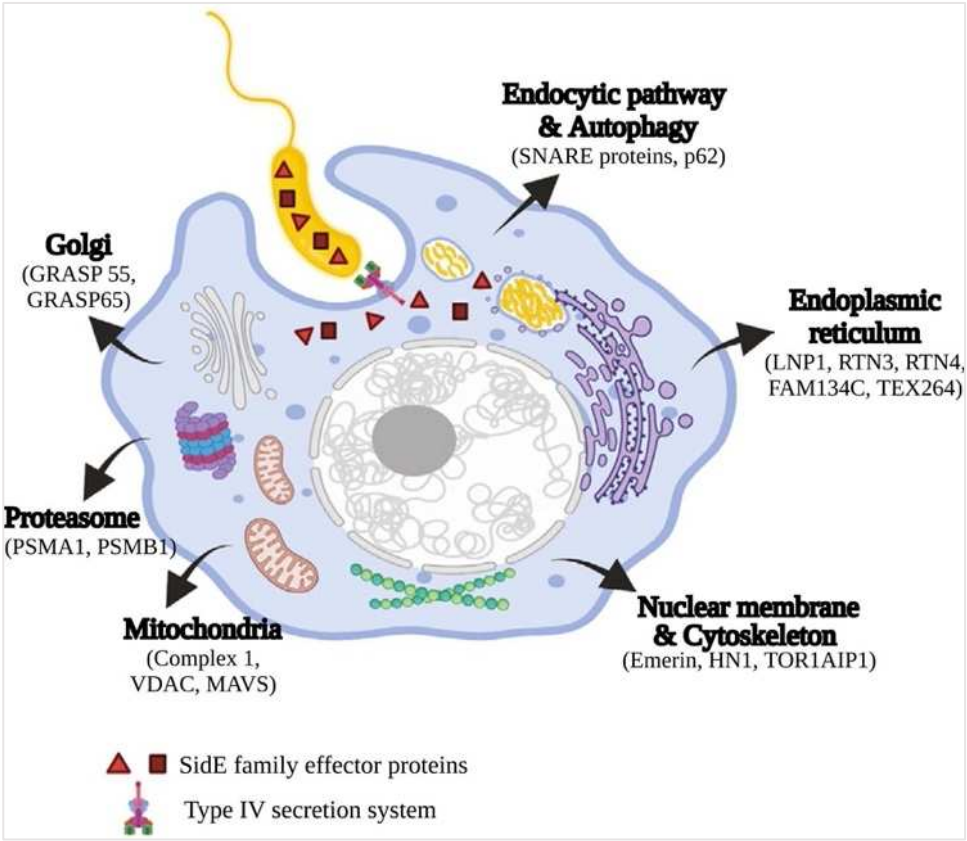

Figure 4.10: Examples of different host pathways which are being targeted by Legionella. (Adapted from Tomaskovic et al 2022)

(A) Assembly of the SNARE complex to form autolysosome

In case of SNARE mediated membrane fusion events, four types of SNARE motifs, namely Q_a, Q_b, Q_c and R motifs gets involved. They form a four alpha-helix bundle to promote membrane fusion. In case of autophagosome and lysosome fusion, Q-SNAREs STX17 and SNAP29 form the Q_{abc} bundle on autophagosome and then it forms a complex with the R SNARE such as VAMP8 which is lysosomal (Itakura et al 2012). SNAP29 is predominantly cytosolic and it gets recruited to autophagosome by its interaction with STX17. The recruitment of STX17 to autophagosomal membrane happens via the transmembrane domain containing glycine zipper like motifs. These motifs on STX17 are not very hydrophobic and that is why it mostly stays cytosolic and only are present on closed autophagosomal membrane. But the actual mechanism leading to its recruitment is not properly known. Targeting of STX17 to autophagosomes is affected in the absence of LAMP2 as well as autophagosomal IRGM (Hubert et al 2016; Kumar et al 2018). But the role of ATG8 proteins for the recruitment of STX17 is not well understood since in the absence of ATG8 proteins, autophagosome still can be formed and STX17 is recruited there but at a slower rate (Tsuboyama et al 2016). The process of SNARE bundle formation can also be altered by post translation modifications. Both STX17 and SNAP29 can be modified by acetylation and *O*-

GlcNAc respectively. These modifications occur under normal condition and prevents premature formation of the SNARE bundle in order to allow the autolysosome formation at a proper time (Shen et al 2020; Guo, B et al 2014). In the next section, the roles of these SNARE proteins will be discussed individually with a focus on their participation in autolysosome formation;

(B) Syntaxin17 (STX17)

STX17 is broadly expressed in several tissues which primarily localises to endoplasmic reticulum (ER) (Steegmaier et al 1998). It is a Q_a-SNARE which is involved in autophagosome and lysosome fusion. The C terminal tail of STX17 contains two transmembrane domains and is required for its ER localisation. The N terminus however is involved in its exit form ER into the ER-Golgi intermediate compartment (ERGIC). The conserved tyrosine residue Y156 is known to be involved in this function (Muppirala et al 2011). The Y156 residue can be phosphorylated by ABL1/c-Abl and dephosphorylated by TC48 and this is important for its interaction with the COPI vesicles. Thus, STX17 can cycle between ER and ERGIC in order to maintain the architecture of ERGIC and the Golgi apparatus (Muppirala et al 2012). STX17 is transferred to the autophagosomes under nutrient starvation conditions and interacts with Q_{bc}-SNARE SNAP29 to mediate autophagosome and lysosome fusion. The absence of STX17 results in the accumulation of autophagosomes which indicates its role in the process. HOPS components, VPS33A, VPS16, or VPS39 are known to play important role in autophagosome maturation as knockdown of these blocks autophagic flux. STX17 interacts with VPS33A using its N terminal and thus regulates the autophagosome localisation of HOPS (Cheng et al 2017; Uematsu et al 2017). PLEKHM1 uses its RUN domain to interact with HOPS complex and colocalises at the vesicle contact sites. Like PLEKHM1, BIRC6/BRUCE, which is a lysosome localized inhibitor of apoptosis protein is also has been shown to promote autolysosome formation by bridging STX17 and LAMP2 labelled lysosomes (Ebner et al 2009). Mitochondria associated membranes or MAMs has been recently shown to be involved in autophagosome formation and STX17 can also be spotted at that site where it recruits ATG14 following starvation (Hamasaki et al 2013). Interestingly ATG14 can stabilise the STX17-SNAP29 binary t-SNARE complex by interacting with the SNARE domain of STX17. Apart from autophagosome maturation, STX17 is also involved in autophagosome formation. During starvation TBK1 phosphorylates STX17 at S202 which causes it to translocate to the phagophore assembly site from Golgi apparatus (Kumar et al 2019). Additionally, ULK1 can interact with STX17 in order to enhance the STX17-SNAP29 coupling and phosphorylation of ULK1 at S243 bocks this interaction (Wang et al 2018). STX17 is also able to interact with ATG8 family member proteins via its two LIR motifs, $LIR1_{172–175}$ and $LIR2_{189–192}$, and mutations

in these LIR motifs reduce autophagosomal recruitment of STX17 (Kumar et al 2018). All these examples indicate the existence a complex molecular signalling around the STX17 which ultimately helps to progress autophagy flux.

(C) SNAP29

SNAP29 is a Q_{ab}-SNARE which belongs to SNAP25 protein family and it contains two SNARE domains but lacks a transmembrane domain which makes it dependent for getting recruited to vesicles through interacting with other syntaxins (Steegmaier et al 1998; Hohenstein et al 2001). In mammalian cells starvation promotes SNAP29 recruitment to STX17 positive LC3 structures and knockdown of it causes accumulation of autophagosomes. As mentioned earlier the cytosolic retention of SNAP29 under normal conditions are regulated by *O*-GlcNAc and O-linked N-acetylglucosamine (GlcNAc) transferase, also known as OGT, is responsible for this modification. A mutant version of SNAP29, $SNAP29_{S2A/S61G/T130A/S153G}$, can enhance autophagy and promote autophagic degradation if protein aggregates even under fed conditions. The importance of this modification has also been shown to be working *in-vivo*. Type I diabetic rat harbouring this mutation shows abnormal autophagic flux showing its importance in the process (Huang et al 2018). In addition, DAPK3 enhances STX17 SNAP29 interaction by binding to SNAP29 (Wang et al 2020). Further research is needed to further delineate the mechanism around SNAP29 which regulates autophagosome and lysosome fusion.

(D) VAMP8; VAMP7

Lysosomal R SNARE VAMP8, and VAMP7 in Drosophila, acts as a coupler between STX17 and SNAP29 and mediates the last step of autophagosome lysosome fusion. Rab21 and MTMR13 regulates the localisation of VAMP8 (and VAMP7) to lysosomes (Jean et al 2015). VAMP7 has been shown to heterodimerize with STX17 which is important for autophagy to function (Saleeb et al 2019). Due to its closer proximity to the STX17-SNAP29 SNARE complex, VAMP7 definitely plays a very important role in the autolysosome formation. VAMP7 belongs to the longin family of SNARE proteins and have a coiled coil domain at their N terminus which helps in membrane fusion (Daste et al 2015).

The domain architecture of these important SNAREs is depicted below:

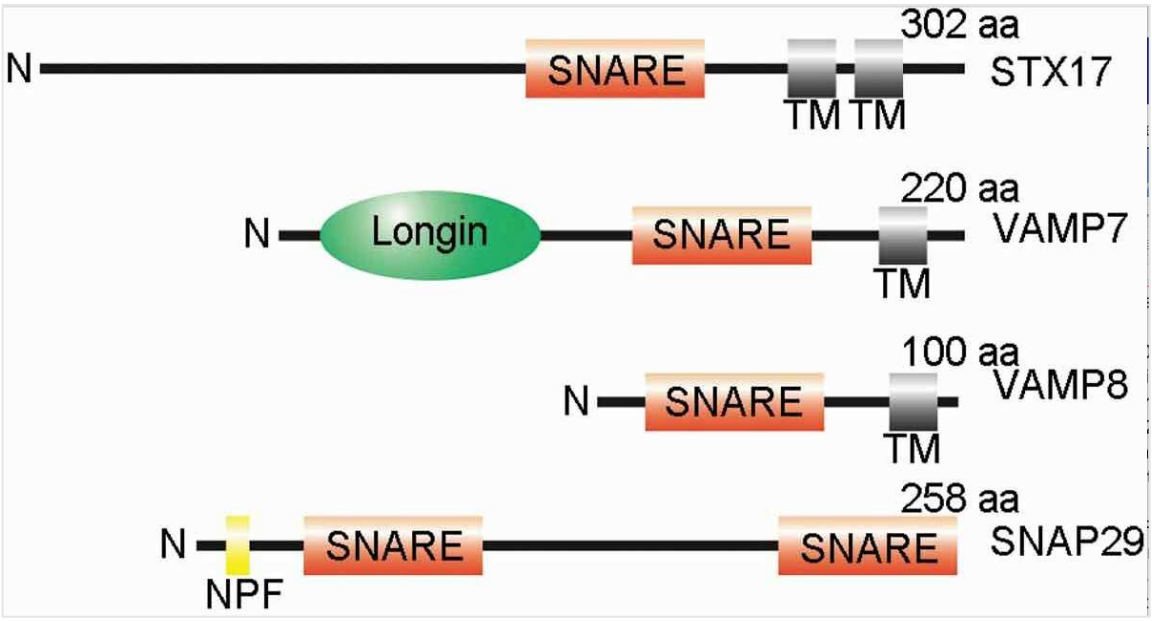

Figure 4.11: Domain architecture of important SNARE proteins for autophagosome and lysosome fusion process. (Adapted from Tian et al 2020)

CHAPTER 5
Objectives

This thesis aims to understand how the autophagy lysosomal system of the cell reacts to extensive lysosomal membrane damage and how the pathogen *Legionella pneumophila* can hijack the autophagy and endolysosomal membrane systems during Legionella infection

The objectives of the thesis can be detailed as follows:

I. To understand the lysosomal regeneration pathway activated in case of extensive lysosomal damage as induced by the lysosomotropic drug LLOMe including the study of the steps of the process, the identification of the molecules involved in the pathway and the possible physiological impact of the process in the cell model of calcium oxalate mediated crystal nephropathy.

II. To understand how phosphoribose linked serine ubiquitination of the SNARE proteins Syntaxin17 and SNAP29 affect the autophagy lysosomal pathway in *Legionella pneumophila* infection and delineate its effect on bacterial replication in lung epithelial (A549) cell line.

CHAPTER 6
Materials and Methods

6.1 Cell culture

HeLa, A549 and HEK 293T cells were cultured in Dulbecco's modified Eagle's medium (DMEM, Gibco) containing 10% foetal bovine serum (FBS) and 1% penicillin–streptomycin. PTEC cells (a kind gift from Tamotsu Yoshimori, Department of Genetics, Osaka University, Japan) were grown in low-glucose DMEM (100 mg/dL glucose, Gibco) containing 10% FBS and 1% penicillin–streptomycin. Transfection with plasmid DNA and siRNA was carried out using Lipofectamine 2000 (Invitrogen) according to the manufacturer's recommendations. Drugs used in this study are listed below:

Name	Treatment conditions	Source
LLOMe	1mM, 2hr	Sigma, Cat ID: L7393
Dynasore	20 μM, 2hr	Sigma, Cat ID: D7693
Wortmanin	300 nM, 6hr	Sigma, Cat ID: W1628
SAR405	10 μM, 6hr	Sigma, Cat ID: 5.33063
MRT68921	10 μM, 6hr	Sigma, Cat ID: SML1644
MLSA1	50 μM, 1hr	Sigma, Cat ID: SML0627
Monensin	100 μM, 1hr	Sigma, Cat ID: M5273
Torin1	500 nM, 6hr	Sigma, Cat ID: 475991
CCCP	10 μM, 4hr	Sigma, Cat ID: C2759

6.2 Plasmids

FLAG-STX17 was a gift from Noboru Mizushima (Addgene #45911; RRID Addgene_45911) and pcDNA 3.2/V5-DEST SNAP29-V5 was a gift from Anne Brunet (Addgene #69821; RRID Addgene_69821). The coding sequence of STX17 from FLAG-STX17 was transferred to vectors pEGFPC1 and pGEX6P1 for expression in mammalian and bacterial cells, respectively. STX17 and SNAP29 serine mutants were generated by mutagenic PCR and site-directed mutagenesis. For proximity labelling experiments, the TBC1D15, STX17 and LAMP1 coding sequences were tagged with the enzyme APEX2 and introduced into the doxycycline-inducible vector pcDNA5 by Gibson assembly. The dual-tag Galectin3 plasmid was acquired from Addgene (ref. 64149). The TBC1D15 coding sequence was subcloned into vectors pEGFPC1 and pGEX6P1 for expression in mammalian and bacterial cells, respectively. The LIRmut and GAPmut variants of TBC1D15 were generated by site-directed mutagenesis. The N-terminal (1–300) and C-terminal (400–697) segments, as well as nested N-terminal deletions ΔN1 (1–100), ΔN2 (1–182) and ΔN3 (1–300) and the loop mutant (57–124) were generated by standard restriction and ligation. The LIR mutations for LIMP2 and TMEM192 were introduced by site

directed mutagenesis. The LIR mutants of LIMP2 are as follows; LIR1: GDYVFL mutated to GDAVAA, LIR2: SDYESV mutated to SDAEAA and LIR3: ETFVDI mutated to ETAVAA. The LIR mutants of TMEM192 are as follows; LIR1: RGYNLI mutated to RGANAA, LIR2: RLYLDL mutated to RLALAA and LIR3: TGFRTI mutated to TGAATI. The full-length and deletion constructs of TBC1D15 were subcloned into pGEX6P1 for bacterial expression. The HA-TBC1D15, LAMP1-GFP, LAMP-RFP, LC3-BFP, GST-GABARAPL2, GST-LC3B and GAL3-GFP constructs were sourced from our in-house plasmid collection. The siRNAs for TBC1D15 (sc-95660), TFEB (sc-38509), TFE3 (sc-38507), ATG3 (sc-72582), ATG12 (sc-72578), ATG13 (sc-97013), ATG16L (sc-72580), Rubicon (sc-78326), DNM2 (sc-35236), LIMP2 (sc-41546) and TMEM192 (sc-89327) were purchased from Santa Cruz Biotechnology.The ProtA-Turbo plasmid was a kind gift from Michiel Vermeulen.

6.3 Antibodies

We used the following antibodies and dilutions: STX17 (cat. no. 17815-1-AP, Proteintech; 1:1000), GAPDH (cat. no. 2118, Cell Signaling Technology; 1:2000), GFP trap beads (cat. no. gta-100, ChromoTek), GFP (cat. no. sc-9996, Santa Cruz Biotechnology; 1:2000), LC3 (cat. no. 2775, Cell Signaling Technology; 1:2000), VAMP8 (cat. no. 13060, Cell Signaling Technology; 1:1000), SNAP29 (cat. no. 3013, Cell Signaling Technology; 1:2000), RAB5 (cat. no. 3547; 1:1,000), RAB7 (cat. no. 9367, Cell Signaling Technology; 1:2000), ATG16L (cat. no. ab188642, Cell Signaling Technology; 1:1000), ATG12 (cat. no. 4180, Cell Signaling Technology; 1:1000), ATG3 (cat no. 3415; Cell signaling technology), ATG13 (cat no. 13468; Cell signaling technology), Rubicon (cat no. 68261; Cell signaling technology), Beclin1 (cat. no. 3738, Cell Signaling Technology; 1:1000), FIP200 (cat. no. 17250-1AP, Proteintech; 1:1000), LAMP1 (cat. no. 9091, Cell Signaling Technology; 1:2000), and *Legionella* (cat. no. 20943, Abcam; 1:4000), Ubiquitin (Cat. no: 3933, Cell Signaling Technology, 1:1000), TBC1D15 (cat. no. 121396; Abcam), GABARAPL1+L2 (cat no. ab109364), DNM2 (cat. no. ab3457; Abcam), CLTC (cat. no. ab2731; Abcam), KIF5B (cat. no. MA1-19352; Thermo Fisher Scientific), TFEB (cat. no. 37785; Cell Signaling Technology), TFE3 (cat no. HPA023881; Sigma), Biotin (cat. no. SC101339; Santa Cruz Biotechnology), HA (cat. no. 7392; Santa Cruz Biotechnology), Myc (cat no. sc-40; Santa cruz biotechnology), GST (cat. no. 2622; Cell Signaling Technology), ATP6V1B2 (cat. no. ab73404; Abcam), phospho-p70s6K Thr389 (cat no. 9205; Cell signalling technology), p70S6K (cat no. 9202; Cell signalling technology), TRPML1 (cat no. ab272608; Abcam) LIMP2 (cat no. 176317; Abcam. We also received aliquots of antibody raised in the lab as a kind gift from Paul Säftig, Institute of Biochemistry, Kiel University, Germany) and

TMEM192 (cat. no. ab185545, Abcam). All primary antibodies were used at 1:1000 dilutions for western blotting and at 1:100 dilutions for Immunofluorescence.

6.4 Immunoprecipitation and western blotting

Cells were lysed in 50 mM Tris-HCl (pH 7.5) containing 150 mM NaCl and 1% Triton X-100. For the immunoprecipitation of STX17-GFP, lysates containing 1 mg protein were incubated with GFP beads in immunoprecipitation buffer (50 mM Tris-HCl pH 7.5, 150 mM NaCl, 0.5% Triton X-100), then washed (50 mM Tris-HCl pH 7.5, 300 mM NaCl, 0.5% Triton X-100) and boiled with SDS sample buffer. For western blotting, 20-µg samples were loaded onto 10% Tris-glycine gels and fractionated at 150 V for 1.5 h, followed by transfer to a PVDF membrane for 2 h at 300 mA and incubation with the antibodies listed above.

6.5 Protein purification

GST-tagged TBC1D15 and its deletions mutants, SNAP29 and STX17 (amino acids 1–224) and their PR-Ub-deficient serine mutants were purified from *E. coli* as previously described (Shin et al., 2020). Briefly, BL21(DE3) competent cells (NEB) were transformed with plasmids and grown in lysogeny broth at 37 °C to an OD_{600} of 0.6–0.8. Protein expression was induced by adding 0.5 mM isopropyl-D-thiogalactopyranoside (IPTG) overnight at 18 °C. Lysates were incubated with glutathione Sepharose resin pre-equilibrated with lysis buffer (50 mM Tris-HCl (pH 7.5), 150 mM NaCl, 3mM DTT), and non-specific proteins were cleared by washing twice with wash buffer (50 mM Tris-HCl (pH 7.5), 300 mM NaCl, 3mM DTT. Proteins were eluted in 50 mM Tris-HCl (pH 7.5), 150 mM NaCl, 15 mM glutathione and exchanged into storage buffer (20 mM Tris-HCl pH 7.5, 100 mM NaCl) before further use.

6.6 In vitro assays

a) GST pulldown assay

Cells were lysed (20 mM Tris-HCl pH 7.5, 150 mM NaCl, 1% Triton X-100) and precleared by incubating with 30 µL GST beads for 1 h to reduce non-specific binding. We then added 1 mg of the precleared lysate to 5 µg of GST-tagged protein and 20 µL glutathione Sepharose resin, and incubated at 4 °C for 2 h on a rotary shaker. The resin is then washed (20 mM Tris-HCl pH 7.5, 300 mM NaCl, 1% Triton X-100), boiled with SDS sample buffer and analyzed by western blot as described above.

b) RILP pulldown assay

GST-tagged RILP was purified from *E. coli*, and 5 µg of the pure GST-RILP protein was mixed with glutathione beads and 1 mg cell lysate in lysis buffer (50 mM Tris.HCl pH 7.5, 150 mM NaCl, 0.1% Triton X-100, protease inhibitor cocktail) overnight at 4 °C. Immunoprecipitated samples were washed (50 mM Tris.HCl pH 7.5, 300 mM NaCl, protease inhibitor cocktail), before

SDS-PAGE and western blotting as described above, using an antibody against Rab7 to determine the proportion of GTP-bound Rab7. Whole cell lysates were blotted and probed with Rab7-specific antibodies to determine the level of total Rab7. Rab7-GTP levels were plotted by normalizing the signal intensities of the GST-RILP pulldown blots against total Rab7.

c) Pure protein interaction assay

Myc tagged LIMP2 constructs (WT and LIR1 mut) and HA tagged TMEM192 construct (WT) were purified from HEK 293T cells by using Myc resin and HA resin respectively. These beads were washed three times with high salt wash buffer (50 mM Tris.HCl pH 7.5, 500 mM NaCl) to remove all cellular interactors. GST tagged ATG8 proteins were incubated with these enriched fractions of LIMP2 and TMEM192 for 1 h at room temperature followed by washing three times with wash buffer (50 mM Tris-HCl pH 7.5, 300 mM NaCl) to remove non-specific binding. These samples were then boiled with 2X SDS sample buffer and subjected to western blotting.

d) In vitro PR-Ub assay

5mM GST-tagged STX17 and SNAP29 were incubated at 37 °C for 1 h with 25 mM of purified untagged ubiquitin, 1 mM NAD^+ and 1–2 mM SdeA in 50 mM Tris-HCl (pH 7.5) and 50 mM NaCl. The reaction mixture was processed as described for western blotting above, and probed with antibodies specific for ubiquitin and GST. PR-Ub-specific deubiquitination assays were performed by incubating PR-Ub proteins with 1 µg of GST-DupA at 37 °C for 1 h in a buffer containing 50 mM Tris-HCl (pH 7.5) and 150 mM NaCl.

e) Vesicle fusion assay

HEK 293T cells were transfected with TMEM192-HA and LAMP1-RFP constructs and the lysosomes were enriched by Lyso-immunoprecipitation (Wyant et al., 2017). To enrich for STX17-GFP vesicles, HEK 293T cells were transfected with STX17-GFP and, after 16 h, treated with Torin-1 for 2 h to induce the formation of $STX17^+$ autophagic vesicles. Cells were then suspended in PBS for mechanical lysis, and the lysates were incubated with GFP beads. The beads were washed in PBS and added to isolated lysosomes in the presence or absence of 1 mM NAD, 3 µg SdeA and 3 µg ubiquitin. The reaction was incubated for 1 h at 37 °C, spotted onto coverslips, and imaged by fluorescence microscopy.

6.7 Microscopy based assays

a) Lysosomal regeneration flux assay using the stable tfGal3 reporter

For stable expression of tfGal3, HeLa cells were transfected with the tfGal3 construct (addgene number: 64149) and maintained in medium containing the selection marker Geneticin(800µg/ml) to obtain a stable expression of the protein. Lysosomal damage was induced by treating cells with 1mM LLOMe for 2 h, and recovery was performed by replacing LLOMe containing medium with

LLOMe free medium after PBS wash for indicated time points. The cells were then fixed immediately with 4% paraformaldehyde, incubated with the appropriate primary antibodies, and red Gal3 puncta, detected by confocal microscopy as described above, were counted manually using FIJI. At least 100 cells from three independent experiments were used for statistical analysis.

b) DQ-BSA assay for hydrolase activity

DQ-BSA green was purchased from ThermoFisher Scientific, cat no. D12050. HeLa cells were treated with siRNA to knockdown TFEB and then transfected with LAMP1-RFP to mark lysosomes. Cells were treated with 1mM LLOMe for 2 h and allowed to recover for different timepoints as mentioned. During the last 40 minutes of every sample, DQ-BSA was loaded into cells at a final conc. of 10µg/ml in prewarmed media. Cells were then imaged by confocal microscopy.

c) Immunocytochemistry

HeLa cells growing on glass coverslips were fixed with 4% paraformaldehyde for 10 min at room temperature, permeabilised and blocked in phosphate-buffered saline (PBS) containing 0.1% saponin and 5% FBS for 1 h at room temperature, and incubated overnight at 4 °C with the appropriate primary antibody. Alexafluor-tagged secondary antibodies were used for visualization by fluorescence imaging.

d) Confocal microscopy and image analysis

Confocal images were observed using a Zeiss LSM780 microscope system fitted with a 63× 1.4 NA oil-immersion objective as well as argon and helium–neon ion lasers for the excitation of GFP (488 nm) and RFP (546 nm), respectively. Images were analyzed in FIJI to determine the colocalization between red and green channels within 50-μm^2 regions of interest by calculating the Manders coefficient. Images were thresholded, converted to 8-bit and analyzed using the 'Analyse particles' plugin in FIJI to count LC3, STX17or SNAP29 puncta in cells.

Airyscan images were acquired on a Zeiss LSM980 Observer in SuperResolution mode using a Plan-Apochromat 40x/1.4 Oil objective with excitation lasers of 405 nm, 488 nm and 561 nm wavelengths. Lysotracker signal intensity after LLOMe treatment was measured using FIJI. Gal3, LC3 and TBC1D15 puncta and lysosomal tubules in cells were counted by thresholding the raw images, then converting them to 8-bit images for processing using the "analyse particles" FIJI plugin. For DQ-BSA imaging, images were converted to 8-bit, mean fluorescent intensity in the green channel was measured in the full cell which were marked by LAMP1-RFP.

e) Analysis of lysosomal tubules in FIJI

For lysosomal tubules, particles with a circularity of 0.8–1.0 were filtered out. The length of the remaining tubular structures was determined, and those exceeding 2.5 µm were classified as long

tubules. At least 75 cells from three independent experiments were used for statistical analysis. Graphs were plotted in MS Excel. A two-tailed type-3 Student's t-test was used to determine statistical significance. For image representation labelled as 'trace' in the figure, the image was split into separate channels. LAMP1, LC3 and TBC1D15 positive structures were manually traced using the Wand (tracing) tool of FIJI. For STED images, at least 30 cells taken from 3 experiments were analysed in FIJI. Images were converted to 8 bit, thresholded, and analysed by the 'Analyze particles' plugin. All lysosomal structures of particle size less than 2µm2 were filtered out. Particles of the size range <2µm2, circularity <0.5 were taken as tubules. Those with higher circularity were classified as rings. The 'include holes' option in the 'Analyze particles' was used to distinguish between open rings and closed ones.

f) STED microscopy

Stimulated Emission Depletion Microscopy (STED) images were taken with an *abberior Instruments* STEDYCON STED setup equipped with an inverted IX83 microscope (Olympus), a 100x oil objective (UPLXAPO100XO, 100x / NA 1.45, oil, Olympus), using pulsed excitation lasers at 640 nm (to excite the *abberior* STAR RED labelled LAMP1), a pulsed STED laser operating at 775 nm, continuous autofocus and gated detection with avalanche photodiode element detectors (APDs). All acquisition operations were controlled by the STEDYCON Software (abberior Instruments).

g) Immuno-electron microscopy

HeLa cells transfected with STX17-GFP and infected with Legionella-DsRed were fixed using freshly made 4% formaldehyde (FA) in 0.1 mol/L phosphate buffer (pH 7.4) by adding an equal amount of fixative to the medium for 5 min. Cells were postfixed using 2% FA in 0.1 mol/L phosphate buffer for 2 h and stored in 1% FA at 4°C. Ultrathin cryosectioning and immunogold labeling were performed as previously described (Slot and Geuze, 2007). GFP-tagged syntaxin 17 was labeled using biotin-conjugated goat anti-GFP and rabbit anti-biotin antibodies from Rockland (610–4120, 600–106-215 and 100–4198, respectively). Antibodies were detected by protein A–10-nm gold particles (Cell Microscopy Core, Utrecht, the Netherlands).

6.8 Legionella infection

a) Protocol for infection

Legionella pneumophila strains were obtained from Dr. Zhao-Qing Luo (Purdue University) and were grown for 3 days on *N*-(2-acetamido)-2-amino-ethanesulfonic acid (ACES)-buffered charcoal (BCYE) extract agar, at 37 °C, followed by growth for 20 h in CYE medium. Bacterial cultures (OD_{600} = 3.2–3.6) were used to infect HEK 293T cells with a multiplicity of infection

(MOI) of 10, and A549 cells with a MOI of 2. For 12-h infection experiments, we used a MOI of 1. HEK 293T cells were transfected with CD32 16 h before infection to facilitate bacterial entry.

b) Intracellular replication of *Legionella*

A549 cells growing in 35-mm dishes were infected with *Legionella* strains at a MOI of 1. The infection was allowed to proceed for 90 min in antibiotic-free medium before switching to medium containing gentamycin for 60 min to kill the remaining extracellular bacteria. The cells were then lysed in 0.4% saponin immediately or after 24 or 48 h to release intracellular bacteria. Lysates were spotted onto BCYE plates at 1:10 and 1:100 dilutions. The intracellular bacterial load was assessed by counting bacterial colonies formed after 48 h. The number of colony forming units (cfu) was calculated using the formula cfu/mL = (number of colonies × dilution factor) / volume of sample plated (mL). The fold-increase in cfu was calculated by normalizing the cfu at 24 or 48 h to that determined immediately after lysis.

6.9 Proteomics related protocols

a) P**roximity labeling of ATX17, TBC1D15 and LAMP1**

Cells expressing APEX2-STX17/TBC1D15/LAMP1 were treated with doxycycline for 24 h to induce protein expression before infection with *Legionella* strains for different time periods. Before lysis, we added 500 μM of biotin-tyramide to the medium, incubated the cells for 1 h, and then treated them with 1 mM H_2O_2 for 1 min to trigger intracellular proximity-induced biotinylation. The reaction was quenched by washing the cells with PBS containing 10 mM sodium azide, 10 mM sodium acorbate and 5mM Trolox. The cells were lysed in 20 mM HEPES-KOH (pH 7.5) containing 150 mM KCl, 0.2 mM EDTA and 0.5% NP-40, then 1 mg of the lysate was incubated with 20 μL streptavidin-agarose resin overnight at 4 °C on a rotating platform. The pulled-down proteins were washed in lysis buffer and water three times and processed for western blotting and MS analysis. In the latter case, the beads were incubated in 8 M urea for 2 h at 37 °C before adding 10 mM DTT for reduction and 40 mM chloroacetamide for alkylation, followed by overnight digestion with 1 μg trypsin and 1 μg Lys-C. The peptides were then acidified with trifluoroacetic acid and desalted using Sep-Pak cartridges. Dried peptides were resuspended in TMT buffer, and labeled by 6-plex TMT before MS analysis.

b) Proximity labeling of bacterial vacuoles using ProtA-Turbo

HEK 293T cells were infected with *Legionella* strains for 2 h before proximity labeling as previously described (Santos-Barriopedro et al., 2021) with modifications. The cells were permeabilized with 0.05% digitonin in 20 mM HEPES/KOH (pH 7.5) containing 150 mM KCl and 2 mM $MgCl_2$ for 5 min at room temperature, then recovered by brief centrifugation (800 × g, 5 min, room temperature) followed by two washes in the same buffer containing 0.02% digitonin.

The cells were then incubated for 1 h at 4 °C in 500 µL of the same buffer without digitonin but containing 1 µg of the *Legionella*-specific antibody. After centrifugation and washing as above, the cells were incubated for 45 min at 4 °C with 1.5 µg ProtA-Turbo in 500 µL of the same buffer. Following another two washes as above, the cells were incubated with biotin reaction buffer (5 µM biotin, 5 mM $MgCl_2$, 1 mM ATP in 0.02% digitonin buffer) in a thermal shaker at 1000 rpm for 15 min at 37 °C. The cells were washed once with 0.5 mL of buffer without digitonin, lysed in 20 mM HEPES/KOH (pH7.5) containing 150 mM KCl, 2 mM $MgCl_2$ and 1% Triton-X-100, and then processed as described above for the streptavidin pulldown assay.

c) Identification of PR-Ub sites by ETD-MS

PR-Ub sites were identified by ETD-MS as previously described (Liu et al., 2021). GST-tagged STX17 and SNAP29 were modified by SdeA *in vitro* then denatured in 0.1 M Tris-HCl (pH 7.5) containing 8 M urea. The samples were washed three times in 200 µL of the same buffer in a 30-kDa Amicon Ultra 0.5-mL centrifugal filter (Merck) to remove free ubiquitin. The eluted protein was washed twice in 50 mM ammonium bicarbonate (pH 7.5) before digestion using a 1:50 ratio of trypsin the same buffer for 6 h. The peptides were desalted on a C18 column, followed by LC-MS/MS analysis. The spectra were collected and deconvoluted, and high-resolution ETD-MS/MS spectra were manually inspected to verify the sequence.

d) Sample preparation for mass spectrometry

Washed immunoprecipitated samples were mixed with 40 µl 8 M urea for 3 h at 37 °C, then the proteins were reduced with 1 mM TCEP and alkylated with 4 mM chloroacetamide for 1 h. The samples were then diluted in 50 mM ammonium bicarbonate to reduce the urea concentration below 1 M and digested with 0.5 µg Lys-c and 1 µg trypsin at 37 °C for 14–18 h. The digested samples were acidified with 1% trifluoroacetic acid and the peptides were desalted using either Sep-Pak cartridges or C-18 stage tips. Dried peptides were resuspended in TMT buffer and labelled with 6-plex TMT for MS analysis as previously described (Shin et al., 2021). All samples were processed as at least three biological replicates.

e) Machine parameters for mass spectrometry

Samples were analysed on a Q Exactive HF coupled to an easy nLC 1200 (ThermoFisher Scientific) using a 35 cm long, 75µm ID fused-silica column packed in house with 1.9 µm C18 particles (Reprosil pur, Dr. Maisch), and kept at 50°C using an integrated column oven (Sonation). TMT6 labelled peptides were eluted by a non-linear gradient from 4-32% acetonitrile over 120 minutes and directly sprayed into the mass-spectrometer equipped with a nanoFlex ion source (ThermoFisher Scientific). Full scan MS spectra (350-1400 m/z) were acquired in Profile mode at a resolution of 120,000 at m/z 200, a maximum injection time of 100 ms and an AGC target

value of 3 x 10^6 charges. Up to 20 most intense peptides per full scan were isolated using a 1.0 Th window and fragmented using higher energy collisional dissociation (normalised collision energy of 35). MS/MS spectra were acquired in centroid mode with a resolution of 15,000, a maximum injection time of 50 ms and an AGC target value of 1 x 10^5. Single charged ions, ions with a charge state above 2 and ions with unassigned charge states were not considered for fragmentation and dynamic exclusion was set to 20s.

IP peptides from label free experiments were eluted by a non-linear gradient from 4-32% acetonitrile over 60 minutes and directly sprayed into the mass-spectrometer equipped with a nanoFlex ion source (ThermoFisher Scientific). Full scan MS spectra (300-1650 m/z) were acquired in Profile mode at a resolution of 60,000 at m/z 200, a maximum injection time of 20 ms and an AGC target value of 3 x 10^6 charges. Up to 10 most intense peptides per full scan were isolated using a 1.4 Th window and fragmented using higher energy collisional dissociation (normalised collision energy of 27). MS/MS spectra were acquired in centroid mode with a resolution of 30,000, a maximum injection time of 54 ms and an AGC target value of 1 x 10^5. Single charged ions, ions with a charge state above 2 and ions with unassigned charge states were not considered for fragmentation and dynamic exclusion was set to 20s**.**

f) Mass spectrometry data analysis

Raw MS data were analysed with Proteome Discoverer v2.4 (Thermo Fisher Scientific) using Sequest HT as the search engine and performing re-calibration of precursor masses with the Spectrum RC-node. Fragment spectra were screened against the human reference proteome and against common contaminants in 'contaminants.fasta' provided with MaxQuant. The accepted static modifications were TMTs on the N-terminus and lysine side chains as well as carbamidomethylated cysteine residues. Accepted dynamic modifications were methionine oxidation and N-terminal acetylation. Matched spectra were filtered with Percolator, applying an FDR of 1% on the peptide spectrum match and protein level. Reporter intensities were normalized to the total protein intensities in Proteome Discoverer, assuming equal sample loading, and also by median normalization using the NormalyzerDE package, if required (Willfross et al., 2018). Label-free data were analysed using MaxQuant v1.65 (Cox and Mann, 2008). Fragment spectra were screened against the *Homo sapiens* SWISSPROT database (TaxID: 9606). Label-free quantification was achieved using MaxLFQ (Cox et al., 2014) with activated matches between runs. Statistically significant changes between samples were determined in Perseus v1.6.6.0 based on a threshold of $p \leq 0.01$ and a $\log_2$ fold change threshold of ±0.5 (Tyanova et al., 2016).

CHAPTER 7 RESULTS
TBC1D15 mediated lysosomal regeneration

7.1 Biphasic phase of lysosomal recovery following LLOMe mediated damage with an initial TFEB independent and later TFEB dependent phase

To track the lysosomal recovery following damage, we sought out to measure two main aspects of lysosomal function. One is its acidity and second is the activity of cathepsins. To track lysosomal acidity after damage, we utilised lysotracker and a tandem fluorescent tagged Gal3 construct. Lysotracker is known to accumulate inside highly acidic vesicles of cells which are lysosomes. We treated Hela cells with 1mM LLOMe for 2 h to damage lysosomes and then we allowed the lysosomes to recover by replenishing the cells with LLOMe free medium for different times points. For the last 30 minutes of each time point 100nM lysotracker was added to the medium to measure the acidity of lysosomes. Cells, treated with control siRNA, showed steady and gradual re-acidification of lysosomes over the course of the entire recovery period. Interestingly, cells depleted for TFEB or TFE3, showed similar trend of re-acidification for the first two hours but after that the lysotracker intensity did not increase anymore (**Fig 7.1A, and B**).

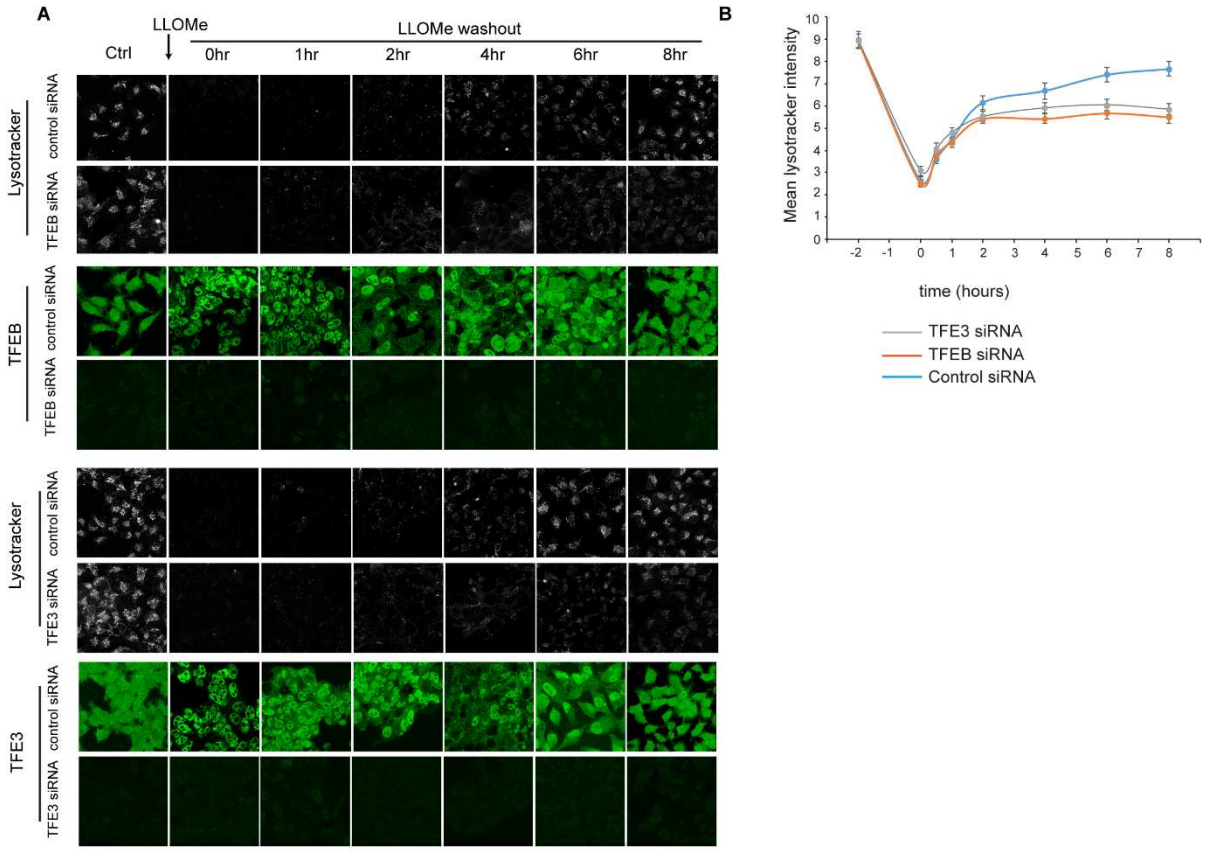

Figure 7.1: Lysosomal re-acidification trend after LLOMe-mediated acute damage. A) HeLa cells were treated with specific siRNA to deplete endogenous TFEB/TFE3 to impair lysosomal biogenesis. 1mM LLOMe was added to the cells for 2h to damage lysosomes followed by washout for the indicated durations. Samples were loaded with LysoTracker Red for last 30 min of each time point followed by fixation and staining with a TFEB/TFE3 specific antibody. B) LysoTracker Red intensities were compared at different time points of LLOMe damage and washout from samples. Data are means ± SEM of 60 cells taken from three independent experiments.

7.2 RFP–GFP (tandem fluorescent)-tagged Gal3 (tfGal3) also showed recovery of lysosomal acidity in 2 phases

We also used a HeLa reporter cell line which stably expresses RFP–GFP (tandem fluorescent)-tagged Gal3 (tfGal3) as a second method to measure lysosomal acidity. Galectin3 is cytosolic protein which specifically localises to damaged lysosomes (Maejima et al., 2013) and this tandem probe works on the principal that the green fluorescence of GFP will be quenched in an acidic environment whereas the red fluorescence of RFP is stable. So, the damaged lysosomes will appear yellow owing to the loss of acidity followed by membrane damage but as soon as the acidity is regained, that population of lysosomes will be emitting only red fluorescence (**Fig7.2A**). We also could see a similar trend of recovery here in terms of acidity; both control cells and cells depleted for TFEB recovered to a similar extent during the first couple of hours in terms of red Gal3 puncta but beyond that point, cells capable of generating new lysosomes showed a better recovery pattern (**Fig 7.2B, and C**). These two experiments led us to the conclusion that after removal of damaging agent, cells can rapidly regenerate active lysosomes from the existing damaged mass and this first phase of rapid recovery is independent of lysosomal biogenesis. Beyond this point cells rely on lysosomal biogenesis to recover that damaged pool of lysosomes and we can term these two phases of recovery as biogenesis independent and biogenesis dependent recovery of damaged lysosomes.

7.3 DQ-BSA fluorescent assay indicated the lysosomal activity of regenerated lysosomes

Next, we wanted to check whether these rapidly regenerated lysosomes are active or not. We utilised DQ-BSA for this experiment which is a fluorogenic substrate of lysosomal hydrolases. Upon reaching lysosomes through the Endo lysosomal pathway, DQ-BSA gets processed by lysosomal hydrolases thus dequenching of the fluorogenic substrate and it can be monitored by convention confocal microscopy. Following treatment with LLOMe, there was a loss of the DQ-BSA fluorescence to < 20% in cells treated with TFEB siRNA or control siRNA. However, during 1h and 2h of wash out, both set of samples showed a recovery of up to ~60% of that compared to the untreated conditions.

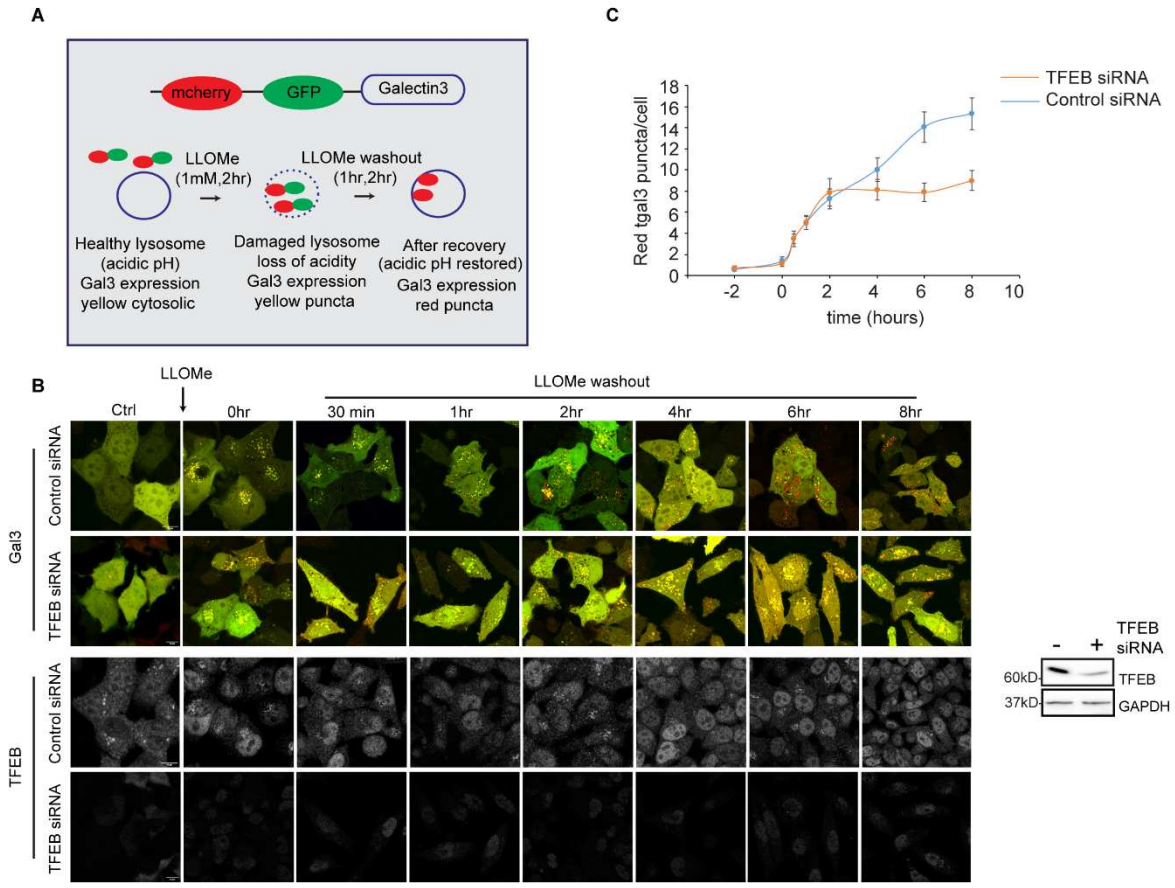

Figure 7.2: Dual tagged Gal3 flux assay shows that lysosomal re-acidification has two distinct phases. A) Schematic of the RFP GFP dual-tagged Gal3 (tfGal3) reporter construct used for the lysosomal regeneration flux assay. B) Stable HeLa cell line was generated using the tfGal3 construct. These cells were then treated with control or TFEB siRNA for 48h. After treating with 1mM LLOMe for 2h cells were cultured in LLOMe-free medium for different durations as mentioned in the panel. The number of red Galectin3 puncta was counted at each time point before and after LLOMe washout as a measure of lysosomal re-acididfication. TFEB knockdown efficiency was additionally checked by western blotting. C)Graph showing numbers of red Galectin3 puncta per cell obtained from this experiment. Data are means ± SEM of 50 cells taken from three independent experiments.

TFEB depleted cells showed a lower signal of DQ-BSA owing to the fact that the lysosomal activity was already compromised even without treating with damaging agent but the recovery pattern was similar for both control cells and cells treated with TFEB siRNA (**Fig. 7.3A, and B**). This indicated that the initial phase lysosomal regeneration is indeed biogenesis independent and the lysosomes which are regenerated during this phase, are not only acidic but also functionally active. A previous report had demonstrated that 1mM LLOMe treatment for 2h causes lysosomal membrane permeabilization (LMP) by destabilizing the lysosomal membrane but molecules of size >10 kDa (like cathepsins) are not released from lysosomes into the cytosol (Repnik et al, 2017). So, these observations suggested the existence of a mechanism by which cells can rapidly

regenerate functional lysosomes from damaged membranes as a primary response to acute lysosomal damage. This phase of recovery will subsequently be followed up by generating new lysosomes via conventional TFEB/TFE3 dependent biogenesis pathway.

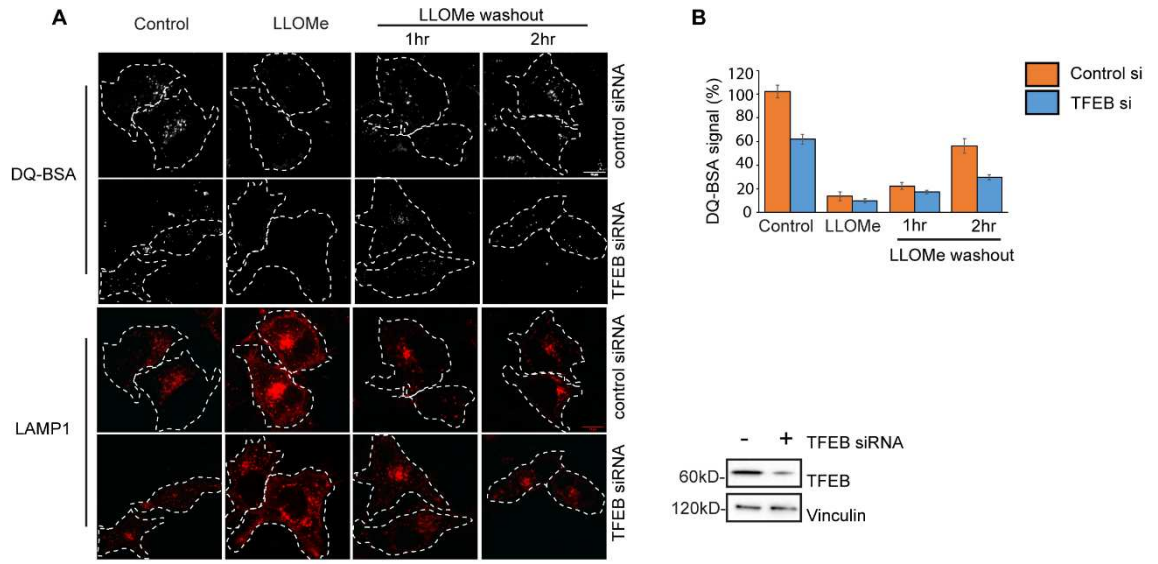

Figure 7.3: Following damage, lysosomes can regain cathepsin function within the first two hours of recovery and this process is also biogenesis independent. A) HeLa cells were depleted for endogenous TFEB using siRNA and LAMP1-RFP was transfected to mark lysosomes. These cells were then treated with LLOMe (1mM, 2 h) followed by washout for indicated timepoints. DQ-BSA was loaded for the last 30 minutes for each treatment conditions prior to imaging the samples by confocal microscopy. TFEB knockdown efficiency was checked by western blotting. B) DQ-BSA signal intensities were compared between control cells and cells lacking endogenous TFEB as a percentage of the signal observed in cells without treatment. Data are means ± SEM from at least 30 cells taken from three independent experiments.

7.4 mTOR activity changes during lysosomal regeneration phases

mTOR (mammalian target of Rapamycin) is known to be involved in lysosomal biogenesis. We also tested whether the activity of mTOR is needed for this first phase of lysosomal regeneration. Activity of mTOR was measured by the extent of phosphorylation of phospho-p70 S6K (Thr389) by western blotting. LLOMe treated cells completely lost the phosphorylation signal compared to control cells and mTOR was reactivated only after at least 4h of recovery and gradually increased from then on **(Fig. 7.4)**. This experiment indicated that the initial phase of recovery is also not dependent on mTOR activity.

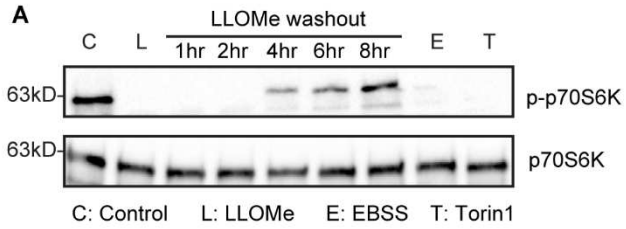

Figure 7.4: mTOR stays inactive during damage and initial recovery time points while regaining activity at the later time points of recovery. mTOR activity was assessed by monitoring the phosphorylation status of p70-S6K by western blotting for indicated treatments. LLOMe:1mM, 2 h, EBSS: 4 h, Torin1: 500nM, 6 h.

7.5 Mass spectrometry revealed the presence of different proteins including TBC1D15 to be present around damaged lysosomal membrane.

To understand this rapid phase of lysosomal recovery in more detail, we used proximity labelling assay by tagging APEX2 to the c terminal of LAMP1, which is cytosolic, and generated an inducible stable LAMP1-APEX HeLa cell line. Followed by LLOMe treatment for 2h, these cells were exposed to biotin and H_2O_2 to induce proximity biotinylation. The biotin labelled candidates were then identified via mass spectrometry (**Fig 7.5A**). By comparing between control and LLOMe treated samples, we could identify several classes of proteins (**Fig 7.5B**). After pathway analysis, we highlighted some interesting and obvious candidates belonging to different categories. Such as proteins related to autophagy ATG3, ATG7, RB1CC1 and GABARAPL1, mTOR pathway candidates LAMTOR1, RAPTOR, TSC and TSC2 and proteins belonging to ESCRT pathway such as VPS50, VPS16, VPS35 and VPS13C. Interestingly, components from lipid metabolism pathway were also enriched as represented by PIP5K1A, PIP4K2A, INPPL1, PLCG2 and INPP5F; as well as some other proteins such as BLOC1S1, TBC1D15, Rab7, DNM2 and kinesins (**Fig 7.5C**). Since autophagy is known to be activated upon LLOMe treatment we decided to use another unbiased mass spectrometry-based approach to identify the proteins which can be enriched after lysosomal damage. Owing to the importance of ATG8 proteins in autophagy, we compared the interactome of GST-tagged LC3B between cells treated with LLOMe or left untreated. Control or LLOme treated HEK 293T cell lysate was incubated with purified GST-LC3B and these samples were analysed by LFQ (label-free quantification) based MS. Along with other candidates, we found TBC1D15 to be significantly enriched by GST-LC3B pulldown from the LLOMe-treated samples (**Fig 7.5D**). Surprisingly, TBC1D15 was also highly enriched in LLOMe treated samples from the previous biotinylation experiment (**Fig 7.5B**). We further validated this finding. HEK293T cells expressing hemagglutinin (HA)-tagged TBC1D15 was

treated with 1mM LLOMe for different timepoints and association of LC3B with TBC1D15 was assessed by HA immunoprecipitation followed by western blotting. LC3B could be seen to strongly associate with TBC1D15 with increasing duration of LLOMe treatment (**Fig 7.5E**). Western blot analysis of biotinylatied samples acquired from LAMP1-APEX cell line suggested the recruitment of TBC1D15 to damaged lysosomal membranes, but after LLOMe washout for 2h, this recruitment was lost (**Fig 7.5F**). This data suggested that upon damage TBC1D15 recruited to damaged lysosomal membranes and is associated with LC3B. In a recent study, TBC1D15 was also reported as significant candidate enriched in the biotin-labelled LC3B interactome from LLOMe-treated cells (Eapen et al., 2021).

7.6 TBC1D15 recruitment to damaged lysosomes is a unique response, not seen in other form of canonical or non-canonical autophagy activation.

Next, we immunostained endogenous TBC1D15 in HeLa cells and confirmed its localisation to damaged lysosomes by immunofluorescence analysis. While TBC1D15 was primarily cytosolic in control cells, LLOMe treatment for 2h resulted in its recruitment to damaged lysosomes which were also positive for Gal3 (**Fig 7.6A**). Interestingly, TBC1D15 recruitment to lysosomes happened only after acute damage (**Fig 7.6B)** while ESCRTs, or Galectin3 are known to get recruited within 30 min-1 h of LLOMe-mediated lysosomal damage (Radulovic et al., 2018, Skowra et al., 2018, Jia et al., 2020). These damaged TBC1D15 positive lysosomal mass was also positive for LC3B and ubiquitin suggesting the involvement of autophagy machinery at this stage of damage response (**Fig 7.6C, and D**). Other form of canonical autophagy activation such as treatment with mTORC1 inhibitor Torin1 or serum starvation with Earle's balanced salt solution (EBSS) did not seem to affect TBC1D15 localisation. Similar results were obtained while stimulating non-canonical autophagy or mitophagy by using Monensin (induces CASM-conjugation of ATG8 to single membrane) or mitochondrial proton gradient un-coupler carbonyl cyanide *m*-chlorophenylhydrazone or CCCP (**Fig 7. 6E**). There data indicates that TBC1D15 localization is specific to acutely damaged lysosomes.

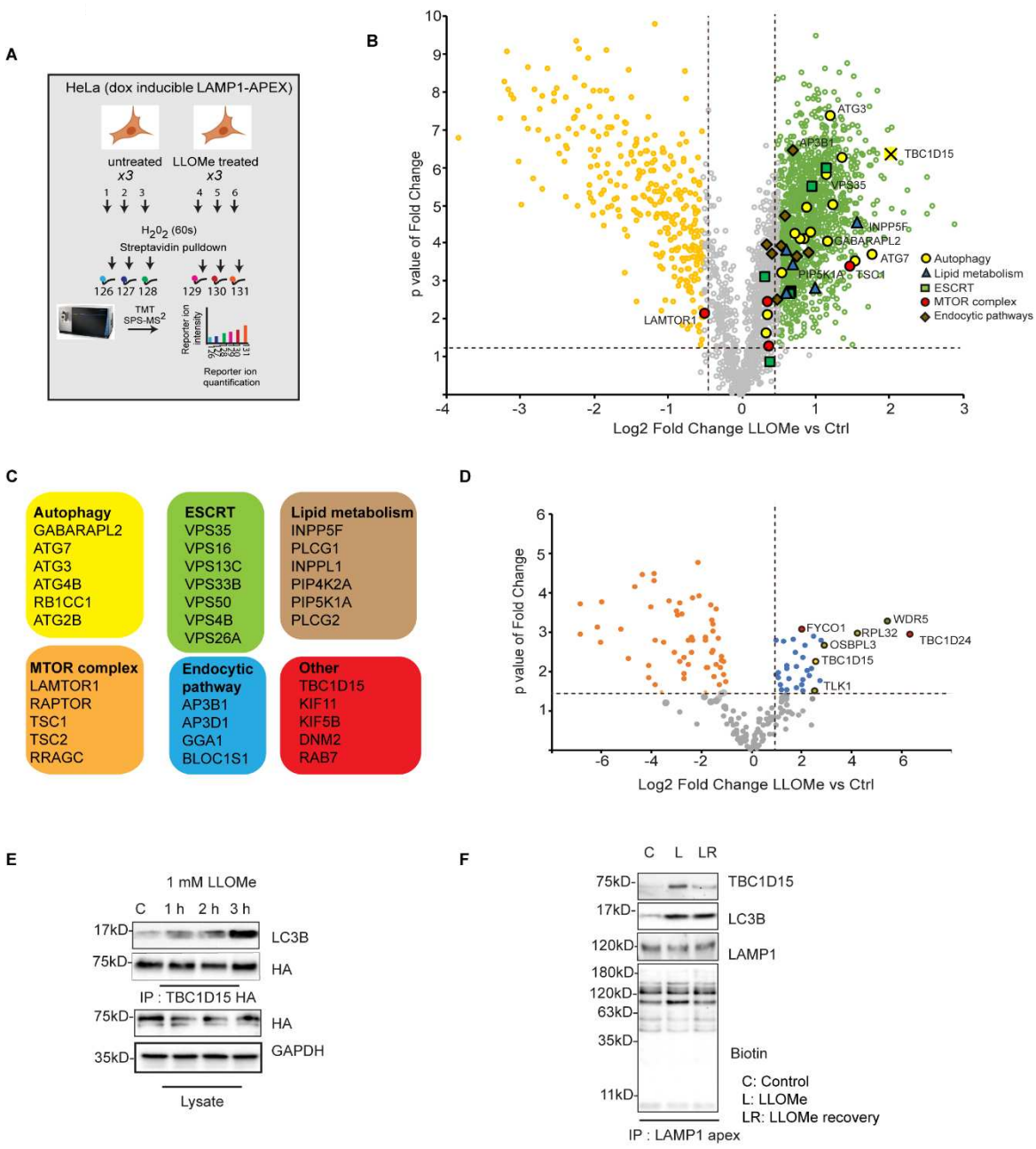

Figure 7.5: Unbiased proteomic approaches followed by biochemical characterisation reveals presence of TBC1D15 near damaged lysosomes. A) Schematic of the LAMP1-APEX proximity labelling assay. B) Volcano plot comparing the biotinylated landscape of APEX2-tagged LAMP1 with and without lysosomal damage. Green and yellow circles indicate significantly enriched and significantly depleted candidates respectively. C)Pathway analysis of significantly enriched proteins after damage revealed several important and relevant categories as shown here. D) GST-LC3B was incubated with cell lysates from control or LLOMe-treated cells followed by the detection of interacting proteins by MS. The volcano plot shows LC3-binding proteins enriched after treating cells with LLOMe. E) HEK 293T cells expressing HA-TBC1D15 were treated with 1 mM LLOMe for 1, 2 or 3h. LC3B bound to TBC1D15 under each condition was assessed by immunoprecipitation using HA beads followed by western blots. F) Cells expressing doxycycline-inducible LAMP1-APEX were treated with LLOMe to damage lysosomes and LLOMe recovery was performed by changing the medium. 500 µM biotin-tyramide was added during the last hour of LLOMe treatment or recovery period and then cells were exposed to 1 mM H_2O_2 for 1 min for inducing biotinylation. Biotinylated proteins were

pulled down using streptavidin-resin. Western blots of samples representing different conditions were probed with antibodies to detect the proteins of interest (TBC1D15, LC3B and LAMP1). C = control. L = treatment with 1 mM LLOMe for 2 h. LR = recovery of 2 h after LLOMe treatment.

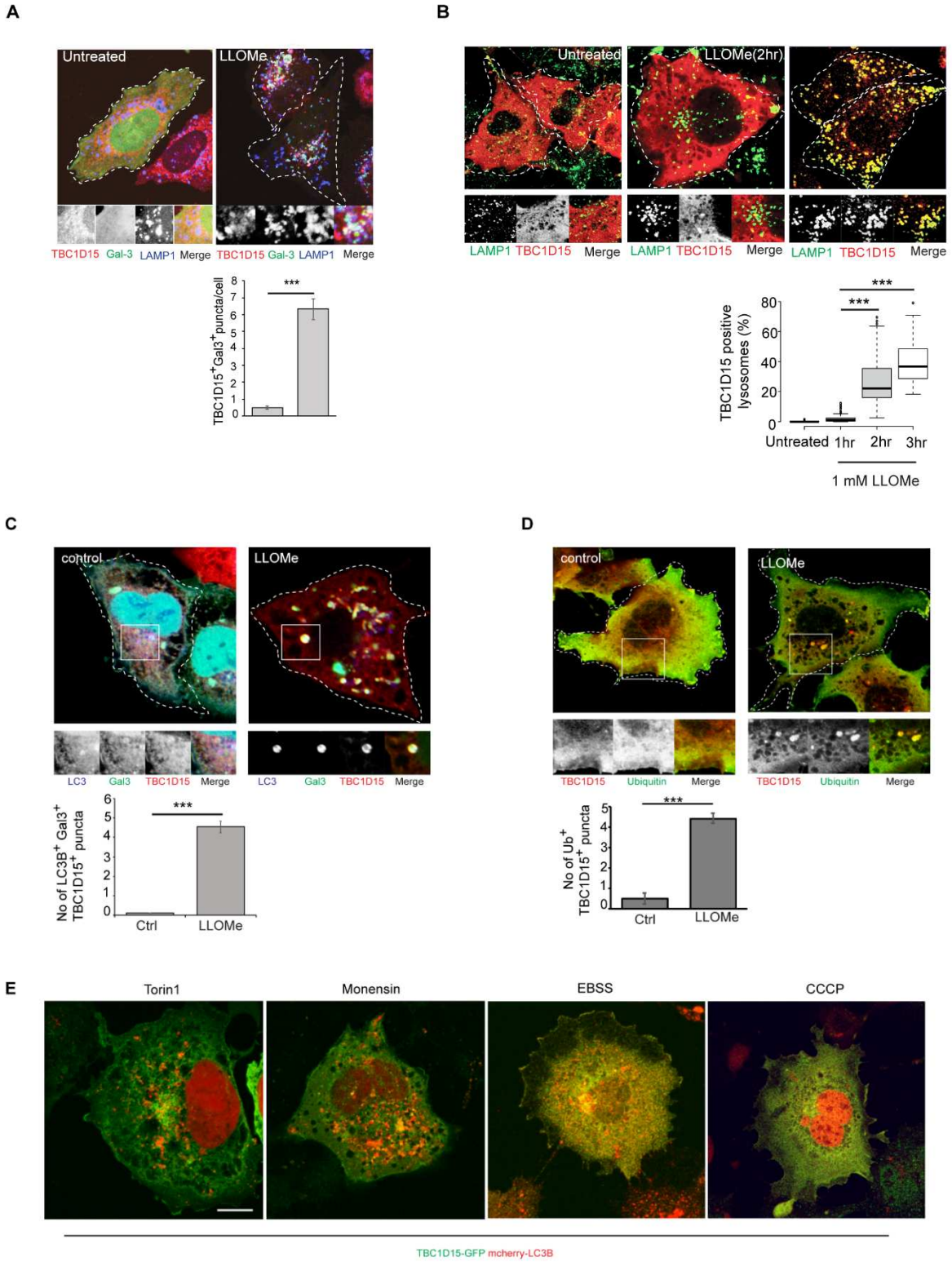

Figure 7.6: TBC1D15 is recruited to acutely damaged lysosomes. A) HeLa cells were treated with1mM LLOMe for 2h followed by staining for endogenous TBC1D15 (red), LAMP1 (blue) and GAL3 (green) using specific antibodies. Data are means ± SEM of 50 cells taken from three independent experiments and were counted for determining the $Gal3^{+}$ $TBC1D15^{+}$ puncta/cell (***$p \leq 0.001$). B) HeLa cells were transfected with HA-TBC1D15 and treated with 1 mM

LLOMe for different time points. Endogenous LAMP1 was stained along with HA-TBC1D15 to assess the degree of TBC1D15 recruitment to lysosomes. Data are means ± SEM of at least 100 cells taken from three different experiments for each time point (***p ≤ 0.001). C) HeLa cells expressing LC3-BFP and GAL3-GFP were treated with 1mM LLOMe for 2h to induce lysosomal damage. Endogenous TBC1D15 was stained to evaluate its recruitment to the damaged lysosomes. Data are means ± SEM of 50 cells (***p ≤ 0.001). D) HeLa cells expressing HA-ubiquitin were treated with LLOMe and endogenous TBC1D15 was stained with an HA-specific antibody to determine the the number of Ub^+ $TBC1D15^+$ puncta/cell. Data are means ± SEM of 50 cells (***p ≤ 0.001). E) HeLa cells expressing TBC1D15-GFP and mCherry-LC3B were treated with Torin1 (500nM, 6h), Monensin (100µM, 1h), EBSS (4h) and CCCP (10µM, 4h) to induce macroautophagy, non-canonical autophagy (inducer of CASM), macroautophagy and mitophagy respectively. TBC1D15 did not form puncta under these conditions. CASM: Conjugation of ATG8 to single membranes.

7.7 TBC1D15 utilises its LIR motif to bind ATG8 proteins.

TBC proteins are known to harbour LC3 interaction region (LIR) motifs (Popovic et al., 2012). We screened TBC1D15 amino acid sequence against the iLIR database (Jacomin et al., 2016) and identified 3 putative LIR motifs (**Fig 7.7A**). To determine the importance of the LIR motifs in response to LLOMe treatment, we introduced multiple point mutations by site directed mutagenesis within each LIR motif of the HA-TBC1D15 construct and overexpressed them in cells. Following treatment with LLOMe, we immunoprecipitated HA-TBC1D15 from the lysates of LLOMe-treated cells and assessed the ability of LC3B binding by western blotting (**Fig 7.7B**). We identified one LIR motif encoded amino acid residues 295–300 (TBC1D15[F297AV299AI300A], LIR2mut) to be a significant candidate as this mutation caused a significant loss of LC3B binding. Our identified motif has also previously been described to be the active LIR motif in TBC1D15 (Yamano et al., 2014). Mutating another LIR motif spanning amino acid residues 540–545 (TBC1D15[F540AF542AL543AI545A], LIR3mut) also resulted in minor reduction in LC3B binding and it prompted us to create a double mutant (LIR2/3mut) which completely lost the ability to interact with LC3B. In contrast, the LIR motif located between amino acids 96–101 (TBC1D15[W98AV101A]) did not show any effect on LC3B binding (**Fig 7.7C**). As TBC1D15 is a known Rab7-GAP (Peralta et al., 2010), we also mutated its GAP motif (TBC1D15[D414AK417A], GAPmut) but this mutation seems to have no effect on LC3B binding in LLOMe-treated cells (**Fig 7.7B**). We also tested the interaction between TBC1D15 and GABARAPL2 and found it to be dependent on the same LIR motifs while GAP mut did not reduce any binding (**Fig 7.7D**).

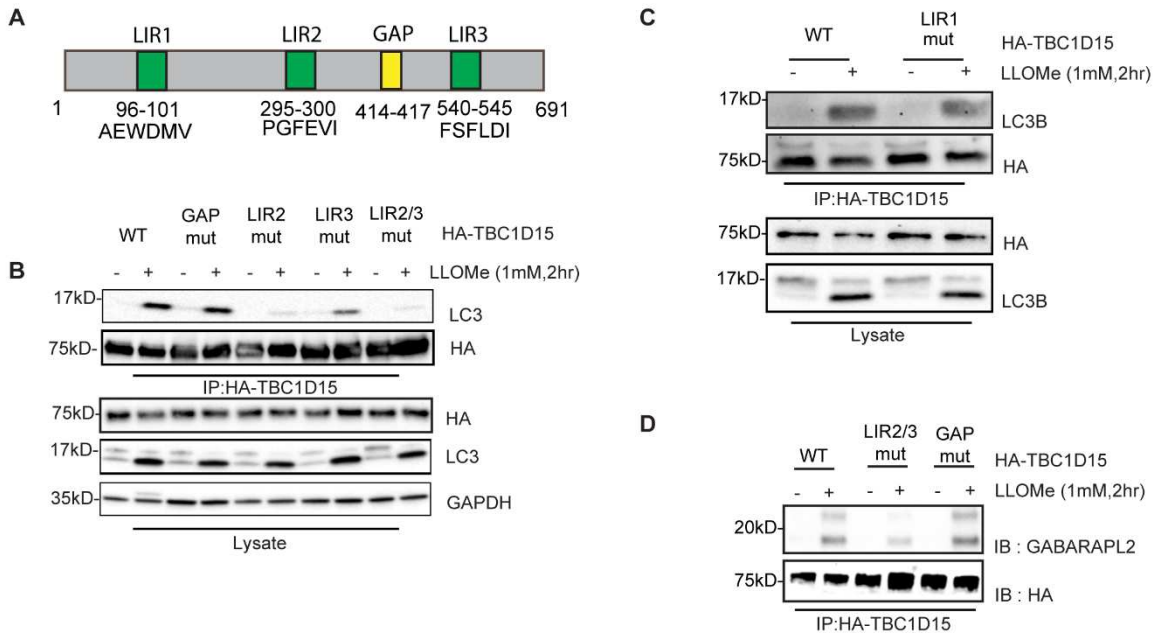

Figure 7.7: TBC1D15 utilises its LIR motif to bind to ATG8 proteins. A) Domain architecture of TBC1D15 showing potential LIR motifs (predicted by screening the iLIR database) and the known GAP motif. B) HEK 293T cells expressing wild-type or HA-tagged mutants of TBC1D15 were treated with 1mM LLOMe for 2 h or left untreated and then tested by HA pulldown to check the effect on LC3B binding. C) HEK 293T cells were transfected with wild-type or LIR1 mut variant of HA tagged TBC1D15. Following 1mM LLOMe treatment for 2 h, HA immunoprecipitation was performed to assess the binding with LC3B by western blotting. D) HEK 293T cells were transfected with different HA tagged variants of TBC1D15, as indicated in the figure. HA immunoprecipitation was performed after LLOMe treatment to assess the binding with GABARAPL2 by western blotting. The lysates used here are the same as those shown in Figure 7B.

7.8 TBC1D15 solely depends on its LIR motif to get recruited to damaged lysosomes and shows enhanced GAP activity under damaged condition.

To determine the importance of LIR and GAP mutants of TBC1D15 for localising to damaged lysosomes, we depleted endogenous TBC1D15 by treating cells with siRNA specific to TBC1D15 and then reconstituted with HA-tagged wild-type or mutant versions (GAPmut and LIR2/3mut). In line with our previous findings, only the LIR mutant failed to localize with LLOMe-damaged lysosomes, whereas wild-type TBC1D15 and the GAP mutant showed robust recruitment (**Fig 7.8A, and B**). Interestingly, knocking down TBC1D15 did not seem to reduce the localisation of LC3B to damaged lysosomes which indicates that TBC1D15 does not serve as a classical lysophagy receptor **(Fig 7.8C)**. Rather, the ATG8 proteins present on damaged lysosomal membranes are required to recruit of TBC1D15 at the site. After figuring out the active LIR motif, we wanted to investigate its GAP activity after using a Rab-interacting lysosomal protein (RILP) pulldown assay. It has been shown that RILP specifically interacts with GTP-bound Rab7 and thus can be used to assess the amount of GTP-bound Rab7 present in cells. This assay can be used

as a measure of GAP activity as TBC1D15 converts Rab7-GTP to Rab7-GDP. In cells treated with TBC1D15 siRNA, the amount of Rab7-GTP was higher after lysosomal damage compared to untreated cells. After reconstituting with wild-type TBC1D15, we saw no difference in the amount of Rab7-GTP between treated and untreated cells indicating that GAP activity was heightened after damage. The GAP mutant accumulated more of the GTP-bound Rab7 as expected. Surprisingly, we could pull down more Rab7-GTP from cells expressing the LIR mutant than from those expressing wild-type TBC1D15, indicating that mutating LIR had compromised its GAP activity (**Fig 7.8D**). It can be hypothesised that following damage, it may be necessary to segregate the damaged lysosomal mass from vesicular traffic which is why TBC1D15 shows higher GAP activity. Further structural and/biophysical characterisation is needed to understand the interdependence of LC3B binding and GAP activity.

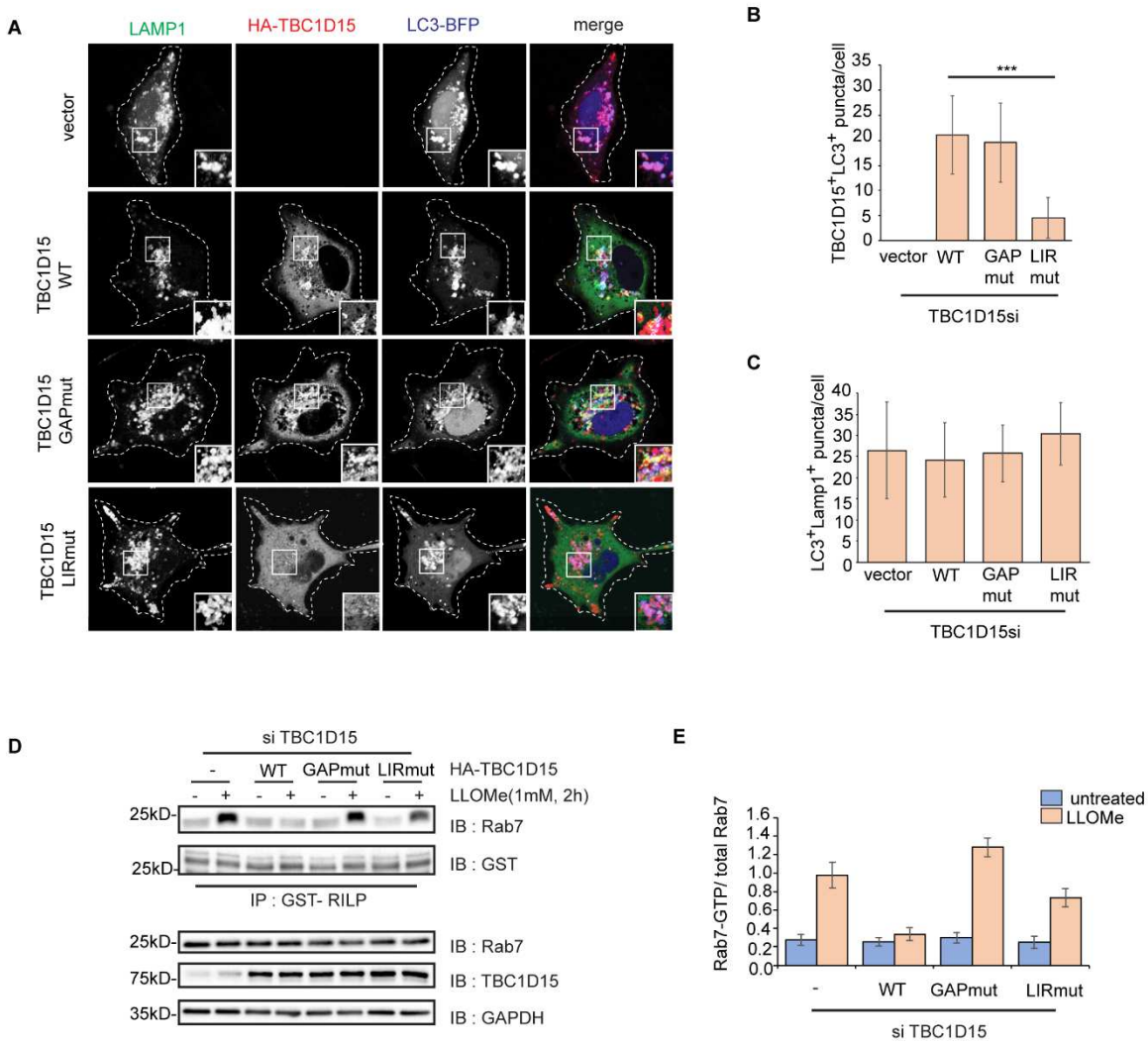

Figure 7.8: The LIR motif of TBC1D15 is important for its localisation to damaged lysosomes while its GAP activity increases at this condition. A) HeLa cells were treated with TBC1D15 siRNA for 48 h followed by transfection with constructs encoding HA-tagged wild-

type or mutant TBC1D15 and LC3-BFP. Cells were treated with 1 mM LLOMe for 2 h, fixed, stained for endogenous LAMP1 and HA, and imaged by confocal microscopy to assess the extent of TBC1D15 recruitment to damaged lysosomes. B) Images from the experiment in panel (a) were analysed using FIJI to evaluate the recruitment of TBC1D15 to LAMP1-labelled lysosomes. Data are means ± SEM of 40 cells from three independent experiments (***$p \leq 0.001$). C) Images from the experiment in panel (a) were analysed using FIJI to check for the colocalization of LC3 and LAMP1. Data are means ± SEM of 40 cells from three independent experiments. D) HeLa cells were treated with siRNA for 48 h to deplete endogenous TBC1D15 followed by reconstitution with HA-tagged wild-type or mutant TBC1D15 for 24 h. The cells were then treated with LLOMe for 2 h followed by lysis. GTP-bound Rab7 was immunoprecipitated from lysates by incubating with GST-RILP. Total Rab7 levels were assessed by western blotting cell lysates with a Rab7-specific antibody.

7.9 Functional TBC1D15 is indispensable for propagating lysosomal regeneration flux

After establishing that TBC1D15 gets recruited to damaged lysosomes, we wanted to dissect its importance in lysosomal regeneration flux. HeLa cells expressing tfGal3 were transfected with HA-TBC1D15 and then were treated with 1mM LLOMe for 2h. Following damage recovery was performed by washing out the damaging agent and then incubating the cells in LLOMe-free medium for another 2h. We saw accumulation of red Gal3 puncta after recovery for 2h which indicated the regeneration of lysosomes (**Fig 7.9A, and B**). Interestingly, TBC1D15 was only present in damaged lysosomes represented by yellow Gal3 puncta but not with recovered acidic lysosomes, indicated by red puncta (**Fig 7.9A, and B**). Next, we knocked down endogenous TBC1D15 using siRNA and then reconstituted with wild-type, LIRmut or GAP mut TBC1D15 and repeated the flux assay. The lysosomal regeneration flux was severely compromised in samples lacking TBC1D15. This phenotype could only be rescued with the wild-type protein, but not with either of the mutants (**Fig 7.9C, and D**). These findings led us to the conclusion that TBC1D15 is important for propagating lysophagy flux and it requires both of its LIR and GAP activity to do so.

7.10 TBC1D15 helps regenerate lysosomes in an autophagy dependent manner

Given the importance of LC3B binding to TBC1D15 for its lysosomal localisation as well as propagating lysosomal regeneration flux, we wanted to explore the role of autophagy in TBC1D15 mediated lysosomal regeneration. To this end, we treated cells with siRNA targeting different key molecules of autophagy: ATG13 (a part of the pre-initiation complex), ATG3 and ATG12 (important for lipidation of ATG8 proteins), and Rubicon (essential for the non-canonical autophagy type LC3 associated phagocytosis (LAP). Depletion of above mentioned

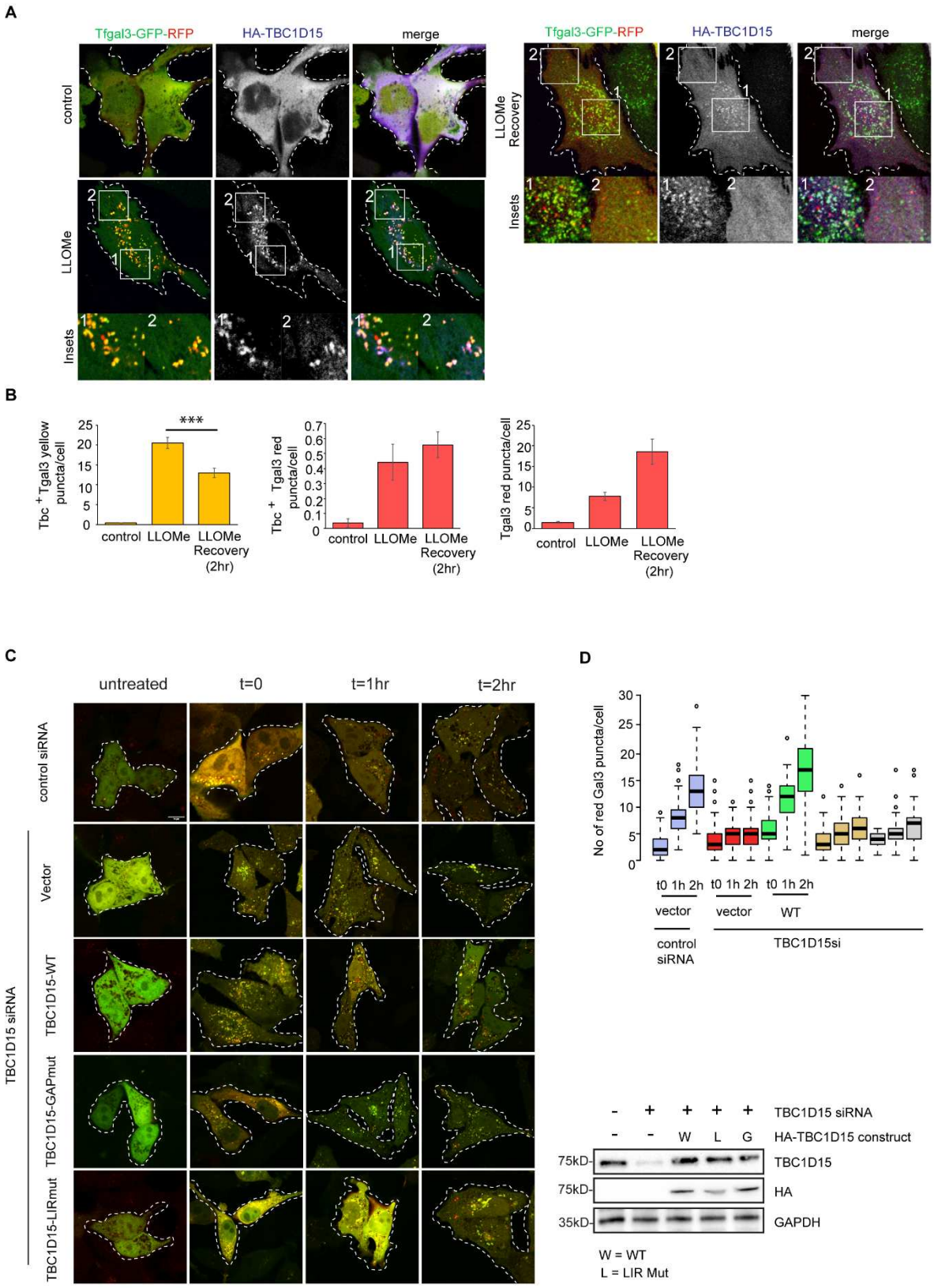

Figure 7.9: TBC1D15 is necessary for lysosomal regeneration. A) HeLa cells with stable expression of the dual-tagged tfGal3 reporter and HA-TBC1D15 were treated with 1 mM LLOMe for 2 h followed by washout (LLOMe recovery). Cells were then fixed and stained with an

antibody specific for HA for confocal imaging. Red gal3 puncta correspond to regenerated lysosomes. B) Images in panel (a) were analysed using FIJI to count the numbers of TBC1D15^{+} yellow gal3 puncta, TBC1D15^{+} red gal3 puncta, and the total number of red gal3 puncta/cell to follow damage and recovery events. Data are means ± SEM of at least 50 cells counted from three independent experiments (***$p \leq 0.001$). C) Endogenous TBC1D15 was silenced with siRNA for 48 h in HeLa cells with stable expression of tfGal3. Wild-type (WT) and mutant TBC1D15 constructs were then transfected into the cells for reconstitution. The cells were then treated with 1 mM LLOMe for 2 h followed by LLOMe washout for 1 or 2 h. Expression levels of TBC1D15 were determined by immunoblotting of lysates made from cells used for imaging. D)The number of red gal3 puncta was counted per cell for each condition in the experiment in panel (c). Data are means ± SEM of 53 cells counted for each condition.

ATGs (ATG13, ATG3, ATG12) led to a significant decrease in TBC1D15 recruitment to damaged lysosomal membranes; while the depletion of Rubicon did not have any effect on TBC1D15 recruitment (**Fig 7.10A**). Knock down of ATG16L also reduced TBC1D15 recruitment to lysosomes. Reconstitution with both WT and the CASM deficient mutant of ATG16L (K490A) (Fletcher et al., 2018) restored the recruitment of TBC1D15 to damaged membranes (**Fig 7.10B**) indicating that CASM is not likely to be involved in this regeneration process.

7.11 Macroautophagy is important for TBC1D15 mediated lysosomal regeneration

Furthermore, we utilised different pharmacological inhibitors of autophagy: the PI3K inhibitor Wortmannin, the ULK1/2 inhibitor MRT68921 and the Vps34 inhibitor SAR405 to test the involvement of autophagy. Treating cells with these drugs significantly reduced the recruitment of TBC1D15 to lysosomes (**Fig 7.11A, and B**). Also, immunoprecipitating HA-TBC1D15 from similarly treated cells showed almost no interaction with LC3B (**Fig 7.11C**). Lysosomal regeneration flux was also compromised upon pharmacological inhibition of autophagy (**Fig 7.11D, and E**). Collectively, all these results indicate that the classical macroautophagy pathway is required for TBC1D15 mediated lysosomal regeneration whereas non-canonical autophagy forms which involves lipidation of ATG8 on single membranes (like LAP and CASM) are not required for this process.

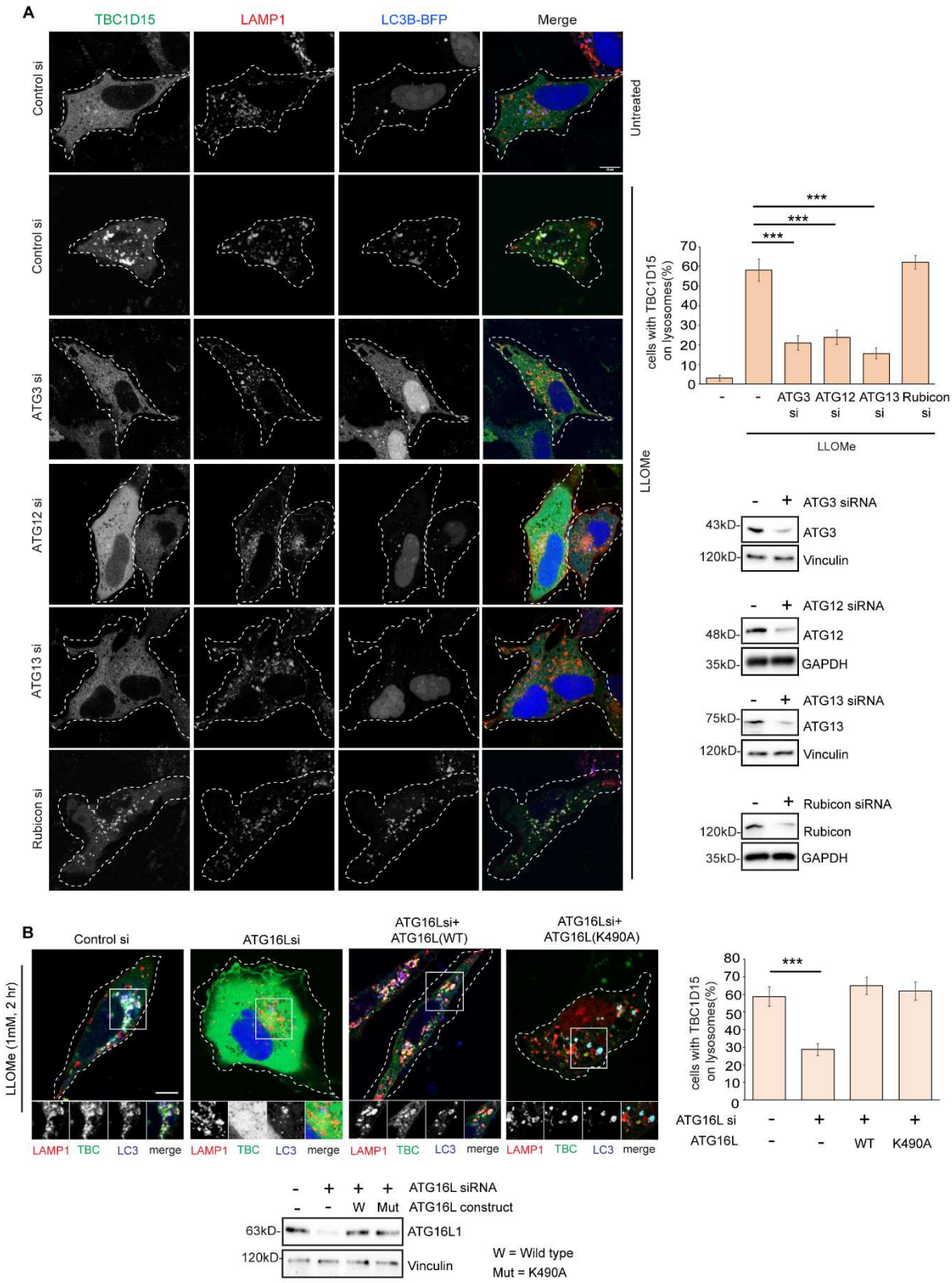

Figure 7. 10: Macroautophagy is important for the recruitment of TBC1D15 to damaged lysosomes. A) HeLa cells were treated with specific siRNA for 48 h to knockdown different autophagy related genes followed by transfection of LC3B-BFP for another 18 hours. Cells were then treated with 1mM LLOMe for 2 h, fixed and stained for LAMP1 and TBC1D15 followed by confocal imaging. Images were analysed in FIJI to determine the number of cells where TBC1D15 is localised on lysosomes. Data are means ± SEM of at least 100 cells taken from three

independent experiments (***p ≤ 0.001). Knockdown efficiency for each gene was checked by western blotting. B) HeLa cells were treated with siRNA to knockdown ATG16L followed by reconstituting with either wild-type or K490A mutant variants. Cells were then transfected with LC3B-BFP for 18 h, followed by 1mM LLOMe treatment for 2 h and stained for LAMP1 and TBC1D15 to quantitate the recruitment of TBC1D15 to damaged lysosomes. Data are means ± SEM of at least 80 cells from three independent experiments (***p ≤ 0.001). Expression levels of ATG16L was checked by western blotting.

7.12 Proximity labelling of TBC1D15 identifies a complex molecular machinery around damaged lysosomes

Since TBC1D15 was found to be instrumental for lysosomal regeneration, we wanted to understand the molecular mechanism by which it helps the regeneration of damaged lysosomes. We again utilised proximity labelling method and generated a stable inducible Flp-in Trex HeLa cells expressing APEX2-TBC1D15. After inducing the expression of TBC1D15 by doxycycline treatment, these cells were treated with LLOMe or left untreated and then the neighbourhood of TBC1D15 was labelled by exposing to biotin followed by a short pulse of 1 mM H_2O_2. Streptavidin beads were used to pull down the biotin-labelled proteome and then was analysed by MS (**Fig 7.12A, and B**). We compared between control and LLOMe treated samples and significant hits were filtered out on the basis of false discovery rate (FDR) correction using Perseus software. Gene Ontology (GO) analysis of significantly enriched proteins identified several interesting groups of proteins. For example, some lysosomal membrane proteins such as SCARB2, TMEM9 and TMEM192, the lysosomal V-ATPase (ATP6V0-V1) complex, and hydrolytic enzymes such as β-hexosaminidase (HEXA, HEXB), α-glucosidase (GAA), and γ-glutamyl hydrolase (GGH). As expected, some autophagy-related proteins were also significantly enriched such as GABARAPL2, FIP200 (RB1CC1) and ATG3 were also enriched by LLOMe treatment. Interestingly, we also could detect several proteins which are known to be involved in lipid metabolism like PLCH1, PLCB3, PLPP6 and GPD2. Some important categories are highlighted in the following panel (**Fig 7.12C**).

7.13 Lysosomal membrane protein can interact simultaneously with LC3B and TBC1D15 in damaged condition.

Since TBC1D15 showed to be very specific in terms of localising to damaged lysosomes only although it does not act as a lysophagy receptor, we wanted to see if there are some other LC3 binding proteins present on damaged lysosomes. From the previous experiment, we found several lysosomal membrane proteins in the proximity of TBC1D15 in LLOMe-treated cells.

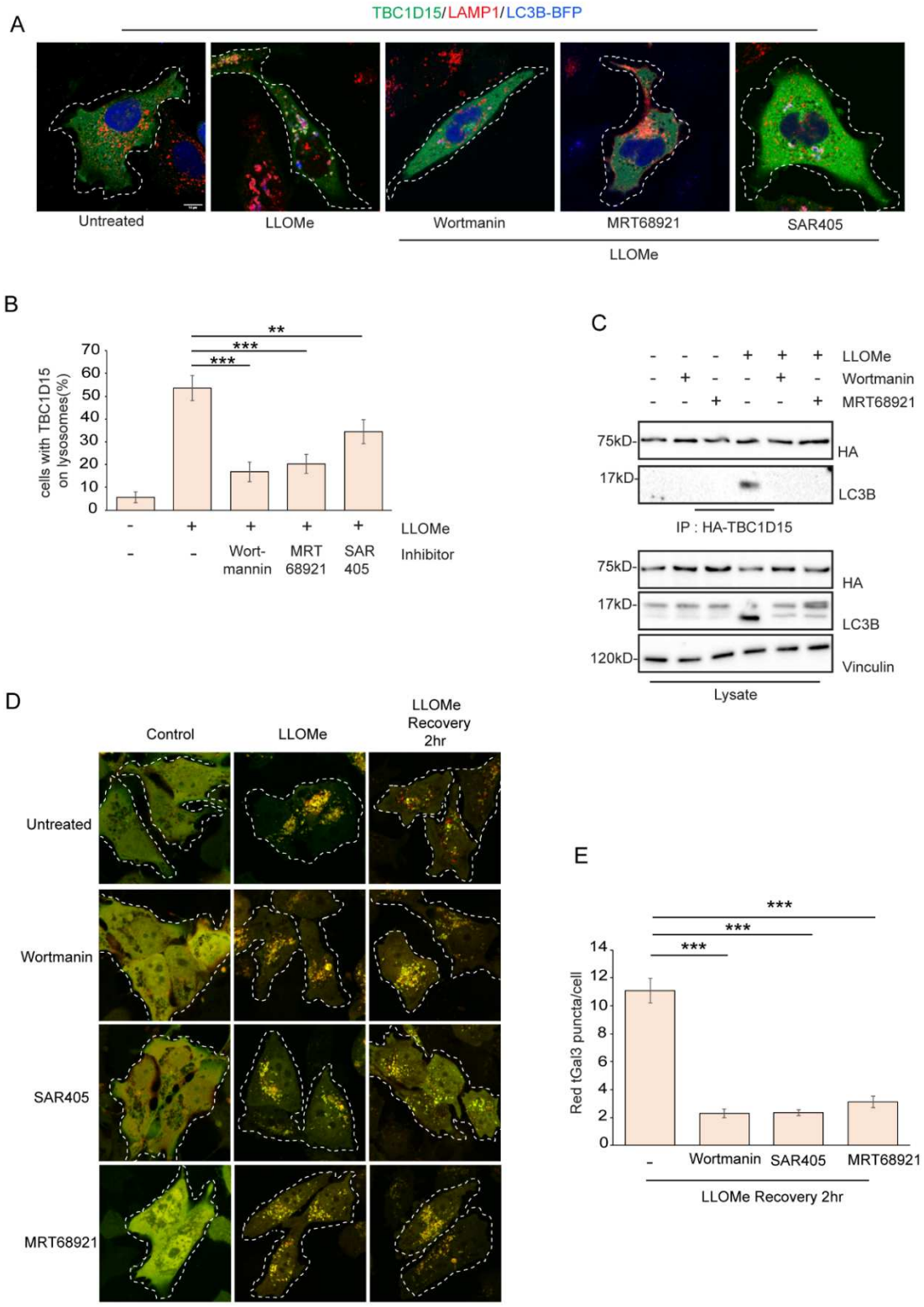

Figure 7. 11: Pharmacological inhibition of autophagy reduces recruitment of TBC1D15 to damaged lysosomes and reduces lysosomal regeneration flux. A) HeLa cells were transfected with HA-TBC1D15 and LC3B-BFP followed by treating them with only 1mM LLOMe for 2 h or LLOMe in combination with different known chemical agents to block autophagy. Cells were then fixed and stained for LAMP1 to check the recruitment of TBC1D15 to damaged lysosomes. B) Recruitment efficiency of TBC1D15 from experiment in panel (a) Data are means ± SEM of at least 80 cells from three independent experiments (***$p \leq 0.001$, **$0.001 < p \leq 0.01$). C) HEK 293T cells were transfected with HA tagged wild-type TBC1D15 followed by treating them with

1mM LLOMe for 2 h or LLOMe in combination with indicated inhibitors. Binding efficiency of TBC1D15 with LC3B under these conditions were assessed by HA immunoprecipitation followed by western blotting. D) Lysosomal regeneration flux assay was performed using HeLa cells stably expressing the tfGal3 reporter after 1mM LLOMe treatment for 2 h followed by LLOMe washout. The indicated drugs were added to the medium 2 h prior to LLOMe treatment, during LLOMe treatment and washout. E) Efficiency of lysosomal regeneration was compared between treatments as shown in experiment in panel (d) by measuring number of red galectin3 puncta/cell. Data are means ± SEM of at least 50 cells from three independent experiments (***p ≤ 0.001). Drug treatments used: Wortmannin (300nM, 6 h), MRT68921 (10μM, 6 h), SAR405 (10μM, 6 h).

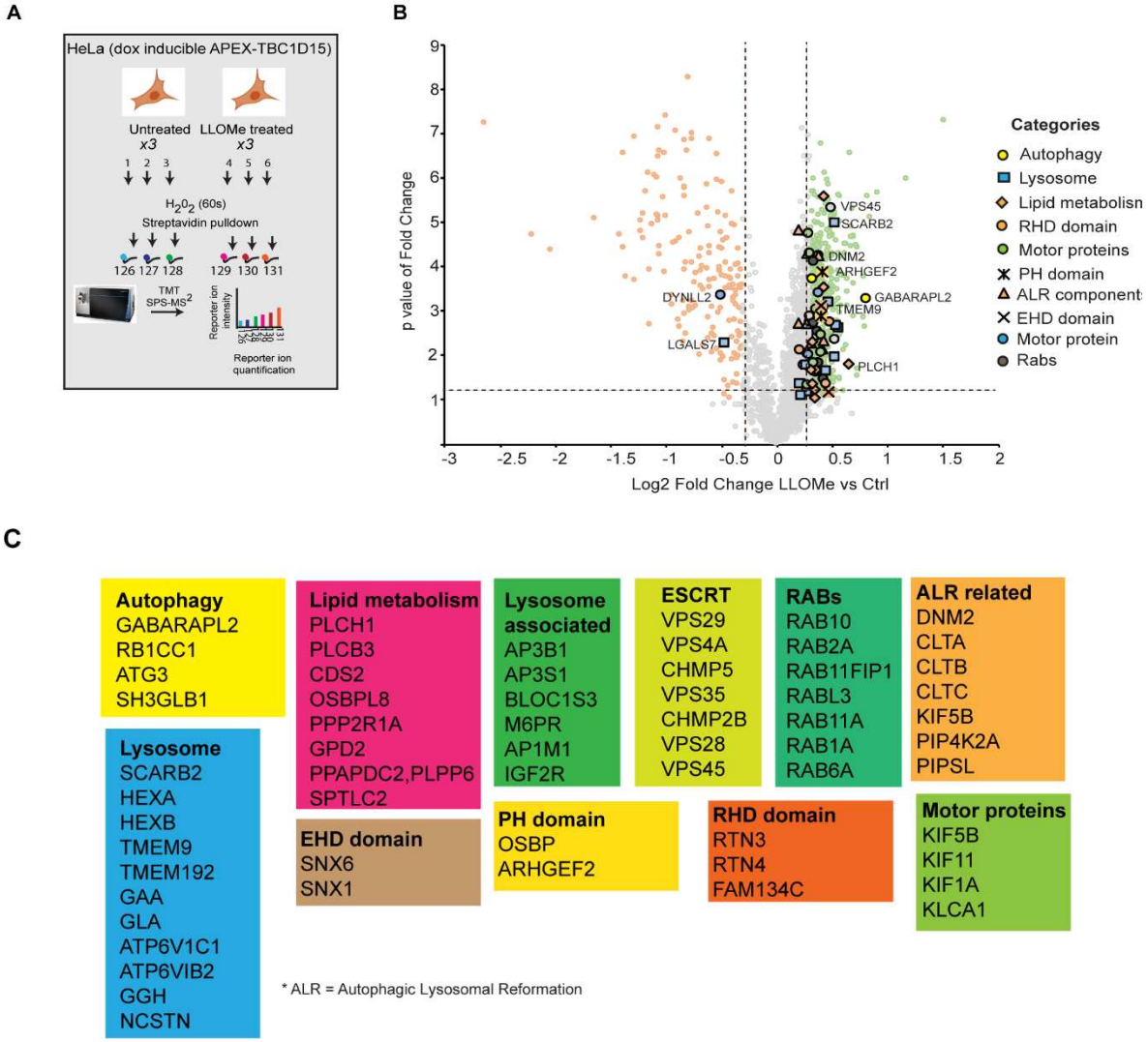

Figure 7. 12: Proximity labelling of TBC1D15 identifies LC3B-binding proteins and ALR machinery near damaged lysosomal membranes. A) Schematic of the APEX2-TBC1D15 proximity labelling assay. B) Volcano plot showing biotinylated proteins enriched by LLOMe treatment. C) Pathway analysis of proteins enriched by LLOMe treatment from the experiment in panel (b)

These candidates were screened against the iLIR database to find out the presence of any potential LIR motifs. Three proteins were found to have putative LIR motifs within them naming:

ATP6V1B2, TMEM192 and SCARB2 (LIMP2) (**Fig 7.13A**). To test the ATG8 binding capability of these proteins we immunoprecipitation HA-tagged TMEM192 and LIMP2 from LLOMe-treated cells (**Fig 7.13B)**. This experiment showed that both proteins interacted with GABARAPL2 and LC3B after damaging lysosomes. Interestingly, we could also immuno-precipitate endogenous TBC1D15 along with ATG8 proteins in this experiment which explains the specificity of TBC1D15 localisation to damaged lysosomes. Although, ATP6V1B2 did not seem to interact with ATG8 proteins upon LLOMe treatment (**Fig** 7.**13C**). Next, we tested the active LIR motifs in LIMP2 and TMEM192 by introducing point mutations. We found that LIR1 (amino acids 211-216, GDYVFL) in LIMP2 is the only active LIR motif since mutating this motif led to significant reduction in binding with GABARAPL2 (**Fig. 7.13D**). Mutating the predicted LIR motifs of TMEM192 did not seem to have any effect on its interaction with GABARAPL2 (**Fig. 7.13E**) suggesting that TMEM192 might not directly bind to ATG8 proteins upon damage but rather stay in the same complex. Next, we also tested this interaction is semi in-vitro setting where we purified WT, the LIR mutant (LIMP2[Y213AF215AL216A], LIR1mut) of LIMP2-Myc and WT TMEM192-HA from HEK293T cells by MYC and HA IP respectively and after removing cellular interactor by high salt wash, we incubated these with GST tagged ATG8 proteins (GABARAPL2 and LC3B) which were purified from *E. coli.* This interaction assay using pure proteins revealed that only LIMP2-Myc can bind to pure GST tagged LC3B and GABARAPL2 using its LIR motif (GDYVFL) as identified from previous experiment. TMEM192 did not interact with LC3B or GABARAPL2 (**Fig 7.13F (i) and (ii)**). This data supported our hypothesis of LIMP2 being a direct interactor of ATG8 proteins in LLOMe treated cells while TMEM192 may be a part of this large protein complex. We also performed a proximity labelling assay of TBC1D15 in absence of LIMP2 and TMEM192 either individually or in combination as looked for its effect on the interaction with ATG8 proteins. The combinatorial knockdown of LIMP2 and TMEM192 significantly reduced the amount of GABARAPL2 biotinylation, suggesting its absence in the vicinity of TBC1D15 (**Fig 7.13G**). This suggested that the binding of ATG8 proteins to LIMP2 is necessary for the recruitment of TBC1D15 to damaged lysosomes and TMEM192 most probably stay in the same complex serving some purpose which is not known yet.

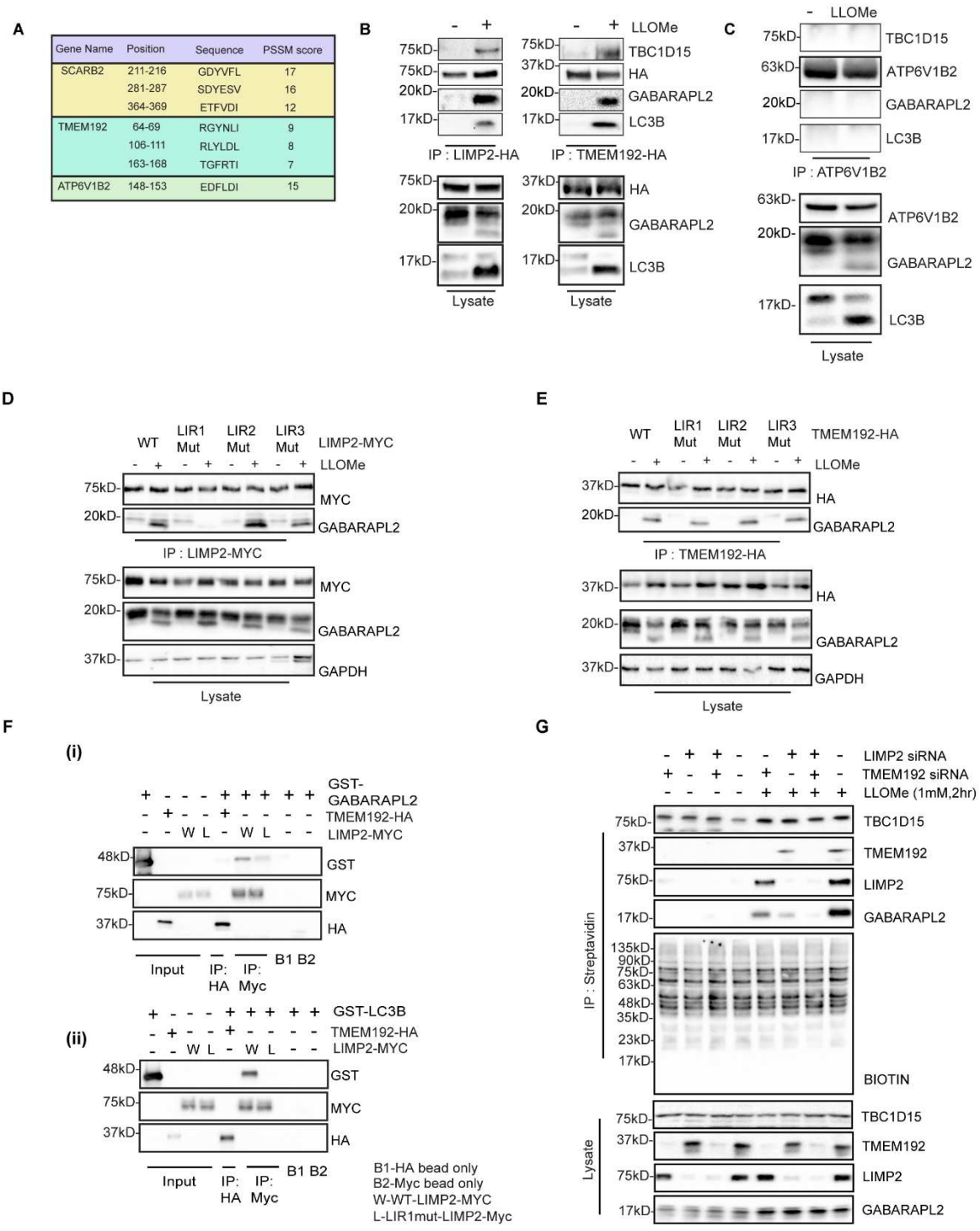

Figure 7.13: Lysosomal membrane protein can bind to ATG8 and TBC1D15 upon damage. A) Lysosomal membrane proteins, significantly enriched after LLOMe treatment were scanned for potential LIR motifs using iLIR database. Putative LIR motifs are listed. B) HEK 293T cells were transfected with HA-tagged LIMP2 and TMEM192 constructs, then treated with 1mM LLOMe for 2 h to induce lysosomal damage. The extent of interaction with ATG8 proteins and TBC1D15 was assessed by HA immunoprecipitation followed by western blotting. C) Endogenous ATP6V1B2 was immunoprecipitated using an antibody coupled to Protein A/G agarose after treating cells with LLOMe and binding with ATG8 proteins were assessed by western blotting. D) Putative LIR motifs for LIMP2 as described in panel (a) were mutated by site

directed mutagenesis. MYC-tagged LIMP2 constructs were transfected in HEK 293T cells and then were treated with 1mM LLOMe for 2 h or left untreated. The interaction with GABARAPL2 and LIMP2 was assessed by MYC immunoprecipitation and western blotting. E) Putative LIR motifs for TMEM192 as described in panel (a) were mutated by site directed mutagenesis. HA-tagged TMEM192 constructs were transfected in HEK 293T cells, treated with 1mM LLOMe for 2 h or left untreated. The efficiency of binding with GABARAPL2 for each construct was assessed by HA immunoprecipitation and western blotting. F) Wild type TMEM192 and wild type or LIR1 mut LIMP2 variants were purified from HEK293T cells and incubated with pure GST-GABARAPL2 and GST-LC3B and extent of binding were assessed by MYC and HA immunoprecipitation followed by western blotting. Efficiency of binding with pure GABARAPL2 and LC3B is shown in panel (f-i) and (f-ii) respectively. G) HeLa cells expressing doxycycline-inducible APEX2-TBC1D15 were treated with siRNA to deplete LIMP2 and TMEM192 either individually or in combination. TBC1D15 expression was then induced with doxycycline, followed by LLOMe treatment and proximity labelling with biotin/H_2O_2. Biotinylated proteins were pulled down using streptavidin-agarose and mentioned proteins were checked by western blotting using specific antibodies.

7.14 LIMP2 and TMEM192 are lysophagy receptors which are important for TBC1D15 recruitment to damaged lysosomes

To test the importance of LIMP2 and TMEM192 for the localisation of TBC1D15, we depleted endogenous LIMP2 and TMEM192 and checked the recruitment of TBC1D15 to damaged lysosomes by confocal microscopy. Knocking down TMEM192 had no discernible impact on the recruitment of TBC1D15 to the damaged lysosomes but knockdown of LIMP2 caused a little albeit statistically significant reduction of TBC1D15 recruitment to lysosomes. In cells lacking both LIMP2 and TMEM192 had significantly fewer TBC1D15 puncta on damaged lysosomes (**Fig 7.14A-C**). Absence of these lysosomal membrane proteins also slowed down lysosomal regeneration flux when measured with the tfGal3 reporter assay (**Fig. 7.14D, and E**). This data altogether suggested that LIMP2 can serve as lysophagy receptor protein which binds to ATG8 proteins after damage and TMEM192 is also a part of this complex serving some function which are yet to be discovered. Following lysosomal damage, cytosolic TBC1D15 gets recruited to this complex and this seems to stabilise it at the damaged spot. We were curious if other ways of accumulating ATG8 proteins on lysosomes can also recruit TBC1D15. Recently it has been shown that one of the major lysosomal calcium channels, TRPML1 can bind ATG8 proteins when cells are treated with its agonist MLSA1 (Nakamura et al., 2020). Treating cells with 50 μM MLSA1 for 1h caused TBC1D15 to colocalize with lysosomes (**Fig 7.14 F**). Under this same condition, LC3, GABARAPL2 and TBC1D15 also seem to be in the proximity of TRPML1 (**Fig 7.14G**). Taken together, these results reinstate that TBC1D15 can indeed be recruited to lysosomes under conditions where the ATG8 proteins binds lysosomal membrane proteins. In case of lysosomal damage response, LIMP2 seems to be the major factor for TBC1D15 recruitment.

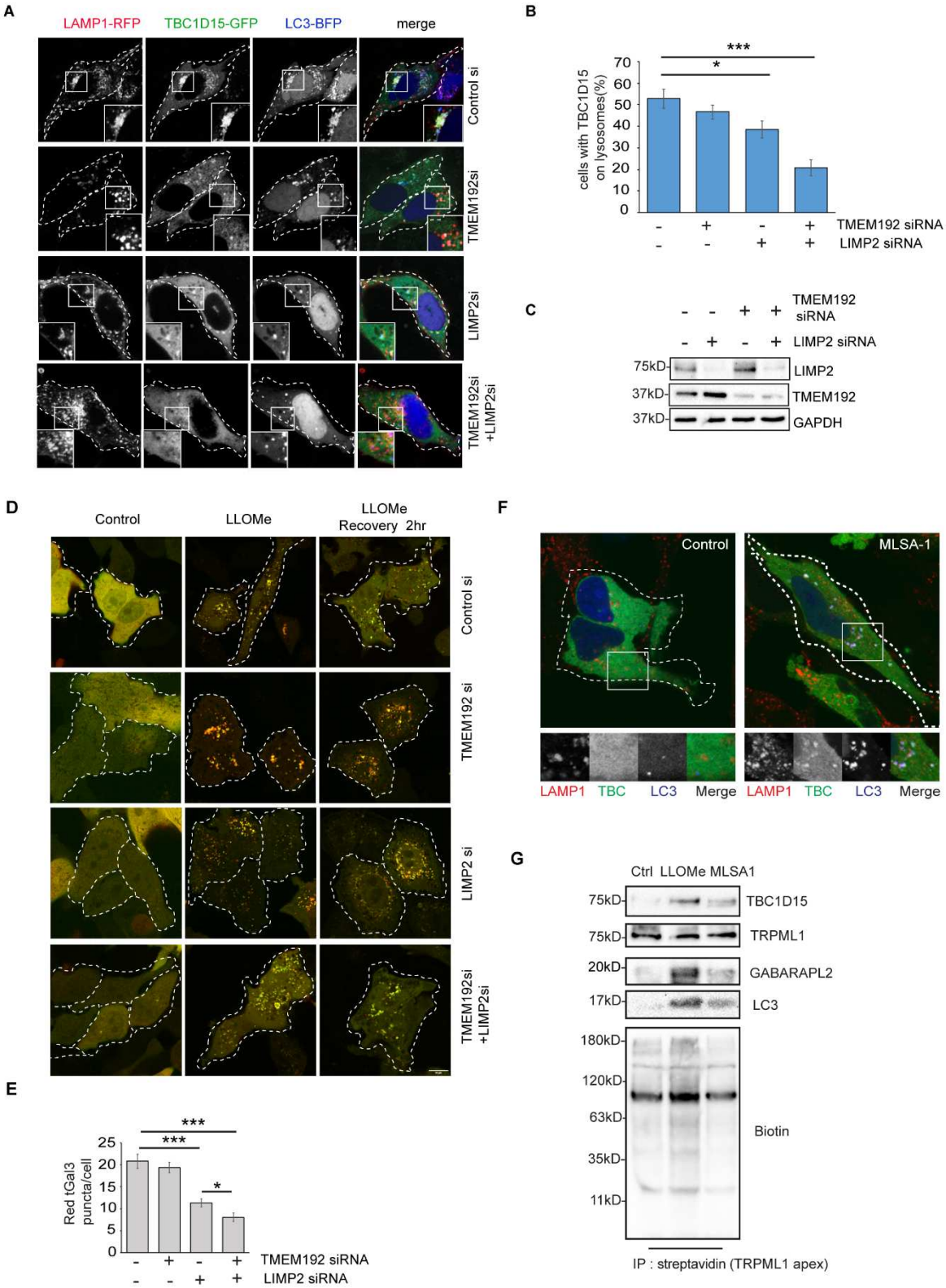

Figure 7.14: ATG8 binding capability of lysosomal membrane protein is crucial for TBC1D15 recruitment and thus is important for lysosomal regeneration. A) HeLa cells were treated with siRNA for 48 h to deplete either LIMP2 and TMEM192 individually or in combination. These cells were then transfected with indicated constructs for 18 h followed by

treatment with 1mM LLOMe for 2 h, fixed and imaged by confocal imaging. B) The number of TBC1D15 puncta was compared between control cells and cells treated with siRNA targeting both genes as described in panel (c). Data are means ± SEM of 100 cells from three independent experiments (***$p \leq 0.001$; *$0.01 \leq p < 0.05$). C) Efficiency of LIMP2 and TMEM192 knockdown were checked by western blotting. D) Importance of LIMP2 and TMEM192 on lysosomal regeneration was assayed by performing the lysosomal regeneration flux assay after LLOMe treatment (1mM, 2 h) and washout (2 h). E) Number of red Gal3 puncta/cell were compared between different samples from experiment in panel (e). Data are means ± SEM of at least 100 cells from three independent experiments (***$p \leq 0.001$). F) HeLa cells were transfected with LC3-BFP and were treated with 50 μM MLSA1 for 1 h followed by confocal imaging. TBC1D15 is recruited to $LAMP1^+$ $LC3^+$ puncta following treatment with MLSA1. G) HeLa cells expressing doxycycline-inducible APEX2-TRPML1 were treated with 1mM LLOMe or 50μM MLSA1 for 2 h followed by proximity labelling using biotin/H_2O_2. Lysates were used in a streptavidin pulldown assay followed by western blotting with the indicated antibodies.

7.15 ALR proteins interact with TBC1d15 in LLOMe treated cells.

Cellular process and Pathway analysis of the significant hits from the TBC1D15 proximity labelling assay using Metascape (Zhou et al., 2019), identified vesicle-mediated transport, and a cluster of ALR proteins (including DNM2, KIF5B and CLTC) (**Fig 7.15A**) (Yu et al., 2010). This led us to hypothesize that these ALR components might be contributing to the regeneration of active lysosomes from damaged membranes. We tested these findings using western blot assay and important candidates of ALR machinery appeared to be in the proximity of TBC1D15 (**Fig 7.15B**). To complement our finding from proximity labelling experiment we analysed the interactome of TBC1D15 followed by HA IP from LLOMe treated cells. This data also revealed that DNM2 and KIF22 may interact directly with TBC1D15 (**Fig 7.15C**). We also could capture ALR proteins after the enriching damaged lysosomal membranes. For this experiment, cells expressing TBC1D15-GFP, LAMP1-RFP and LC3-BFP were treated with LLOMe followed by permeabilization with 0.05% digitonin to reduce cytosolic fraction and enrichment of membranous fraction. Confocal microscopy confirmed extensive colocalization of TBC1D15, LAMP1 and LC3 in the LLOMe-treated samples and this signal was unperturbed even after digitonin treatment (**Fig 7.15D**). GFP pulldown from these samples was subjected to mass spec and subsequent interactome analysis revealed the presence of LC3B and the ALR components such as CLTC and KIF5B to be associated with TBC1D15 suggesting that TBC1D15 is instrumental in recruiting these proteins to damaged lysosomes (**Fig 7.15E**).

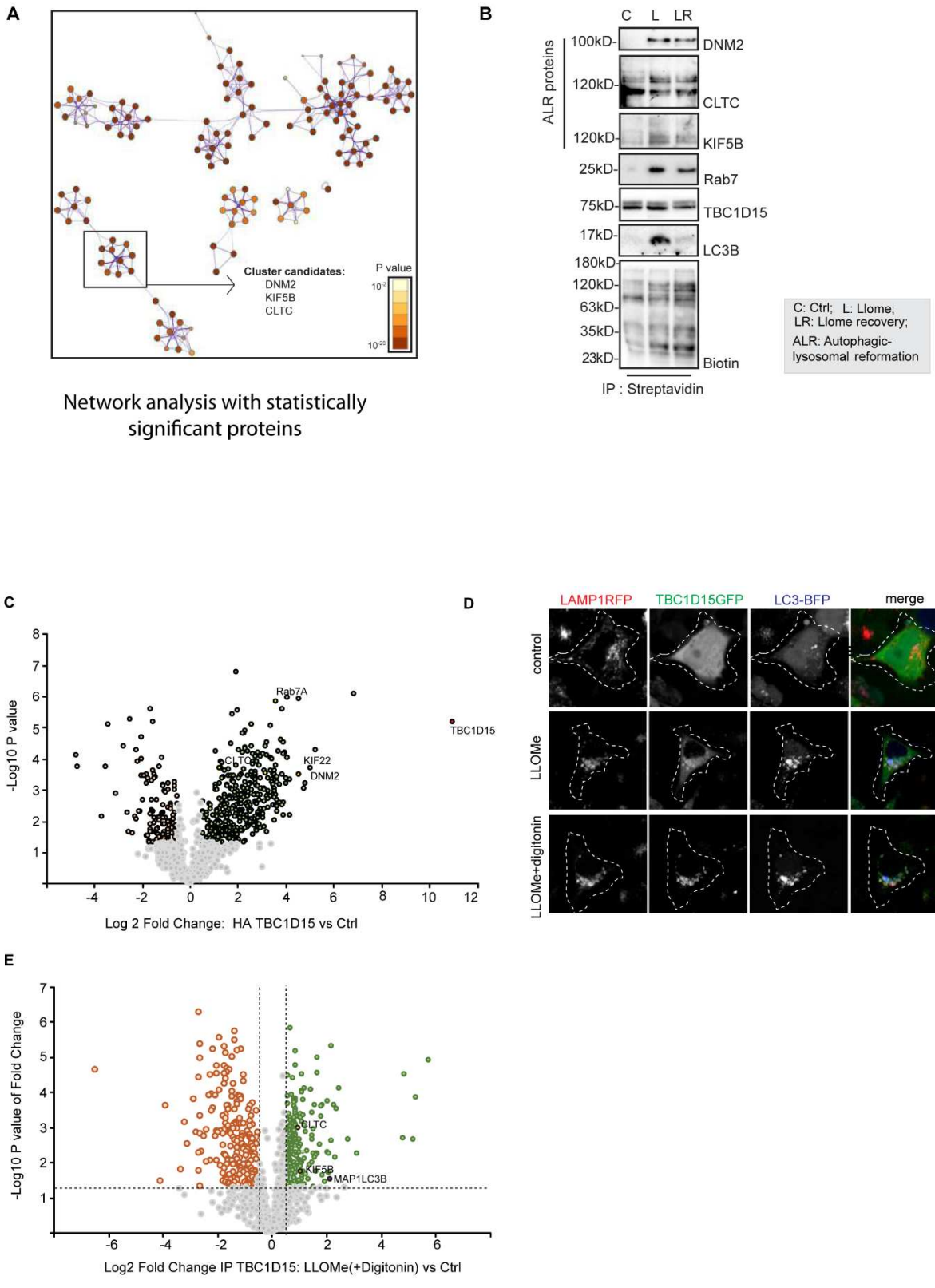

Figure 7.15: ALR proteins interact with TBC1D15 in LLOMe-treated cells. A) Metascape network analysis of proteins significantly enriched in the proximity labelling experiment shown in Fig 712A and 7.12B. B) Cells expressing doxycycline-inducible APEX2-TBC1D15 were treated as indicated and exposed to biotin/H_2O_2 before a proximity labelling assay. Following streptavidin pulldown, samples representing different conditions were analysed by western

blotting and the proteins of interest (DNM2, CLTC, KIF5B, Rab7, TBC1D15 and LC3B) were detected using specific antibodies. C = control; L = treatment with 1 mM LLOMe for 2 h; LR = LLOMe treatment followed by 2 h recovery; ALR = autophagic lysosomal reformation. C) HA-TBC1D15 was immunoprecipitated from cells after 1mM LLOMe treatment for 2 h followed by MS analysis. Proteins related to ALR (KIF22, CLTC and DNM2) were enriched by LLOMe treatment. Control = lysates from cells treated with LLOMe but not expressing HA-TBC1D15. D) Cells expressing LAMP1-RFP, TBC1D15-GFP and LC3-BFP were treated with 1 mM LLOMe for 2 h. Before fixing the cells, 0.05% digitonin was added to reduce the cytosolic background of TBC1D15 staining. Digitonin-treated cells show the presence of TBC1D15 in LAMP1-RFP$^+$ LC3-BFP$^+$ membrane mass. E) TBC1D15-GFP in lysates from cells treated with LLOMe and digitonin similar to panel (d) was immunoprecipitated using anti-GFP beads followed by MS analysis. ALR proteins were enriched by LLOMe treatment.

7.16 TBC1D15 utilises its N terminal domain to act as a scaffold protein for recruiting proteins required for lysosomal regeneration and this assembly is indispensable for propagating lysosomal regeneration flux.

Since, DNM2 was found to be a significant candidate in almost every TBC1D15 interactome after LLOMe treatment, we asked if DNM2 interacts directly with TBC1D15. The C-terminal of TBC1D15 harbours the catalytic GAP domain and LIR motifs and it has already been structurally characterized (Chen et al., 2017). However, there is not much information about the N-terminal stretch of TBC1D15. So, we analysed the complete protein using the structure available in AlphaFold database (Jumper et al., 2021). The predicted structure of TBC1D15 showed that it has two distinct domains and the N-terminal domain and C-terminal domain is connected by a linker (**Fig 7.16A**). To identify which domain is being used for interaction, we purified full-length GST-tagged TBC1D15, and two versions without the N-terminus (ΔNter, TBC1D15 amino acids 301–697) and without the C-terminus (ΔCter, TBC1D15 amino acids 1–399) from *Escherichia coli*. We then incubated these purified proteins with the lysates from LLOMe-treated cells and after GST pulldown we analysed the samples by western blotting. The result suggested that TBC1D15 uses its N terminal domain to bind with DNM2 and CLTC (**Fig 7.16B**) and further testing of several deletion mutations of the N terminal revealed that the first 190 amino acids were most important for the interaction with DNM2, especially residues 102–183 (**Fig 7.16C**). From the AlphaFold model, we spotted the presence of a loop spanning residues 57–124, which can be considered as a likely structure to interact with DNM2 (**Fig 7.16D**). We therefore deleted this loop (TBC1D15Δ [57-124], loop mutant) and compared the interaction between TBC1D15 and ALR candidates DNM2 and CLTC. GFP pulldown analysis from cells expressing this deletion variant showed weaker interaction between TBC1D15 and ALR component while comparing to the full-length protein (**Fig 7.16E**). We therefor concluded that TBC1D15 utilises its C-terminal region for LC3 binding and its GAP activity while the N-terminal region interacts with DNM2.

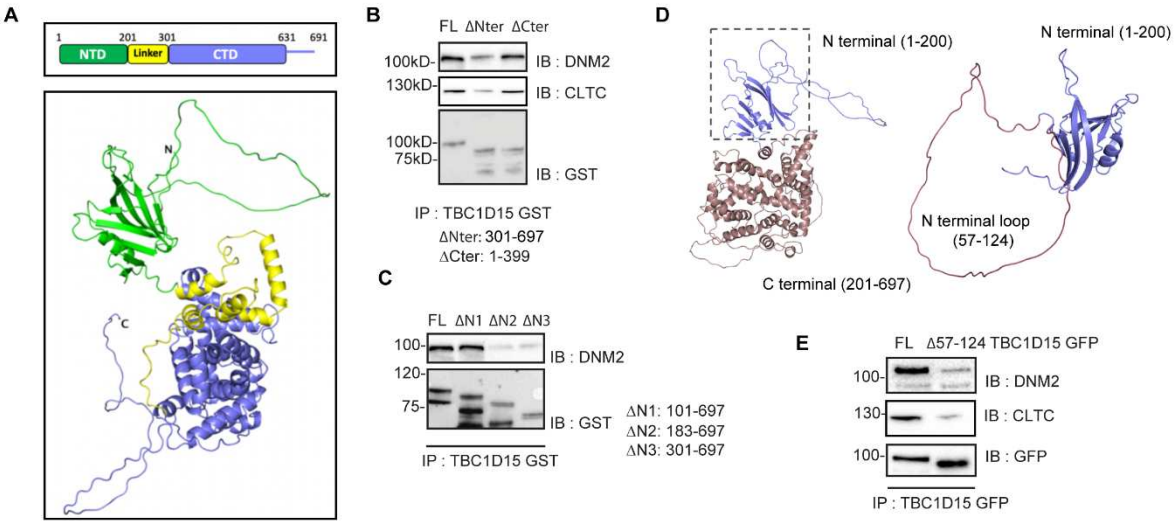

Figure 7.16: TBC1D15 can directly bind DNM2 using its N terminal domain. A) AlphaFold predicted structure of full-length TBC1D15 showing N-terminal domain (NTD) in green, the linker in yellow and the C-terminal domain (CTD) in blue. B) GST-tagged deletion constructs of TBC1D15 were incubated with cell lysates from HEK 293T cells in a GST pulldown assay and detected by western blotting with the indicated antibodies. C) GST-tagged N-terminal deletion constructs of TBC1D15 were incubated with HEK 293T cell lysates in a GST pulldown assay and detected by western blotting with the indicated antibodies. D) AlphaFold predicted structure showing the N-terminal loop required for DNM2 binding. E) GFP-tagged wild-type TBC1D15 or the loop mutant were enriched from LLOMe-treated cells using anti-GFP beads followed by western blotting with the indicated antibodies.

7.17 TBC1D15 acts as a scaffold to assemble ALR machinery

To conclusively prove the scaffolding function of TBC1D15, we utilised a specific antibody to immunoprecipitate endogenous DNM2 from LLOMe-treated cells. Both TBC1D15 and CLTC seem to bind with DNM2 after LLOMe treatment but the interaction between DNM2 and CLTC was weaker when we depleted TBC1D15 using siRNA (**Fig. 7.17A**) This data supported our hypothesis that TBC1D15 acts as a scaffold to assemble the ALR molecular machinery. But this machinery along with TBC1D15 can still be part of a multi-protein complex but this requires further testing. To establish the role of TBC1D15 and DNM2 in lysosomal regeneration, we either utilised dynasore, a pharmacological inhibitor the DNM2-mediated scission of lysosomal tubules or depleted endogenous DNM2 using siRNA and repeated the RFP-GFP-Gal3 flux assay. In both experiments a significant reduction in the number of red Gal3 puncta was noticed after 2 h of LLOMe washout (**Fig 17B, and C**) indicating its importance for lysosomal regeneration. This effect could be rescued by expressing full length TBC1D15 but not the loop mutant, confirming that TBC1D15-DNM2 interaction is indeed instrumental for lysosomal regeneration (**Fig 17D**).

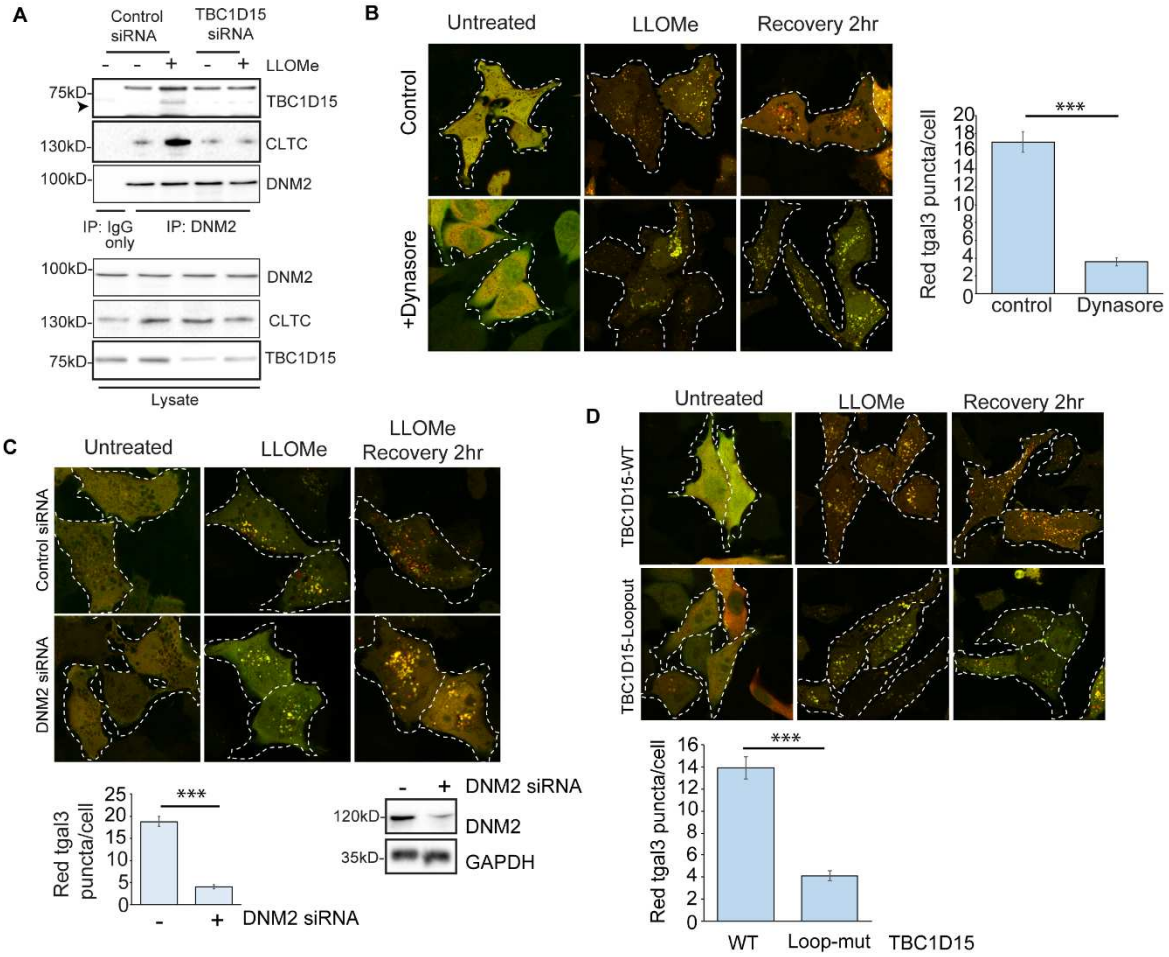

Figure 7.17: TBC1D15 and DNM2 interaction in indispensable for lysosomal regeneration. A) Endogenous DNM2 was immunoprecipitated from TBC1D15-depleted cells (untreated or treated with 1 mM LLOMe, 2 h) and the interactions of DNM2 with CLTC and TBC1D15 were assessed by western blotting. B) HeLa cells stably expressing the tfGal3 flux reporter were subjected to a lysosomal regeneration flux assay in cells with or without 20 µM Dynasore added in LLOMe-free medium during washout. The number of red tGal3 puncta per cell was counted. Data are means ± SEM of at least 50 cells from three independent experiments (***$p \leq 0.001$). C) HeLa cells expressing the tfGal3 flux reporter were treated with DNM2 siRNA and then were subjected to a lysosomal regeneration flux assay. The number of red tfGal3 puncta per cell was counted. Data are means ± SEM of at least 50 cells from three independent experiments. (***$p \leq 0.001$). D) HeLa cells stably expressing tfGal3 were depleted of endogenous TBC1D15 for 48 h followed by transfection of wild-type TBC1D15 or the loop mutant. Cells were treated with 1mM LLOMe for 2h followed by LLOMe washout and imaged by confocal microscopy. The number of red tGal3 puncta per cell was counted. Data are means ± SEM of at least 50 cells from three independent experiments (***$p \leq 0.001$).

7.18 In response to LLOMe-mediated damage, damaged lysosomes undergo tubulation to form proto-lysosomes followed by subsequent scission to generate functional lysosomes.

A hallmark structure of lysosomal regeneration involves the formation of tubules from LC3 and LAMP1 positive structures which gets subsequently cleaved by DNM2 to yield proto-lysosomes (Yu et al., 2010; Khundadze et al., 2021). We performed high resolution (STED) imaging of

endogenous LAMP1 in untreated, LLOMe treated, and during LLOMe washout to look for these structures. In comparison to untreated cells, where LAMP1 was present on lysosomes, LLOMe treated cells showed the dispersed staining of LAMP1 which indicated the loss of lysosomal membrane integrity. However, during LLOMe washout different LAMP1 structures could be found to be emerging from this damaged mass which can be roughly categorised into three different categories such as short LAMP1 positive membranes, longer curved tubules resembling open ring, and larger closed vesicles were evident (**Figure 7.18A, and C**). Knockdown of TBC1D15 caused a decrease in formation of tubules while depletion of DNM2 increased the length of these tubules (**Figure 7.18B, and C**).

7.19 Lysosomal tubulation occurs in a TBC1D15 dependent manner.

To determine the distribution of LC3B and TBC1D15 on these LAMP1 positive structures, we treated HeLa cells expressing LAMP1-RFP, TBC1D15-GFP and LC3-BFP with LLOMe, followed by LLOMe washout and imaged them by airy-scan confocal microscopy. LAMP1-GFP tubules were often appeared as a curved structure in the form of open (unsealed) rings and TBC1D15 and LC3B were closely associated with LAMP1 structures. Dynasore treatment led to the formation of longer tubules which often appeared like a tangled mass of membranes at airy-scan resolution reinstating the importance of Dynamin2 activity which is required for the scission of these tubules (**Fig 7.19A-D**).

7.20 Time-lapse imaging reveals positioning of TBC1D15 on lysosomal tubules

We tried to capture this phenomenon using time-lapse imaging of cells expressing LAMP1-RFP and TBC1D15-GFP. After damaging lysosomes using LLOMe, lysosomes were allowed to regenerate during 2h of LLOMe washout and at this stage we saw the presence of large

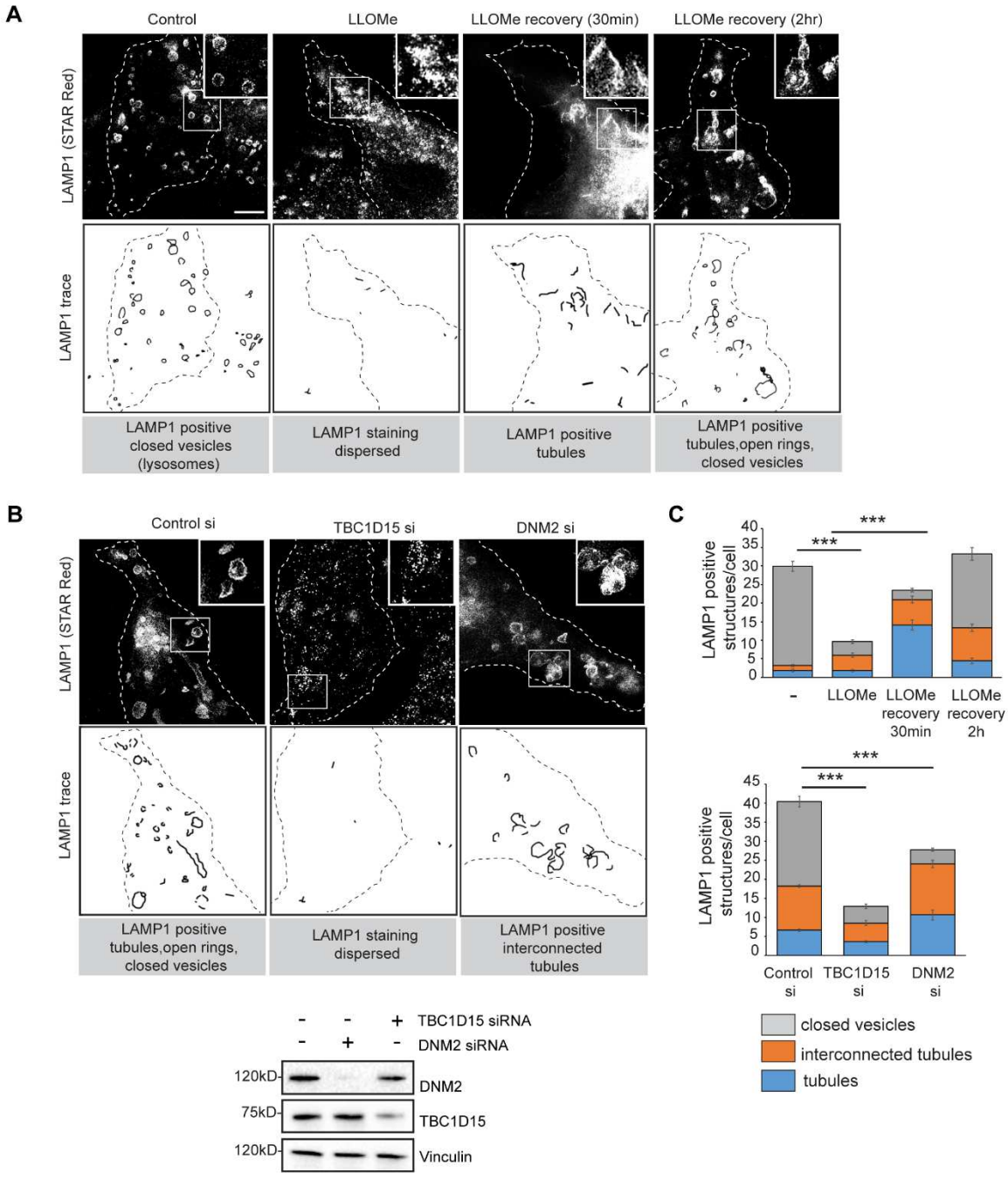

Figure 7.18: Lysosomal regeneration from damaged membranes occurs via tubulation and successive scission in a TBC1D15 and DNM2 dependent manner. A) HeLa cells were treated with LLOMe and were allowed to recover for the indicated timepoints. Cells were fixed and stained for LAMP1 and imaged by STED microscopy. B) HeLa cells were treated with siRNA to deplete either TBC1D15 or DNM2 individually. These cells were the allowed to recover for 2hr after LLOMe treatment and were then fixed and stained for LAMP1 to assess the effect of the TBC1D15 and DNM2 on lysosomal tubulation events by STED microscopy. C) Different lysosomal structures, from experiments in panel (a) and (b) were analysed in FIJI and classified into closed rings, interconnected tubules and tubules Data are means ± SEM of at least 50 cells from three independent experiments (***$p \leq 0.001$). **(STED imaging in Figure 7.18 was performed by Rukmini Mukherjee)**

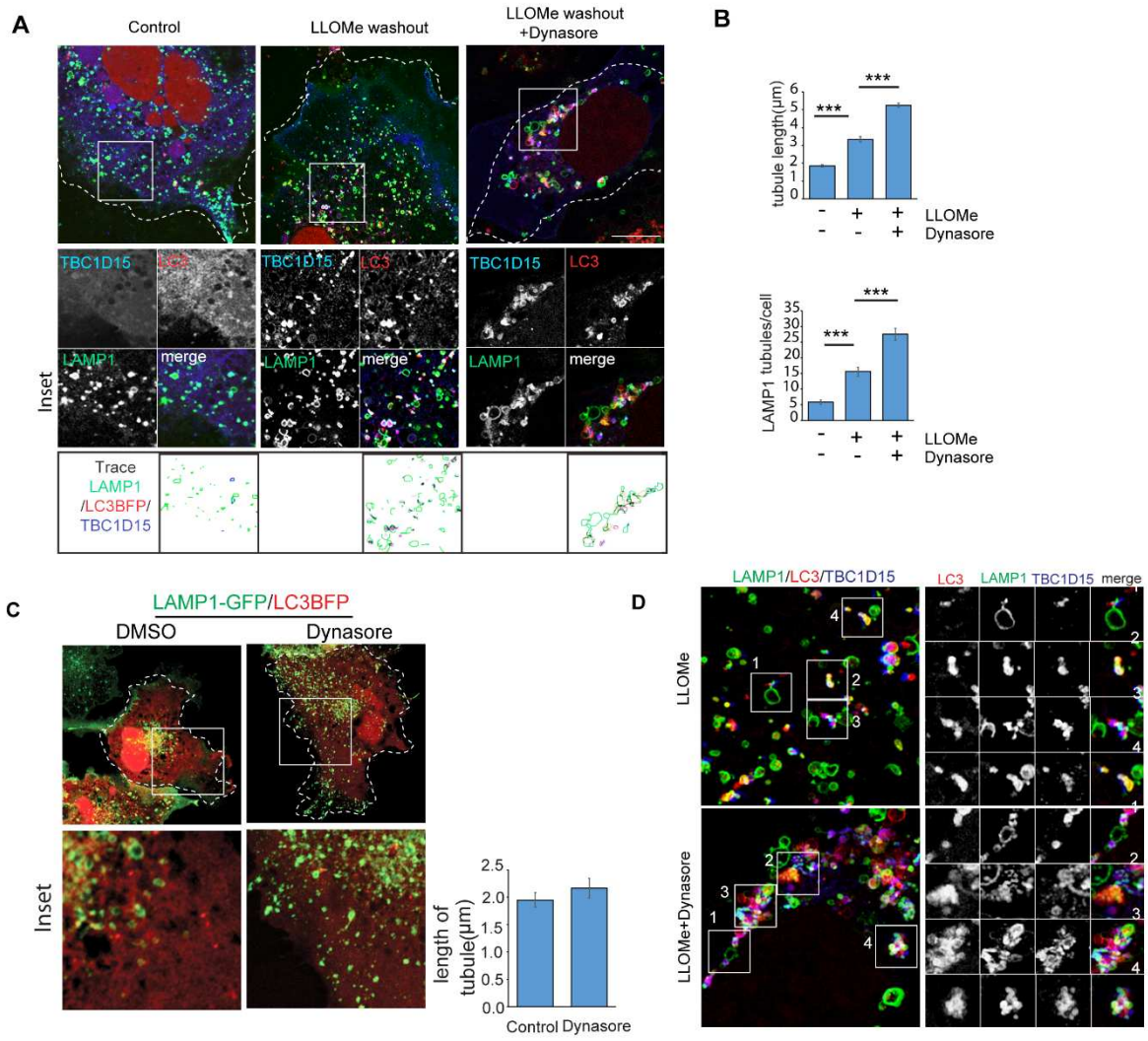

Figure 7.19: Regenerating lysosomal tubules are a mixture of LC3 and LAMP1 positive membranes and DNM2 is important for their scission. A) Cells expressing LC3B-BFP were treated with 1mM LLOMe for 2hr followed by recovery in LLOMe free medium with or without 20 μM Dynasore for 2 h, and were fixed and stained for TBC1D15 and LAMP1. These samples were then imaged by airy-scan confocal microscopy. Images were analysed in FIJI to obtain the trace of LAMP1 membranes (green), LC3BFP (red) and TBC1D15 (blue). B) Cells from experiment in panel (a) were analysed with FIJI to measure the length and number of lysosomal tubules. LAMP1 structures greater than 2.5 μm in length were defined as a lysosomal tubule when counting number of tubules per cell. Data are means ± SEM of 60 cells from three independent experiments (***$p \leq 0.001$). C) Effect of 20μM dynasore treatment for 2 h in the absence of LLOMe. D) 3D projections made from Z-stacks of airy-scan images as seen in Fig 7.19A. **(Airy-scan imaging in Figure 7.19 was performed by Rukmini Mukherjee)**

closed rings which were LAMP1 positive. TBC1D15 was present on certain regions of these large rings from where small membrane buds protrude and were being pulled outwards and then subsequently got cleaved to form small LAMP1 positive vesicles (proto-lysosomes) (**Fig 7.20A and B, supplementary videos 3, 4**).

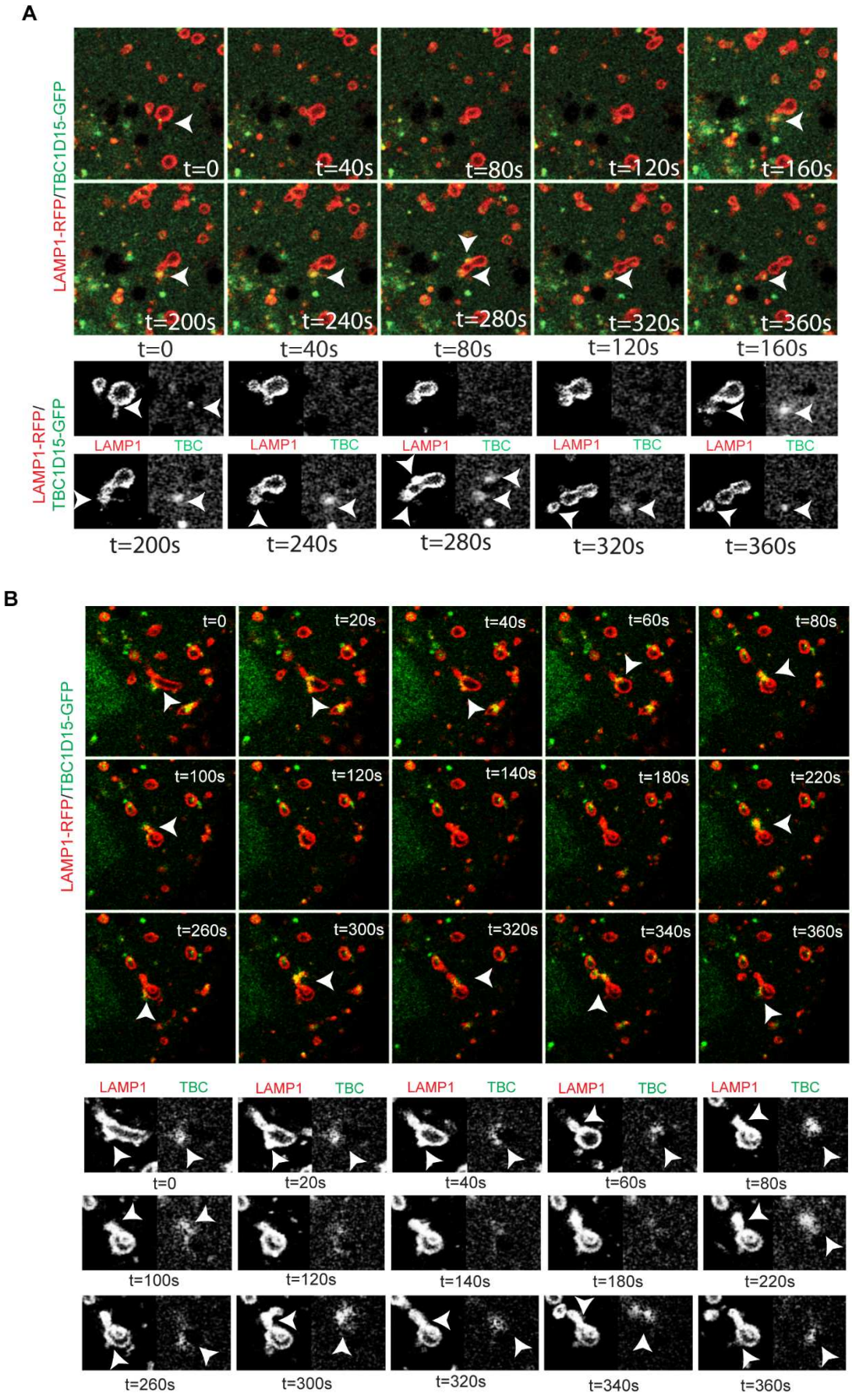

Figure 7.20: Live imaging shows lysosomal tubulation events following damage. A) Time-lapse imaging of cells expressing LAMP-RFP and TBC1D15-GFP treated with 1mM LLOMe for

2 h followed by LLOMe recovery for 1 h. Arrows indicate position of TBC1D15 on the LAMP1 tubule. B) Time-lapse imaging of 1mM LLOMe treated cells expressing LAMP-RFP and TBC1D15-GFP. **(Time-lapse imaging in Figure 7.20 was performed by Rukmini Mukherjee)**

7.21 TBC1D15 depleted cells have reduced number and shorter length of LAMP1 tubules

Cells depleted for TBC1D15 showed a significant reduction in the number and length of LAMP1 tubules in the cells and this phenotype could only be rescued by reconstitution with wild-type TBC1D15 but not the loop mutant (**Fig. 7.21A, and B**). Tubules observed by airy scan confocal imaging in previous experiment showed to have either LC3 or LAMP or containing both markers which suggested that they are a mixture of lysosomal and autolysosomal membranes. These experiments suggest that following extensive damage, the broken lysosomal mass undergoes a rapid regeneration process which requires TBC1D15 and the ALR machinery to create proto-lysosomes which subsequently generates new functional lysosomes to mitigate the crisis.

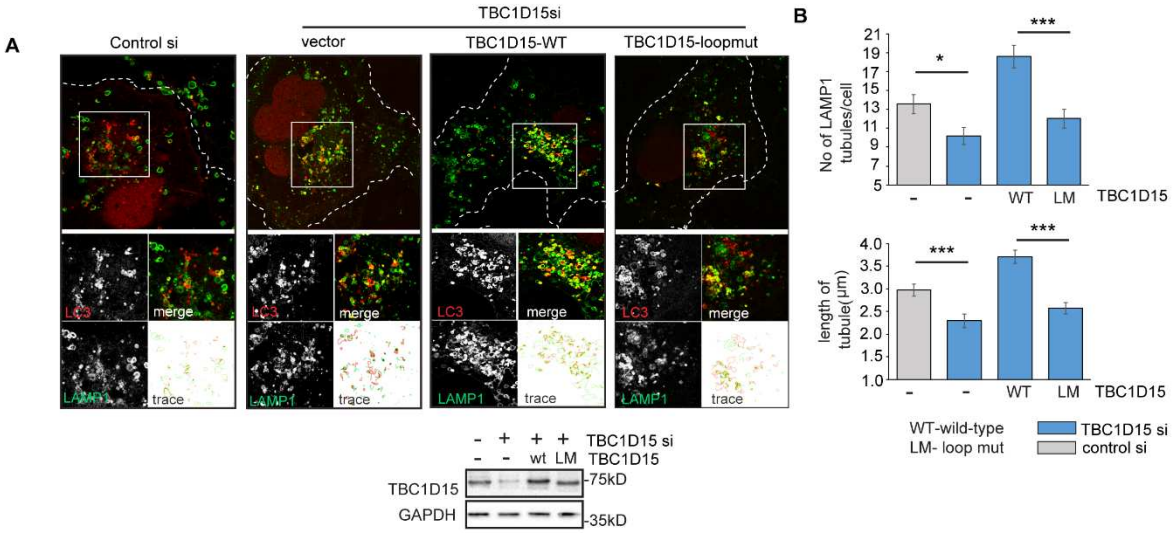

Figure 7.21: Lysosomal tubulation requires TBC1D15 and its scaffolding activity. A) HeLa cells were treated with TBC1D15-specific siRNA to deplete the endogenous pool followed by reconstitution with either full-length TBC1D15 or the loop mutant. These cells were then treated with 1mM LLOMe for 2 h and were allowed to recover in LLOMe free medium for 2 h. Cells were then fixed and stained for TBC1D15 and LAMP1 and lysosomal tubulation events were observed by airyscan confocal microscopy. Images were analysed in FIJI to obtain the trace of LAMP1 membranes (green), LC3BFP (red) and TBC1D15 (blue). B) Cell counts corresponding to the images in panel (). Data are means ± SEM of 50 cells counted for all conditions to compare the number and length of LAMP1 tubules (***$p \leq 0.001$, *$0.01 \leq p < 0.05$).

7.22 TBC1D15 dependent lysosomal regeneration is also active in a cell model of crystal nephropathy.

Finally, we tested if TBC1D15 dependent lysosomal regeneration can be seen in a physiological condition where lysosomes are known to be damaged. We utilised a model of crystal nephropathy for this effort. Recent report has shown that exposure to calcium oxalate crystals in immortalized

kidney proximal tubular epithelial cells (PTECs) can damage lysosomes and this damage can cause the lipidation of ATG8 on the lysosomal membrane and prompts TFEB to translocate to the nucleus (Nakamura et al., 2020). In our hands, oxalate-induced damage led to the formation of Gal3-GFP puncta which pointed the occurring of lysosomal membrane damage (**Fig 7.22A**) and HA-TBC1D15 was recruited to this damaged lysosome as expected (**Fig 7.22B**). Oxalate-induced damaged lysosomes were also capable of regenerating themselves as we could see formation of LAMP1-GFP tubules which we previously characterised as a hallmark of lysosomal regeneration process. Treating these cells with dynasore increased the number of tubules indicating that DNM2 is needed for the cleavage of proto-lysosomal tubules (**Fig 7.22C**). Finally, the depletion of TBC1D15 led to a significant reduction in tubule number and length reconfirming its importance for this whole process (**Fig 7.22D**). Our PTEC/calcium oxalate model therefore confirmed that lysosomal regeneration also takes place under physiological conditions where lysosomes are damaged such as oxalate nephropathy and this process is dependent on TBC1D15.

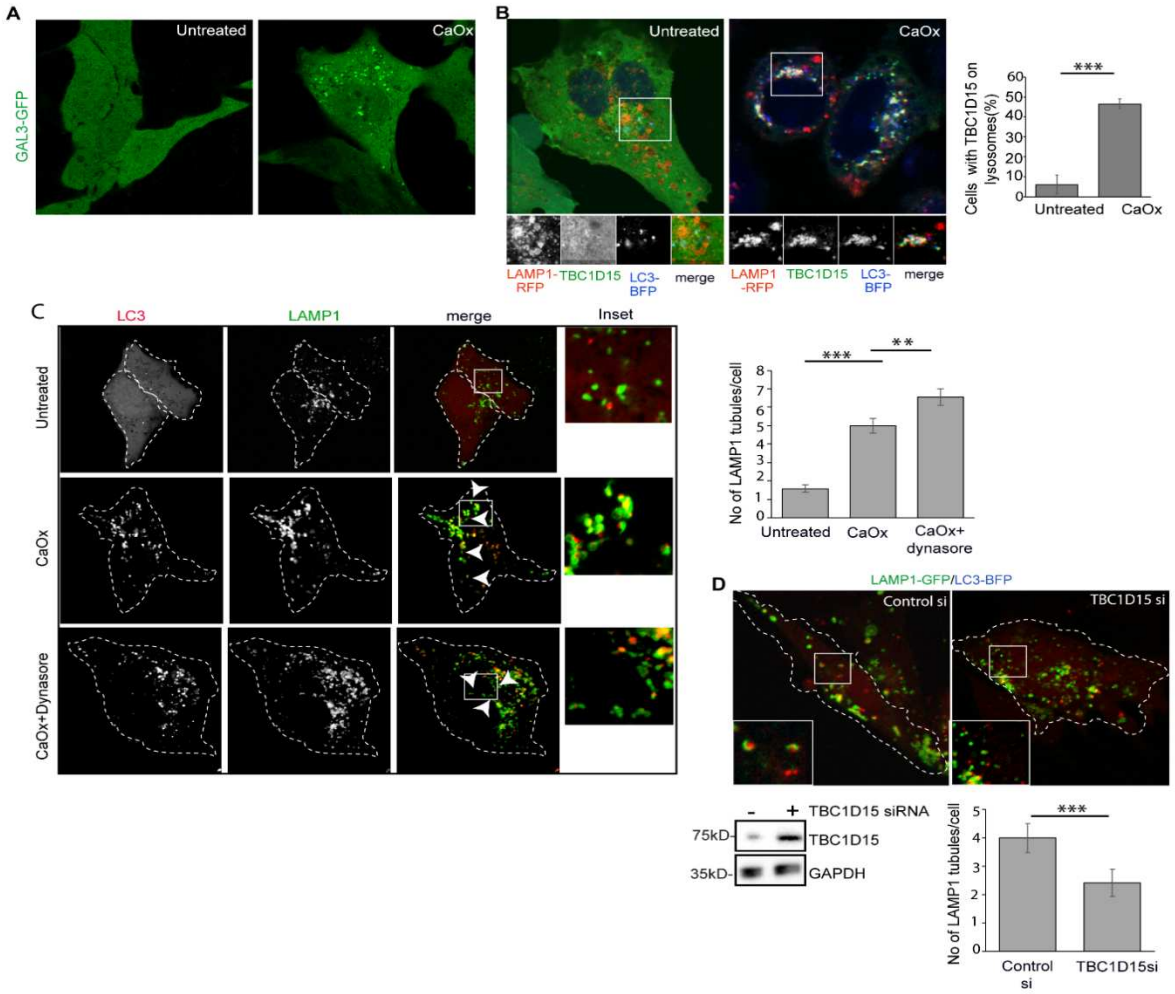

Figure 7.22: TBC1D15 regulates lysosomal tubulation in PTEC cells treated with calcium oxalate. A) PTEC cells expressing GFP-GAL3 were treated with 100 µg/ml calcium oxalate (CaOx) for 2 h to induce lysosomal damage, and the extent of damage was determined by the analysis of GFP-Gal3 puncta. B) PTEC cells were transfected with LAMP1-RFP and LC3-BFP,

and the colocalization of TBC1D15 with LAMP1 was assessed by confocal microscopy based on the staining of endogenous TBC1D15. Data are means ± SEM of at least 100 cells from three independent experiments (***$p \leq 0.001$). C) PTEC cells expressing LAMP1-RFP and LC3-BFP were treated with 100 μg/ml CaOx or 100 μg/ml CaOx plus 20 μM Dynasore to check for lysosomal tubulation events. Data are means ± SEM of 70 cells imaged to determine the number of lysosomal tubules under different conditions (***$p \leq 0.001$, **$0.001 < p \leq 0.01$). D) PTEC cells expressing LAMP1-GFP and LC3-BFP were treated with either control siRNA or siRNA specific for TBC1D15 and then with 1 mM LLOMe to determine the number of LAMP1 tubulation events. Data are means ± SEM of 50 cells counted to compare the two conditions (***$p \leq 0.001$). Knockdown efficiency of TBC1D15 was checked by western blotting.

CHAPTER 8 RESULTS
Serine ubiquitination regulates the autophagy-lysosomal pathway in *Legionella pneumophila* infection

8.1 *Legionella pneumophila* modulate autophagy via the effectors SidE and RavZ

Upon infection cell activates autophagy to degrade invading pathogens, this is also known as xenophagy. To avoid this degradation *L. pneumophila* delipidates ATG8 proteins to block autophagosome formation by using an effector protein named RavZ. This situation is phenotypically similar to ATG8 conjugation-deficient cells. We wanted to investigate the mechanism of this fusion block and according to recent study (Shin et al., 2020), the autophagosomal SNARE proteins STX17 and SNAP29 were identified as putative substrate of PR-linked serine ubiquitination via another effector protein of legionella naming SdeA (**Fig 8.1A, and B**). These two SNAREs are known to be important for autophagosome–lysosome fusion so to determine the effect of SdeA on autophagy, we measured autophagic flux in HEK 293T cells expressing GFP-tagged WT SdeA or a catalytic dead version where the mART domain of this protein was mutated (E860AE862A). Autophagy was activated by the mTORC1 inhibitor Torin-1 for different periods of time, followed by western blotting to detect LC3-II. WT SdeA expressing cells converted LC3-I to LC3-II more slowly than cells expressing catalytically dead SdeA or those transfected with the control vector indicating a slower autophagic turnover rate (**Fig 8.1C, and D**). We also determined the effect of PR-Ub on autophagic flux within infected cells. To this end, we infected HEK 293T cells by *Legionella* strains with various deletions, as previously reported (Choy et al., 2012), and measured LC3-II levels during the course of infection. LC3-II levels appeared to be lower in cells infected with wild-type (WT) bacteria compared to uninfected cells and those infected with a ΔRavZ strain. The inhibition of LC3-II formation was more prominent when cells were additionally treated with bafilomycin A1 indicating a blockade in autophagic turnover. The lack of SidE (ΔSidE and ΔRavZΔSidE) did not affect LC3-II formation in infected cells (**Fig 8.1E**). Next, immunostained endogenous LC3 in A549 cells infected with different strains of *Legionella*. RavZ-deficient bacteria (ΔRavZ and ΔRavZΔSidE) produced a significantly higher number of autophagosomes. Between ΔRavZΔSidE and ΔRavZ, cells infected with ΔRavZ strain had a significantly higher number of autophagosomes compared suggesting that PR-Ub may regulate autophagic flux by modulating the clearance of autophagosomes (**Fig 8.1F, and G**). However, the conversion of LC3-I to LC3-II may not provide a satisfactory direct readout to decipher the role of this modification because *Legionella*-infected cells contained negligible levels of LC3-II due to the presence of RavZ.

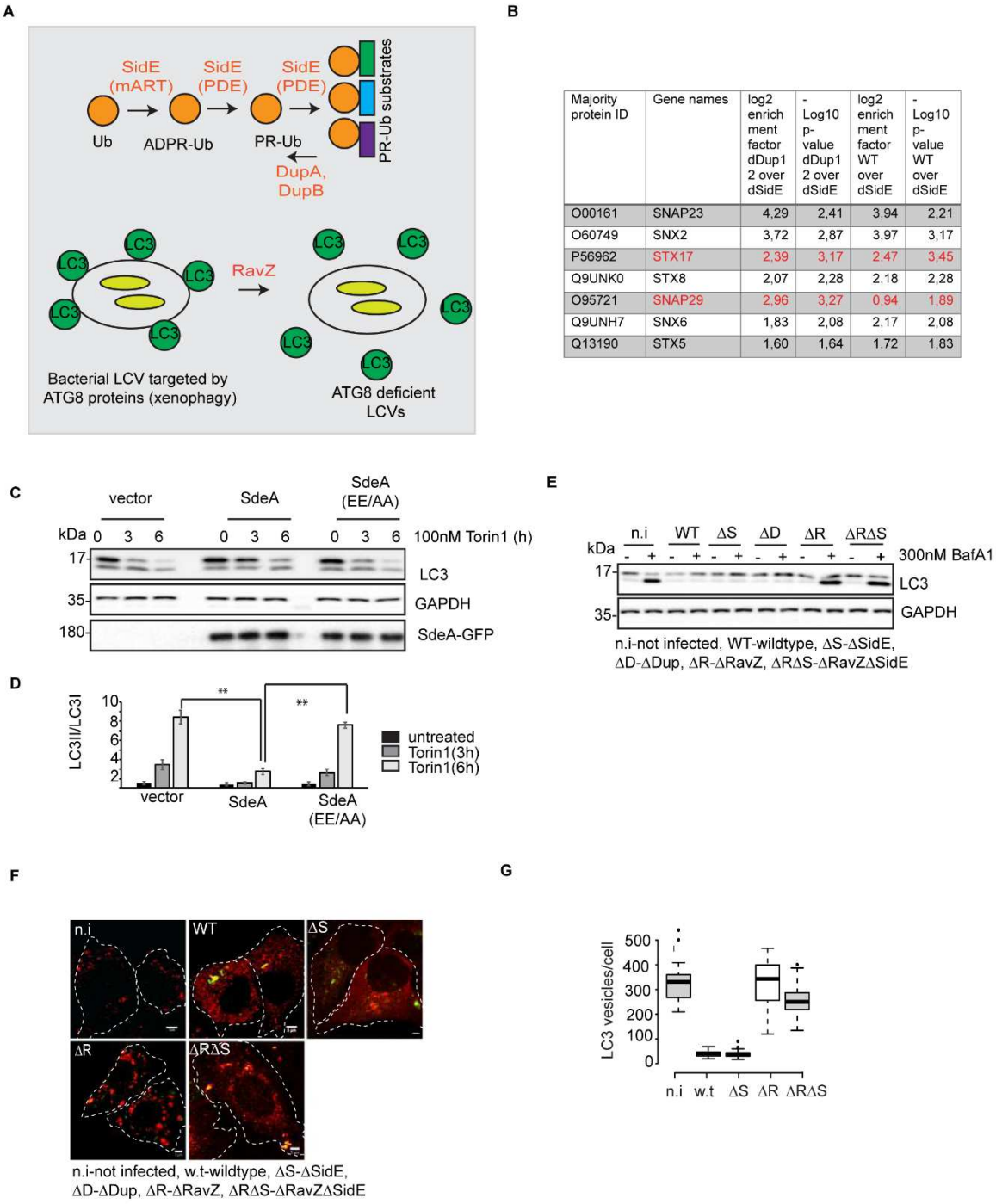

Majority protein ID	Gene names	log2 enrichment factor dDup12 over dSidE	-Log10 p-value dDup12 over dSidE	log2 enrichment factor WT over dSidE	-Log10 p-value WT over dSidE
O00161	SNAP23	4,29	2,41	3,94	2,21
O60749	SNX2	3,72	2,87	3,97	3,17
P56962	STX17	2,39	3,17	2,47	3,45
Q9UNK0	STX8	2,07	2,28	2,18	2,28
O95721	SNAP29	2,96	3,27	0,94	1,89
Q9UNH7	SNX6	1,83	2,08	2,17	2,08
Q13190	STX5	1,60	1,64	1,72	1,83

Figure 8.1: ***Legionella pneumophila*** **regulate autophagy via effectors SidE and RavZ during infection.** A) *Legionella* effectors involved in regulating autophagy. B) SNARE proteins that were identified as PR-Ub substrates (Shin et al., 2020). C) HEK 293T cells were transfected with SdeA, its catalytic mutant SdeA(EE/AA) or a control vector for 16 h. Cells were treated with 100 nM Torin-1 as shown, then lysed and analysed by western blot to check for LC3 levels. GAPDH was used as a loading control. D) Quantitation of LC3II/LC3I as depicted in panel (C). D) A549 cells were infected with different strains of *Legionella* for 4 h in the presence of 300 nM bafilomycin A1, then lysed and analysed by western blot with antibodies against LC3 (and GAPDH as a loading control). E) A549 cells were infected with *Legionella* strains for 4 h, then endogenous LC3 was immunostained for confocal imaging. F) In the box-plot, centre lines show the medians; box limits indicate the 25th and 75th percentiles as determined by R software; whiskers extend 1.5 times the interquartile range from the 25th and 75th percentiles, outliers are represented by

dots. n = 34, 31 cells. p value was calculated using 2 tailed, type 3 Student's t-test, ***p ≤ 0.001, **0.01 ≤ p <0.001. Scale bar: 5µm.

8.2 STX17 is modified by serine ubiquitination

Given its role in the initial steps of phagophore formation (preceding LC3 conjugation) we focused on dissecting the role of STX17. This protein was also reported to form autophagosomes in the absence of LC3 (Tsuboyama et al., 2016). STX17 was identified as a putative PR-ubiquitination substrate for SidE proteins (Shin et al., 2020). To confirm this, we checked for PR-ubiquitination of STX17 in infected cells. HEK 293T cells expressing FLAG-STX17 showed significantly higher level of PR-ubiquitination after infecting the cells with *Legionella* (**Fig 8.2A**). Furthermore, wild-type SdeA could induce PR-ubiquitination of STX17 but not the inactive mART mutant. This modification was lost when lysates were treated *in vitro* with WT DupA (**Fig 8.2B, and C**).

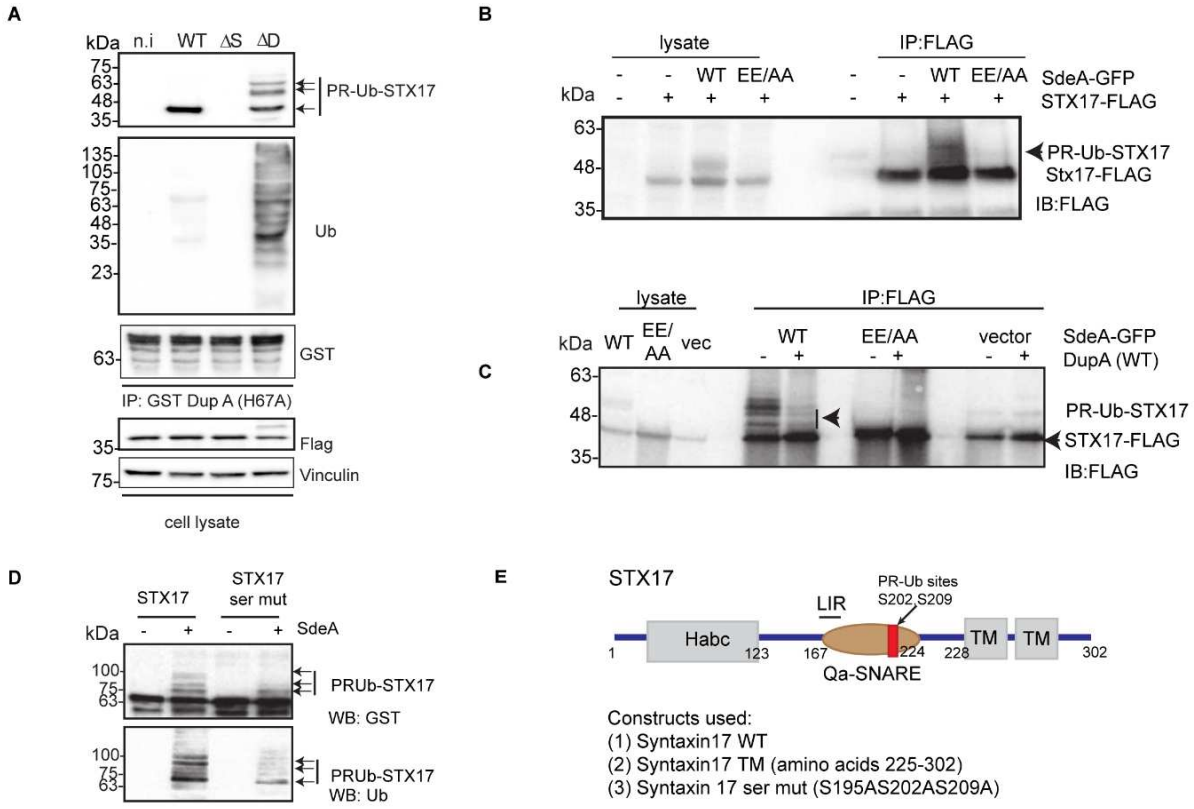

Figure 8.2: ***Legionella pneumophila*** **modifies STX17 by PR-ubiquitination.** A) HEK 293T cells expressing FLAG-STX17 were infected with different strains of *Legionella* for 2 h. Lysates were used for GST pulldown with the DupA trapping mutant GST-DupA(H67A), followed by western blots with antibodies against FLAG, GST and ubiquitin. Whole cell lysates were blotted with antibodies against FLAG and vinculin as a loading control. B) HEK 293T cells were co-transfected with FLAG-STX17 and GFP-tagged SdeA/SdeA(EE/AA) or a control vector for 16 h. FLAG-STX17 was immunoprecipitated using FLAG resin and analysed by western blot using antibodies against FLAG to detect PR-Ub-modified and unmodified FLAG-STX17. C) HEK 293T cells were co-transfected with FLAG-STX17 and GFP-tagged SdeA/SdeA(EE/AA) or a control vector and immunoprecipitated as shown in panel (B). The samples were then treated with or without pure DupA for 1 h before western blotting with antibodies against FLAG to detect PR-Ub-modified and unmodified FLAG-STX17. D) GST-STX17 and GST-

STX17(S195AS202AS209A) were incubated with or without SdeA in the presence of 1 mM NAD^+ and ubiquitin for 1 h. The samples were analysed by western blot using antibodies against ubiquitin and GST to detect PR-Ub. E) Domain architecture of Syntaxin17 showing the serine ubiquitination sites.

Next, we wanted to identify the serine residues of STX17 which were modified by SdeA. We utilized in an *in vitro* ubiquitination assay where we purified GST-STX17 from *Escherichia coli* and incubated this with pure SdeA, ubiquitin and NAD^+ (**Fig 8.2D**). The products of this *in vitro* PR-Ub assay were analysed by high-resolution electron-transfer dissociation mass spectrometry (ETD-MS) which revealed two STX17 serine residues (S202 and S209) linked to PR-Ub (**Fig S1**). By analysing the STX17 amino acid sequence, we found both PR-Ub sites to be located within the Qa-SNARE domain of STX17 (**Fig 8.2E**).

8.3: Triple serine mutant of STX17 has severe reduction in PR-Ub.

Mutating three serine residues GFP-STX17 (S195AS202AS209A) resulted in significant reduction the PR-ubiquitination of STX17 in cells infected with WT or ΔSidE *Legionella* strains (**Fig 8.3**). The transmembrane hairpins of STX17 (STX17TM) are necessary and sufficient for its localization to the autophagosome (Itakura et al., 2012). STX17TM-GFP was not modified by PR-Ub in infected cells (**Fig 8.3**).

8.4 Serine ubiquitination of STX17 by *Legionella* facilitates the formation of $STX17^+$ pre-autophagosomes that are recruited to bacterial vacuoles.

After confirming the modification of STX17, we wanted to investigate the formation of $STX17^+$ autophagosomes in A549 cells infected for 2 h with different strains of *Legionella*. STX17 was seen to be predominantly distributed in the ER of uninfected cells but the induction of autophagy by adding Torin-1 caused STX17 to form autophagosomal puncta as expected. Infection with WT *Legionella* led to the formation of STX17-GFP vesicles, but cells infected with RavZ-deficient *Legionella* strains (ΔR or ΔRΔS) contained a significantly higher number of $STX17^+$ vesicles due to the unhindered formation of $ATG8^+$ autophagosomes. However, the

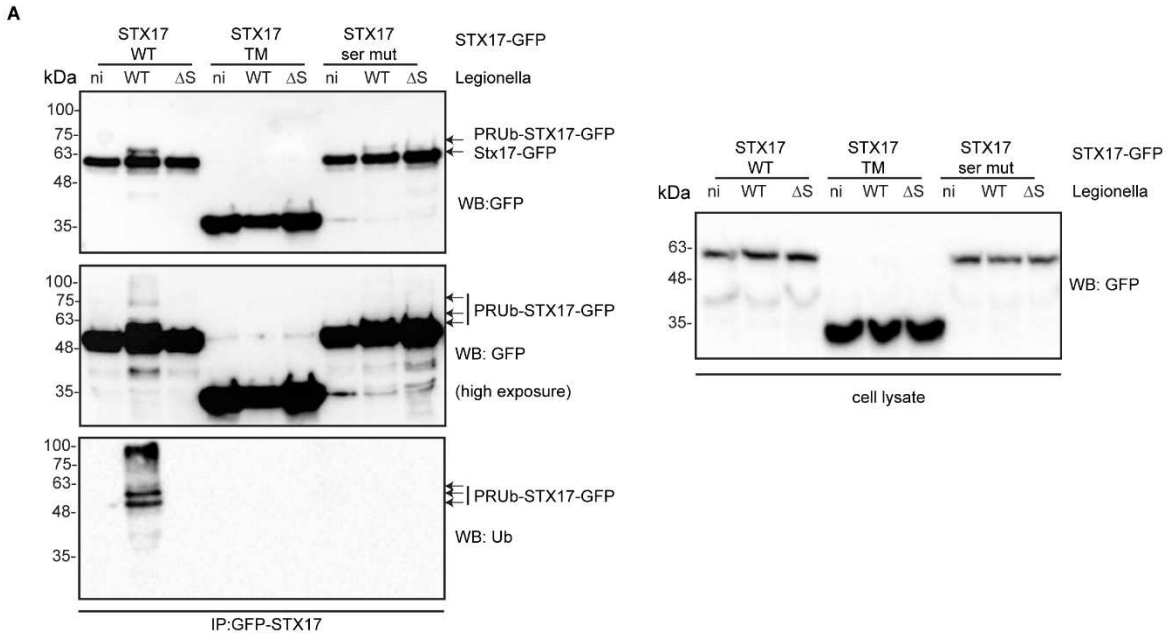

Figure 8.3: Validating the serine residues of STX17 which are modified by PR-Ub during *Legionella* infections. HEK 293T cells were transfected with GFP-tagged WT STX17, STX17TM, or the STX17 serine mutant (S195AS202AS209A) followed by *Legionella* infection for 2 h. STX17 was then immunoprecipitated using anti-GFP beads followed by western blotting with antibodies against GFP and ubiquitin. Cell lysates were analysed by western blot with an antibody against GFP to check the expression levels of GFP-STX17 constructs.

number of vesicles were significantly lower in cells infected with the ΔS strain. This observation indicates that STX17$^+$ vesicles formed during infections with WT *Legionella*, even in the absence of LC3, and were actually dependent on PR-Ub (**Fig 8.4A**). Interestingly, we also observed PR-Ub-dependent of STX17 led to its recruitment to bacterial vacuoles in cells infected with WT and ΔR *Legionella*, whereas STX17 did not localize to bacterial vacuoles in cells infected with SidE deletion strains (ΔS and ΔRΔS) (**Fig 8.4A**). This experiment was repeated in cells expressing the STX17-GFP serine mutant (S95S202AS209A) where the formation of STX17$^+$ autophagosomal puncta seemed to be significantly reduced following infection with either WT or ΔS *Legionella* strains. The lack of serine ubiquitination also blocked the recruitment of mutant STX17 to bacterial vacuoles (**Fig 8.4B**). STX17TM-GFP, which was not modified by PR-Ub in infected cells, still formed autophagosomal puncta in cells infected with the ΔRavZ strain of *Legionella* (**Fig 8.4C**). We also could spot STX17 recruitment to bacterial vacuoles using transmission electron microscopy (**Fig 8.4D**). All these results shows that modification of STX17 by serine ubiquitination facilitates the formation of STX17$^+$ vesicles, which may be constituents of the early bacterial vacuole (2 h post-infection).

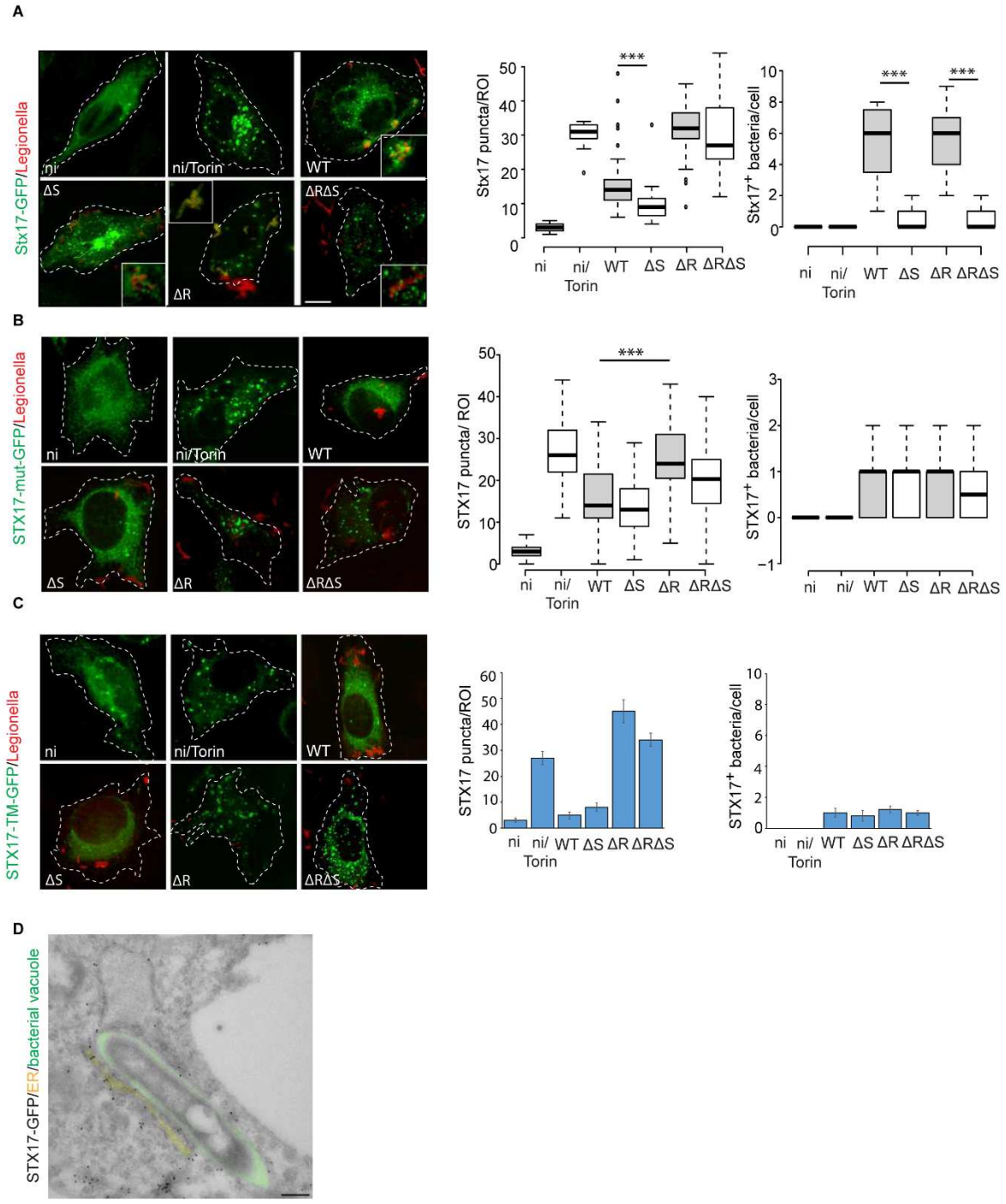

Figure 8.4: Modification of STX17 by PR-ubiquitination lead to the formation of STX17 positive vacuoles which are recruited to bacteria. A) A549 cells expressing STX17-GFP were infected with *Legionella* strains for 2 h before fixation and immunostaining with a *Legionella*-specific antibody for analysis by confocal microscopy. Control cells were treated with 300 nM Torin-1 for 4 h. The number of $STX17^+$ puncta in 50-μm^2 regions of interest and the number of $STX17^+$ bacteria per cell were counted for ~50 cells in three different experiments. In the box-plots, center lines show the medians; box limits indicate the 25^{th} and 75^{th} percentiles as determined by R software; whiskers extend 1.5 times the interquartile range from the 25^{th} and 75^{th} percentiles, outliers are represented by dots. N = 52, 56 cells. p value was calculated using 2 tailed, type 3 Student's t-test, ***$p \leq 0.001$. Scale bar: 5µm. B) A549 cells expressing the PR-Ub-deficient mutant of STX17-GFP were infected with *Legionella* strains for 2 h before fixation and immunostaining with *Legionella*-specific antibodies for confocal imaging. Control cells were

treated with 300 nM Torin-1 for 4 h. We counted $STX17^+$ puncta in 50-μm^2 regions of interest and the number of $STX17^+$ bacteria per cell. In the box-plot, center lines show the medians; box limits indicate the 25th and 75th percentiles as determined by R software; whiskers extend 1.5 times the interquartile range from the 25th and 75th percentiles. n >50 cells taken from 3 independent experiments. p value was calculated using 2 tailed, type 3 Student's t-test, ***$p \leq 0.001$. Scale bar: 5μm. C) The experiment is panel (A and B) was repeated in cells expressing STX17TM-GFP. Control cells were treated with 300 nM Torin-1 for 4 h. We counted $STX17^+$ puncta in 50-μm^2 regions of interest and the number of $STX17^+$ bacteria per cell. The data are means ± SEM of 20 cells in two different experiments. (ni-not infected, WT-wild-type *Legionella*, ΔS-ΔSidE, ΔR-ΔRavZ, ΔRΔS-ΔRavZΔSidE *Legionella*). D) HeLa cells were transfected with STX17-GFP for 16h, followed by *Legionella* infection for 4 h. Cells were fixed and subjected to transmission electron microscopy after gold labelling of GFP tag in cells. Bacterial vacuole is marked in green, ER like membranes are marked in yellow.
(Transmission electron microscopy in Figure 8.4D was performed by Tineke veenendaal and Judith Klumperman)

8.5 $STX17^+$ vesicles are originated from the Golgi body in a PR-Ubiquitination dependent manner.

It has been previously reported that upon serum starvation STX17 translocate from the ER to the Golgi body where it associates with FIP200 and ATG13 to form pre-autophagosomal structures (Kumar et al., 2019). To determine whether PR-Ub of STX17 is affecting this phenomenon, we co-stained *Legionella*-infected cells for STX17 and the Golgi marker GM130. While in uninfected cells, STX17 was seen to be localized to the ER, infection with WT *Legionella* caused it to spread beyond the ER to the Golgi body, and also resulted in the formation of $STX17^+$ vesicles. Infection with ΔS *Legionella* significantly increased the colocalization of STX17 with GM130 compared to the WT strain, and fewer $STX17^+$ vesicles were observed. Treating cells with brefeldin A, which inhibits protein transport from the ER to the Golgi body, blocked the formation of $STX17^+$ vesicles in cells infected with WT *Legionella* (**Fig 8.5A, and B**). The formation of $STX17^+$ autophagic vesicles as well as the recruitment of STX17 to bacteria were also reduced in cells treated with the PI3K inhibitor wortmannin (**Fig 8.5C**). These results suggest upon that *Legionella* infection, STX17 translocate from the ER to the Golgi body and the PR-Ub of STX17 is important for the formation of $STX17^+$ pre-autophagosomes from the Golgi body.

8.6 The serine ubiquitination of STX17 is important for bacterial replication

As the serine ubiquitination led to the recruitment of STX17 to bacterial vacuoles, we used an intracellular *Legionella* replication assay in A549 cells depleted of endogenous STX17 to determine the importance of STX17 for intracellular bacterial replication. Depletion of endogenous STX17 by using a specific siRNA for 48 h before infection led to a decrease of intracellular bacterial load compared to mock siRNA treatment. This effect was negligible in cells

infected with the Δ*S Legionella* strains, indicating that the bacterial replication process is dependent on PR-Ubiquitinated STX17 (**Fig 8.6A**).

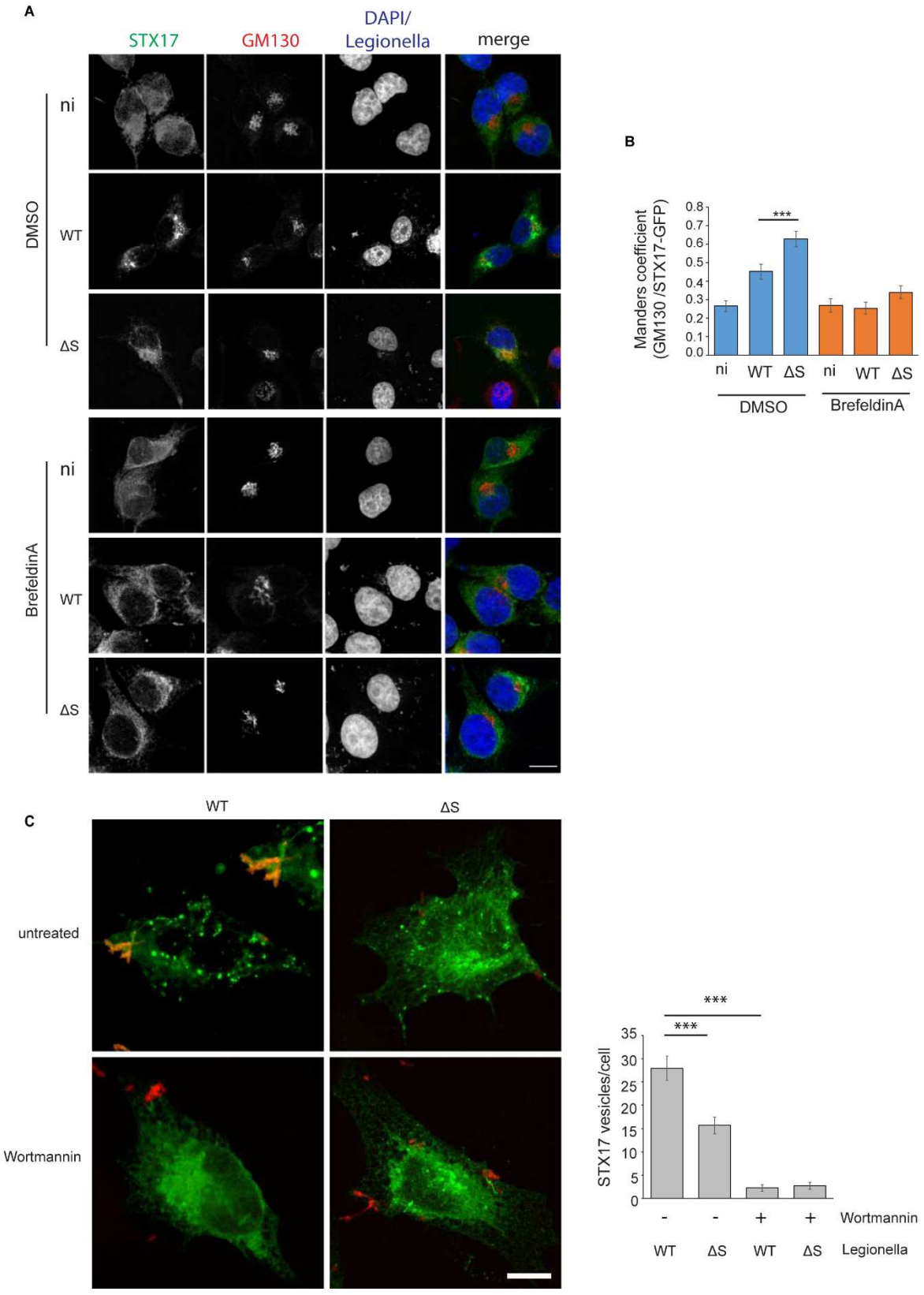

Figure 8.5: The formation of STX17^{+} vesicles is blocked by inhibiting ER-to-Golgi transport with brefeldin A and PI3K with wortmannin. A) A549 cells expressing STX17-GFP were

infected with *Legionella* (WT/ΔS) for 2 h in the presence or absence of 100 nM brefeldin A before fixation and immunostaining with antibodies against the Golgi marker GM130 and *Legionella*. Scale bar:10µm. B) The colocalization of STX17-GFP and GM130 was measured in the images from panel (A) by calculating the Manders coefficient in FIJI. The Manders coefficient in the left set of bars (blue) represents the proportion of GM130 pixels that are $STX17^{+}$. The Manders coefficient in the right set of bars (orange) represents the proportion of calnexin pixels that are $STX17^{+}$. The data are means ± SEM of Manders coefficient counted from 30 cells taken from 3 experiments (***$p \leq 0.001$). C) A549 cells expressing STX17-GFP were infected with *Legionella* (WT/ΔS) for 2 h in the presence or absence of 100 nM wortmannin before fixation and immunostaining with antibodies against *Legionella*. Scale bar:5µm. (ni-not infected, WT-wild-type *Legionella*, ΔS-ΔSidE *Legionella*)

This phenotype could only be rescued with WT STX17 but not with the PR-Ub-deficient mutant (S95S202AS209A) (**Fig 8.6B**). The immunostaining of LCVs 12 h post-infection revealed that bacterial vacuoles were indeed larger in cells infected with WT compared to ΔS *Legionella*, and in untreated cells compared to those treated with STX17 siRNA (**Fig 8.6C**).

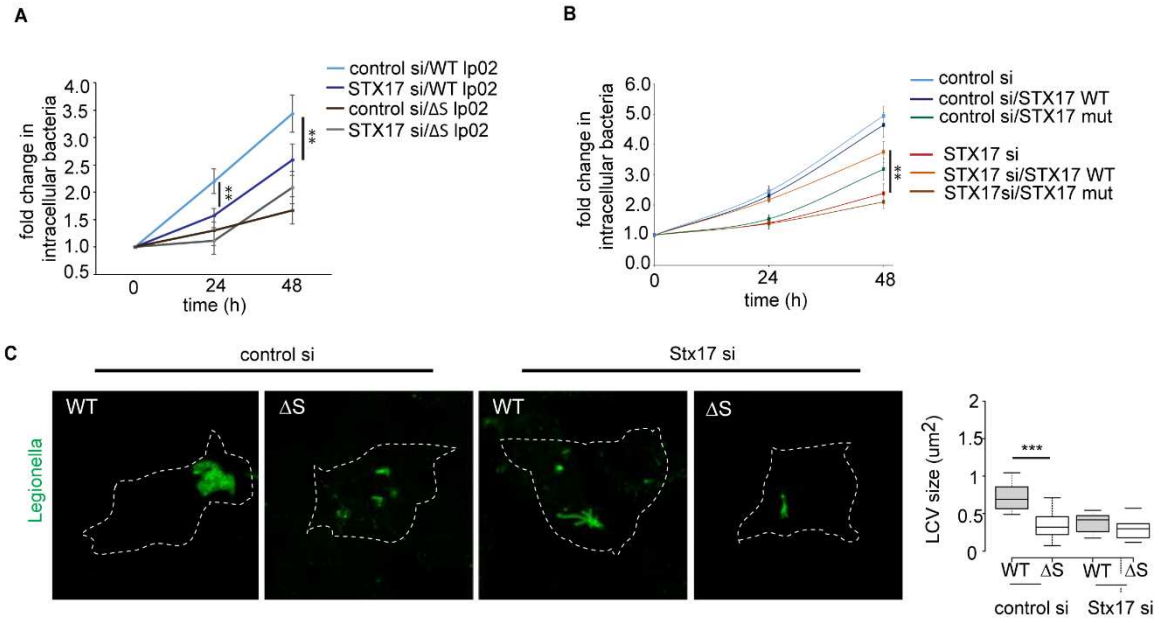

Figure 8.6: Serine ubiquitination of STX17 is important for LCV biogenesis and bacterial replication. A) A549 cells were treated with control or STX17 siRNA for 48 h followed by infection with WT or ΔS *Legionella*. Intracellular bacterial replication was assessed after 0, 24 and 48 h. Data are means ± SEM of three independent experiments. p value was calculated using 2 tailed type 3 Student's t-test, p 0.001 < **$p \leq 0.01$. B) A549 cells were treated with STX17 or control siRNA for 48 h followed by transfection with WT or PR-Ub-deficient STX17 for 24 h. Intracellular bacterial replication was assessed after 0, 24 and 48 h. Data are means ± SEM of three independent experiments (0.001 < **$p \leq 0.01$). C) A549 cells were treated with STX17 or control siRNA for 48 h followed by infection with WT or ΔS *Legionella* for 12 h (MOI = 1). Cells were fixed for immunostaining with a *Legionella*-specific antibody followed by confocal microscopy. The LCV size was estimated in FIJI. In the box-plot, centre lines show the medians; box limits indicate the 25th and 75th percentiles as determined by R software; whiskers extend 1.5 times the interquartile range from the 25th and 75th percentiles, outliers are represented by dots. n = 32, 31 cells taken from 3 independent experiments. p value was calculated using 2 tailed, type 3 Student's t-test, ***$p \leq 0.001$. (WT-wild-type *Legionella*, ΔS-ΔSidE *Legionella*)

8.7 Proximity labelling of STX17 reveals different components of the autophagic and endosomal pathways to be in close proximity of STX17 after infection

To investigate the role of STX17 in bacterial replication, we carried out STX17 proximity labelling experiments using infected cells. HeLa cells expressing doxycycline-inducible APEX2-STX17 were infected with WT, ΔS, ΔR or ΔRΔS *Legionella* for 1 h, followed by H_2O_2 treatment and MS analysis of the biotin-labelled proteome (**Fig 8.7A**). Samples were analysed by 6-plex tandem mass tag (TMT) labelling for all cases. Comparing between WT infected cells and uninfected cells (**Fig 8.7B**), the biotin-labelled proteome of STX17 included proteins representing the interconnected autophagic, secretory and endocytic pathways (**Fig. 8.7C, and D**). Proteins that were significantly enriched by infection with WT *Legionella* compared to uninfected cells included those related to autophagy (ATG3, ATG16L and BECN1), endocytosis (RAB5C, RAB8A, HGS1 and TFRC), ER-to-Golgi trafficking (ERGIC1, SEC23A, COPG1 and COPG2) and the Golgi and *trans*-Golgi network (STT3A, STT3B, LMAN2, B4GALT1, RAB34, ARF3 and ARF4). In uninfected cells, STX17 were in proximity with ER proteins, components of the protein translation machinery and ribosomal components (SIGMAR1, EIF2, SRP9, SRP14, RPL35, RPL23 and RPL14) (**Fig 8.7C, and D**).

8.8 Biotin labelled interaction landscape of STX17 in Legionella infection (WT and ΔS Legionella strains)

Comparing the biotin labelled-interaction landscape of infections with WT and ΔS *Legionella* strains, we observed the enrichment of proteins related to autophagosome formation (PIK3C3, PIK3C2, BECN and ATG16L), endocytosis (HGS, TFRC, AP2M1, AP2B1 and SNX6), and the *trans*-Golgi network (ARF6, ARF1, RAB10 and M6PR) in WT infections, whereas STX17 preferentially interacted with proteins of the ER-Golgi intermediate compartment (ERGIC) and Golgi body (SEC23B, SEC24C, SEC31A, ERGIC2, GOLGA2, GOLGA5, LMAN2 and LMAN1), SNARE proteins needed for vesicle fusion (SNAP29 and SNAP47), components of the HOPS complex needed for lysosomal fusion (VPS41, VPS18 and VPS11) and mitochondrial proteins (MAVS, MFN2 and TIMM21) in infections with the ΔS strain (**Fig 8.8A, and B**).

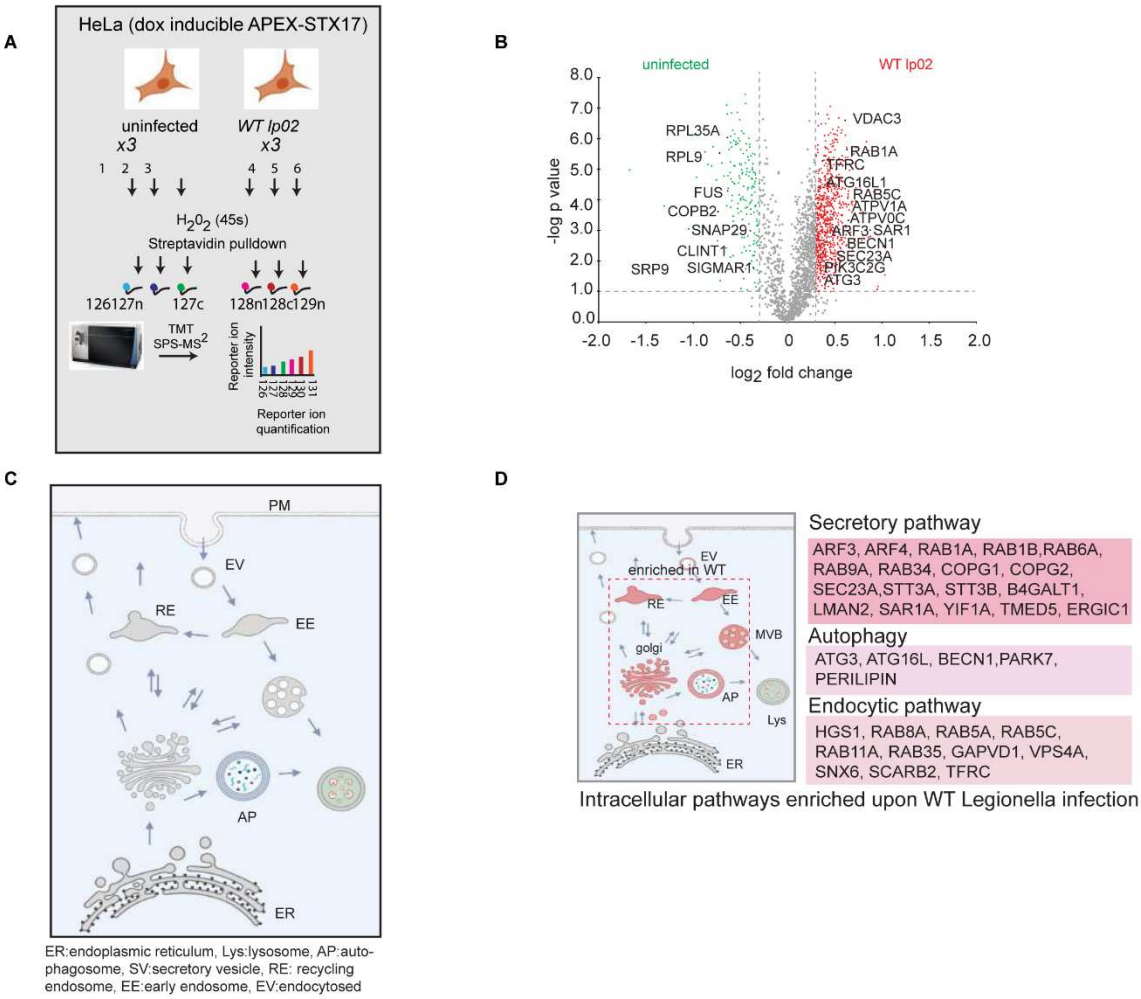

Figure 8.7: Proximity labelling of STX17 reveals serine ubiquitination-dependent changes in the STX17 neighbourhood in the absence of LC3 conjugation. A) Proximity labelling assay workflow. HeLa cells expressing doxycycline-inducible APEX-STX17 were infected with *Legionella* for 2 h before treatment with biotin-tyramide and H_2O_2 followed by streptavidin pulldown. The samples were reduced, alkylated and digested with trypsin before MS analysis. Samples representing three biological replicates each of non-infected and *Legionella*-infected cells were analysed in a single reaction by 6plex TMT labelling. B) Volcano plot showing how the biotin-labelled proteome changes when HeLa cells expressing APEX-STX17 are infected with WT *Legionella* for 2 h. C) Depiction of cross-talk between the autophagic, endocytic and secretory pathways in the cell. D) Pathways and proteins enriched in WT *Legionella* infection (compared to uninfected cells) revealed by Gene Ontology analysis of the MS data from panel (B). Compartments marked in red include proteins that are enriched during a WT *Legionella* infection. Western blots of these samples after streptavidin pulldown showed the proximity of STX17 to different autophagy related proteins such as autophagy initiation factors (FIP200, ATG13, ULK1, ATG14L and Beclin1), the PI3P binding protein WIPI2, and the LC3 conjugation machinery (ATG5, ATG12 and ATG16L) in cells infected with WT *Legionella* but not in uninfected cells or those infected with ΔS strains. Proteins of the endosomal pathway (Rab5 and EEA1) were also enriched in the pulldown fraction of cells infected with WT *Legionella*. On the other hand, STX17 did not interact with autophagosomal SNARE components (VAMP8 and SNAP29) in cells infected with WT *Legionella*, and association with the lysosomal marker LAMP1 was less

prevalent (**Fig 8.8C**). Moreover, the interaction between STX17 and the autophagosome initiation machinery peaked after 1 h and was significantly reduced after 2 h post-infection. The interaction of STX17 with WIPI2, the ATG5-ATG12-ATG16 complex and endosomal markers (Rab5 and EEA1) peaked 2 h post-infection but still persisted 3 h post-infection. The interaction between STX17 and the proteins of the autophagic and endosomal pathways was reduced and delayed in absence of PR-Ub, as observed in cells infected with ΔS *Legionella* (**Fig 8.8D, and E**).

8.9 Biotin labelled interaction landscape of STX17 in Legionella infection (ΔRΔS and ΔR Legionella strains)

Next, we compared the biotin-labelled proteome of cells expressing APEX2-STX17 and infected with *Legionella* strains ΔR or ΔRΔS. In the absence of RavZ, autophagy components such as GABARAPL1, ATG16L1 and FIP200 were enriched following infection with the ΔR strain, whereas STX17 interacted with several lysosomal proteins including cathepsins (CTSB and CTSD), LAMP proteins, the mTOR complex (LAMTOR3, LAMTOR5 and TSC2) and the lysosomal V-ATPase (ATP6V0A1, ATP6V0A2, ATPV0C and ATP6V1H) following infection with the ΔRΔS strain (**Fig 8.9A, and B**). To determine whether PR-Ub directly affected the interaction between STX17 and autophagy proteins, we modified GST-STX17 *in vitro* with SdeA and incubated it with HEK 293T cell lysates in a GST-pulldown assay. The presence of PR-Ub on STX17 facilitated its interaction with FIP200, ATG13 and ATG14L, whereas the PR-Ub-deficient mutant of STX17 was not modified by SdeA and these protein–protein interactions were unaffected (**Fig 8.9C**). These results collectively suggest that PR-Ub drives the formation of pre-autophagic vesicles from the Golgi body, which interact with the early endocytic pathway in the absence of lipidated ATG8 proteins.

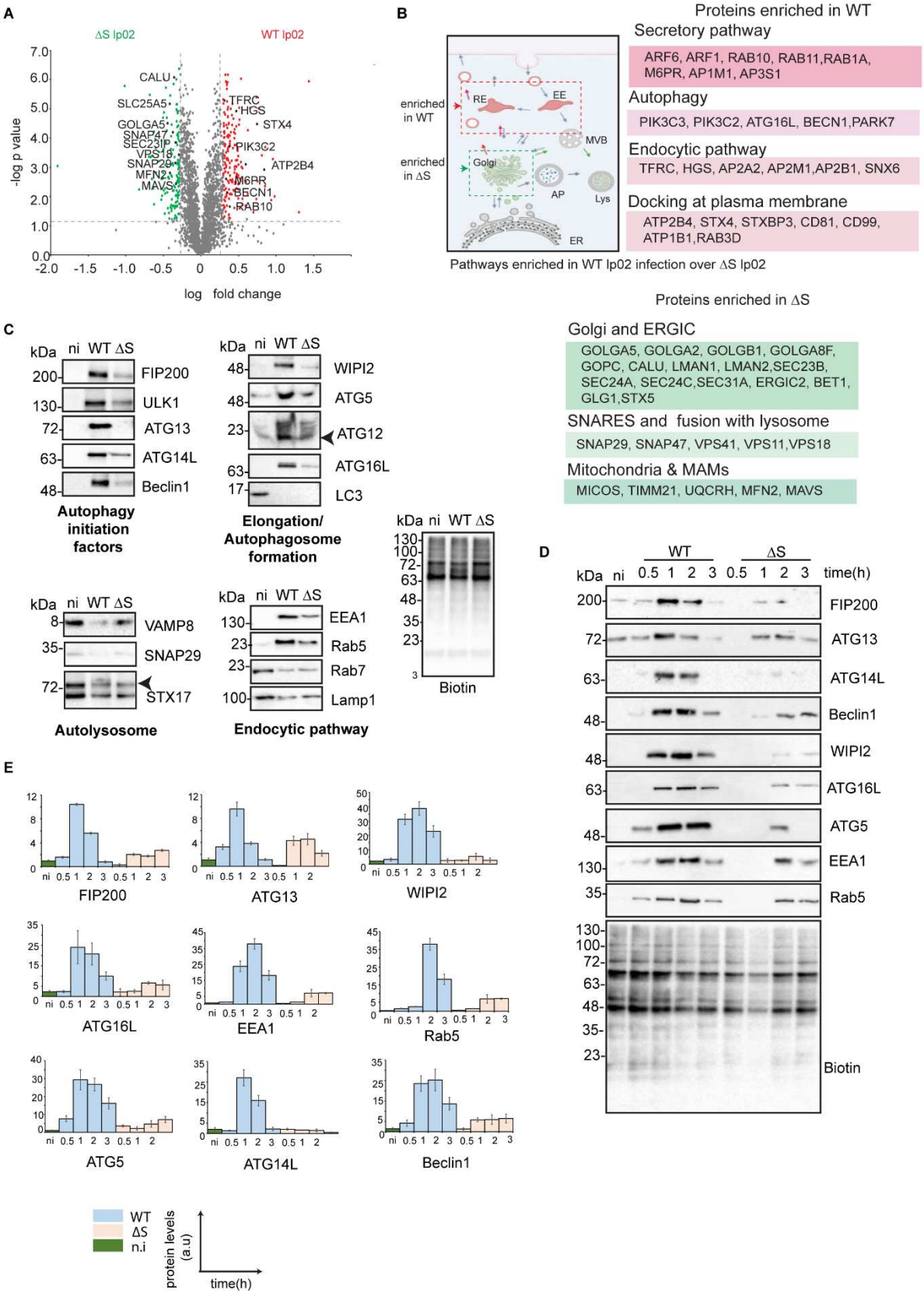

Figure 8.8: Proximity labelling of STX17 reveals differential accumulation of several autophagy factors in a serine ubiquitination-dependent manner. A) Volcano plot showing changes in the biotin-labelled proteome following the infection of HeLa cells expressing APEX-STX17 with WT and ΔS *Legionella* for 2 h. B) GO analysis of the biotin-labelled proteome showing pathways upregulated by infection with WT vs ΔS *Legionella*. Red and green indicate

compartments containing proteins enriched following infection with WT and ΔS *Legionella*, respectively. C) Cells expressing doxycycline-inducible APEX-STX17 were infected with *Legionella* for 2 h before treatment with biotin-tyramide and H_2O_2 followed by streptavidin pulldown. The samples were analysed by western blot with antibodies against proteins of the autophagic and endosomal pathways. D) The experiment in panel (C) was repeated at different time points of *Legionella* infection. E) Graphs represent protein levels determined by western blot analysis. The data are means ± SEM of three independent experiments.

When ATG8 lipidation is possible (infection with ΔRavZ *Legionella* strains), these vesicles can develop into $ATG8^+$ autophagosomes, but the absence of both RavZ and SidE causes the fusion of $STX17^+$ vesicles with lysosomes.

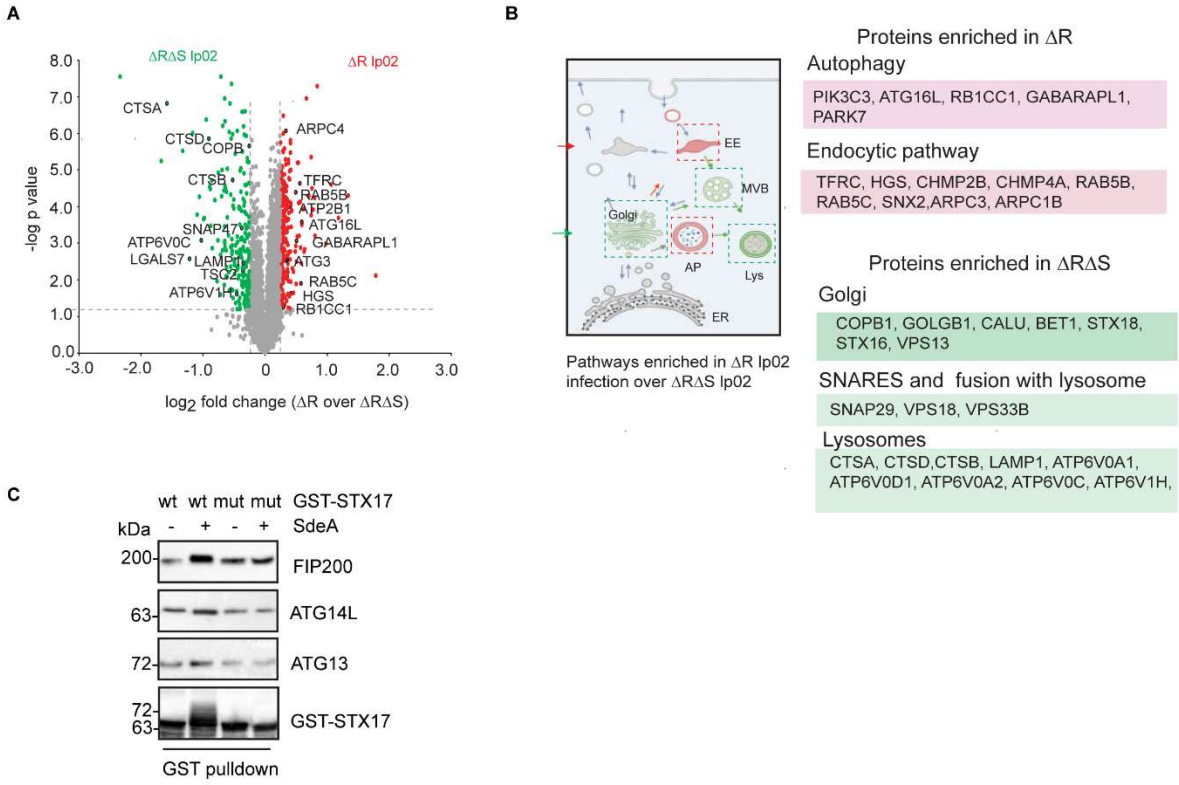

Figure 8.9: STX17 is able to recruit autophagy proteins in a serine ubiquitination-dependent manner. A) Volcano plot showing changes in the biotin-labelled proteome following the infection of HeLa cells expressing APEX-STX17 with ΔR and ΔRΔS *Legionella* for 2 h. B) GO analysis of the biotin-labelled proteome showing pathways upregulated by infection with ΔR vs ΔRΔS *Legionella*. Red and green indicate compartments containing proteins enriched following infection with ΔR and ΔRΔS *Legionella*, respectively. (ni-not infected, WT-wild-type *Legionella*, ΔS-ΔSidE, ΔR-ΔRavZ, ΔRΔS-ΔRavZΔSidE *Legionella*). C) GST-tagged WT or PR-Ub-deficient STX17 was modified by SdeA *in vitro* and incubated with lysates from HEK 293T cells in a GST pulldown assay. The samples were analyzed by western blot with antibodies against ATG14L, ATG13 and FIP200. (ni-not infected, WT-wild-type *Legionella*, ΔS-ΔSidE *Legionella*)

8.10 Identification of proteins recruited to bacterial vacuoles in *Legionella*-infected cells

Having already observed the recruitment of STX17 to bacteria, we sought to determine whether other autophagy markers were also recruited to the bacterial vacuole 2 h post-infection. The early

endosome marker Rab5 was recruited to intracellular bacteria along with autophagosome initiation markers STX17, FIP200 and ULK2, and the LC3 conjugation machinery (ATG5, ATG12 and ATG16L). Surprisingly, the recruitment of Rab5, WIPI2 and ATG5-ATG12-ATG16L was independent of PR-Ub, whereas the recruitment of STX17, FIP200 and ULK2 was dependent on PR-Ub. LC3 was not recruited to either strain of *Legionella* (**Fig 8.10A, and B**). We investigated the recruitment of these proteins to WT *Legionella* at different times post-infection (10 min, 30 min, 1 h, 2 h and 3 h), revealing that Rab5 is recruited first, followed by ATG16L. Bacteria acquire STX17 and FIP200 later (2 h post-infection). Most of the autophagic markers were absent from the bacterial vacuoles 3 h post-infection, and instead they displayed the ER marker calnexin (**Fig 8.10C, and D**).

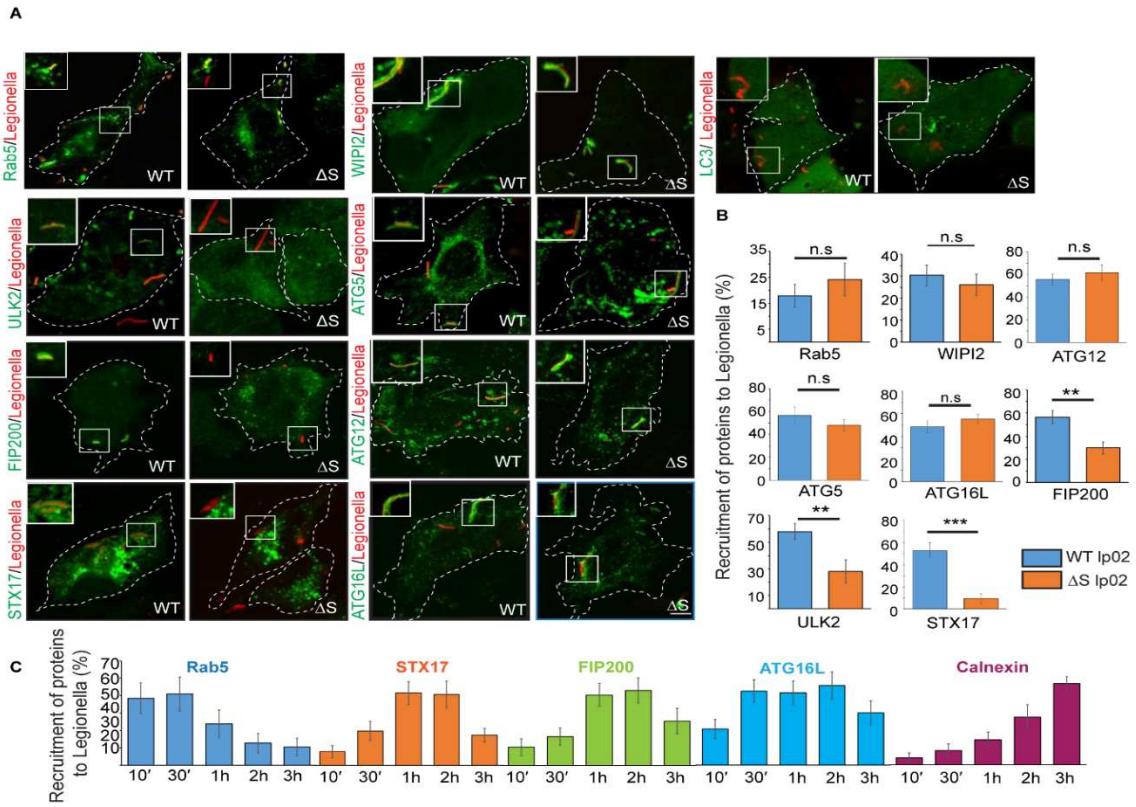

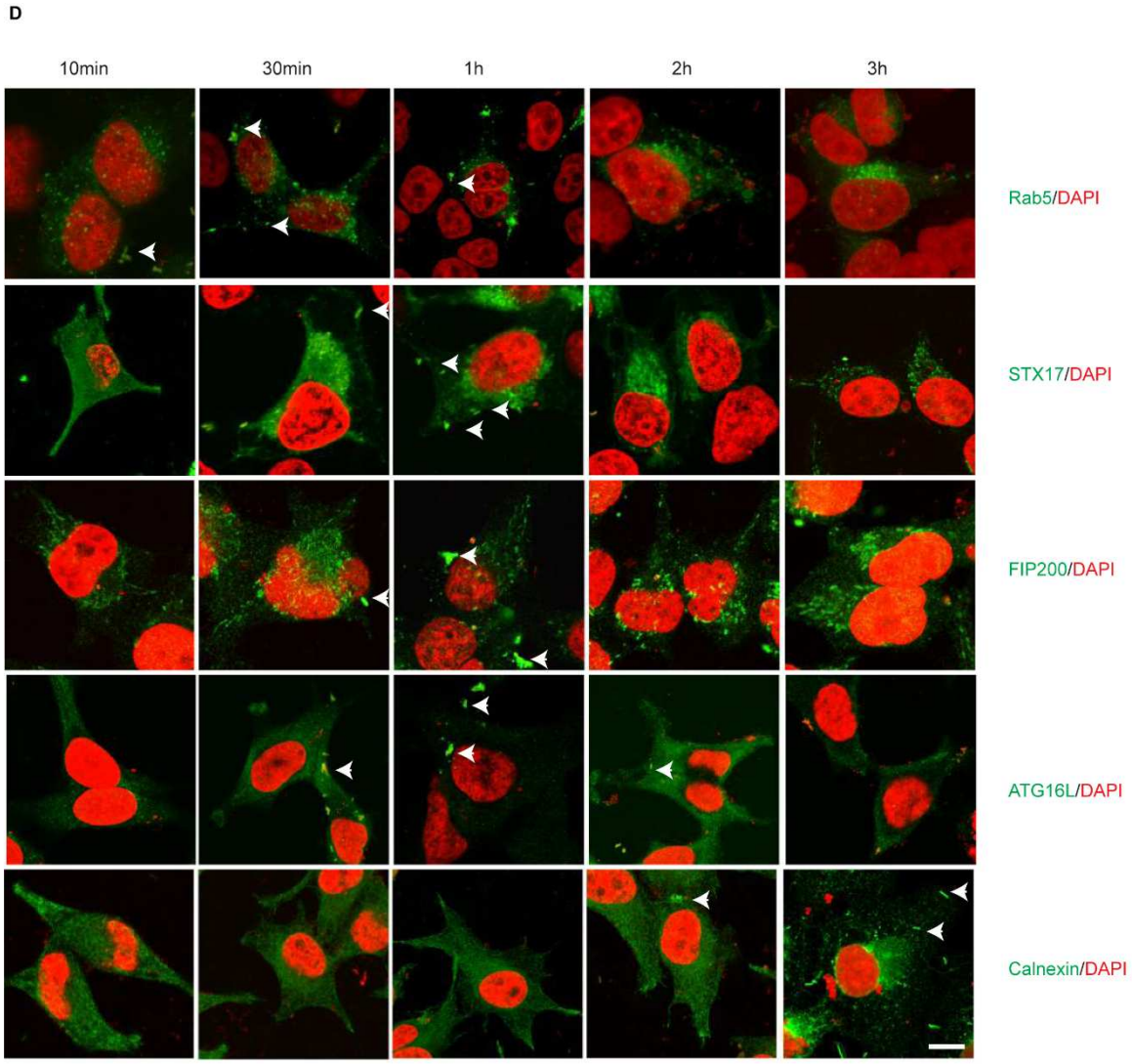

Figure 8.10: Autophagy proteins are recruited to bacteria 1 h post-infection. A) A549 cells were infected with WT or ΔS *Legionella* for 1 h, fixed and immunostained with the indicated antibodies to check for the recruitment of endocytic and autophagic markers to intracellular bacteria. Scale bar: 5µm. B) The experiment in panel (A) was quantified to measure the recruitment of each protein to intracellular bacteria. The data are means ± SEM of 50 cells representing three experiments. p value was calculated using 2 tailed type 3 Students t-test ($0.001 < **p \leq 0.01$, $***p \leq 0.001$). C) The experiment from panel (A) was repeated at different time points (10 min, 30 min, 1 h, 2 h and 3 h) post-infection to monitor the recruitment of Rab5, STX17, FIP200, ATG16L and calnexin. The data are means ± SEM of 50 cells representing three experiments. D) A549 cells were infected with WT *Legionella* for 10 min, 30 min, 1 h, 2 h or 3 h before fixation and immunostaining with antibodies against the indicated endocytic and autophagic markers to check for their recruitment to intracellular bacteria. DAPI counterstaining shows nuclear and bacterial DNA. Scale bar:5µm. (**Imaging in Figure 8.10 was performed by Rukmini Mukherjee)**

8.11 Proximity labelling of the bacterial vacuole

To confirm our immunofluorescence data, we used proximity labelling of the bacterial vacuole in cells fixed 2 h post-infection with WT or ΔS *Legionella*, permeabilized with 0.05% digitonin, and incubated with a *Legionella*-specific antibody to label the vacuole. We then added TurboID-

tagged protein A, which binds the *Legionella* antibody and biotinylates proteins in the vicinity of the bacterial vacuole (**Fig 8.11A**).

Endosomal markers (Rab5 and EEA1) and LC3 conjugation markers (ATG5, ATG16L1 and WIPI2) were found in the proximity of intracellular WT and ΔS *Legionella*. The recruitment of STX17, ATG14L and FIP200 was facilitated by PR-Ub (**Fig 8.11B**). These experiments highlight the role of PR-Ub in the maturation of the bacterial phagosome during the early phase of infection (**Fig 8.11C**).

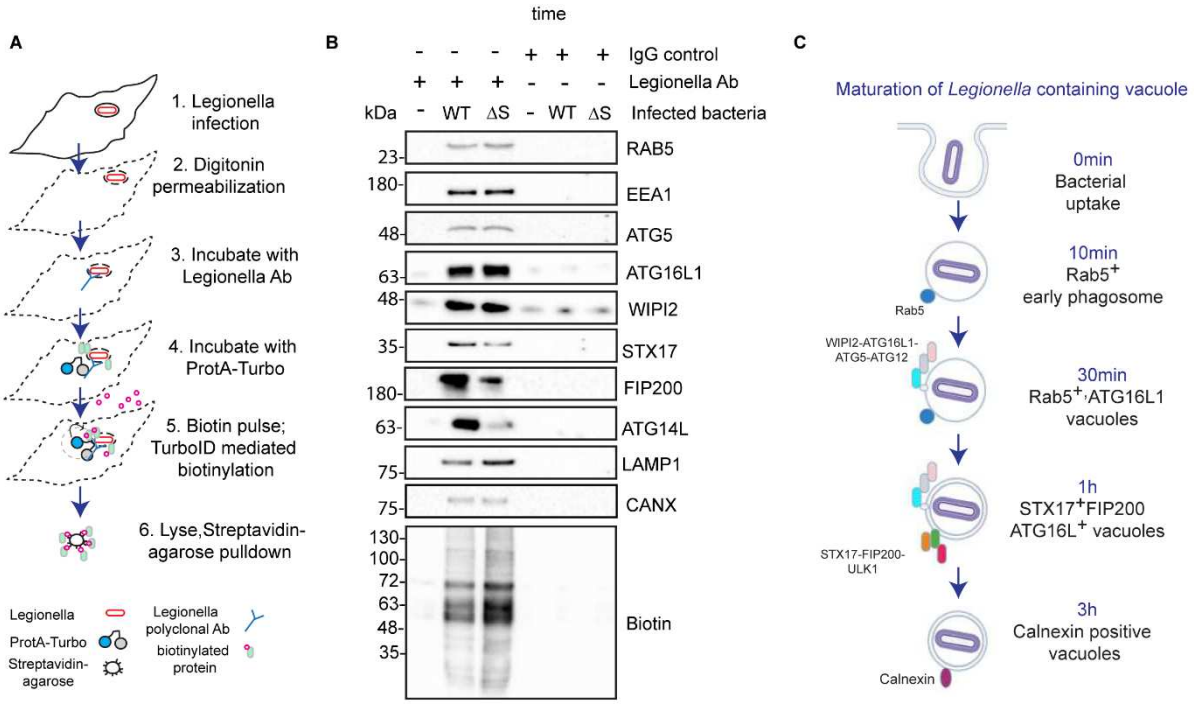

Figure 8.11: Proximity labelling of bacterial vacuole. A) Proximity labelling of bacterial vacuoles in digitonin-permeabilized cells 2 h post-infection. B) Western blots of the indicated proteins after streptavidin pulldown from lysates derived from cells treated with TurboID-ProtA and *Legionella* antibody. C) Schematic illustration showing the maturation of *Legionella*-containing vacuoles after infection. (WT-wild-type *Legionella*, ΔS-ΔSidE *Legionella*)

8.12 PR-ubiquitination of SNAP29 prevents its recruitment to bacterial vacuoles

Given that STX17 is a component of bacterial vacuoles, we investigated whether its SNARE partner (SNAP29) was also recruited to bacteria. SNAP29 is also modified by PR-Ub during *Legionella* infections, as confirmed by enriching for PR-Ub substrates with a GST-DupA(H67A) trapping matrix (Shin et al., 2020; **Fig 8.12A**). The expression of WT SdeA, but not the inactive mART mutant, resulted in the appearance of PR-Ub SNAP29, but the modification was lost when lysates were treated with WT DupA *in vitro* (**Fig 8.12B**). The modification of SNAP29 by *in vitro* PR-Ub followed by high-resolution ETD-MS revealed that residue S63 of SNAP29 is the PR-Ub site (**Fig S2, 8.12C**). The mutation of S63 and the two flanking serine residues (S61AS63AS70A) abolished the modification in infected cells (**Fig 8.12D, and E**).

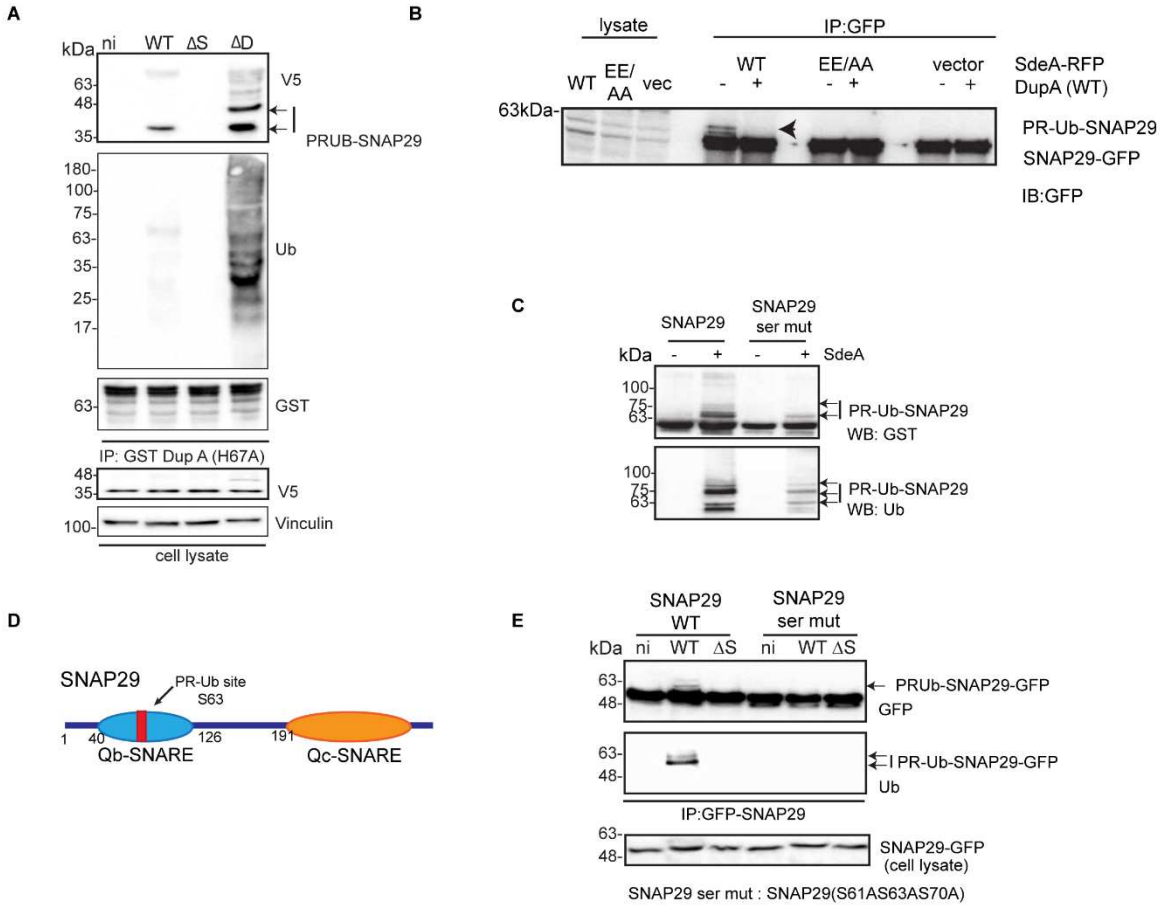

Figure 8.12: SNAP29 is modified by PR-Ub during infection. A) HEK 293T cells expressing V5-SNAP29 were infected with different *Legionella* strains for 2 h. Lysates were used for GST pulldown with the DupA trapping mutant GST-DupA(H67A) followed by western blotting with antibodies against V5, GST and ubiquitin. Whole cell lysates were probed with antibodies against V5 and vinculin as a loading control. **B)** HEK 293T cells were co-transfected with GFP-SNAP29 and HA-tagged SdeA/SdeA(EE/AA) or a control vector for 16 h. GFP-SNAP29 was immunoprecipitated with anti-GFP beads, treated with or without pure DupA for 1 h and analysed by western blot with antibodies against GFP to detect PR-Ub-modified and unmodified SNAP29. **C)** GST-SNAP29 and its PR-Ub-deficient mutant (S61AS63AS70A) were modified with or without SdeA, in the presence of 1 mM NAD^+ and ubiquitin for 1 h. Samples were analysed by western blot with antibodies against ubiquitin and GST to detect PR-Ub. **D)** Domain architecture of SNAP29 showing the serine ubiquitination sites. **E)** HEK 293T cells were transfected with WT SNAP29 or its serine mutant (S61AS63AS70A) followed by *Legionella* infection for 2 h. SNAP29 was immunoprecipitated using anti-GFP beads followed by western blotting with antibodies against GFP and ubiquitin. Cell lysates were probed with an antibody against GFP to check the expression levels of GFP-SNAP29 constructs.

8.13 PR-Ub of SNAP29 blocks its recruitment to intracellular Legionella

SNAP29 is a cytosolic protein that is recruited to autophagosomes when autophagy is induced. However, no SNAP29-GFP puncta were observed in $RavZ^+$ bacteria (WT or ΔS) in which autophagosome formation was blocked because SNAP29 was not recruited to intracellular bacteria in these cells. In absence of RavZ, cells infected with the ΔRΔS strain contained a

significantly greater number of SNAP29 puncta than in ΔR infected cells; also SNAP29 was recruited to bacteria in absence of PR-Ub (in ΔRΔS infection). This difference between ΔR and ΔRΔS strains was insignificant when the PR-Ub-deficient mutant of SNAP29 (S61AS63AS70A) was used (**Fig 8.13A**), suggesting that PR-Ub inhibits the recruitment of SNAP29 to autophagosomes and bacterial vacuoles. Similarly, the formation of SNAP29-GFP puncta was inhibited in Torin-1 treated cells expressing SdeA compared to cells expressing the catalytic mutant of SdeA or a control vector. The PR-Ub-deficient mutant of SNAP29 (S61AS63AS70A) formed autophagosomal puncta in SdeA-expressing cells treated with Torin-1 (**Fig 8.13B**).

8.14 PR-ubiquitination of STX17 and SNAP29 inhibits the formation of autophagosomal SNARE complexes

SNAP29 was not recruited to autophagosomes in the presence of SidE so we determined whether its interaction with other components of the autophagosomal SNARE complex was affected by PR-Ub. Structural rearrangements were recently characterized in the STX17-SNAP29-VAMP8 complex during autophagosome–lysosome fusion (Li et al., 2020). Based on this structure, it was evident that the PR-Ub site of SNAP29 is at the interface that binds STX17 and VAMP8. We added PR-Ub (PDB ID: 5M93) manually to the S63 residue of SNAP29 in the structure of the STX17-SNAP29-VAMP8 complex (7BV6) using Pymol, revealing that the modification is likely to sterically hinder the formation of the four-helix bundle that triggers the fusion of opposing membranes (**Fig 8.14A**). To test this hypothesis, we enriched GST-STX17 and its serine mutant (S195AS202AS209A) on GST resin, and incubated the proteins with lysates from cells infected with *Legionella* ΔDup or ΔSidE strains. GST-STX17, but not the PR-Ub-deficient mutant, was modified by SidE in the ΔDup-infected cell lysates. The interaction of GST-STX17 with both VAMP8 and SNAP29 was inhibited by PR-Ub (**Fig 8.14B**). Similarly, the interaction of GST-SNAP29 with STX17 was inhibited by the PR-ubiquitination of SNAP29, as shown by the stronger interaction of the PR-Ub-deficient SNAP29 mutant (S61AS63AS70A) (**Fig 8.14C**). These results suggest that the PR-ubiquitination of SNAP29 and STX17 in their Qb and Qa domains, respectively, block the formation of the autophagosomal SNARE complex needed for the $STX17^{+}$ autophagosome (or bacterial vacuole) to fuse with the lysosome.

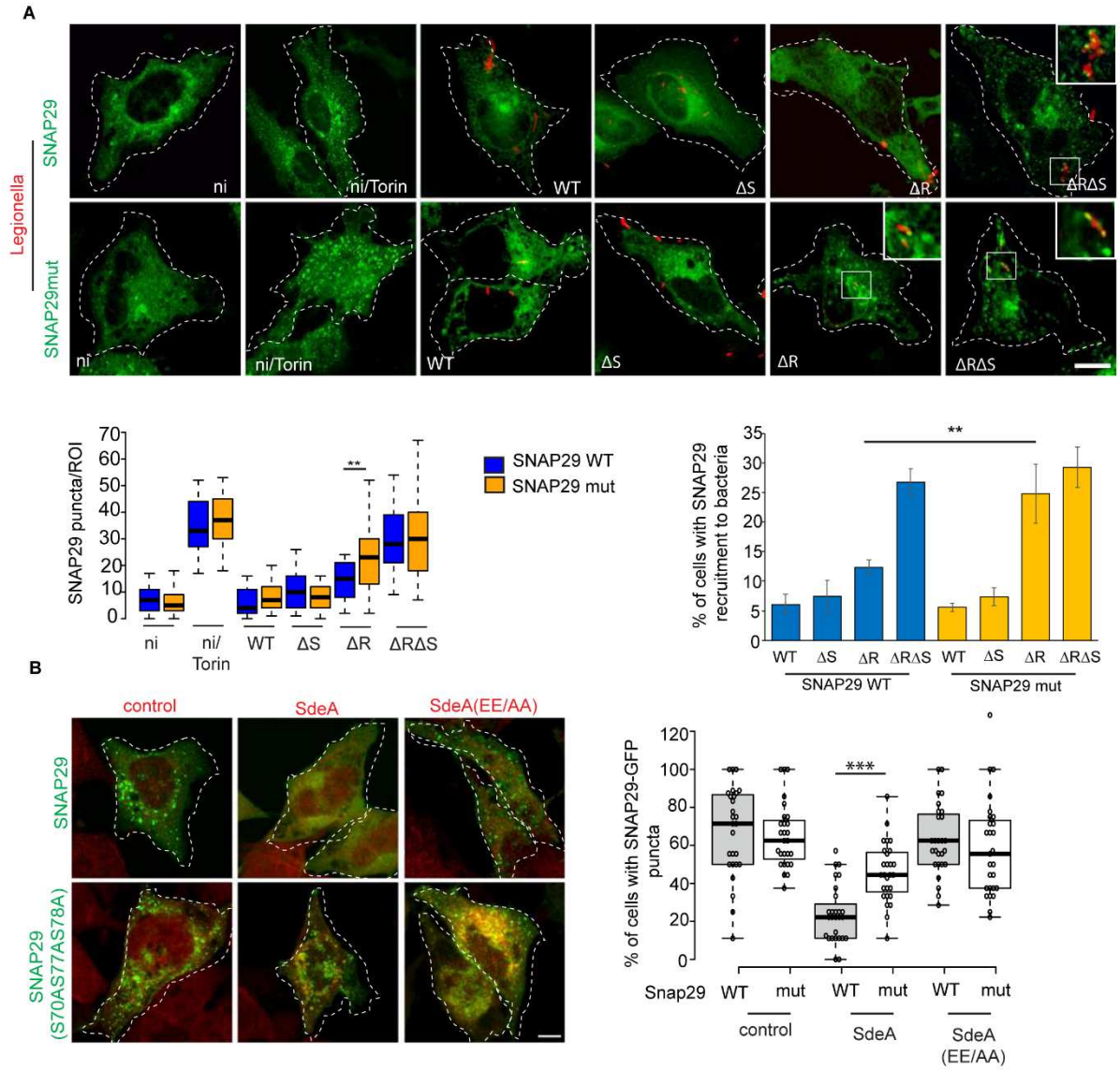

Figure 8.13: Serine-ubiquitinated SNAP29 is not recruited to autophagosomes. HeLa cells were co-transfected with RFP-tagged SdeA or its catalytic mutant (E860AE862A) and GFP-tagged WT SNAP29 or its PR-Ub-deficient mutant. Cells were treated with 300 nM Torin-1 for 4 h to induce autophagy before fixation and confocal imaging. The graph shows the number of cells with SNAP29-GFP puncta counted in FIJI. In the box-plot, centre lines show the medians; box limits indicate the 25th and 75th percentiles as determined by R software; whiskers extend 1.5 times the interquartile range from the 25th and 75th percentiles. n >30 cells taken from 3 independent experiments. p value was calculated using 2 tailed, type 3 Student's t-test, $0.001 < **p \leq 0.01$. In bar graph, the data are means ± SEM of n>30 cells from three independent experiments. Scale bar:5µm. B) The formation of WT and PR-Ub-deficient SNAP29-GFP puncta was monitored in *Legionella*-infected cells 4 h post-infection. SNAP29 puncta were counted in 50-µm^2 regions of interest using FIJI. In the box-plot, centre lines show the medians; box limits indicate the 25th and 75th percentiles as determined by R software; whiskers extend 1.5 times the interquartile range from the 25th and 75th percentiles. n >50 cells taken from 3 independent experiments. p value was calculated using 2 tailed, type 3 Student's t-test, $***p \leq 0.001$. Scale bar: 5µm. (ni-not infected, WT-wild-type *Legionella*, ΔS-ΔSidE, ΔR-ΔRavZ, ΔRΔS-ΔRavZΔSidE *Legionella*)

To check for the fusion of $STX17^+$ autophagosomes with lysosomes, we immunostained LAMP1 in HeLa cells expressing GFP-tagged WT STX17 or the PR-Ub-deficient mutant (S95S202AS209A) along with HA-tagged SdeA or its catalytic mutant (E860AE862A). Cells expressing SdeA produced fewer $STX17^+LAMP1^+$ puncta than cells expressing the catalytic mutant following treatment with 300 nM Torin-1, indicating that autophagosome–lysosome fusion was blocked. Cells expressing the PR-Ub-deficient mutant STX17 contained more $STX17^+LAMP1^+$ puncta, indicating a partial rescue of autophagosome–lysosome fusion (**Fig 8.14D**). We also enriched GFP-tagged $STX17^+$ vesicles from cells, incubated them with or without SdeA to cause PR-ubiquitination, and then mixed them with lysosomes expressing RFP-LAMP1 *in vitro* to screen for vesicle fusion (**Fig 8.14E**). PR-Ub-modified STX17 formed fewer fused or tethered vesicles compared to the control reaction lacking SdeA (**Fig 8.14F**).

8.15 SidE and RavZ are both necessary to block host xenophagy

RavZ and SidE may cooperate to shield bacteria from autophagy, the former conjugating LC3 to autophagosomes and the latter potentially preventing autophagosome–lysosome fusion. We therefore monitored autophagosomal turnover in infected cells treated with combinations of Torin-1 (which induces autophagy) and chloroquine (which blocks lysosomal degradation). The difference in the amount of LC3-II between samples with and without chloroquine represents the level of autophagic flux. LC3-II levels were higher in ΔRavZ-infected cells treated with Torin-1 than ΔRavZΔSidE-infected cells, indicating that SidE modulates the turnover of autophagosomes (**Fig 8.15A**). We visualized the transition from autophagosomes to autolysosomes by transfecting A549 cells with the tandem construct mRFP-GFP-LC3 prior to infection. Autophagosomes emit GFP and RFP fluorescence and thus appear as yellow puncta, whereas acidic autolysosomes quench GFP fluorescence and thus appear as red puncta. The induction of autophagy increases the quantity of yellow and red puncta whereas late inhibition of autophagy (maturation of autophagosome or fusion with lysosome) increases the number of yellow puncta while reducing the number of red puncta. A549 cells treated with Torin-1 contained both red and yellow puncta before infection.

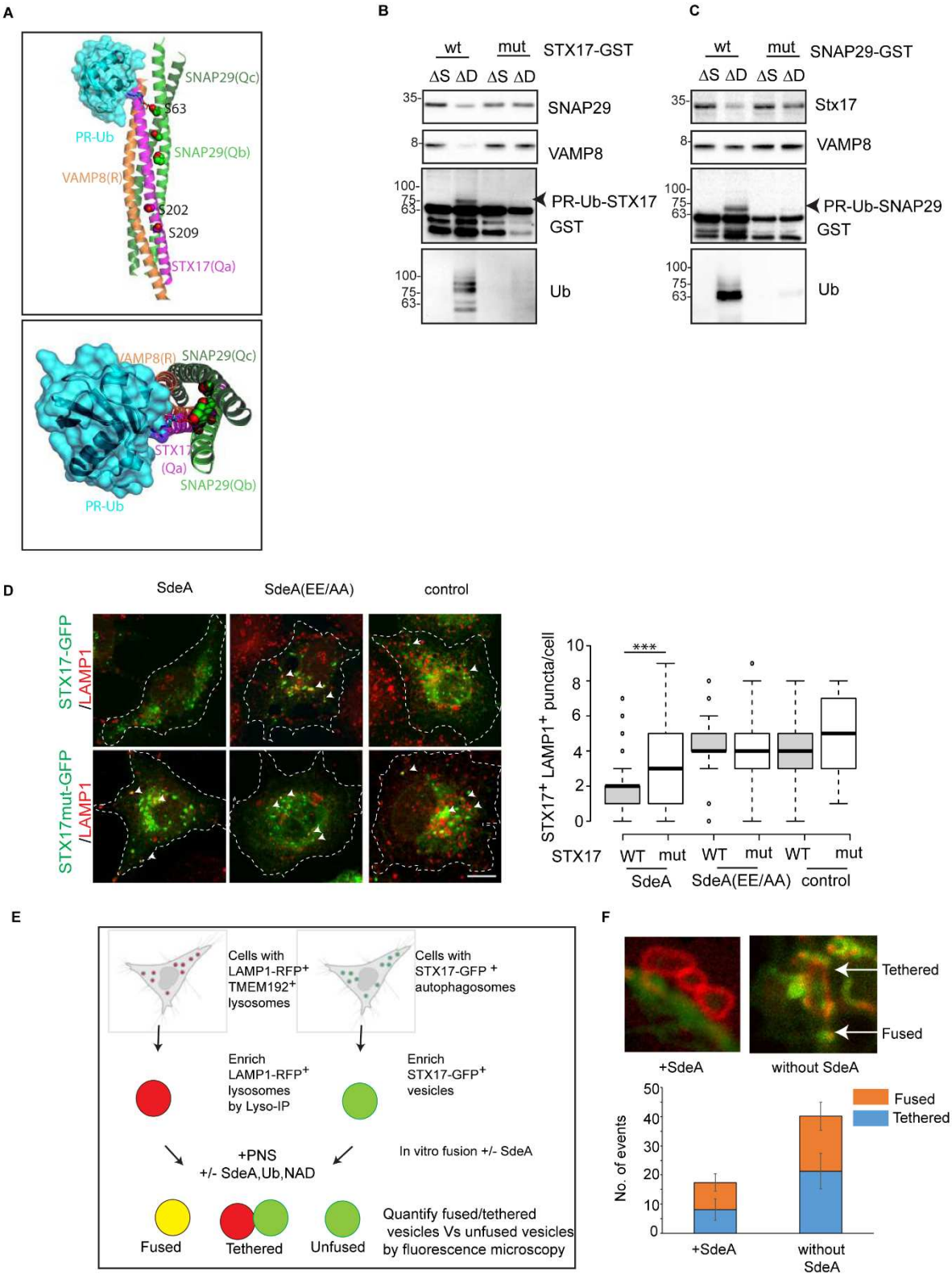

Figure 8.14: PR-Ub of STX17 and SNAP29 blocks their mutual interaction. A) PR-Ub (PDB ID: 5M93) was manually attached to residue S63 of SNAP29 in the structure of the STX17-SNAP29-VAMP8 complex (7BV6) using Pymol. B) STX17-GST was purified from *E. coli* and incubated with lysates from HEK 293T cells infected with *Legionella* strains for 2 h in a GST pulldown assay. Samples were analysed by western blot using antibodies against SNAP29, VAMP8, GST and ubiquitin. (ΔS-ΔSidE, ΔD-ΔDup *Legionella*). C) SNAP29-GST was purified from *E. coli* and incubated with lysates from infected cells similar to the assay in panel (B). After

GST pulldown, the samples were analyzed by western blot using antibodies against STX17, VAMP8, GST and ubiquitin. (ΔS-ΔSidE, ΔD-ΔDup *Legionella*). D) HeLa cells were cotransfected with HA-tagged SdeA or its catalytic mutant (E860AE862A) and GFP-tagged WT STX17 or its PR-Ub-deficient mutant. Cells were treated with 300 nM Torin-1 for 4 h to induce autophagy before fixation and immunostaining with an antibody against LAMP1 for confocal imaging. We counted the number of yellow puncta ($STX17^+LAMP1^+$) per cell in FIJI. In the box-plot, center lines show the medians; box limits indicate the 25th and 75th percentiles as determined by R software; whiskers extend 1.5 times the interquartile range from the 25th and 75th percentiles. n >50 cells taken from 3 independent experiments. p value was calculated using 2 tailed, type 3 Student's t-test, ***$p \leq 0.001$. Scale bar: 5µm. E) Schematic representation of the vesicle fusion assay. F) The number of fused or tethered vesicles detected in the vesicle fusion assay with and without SdeA treatment. Tethered and fused vesicles of $LAMP1^+$ (red) and $STX17^+$ (green) membranes are shown in the accompanying images. Graph represents 30 slides prepared from 3 independent experiments. Error bars indicate means ± SEM.
(Experiment in Figure 8.14A was performed by Mohit Mishra, 8.14 E and F was performed by Rukmini Mukherjee)

Cells infected with WT *Legionella* contained very few $LC3^+$ puncta due to the activity of RavZ, but the ΔRavZ-infected contained a larger number of yellow autophagosomes that were not acidified to form red autolysosomes. The cells infected with ΔRavZΔSidE contained a greater proportion of red puncta and a larger number of $LC3^+$ bacteria compared to ΔRavZ-infected cells (**Fig 8.15B**). Similarly, transient overexpression of SdeA and mRFP-GFP-LC3 also reduced the abundance of acidic red vesicles compared to the SdeA catalytic mutant E860AE862A (**Fig 8.15C**).

8.16 RavZ and SidE are both essential to facilitate bacterial replication

Moreover, to check whether these early $LC3^+$ bacteria fuse with the lysosome, we measured the recruitment of LAMP1 to the different *Legionella* strains. Infection with ΔRavZΔSidE led to the delivery of bacteria to $LAMP1^+$ lysosomes (**Fig 8.16A, and B**). We also tested the intracellular replication of these strains in A549 cells. The single deletion strains ΔSidE and ΔRavZ replicated less efficiently than WT controls, whereas the ΔRavZΔSidE strain showed the lowest replicative potential (**Fig 8.16C**). These results indicated that SidE and RavZ are both important to prevent the xenophagic targeting of bacteria.

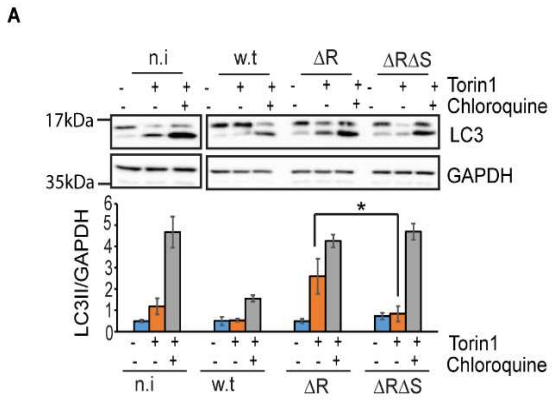

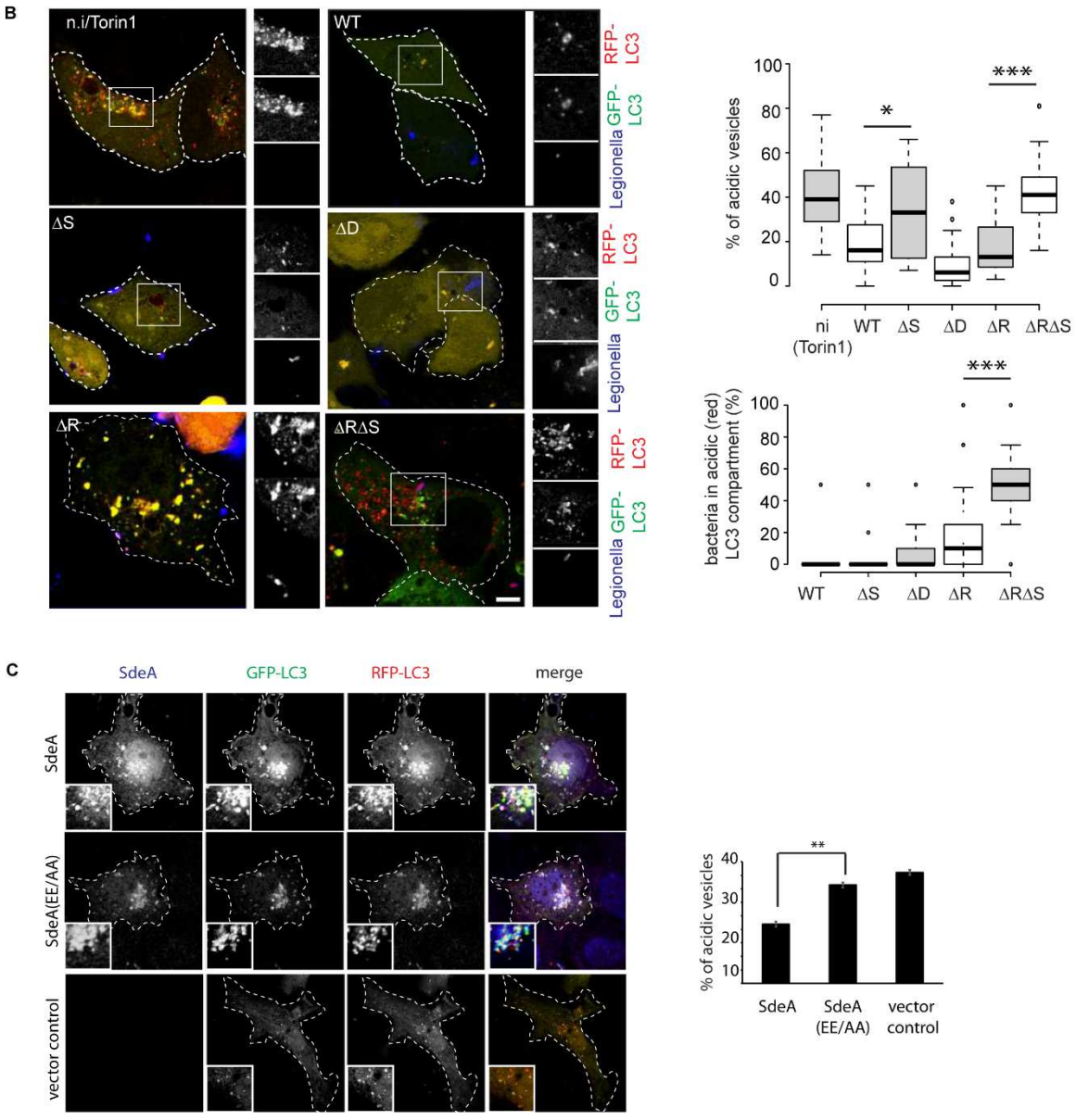

Figure 8.15: Serine ubiquitination blocks autophagosome–lysosome fusion and prevents the xenophagic targeting of intracellular bacteria. A) A549 cells were infected with *Legionella* strains for 4 h in the presence of 200 nM Torin-1 and/or 100 µM chloroquine as indicated. The cells were lysed and analysed by western blot with antibodies against LC3 and GAPDH. The data are means ± SEM of chemiluminescent intensity detected from 3 western blots taken from 3 independent experiments (*0.05<p ≤ 0.01). B) A549 cells were transfected with RFP-GFP-LC3 before infection with *Legionella* strains in the presence of 100 nM Torin-1 for 4 h. The cells were then fixed for immunostaining with a *Legionella*-specific antibody and confocal imaging. We counted the total number of puncta and the number of red puncta per cell in FIJI. In the box-plots, centre lines show the medians; box limits indicate the 25th and 75th percentiles as determined by R software; whiskers extend 1.5 times the interquartile range from the 25th and 75th percentiles. n >50 cells taken from 3 independent experiments. p value was calculated using 2 tailed, type 3 Student's t-test, ***p ≤ 0.001. Scale bar: 5µm. C) HeLa cells were co-transfected with RFP-GFP-LC3 and HA-tagged SdeA/SdeA(EE/AA) or a control vector for 16 h before treatment with 300 nM Torin-1 for 4 h to induce autophagy. The cells were then fixed and incubated with an anti-HA antibody for confocal imaging. We counted the total number of puncta and the number of red

puncta per cell in FIJI. The data are means ± SEM of 30 cells from three independent experiments (**0.01 ≤ p < 0.001).

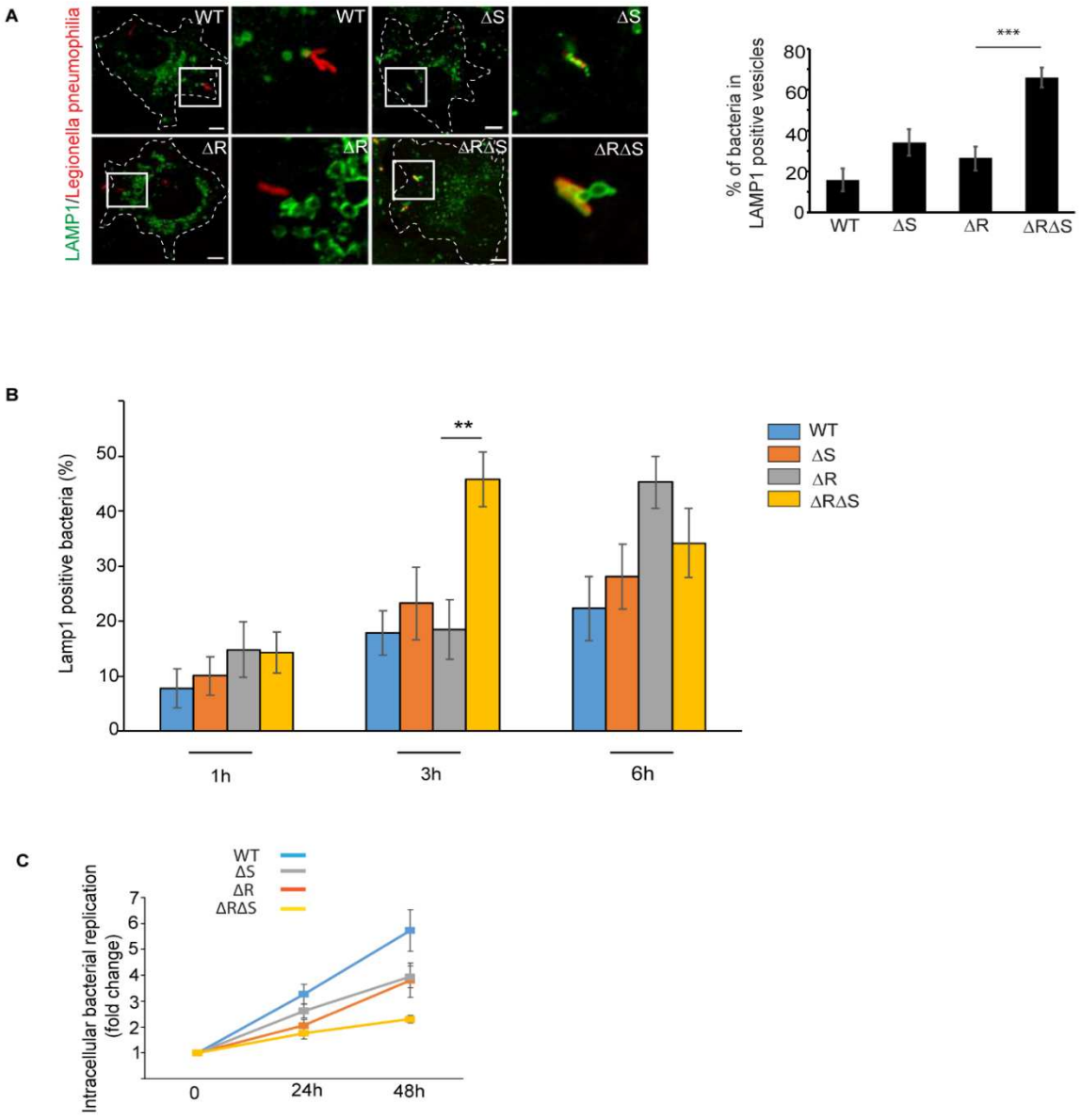

Figure 8.16: RavZ and SidE are both necessary for the evasion of host cell autophagy. A) A549 cells were infected with different strains of *Legionella* for 4 h before fixation and immunostaining with a LAMP1-specific antibody. We counted the number of LAMP1$^+$ bacteria per cell. The data are means ± SEM of 30 cells from three independent experiments (***p ≤ 0.001). Scale bar: 5µm. B) A549 cells were infected with *Legionella* strains for 1, 3 or 6 h before fixation and immunostaining with a LAMP1-specific antibody. We counted the number of LAMP1$^+$ bacteria per cell. The data are means ± SEM of 30 cells from three independent experiments (0.001 < **p ≤ 0.01). (ni-not infected, WT-wild-type *Legionella*, ΔS-ΔSidE, ΔD-ΔDup, ΔR-ΔRavZ, ΔRΔS-ΔRavZΔSidE *Legionella*). C) A549 cells were infected with the indicated strains of *Legionella*, and their intracellular replication was assessed at 0, 24 and 48 h post-infection. The data are means ± SEM of three independent experiments.

CHAPTER 9
Discussion

The endolysosomal system is extremely important to most aspects of cellular function Cellular protein cargo is trafficked through the endolysosomal system to reach their destinations within the cell, get secreted or get degraded in the terminal compartment of the pathway which is the lysosome. This thesis explores two important questions pertaining to the maintenance of lysosomal homeostasis: (1) how does the cell maintain a healthy pool of lysosomes when extensive lysosomal membrane damage is induced; and (2) how is the endolysosomal system affected in a cell infected by the pathogen *Legionella pneumophila?*

Lysosomal damage elicits several complex molecular signalling pathways which are often intertwined. Although several studies have been carried out to decipher these pathways how cells immediately cope with acute lysosomal damage stays elusive. Using unbiased proteomics, regular biochemistry and cell biology approaches, we have unravelled a new pathway using which cells can rapidly regenerate functional lysosomes by repurposing the damaged membrane. This pathway can function independently of lysosomal biogenesis. Some key molecules of this process are TBC1D15, DNM2 and LIMP2 while the later binds to ATG8 proteins after damage. We have termed this process as Lysosomal regeneration and it shares common features with ALR (Autophagic lysosomal reformation). While lysosomal regeneration is dependent of TBC1D15 and is independent of mTOR activity and lysosomal biogenesis, ALR has been shown to be dependent on mTOR activity and is usually gets activated after long starvation. TBC1D15 does not play any role in ALR according to our experiments. Although the initiation of these two processes is different and TBC1D15 is exclusively active only in lysosomal regeneration, both processes depends on ATG8 proteins to initiate the formation of lysosomal tubules, which are then elongated by pulling along the microtubules using kinesin proteins, and then subsequently get cleaved by DNM2 to generate new functional lysosomes. Analysis of the structural model of TBC1D15 followed by exhaustive mutational analysis showed that the TBC1D15 C-terminal domain binds to ATG8 proteins while the N-terminal domain interacts with DNM2 and CLTC which are instrumental for this process. TBC1D15 is anchored to damaged lysosomes by interacting with ATG8 proteins bound to lysosomal membrane proteins, and acts as a scaffold to assemble the regeneration machinery that is needed to produce new lysosomes (**Fig 9.1**).

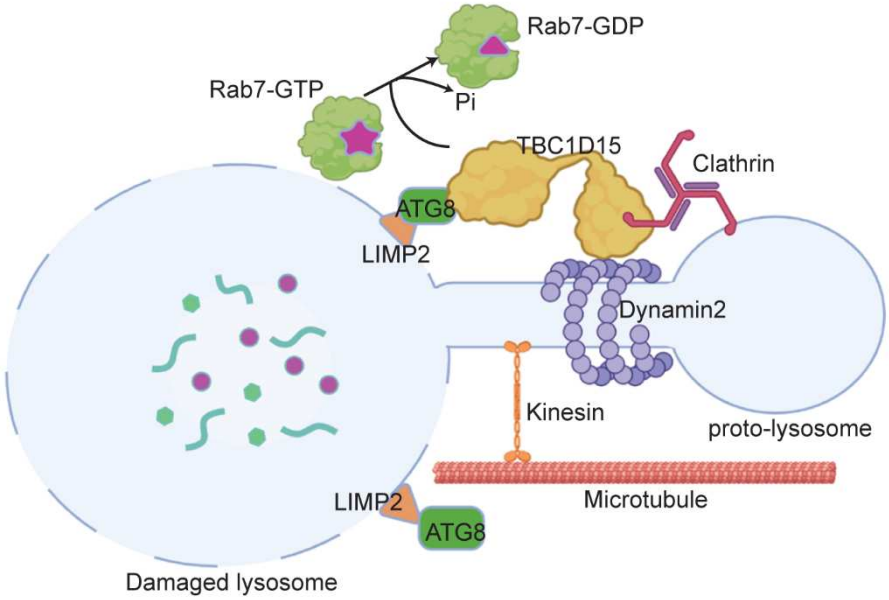

Figure 9.1: Molecular basis of TBC1D15 mediated lysosomal regeneration. TBC1D15 orchestrates the tubulation and dynamin2 dependent cleavage to generate new proto-lysosomes from damaged membranes

TBC1D15 utilises its LIR motif in order to localise to damaged lysosomes. Our proximity-labelling experiments suggested LIMP2 and TMEM192 as potential lysophagy receptors. However, experiments with pure proteins showed that only LIMP2 binds to ATG8 proteins utilising its LIR motif while TMEM192 is not a direct interactor but resided in the same complex. Therefore, LIMP2 can be acknowledged as a bonafied lysophagy receptors but this does not exclude the possibility of existence of other lysophagy receptors. Depletion of LIMP2 (but not TMEM192) caused a reduction in lysosomal regeneration flux but the concurrent depletion of both these genes led to a greater decrease in lysosomal regeneration. This suggests that though TMEM192 is not a lysophagy receptor, it may be a part of the multi-protein complex which binds ATG8 proteins in LLOMe treated cells. LIMP2 binding to ATG8 proteins is probably contributing to the specificity of TBC1D15 to damaged lysosomal membranes since depletion of LIMP2 significantly reduces lysosomal recruitment of TBC1D15 even though LC3B is still recruited to lysosomes.

Given the importance of the interaction between ATG8 and lysosomal membrane protein for TBC1D15 recruitment, we also checked other known scenario of accumulating ATG8 at the lysosomal membrane without using a damaging agent. In a recent study, one of the major lysosomal calcium channels TRPML1 was shown to bind lipidated LC3 after treating cells with its agonist MLSA-1 (Nakamura et al., 2020). In our proximity experiment using TRPML1-APEX2, we saw that treating cells with MLSA1 not only brings ATG8 proteins in the proximity

of TRPML1 but has TBC1D15 in its vicinity. Although further molecular and structural based approaches are needed to achieve better insight into the specificity of TBC1D15 recruitment and its function in this particular scenario.

Engagement of macro-autophagy and the formation of autophagosomal membranes is also proved to be essential for TBC1D15 dependent process of lysosomal regeneration. Pharmacological inhibition with known chemical agents of autophagosome formation and siRNA mediated depletion of different crucial autophagy genes led to a significant decrease in this lysosomal regeneration flux. Lipidated ATG8 proteins, present on autophagosomal membranes, binds to lysosomal membrane protein LIMP2, which can act as a lysophagy receptor on the damaged lysosome. TBC1D15 is also seen to be bound to this macro molecular complex. This localised TBC1D15 in turn recruits the machinery by which damaged lysosomal membranes form elongated tubules, open or closed LAMP1 rings which are quite distinct in morphology when compared to the tubules formed during ALR (Yu et al., 2010, Khundadze et al., 2021). By the effect of clathrin and kinesis proteins respectively, membrane buds are formed which are then pulled along microtubules to generate the aforementioned distinct membranous structures. These structures then get cleaved by the activity of a well-known GTPase protein Dynamin2 to form new LAMP1+ proto-lysosomes in a process which closely resembles ALR. These newly formed protolysosomes are acidic and have sub-optimal hydrolase activity when compared to that of mature lysosomes in untreated cells. To avoid ambiguity, we have termed this process as lysosomal regeneration since the process is similar but not identical to ALR.

Although TBC1D15-mediated lysosomal regeneration requires the ALR machinery to form new functional lysosomes, but other proteins may also serve important role. Proximity labelling of TBC1D15 after damage revealed several groups of proteins that may be indispensable for the process. This list includes several ESCRT proteins that are well-known for their membrane budding and scission activities. Some other proteins featured lipid-binding domains such as the PH domain (OSBP, ARHGEF2, KIF1A and OSBPL8), BAR domain (SNX6 and SH3GLB1), C2 domain (PLCH1, RABL1FIP1, PLCB3 and ESYT2), and ENTH domain (HIP1 and PICALM), was also found suggesting that the regeneration of damaged membranes involves the complex remodelling of lipids. Although the exact mechanism of this complex process is yet to be resolved. Furthermore, it is of extreme importance to understand the physiological context in which lysosomal regeneration may serve an important role. The lysosomal damage response is quite diverse and it is dependent on the duration and extent of damage. It has been reported that minor membrane perturbations trigger the calcium-dependent recruitment of ESCRT proteins for membrane repair (Skowra et al., 2018; Radulovic et al., 2018) whereas greater damage is capable

of triggering lysophagy. In this case lysosomal membrane is severely damaged and autophagy comes into play which then recruits selective autophagy receptors such as TAX1BP1, SQSTM1 and NDP52 (Koerver et al., 2019; Eapen et al., 2021). Like other organellophagy, it has been shown that autophagosomes containing cargos of damaged organelles (lysosomes) then fuse with healthy lysosomes for clearance. But in case of acute damage of lysosomes, we found that the proportion of functional (acidic) degradative lysosomes are far below than that of the damaged organelles thus making it difficult to clear damaged lysosomes through conventional autophagosome–lysosome fusion. This crisis condition then causes the induction of an instantaneous regeneration program which requires autophagy proteins, but its contribution becomes significant when the damage is most severe (as seen after 2–3 h of treatment with LLOMe, when TBC1D15 distribution is almost completely lysosomal). This mechanism is probably used by the cell to generate a population of healthy lysosomes even before TFEB/TFE3-mediated gene expression can initiate the program of lysosomal biogenesis. The treatment of PTECs with calcium oxalate also caused the recruitment of TBC1D15 to lysosomes and the formation of LAMP1 tubules, which are dependent on TBC1D15 and DNM2 for their formation and conversion to proto-lysosomes, respectively. The regeneration process may therefore contribute to the maintenance of lysosomal homeostasis in diseases such as crystal nephropathy.

In the second part of the thesis we have dissected how the endolysosomal pathway reacts to another stimulus which is *Legionella pneumophila* infection. Legionella enters the cell using receptor mediated endocytosis. It traverses the endosomal pathway residing in a vacuole which has components of the endosomal pathway and autophagy proteins but does not fuse with the lysosome. Legionella utilizes multiple effector proteins to segregate the lysosome from the early endosomal pathway with the intention of hijacking endosomal trafficking pathways to facilitate bacterial replication and at the same time avoiding lysosomal degradation through autophagy.

During the first 10 min of infection, a sub-population of *Legionella* is present in $Rab5^+$ phagosomes, which lack late endosome markers and escape fusion with the lysosome (Ku et al., 2012; Gasper et al., 2014). We found that early phagosomes acquire the PI3P-binding protein WIPI2 and proteins of the ATG8 conjugation machinery (ATG12-5-16L1 complex) within 30 min post-infection. These phagosomes fuse with $STX17^+$ vesicles to form autophagosome-like vacuoles displaying markers of autophagy but are devoid of ATG8 proteins. I investigated the role of serine ubiquitination in the formation of autophagosomal bacterial vacuoles during the early steps of *Legionella* infection while preventing the fusion of these vacuoles with lysosomes. Absence of ATG8 lipidation (due to RavZ activity) and serine ubiquitination of autophagosomal SNARE proteins prevent the fusion of these vacuoles with the lysosome (**Fig 9.2**).

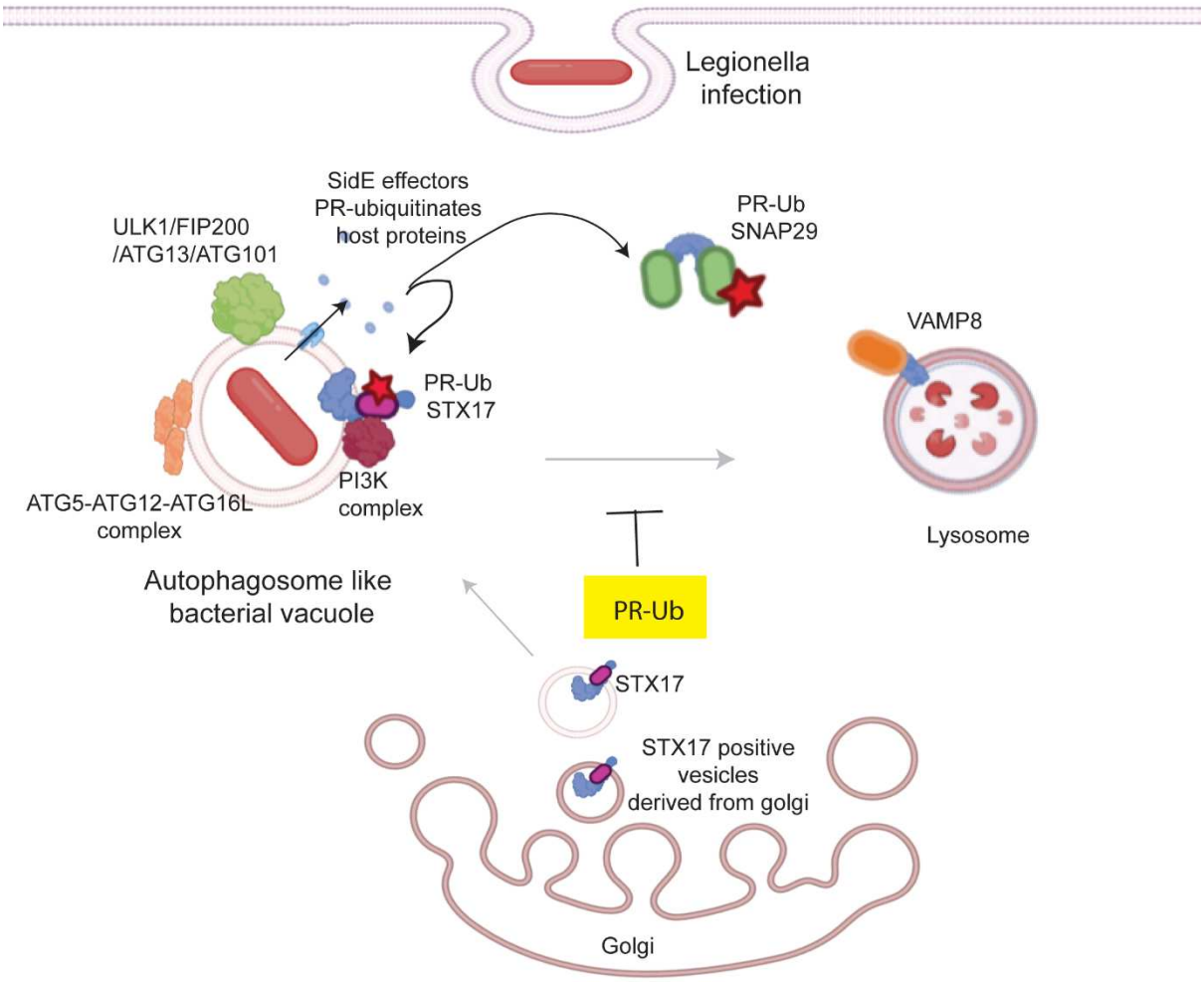

Figure 9.2: PR-Ub of STX17 and SNAP29 prevents fusion of autophagosome-like Legionella containing vacuoles with the lysosome.

The PR-ubiquitination of STX17 is necessary for its recruitment to bacterial vacuoles, but it is unclear whether the PR-Ub-modified form of STX17 is solely present on the bacterial vacuole and if so how PR-Ub promotes membrane recruitment. It is also interesting to consider whether conventional ubiquitination regulates STX17 during autophagosome biogenesis and lysosomal fusion. The PR-ubiquitination of SNAP29 in the Qb SNARE domain sterically hinders the formation of the four-helix bundle required to form the autophagosomal SNARE complex. SNAP29 is also implicated in several other vesicle trafficking events, including the regulation of secretory traffic from the Golgi body (Rapaport et al., 2018). SNAP29 activity is also regulated by post-translational modifications such as phosphorylation and the addition of *O*-linked β-*N*-acetylglucosamine (Smeele and Vaccari, 2022); whether PR-Ub affects these non-canonical functions or modifications of SNAP29 will be interesting to study.

We can also speculate whether the generation of bacterial vacuoles is similar to non-canonical autophagic mechanisms such as LC3-associated phagocytosis (LAP) (Martinez et al., 2015). Electron microscopy revealed the presence of bacteria within single-membrane vesicles during

the early stage of infection, but we did not detect the essential LAP marker Rubicon (data not shown). Since the discovery of RavZ, *Legionella*-infected cells have been considered a mostly autophagy-deficient system due to the defect in LC3 conjugation. However, to maintain a cellular niche that is suitable for bacterial proliferation, the housekeeping functions of autophagy should remain operational. Low levels of autophagy may be needed to recycle macromolecules into nutrients necessary for bacterial survival. Basal levels of autophagy may reflect the use of STX17-mediated autophagy, which occurs in ATG-conjugation-deficient systems (Tsuboyama et al., 2016). In this case, the autophagosome is often elongated due to the inefficient degradation of the inner autophagosomal membrane (Tsuboyama et al., 2016). In our experiments using *Legionella*-infected cells, we observed elongated STX17-coated bacterial vacuoles surrounding individual rod-shaped bacteria 2 h post-infection.

During the initial stages of infection, the bacteria reside in PI(3)P^+ phagosomes that are soon converted to PI(4)P^+ vesicles (Weber et al., 2014), which recruit ER markers such as calnexin. PI(4)P is mainly found on Golgi membranes and on secretory vesicles derived from the Golgi body. We found that Golgi-derived STX17$^+$ vesicles are recruited to bacterial phagosomes, so early bacterial vacuole formation, including the conversion of PI(3)P^+ phagosomes to PI(4)P^+ vacuoles, may be dependent on SidE. In contrast, vacuolar expansion is dependent on Atlastin-mediated membrane remodelling. This was shown in *Dictyostelium discoideum*, where the ER GTPase Atlastin3 (Sey1) was needed for ER remodelling around the vacuole to facilitate expansion (Steiner et al., 2017).

FAM134B and FAM134C were also serine ubiquitinated by SidE during bacterial infection (Shin et al., 2020). These proteins have reticulon homology domains (which induce curvature in membranes) and LIR motifs (which interact with LC3) and can therefore generate ER-derived autophagosomes by ER-phagy (Hubner and Dikic, 2020). It is unclear whether this process, mediated by FAM134, contributes to the recruitment of membranes to bacteria in the absence of ATG8 conjugation. Our analysis of SidE effectors and their substrates indicates that serine ubiquitination is an important mechanism utilized by *Legionella* to hijack intracellular membranes from both the ER and Golgi body.

STX17 is a substrate of the *Legionella* serine protease Lpg1137, and although the levels of STX17 are unaffected by the protease 1 h post-infection, almost complete Lpg1137-dependent degradation has occurred after 4 h (Arasaki et al., 2017). We observed STX17$^+$ vesicles and the recruitment of STX17 to bacteria during the first 2 h post-infection. At later time points, intracellular bacteria do not display STX17 or other autophagy markers but are instead enclosed

in ER-like compartments. We speculate that the transition from bacterial vacuoles resembling pre-autophagosomes to ER-derived LCVs may reflect the degradation of STX17 by Lpg1137.

Following serum starvation, STX17 is phosphorylated on S202 by TBK1. Phosphorylation causes a change in the localization of STX17 from the ER to the Golgi body and to peripheral puncta representing mammalian pre-autophagosomal structures (Kumar et al., 2019). We found that STX17 was distributed in the ER, Golgi body and peripheral puncta of cells infected with WT *Legionella*, whereas STX17 was extensively colocalized with the Golgi marker GM130 in cells infected with ΔS *Legionella*, which also contain fewer $STX17^{+}$ puncta. The formation of $STX17^{+}$ vesicles was also inhibited by brefeldin A and wortmannin, which block COPI-mediated transport and PI3K, respectively. These data suggest that $STX17^{+}$ puncta are derived from the Golgi body and their formation is dependent on serine ubiquitination. Given that the TBK1 phosphorylation site is also a target for ubiquitination, it is important to dissect the individual roles of STX17 phosphorylation and serine ubiquitination during *Legionella* infection.

STX17 is required for the formation of HyPAS, which appear to be derived from $FIP200^{+}$ vesicles originating from the *cis*-Golgi and $ATG16L1^{+}$ endosomal membranes. STX17 and its interactors SERCA2, extended synaptotagmin E-SYT2, and SIGMAR1, are needed to form HyPAS, and the process can be blocked by the SARS-CoV-2 protein NSP6 (Kumar et al., 2021). It is interesting to reflect on whether STX17+ HyPAS membranes build bacterial vacuoles. Unlike SARS-CoV-2, which blocks HyPAS formation, it is possible that *Legionella* may upregulate the formation of HyPAS membranes in a serine ubiquitination-dependent manner to generate replication vacuoles.

CHAPTER 10
References

Aflaki, E., Westbroek, W. and Sidransky, E., 2017. The complicated relationship between Gaucher disease and parkinsonism: insights from a rare disease. *Neuron*, *93*(4), pp.737-746.

Akturk, A., Wasilko, D. J., Wu, X., Liu, Y., Zhang, Y., Qiu, J., ... & Mao, Y. , 2018. Mechanism of phosphoribosyl-ubiquitination mediated by a single Legionella effector. *Nature*, *557*(7707), 729-733.

Alix, E., Godlee, C., Cerny, O., Blundell, S., Tocci, R., Matthews, S., Liu, M., Pruneda, J.N., Swatek, K.N., Komander, D. and Sleap, T., 2020. The tumour suppressor TMEM127 Is a Nedd4-Family E3 ligase adaptor required by Salmonella SteD to ubiquitinate and degrade MHC class II molecules. *Cell Host & Microbe*, *28*(1), pp.54-68.

Aman, Y., Schmauck-Medina, T., Hansen, M., Morimoto, R. I., Simon, A. K., Bjedov, I., ... & Fang, E. F., 2021. Autophagy in healthy aging and disease. *Nature aging*, *1*(8), 634-650.

Antonin, W., Holroyd, C., Fasshauer, D., Pabst, S., von Mollard, G.F. and Jahn, R., 2000. A SNARE complex mediating fusion of late endosomes defines conserved properties of SNARE structure and function. *The EMBO journal*, *19*(23), pp.6453-6464.

Appelqvist, H., Wäster, P., Kågedal, K. and Öllinger, K., 2013. The lysosome: from waste bag to potential therapeutic target. *Journal of molecular cell biology*, *5*(4), pp.214-226.

Arasaki, K., & Tagaya, M., 2017. Legionella blocks autophagy by cleaving STX17 (syntaxin 17). *Autophagy*, *13*(11), 2008-2009.

Arasaki, K., Mikami, Y., Shames, S.R., Inoue, H., Wakana, Y. and Tagaya, M., 2017. Legionella effector Lpg1137 shuts down ER-mitochondria communication through cleavage of syntaxin 17. *Nature communications*, *8*(1), p.15406.

Bakula, D., Müller, A.J., Zuleger, T., Takacs, Z., Franz-Wachtel, M., Thost, A.K., Brigger, D., Tschan, M.P., Frickey, T., Robenek, H. and Macek, B., 2017. WIPI3 and WIPI4 β-propellers are scaffolds for LKB1-AMPK-TSC signalling circuits in the control of autophagy. *Nature communications*, *8*(1), p.15637.

Balderhaar, H.J.K. and Ungermann, C., 2013. CORVET and HOPS tethering complexes–coordinators of endosome and lysosome fusion. *Journal of cell science*, *126*(6), pp.1307-1316.

Ballabio, A. and Bonifacino, J.S., 2020. Lysosomes as dynamic regulators of cell and organismal homeostasis. *Nature reviews Molecular cell biology*, *21*(2), pp.101-118.

Ballabio, A. and Gieselmann, V., 2009. Lysosomal disorders: from storage to cellular damage. *Biochimica et Biophysica Acta (BBA)-Molecular Cell Research*, *1793*(4), pp.684-696.

Bandyopadhyay, U., Kaushik, S., Varticovski, L. and Cuervo, A.M., 2008. The chaperone-mediated autophagy receptor organizes in dynamic protein complexes at the lysosomal membrane. *Molecular and cellular biology*, *28*(18), pp.5747-5763.

Banga, S., Gao, P., Shen, X., Fiscus, V., Zong, W.X., Chen, L. and Luo, Z.Q., 2007. Legionella pneumophila inhibits macrophage apoptosis by targeting pro-death members of the Bcl2 protein family. *Proceedings of the National Academy of Sciences*, *104*(12), pp.5121-5126.

Bardill, J.P., Miller, J.L. and Vogel, J.P., 2005. IcmS-dependent translocation of SdeA into macrophages by the Legionella pneumophila type IV secretion system. *Molecular microbiology*, *56*(1), pp.90-103.

Bargal, R., Avidan, N., Ben-Asher, E., Olender, Z., Zeigler, M., Frumkin, A., Raas-Rothschild, A., Glusman, G., Lancet, D. and Bach, G., 2000. Identification of the gene causing mucolipidosis type IV. *Nature genetics*, *26*(1), pp.118-122.

Bartolomeo, R., Cinque, L., De Leonibus, C., Forrester, A., Salzano, A.C., Monfregola, J., De Gennaro, E., Nusco, E., Azario, I., Lanzara, C. and Serafini, M., 2017. mTORC1 hyperactivation arrests bone growth in lysosomal storage disorders by suppressing autophagy. *The Journal of clinical investigation*, *127*(10), pp.3717-3729.

Bassi, M.T., Manzoni, M., Monti, E., Pizzo, M.T., Ballabio, A. and Borsani, G., 2000. Cloning of the gene encoding a novel integral membrane protein, mucolipidin—and identification of the two major founder mutations causing mucolipidosis type IV. *The American Journal of Human Genetics*, *67*(5), pp.1110-1120.

Bhogaraju, S., Bonn, F., Mukherjee, R., Adams, M., Pfleiderer, M. M., Galej, W. P., ... & Dikic, I., 2019. Inhibition of bacterial ubiquitin ligases by SidJ–calmodulin catalysed glutamylation. *Nature*, *572*(7769), 382-386.

Bhogaraju, S., Kalayil, S., Liu, Y., Bonn, F., Colby, T., Matic, I., & Dikic, I., 2016. Phosphoribosylation of ubiquitin promotes serine ubiquitination and impairs conventional ubiquitination. *Cell*, *167*(6), 1636-1649.

Bian, B., Mongrain, S., Cagnol, S., Langlois, M.J., Boulanger, J., Bernatchez, G., Carrier, J.C., Boudreau, F. and Rivard, N., 2016. Cathepsin B promotes colorectal tumorigenesis, cell invasion, and metastasis. *Molecular carcinogenesis*, *55*(5), pp.671-687.

Black, M. H., Osinski, A., Gradowski, M., Servage, K. A., Pawłowski, K., Tomchick, D. R., & Tagliabracci, V. S., 2019. Bacterial pseudokinase catalyzes protein polyglutamylation to inhibit the SidE-family ubiquitin ligases. *Science*, *364*(6442), 787-792.

Blatt, S.P., Parkinson, M.D., Pace, E., Hoffman, P., Dolan, D., Lauderdale, P., Zajac, R.A. and Melcher, G.P., 1993. Nosocomial Legionnaires' disease: aspiration as a primary mode of disease acquisition. *The American journal of medicine*, *95*(1), pp.16-22.

Bonam, S.R., Wang, F. and Muller, S., 2019. Lysosomes as a therapeutic target. *Nature Reviews Drug Discovery*, *18*(12), pp.923-948.

Boya, P. and Kroemer, G., 2008. Lysosomal membrane permeabilization in cell death. *Oncogene*, *27*(50), pp.6434-6451.

Boyle, K.B. and Randow, F., 2013. The role of 'eat-me'signals and autophagy cargo receptors in innate immunity. *Current opinion in microbiology*, *16*(3), pp.339-348.

Brenner, D.J., STEIGERWALT, A.G. and McDADE, J.E., 1979. Classification of the Legionnaires' disease bacterium: Legionella pneumophila, genus novum, species nova, of the family Legionellaceae, familia nova. *Annals of internal medicine*, *90*(4), pp.656-658.

Camões, J., Lobato, C.T., Beires, F. and Gomes, E., 2021. Legionella and SARS-CoV-2 coinfection in a patient with pneumonia–an outbreak in northern Portugal. *Cureus*, *13*(1).

Cantuti-Castelvetri, L., Fitzner, D., Bosch-Queralt, M., Weil, M.T., Su, M., Sen, P., Ruhwedel, T., Mitkovski, M., Trendelenburg, G., Lütjohann, D. and Möbius, W., 2018. Defective cholesterol clearance limits remyelination in the aged central nervous system. *Science*, *359*(6376), pp.684-688.

Castellano, B.M., Thelen, A.M., Moldavski, O., Feltes, M., Van Der Welle, R.E., Mydock-McGrane, L., Jiang, X., Van Eijkeren, R.J., Davis, O.B., Louie, S.M. and Perera, R.M., 2017. Lysosomal cholesterol activates mTORC1 via an SLC38A9–Niemann-Pick C1 signaling complex. *Science*, *355*(6331), pp.1306-1311.

Cesar-Silva, D., Pereira-Dutra, F.S., Moraes Giannini, A.L. and Jacques G. de Almeida, C., 2022. The endolysosomal system: the acid test for SARS-CoV-2. *International Journal of Molecular Sciences*, *23*(9), p.4576.

Chadt, A., Leicht, K., Deshmukh, A., Jiang, L.Q., Scherneck, S., Bernhardt, U., Dreja, T., Vogel, H., Schmolz, K., Kluge, R. and Zierath, J.R., 2008. Tbc1d1 mutation in lean mouse strain confers leanness and protects from diet-induced obesity. *Nature genetics*, *40*(11), pp.1354-1359.

Chauhan, S., Ahmed, Z., Bradfute, S.B., Arko-Mensah, J., Mandell, M.A., Won Choi, S., Kimura, T., Blanchet, F., Waller, A., Mudd, M.H. and Jiang, S., 2015. Pharmaceutical screen identifies novel target processes for activation of autophagy with a broad translational potential. *Nature communications*, *6*(1), p.8620.

Chauhan, S., Kumar, S., Jain, A., Ponpuak, M., Mudd, M.H., Kimura, T., Choi, S.W., Peters, R., Mandell, M., Bruun, J.A. and Johansen, T., 2016. TRIMs and galectins globally cooperate and TRIM16 and galectin-3 co-direct autophagy in endomembrane damage homeostasis. *Developmental cell*, *39*(1), pp.13-27.

Chen, Y. and Yu, L., 2017. Recent progress in autophagic lysosome reformation. *Traffic*, *18*(6), pp.358-361.

Cheng, X., Ma, X., Ding, X., Li, L., Jiang, X., Shen, Z., Chen, S., Liu, W., Gong, W. and Sun, Q., 2017. Pacer mediates the function of class III PI3K and HOPS complexes in autophagosome maturation by engaging Stx17. *Molecular cell*, *65*(6), pp.1029-1043.

Chiang, H.L., Terlecky, S.R., Plant, C.P. and Dice, J.F., 1989. A role for a 70-kilodalton heat shock protein in lysosomal degradation of intracellular proteins. *Science*, *246*(4928), pp.382-385.

Choy, A., Dancourt, J., Mugo, B., O'Connor, T. J., Isberg, R. R., Melia, T. J., & Roy, C. R. , 2012. The Legionella effector RavZ inhibits host autophagy through irreversible Atg8 deconjugation. *Science*, *338*(6110), 1072-1076.

Chu, B.B., Liao, Y.C., Qi, W., Xie, C., Du, X., Wang, J., Yang, H., Miao, H.H., Li, B.L. and Song, B.L., 2015. Cholesterol transport through lysosome-peroxisome membrane contacts. *Cell*, *161*(2), pp.291-306.

Clague, M.J., Urbé, S. and Komander, D., 2019. Breaking the chains: deubiquitylating enzyme specificity begets function. *Nature reviews Molecular cell biology*, *20*(6), pp.338-352.

Coen, K., Flannagan, R.S., Baron, S., Carraro-Lacroix, L.R., Wang, D., Vermeire, W., Michiels, C., Munck, S., Baert, V., Sugita, S. and Wuytack, F., 2012. Lysosomal calcium homeostasis defects, not proton pump defects, cause endo-lysosomal dysfunction in PSEN-deficient cells. *Journal of Cell Biology*, *198*(1), pp.23-35.

Cox, J. and Mann, M., 2008. MaxQuant enables high peptide identification rates, individualized ppb-range mass accuracies and proteome-wide protein quantification. *Nature biotechnology*, *26*(12), pp.1367-1372.

Cox, J., Hein, M.Y., Luber, C.A., Paron, I., Nagaraj, N. and Mann, M., 2014. Accurate proteome-wide label-free quantification by delayed normalization and maximal peptide ratio extraction, termed MaxLFQ. *Molecular & cellular proteomics*, *13*(9), pp.2513-2526.

Cuervo, A.M. and Dice, J.F., 1996. A receptor for the selective uptake and degradation of proteins by lysosomes. *Science*, *273*(5274), pp.501-503.

Cuif, M.H., Possmayer, F., Zander, H., Bordes, N., Jollivet, F., Couedel-Courteille, A., Janoueix-Lerosey, I., Langsley, G., Bornens, M. and Goud, B., 1999. Characterization of GAPCenA, a GTPase activating protein for Rab6, part of which associates with the centrosome. *The EMBO journal*, *18*(7), pp.1772-1782.

Dash, S., Sano, H., Rochford, J.J., Semple, R.K., Yeo, G., Hyden, C.S., Soos, M.A., Clark, J., Rodin, A., Langenberg, C. and Druet, C., 2009. A truncation mutation in TBC1D4 in a family with acanthosis nigricans and postprandial hyperinsulinemia. *Proceedings of the National Academy of Sciences*, *106*(23), pp.9350-9355.

Daste, F., Galli, T. and Tareste, D., 2015. Structure and function of longin SNAREs. *Journal of cell science*, *128*(23), pp.4263-4272.

De Duve, C., Pressman, B.C., Gianetto, R., Wattiaux, R. and Appelmans, F., 1955. Tissue fractionation studies. 6. Intracellular distribution patterns of enzymes in rat-liver tissue. *Biochemical Journal*, *60*(4), p.604.

De Leon, J.A., Qiu, J., Nicolai, C.J., Counihan, J.L., Barry, K.C., Xu, L., Lawrence, R.E., Castellano, B.M., Zoncu, R., Nomura, D.K. and Luo, Z.Q., 2017. Positive and negative regulation of the master metabolic regulator mTORC1 by two families of Legionella pneumophila effectors. *Cell reports*, *21*(8), pp.2031-2038.

Decressac, M., Mattsson, B., Weikop, P., Lundblad, M., Jakobsson, J. and Björklund, A., 2013. TFEB-mediated autophagy rescues midbrain dopamine neurons from α-synuclein toxicity. *Proceedings of the National Academy of Sciences*, *110*(19), pp.E1817-E1826.

Dehay, B., Bové, J., Rodríguez-Muela, N., Perier, C., Recasens, A., Boya, P. and Vila, M., 2010. Pathogenic lysosomal depletion in Parkinson's disease. *Journal of Neuroscience*, *30*(37), pp.12535-12544.

Di Malta, C., Siciliano, D., Calcagni, A., Monfregola, J., Punzi, S., Pastore, N., Eastes, A.N., Davis, O., De Cegli, R., Zampelli, A. and Di Giovannantonio, L.G., 2017. Transcriptional activation of RagD GTPase controls mTORC1 and promotes cancer growth. *Science*, *356*(6343), pp.1188-1192.

di Ronza, A., Bajaj, L., Sharma, J., Sanagasetti, D., Lotfi, P., Adamski, C.J., Collette, J., Palmieri, M., Amawi, A., Popp, L. and Chang, K.T., 2018. CLN8 is an endoplasmic reticulum cargo receptor that regulates lysosome biogenesis. *Nature cell biology*, *20*(12), pp.1370-1377.

Dierks, T., Schmidt, B., Borissenko, L.V., Peng, J., Preusser, A., Mariappan, M. and von Figura, K., 2003. Multiple sulfatase deficiency is caused by mutations in the gene encoding the human Cα-formylglycine generating enzyme. *Cell*, *113*(4), pp.435-444.

Dikic, I., & Elazar, Z., 2018. Mechanism and medical implications of mammalian autophagy. *Nature reviews Molecular cell biology*, *19*(6), 349-364.

Ding, X., Jiang, X., Tian, R., Zhao, P., Li, L., Wang, X., Chen, S., Zhu, Y., Mei, M., Bao, S. and Liu, W., 2019. RAB2 regulates the formation of autophagosome and autolysosome in mammalian cells. *Autophagy*, *15*(10), pp.1774-1786.

Dong, Y., Mu, Y., Xie, Y., Zhang, Y., Han, Y., Zhou, Y., ... & Feng, Y., 2018. Structural basis of ubiquitin modification by the Legionella effector SdeA. *Nature*, *557*(7707), 674-678.

Dooley, H.C., Razi, M., Polson, H.E., Girardin, S.E., Wilson, M.I. and Tooze, S.A., 2014. WIPI2 links LC3 conjugation with PI3P, autophagosome formation, and pathogen clearance by recruiting Atg12–5-16L1. *Molecular cell*, *55*(2), pp.238-252.

Du, W., Su, Q.P., Chen, Y., Zhu, Y., Jiang, D., Rong, Y., Zhang, S., Zhang, Y., Ren, H., Zhang, C. and Wang, X., 2016. Kinesin 1 drives autolysosome tubulation. *Developmental cell*, *37*(4), pp.326-336.

Eapen, V.V., Swarup, S., Hoyer, M.J., Paulo, J.A. and Harper, J.W., 2021. Quantitative proteomics reveals the selectivity of ubiquitin-binding autophagy receptors in the turnover of damaged lysosomes by lysophagy. *Elife*, *10*, p.e72328.

Ebner, M., Koch, P.A. and Haucke, V., 2019. Phosphoinositides in the control of lysosome function and homeostasis. *Biochemical Society Transactions*, *47*(4), pp.1173-1185.

Ebner, P., Poetsch, I., Deszcz, L., Hoffmann, T., Zuber, J. and Ikeda, F., 2018. The IAP family member BRUCE regulates autophagosome–lysosome fusion. *Nature communications*, *9*(1), p.599.

Emmerson, B.T., Cross, M., Osborne, J.M. and Axelsen, R.A., 1990. Reaction of MDCK cells to crystals of monosodium urate monohydrate and uric acid. *Kidney international*, *37*(1), pp.36-43.

Fleming, A., Bourdenx, M., Fujimaki, M., Karabiyik, C., Krause, G. J., Lopez, A., ... & Rubinsztein, D. C., 2022. The different autophagy degradation pathways and neurodegeneration. *Neuron*.

Fletcher, K., Ulferts, R., Jacquin, E., Veith, T., Gammoh, N., Arasteh, J. M., ... & Florey, O. (2018). The WD 40 domain of ATG 16L1 is required for its non-canonical role in lipidation of LC 3 at single membranes. *The EMBO journal*, *37*(4), e97840.

Fraldi, A., Annunziata, F., Lombardi, A., Kaiser, H.J., Medina, D.L., Spampanato, C., Fedele, A.O., Polishchuk, R., Sorrentino, N.C., Simons, K. and Ballabio, A., 2010. Lysosomal fusion and SNARE function are impaired by cholesterol accumulation in lysosomal storage disorders. *The EMBO journal*, *29*(21), pp.3607-3620.

Fraser, D.W., Tsai, T.R., Orenstein, W., Parkin, W.E., Beecham, H.J., Sharrar, R.G., Harris, J., Mallison, G.F., Martin, S.M., McDade, J.E. and Shepard, C.C., 1977. Legionnaires' disease: description of an epidemic of pneumonia. *New England Journal of Medicine*, *297*(22), pp.1189-1197.

Fujita, N., Morita, E., Itoh, T., Tanaka, A., Nakaoka, M., Osada, Y., Umemoto, T., Saitoh, T., Nakatogawa, H., Kobayashi, S. and Haraguchi, T., 2013. Recruitment of the autophagic

machinery to endosomes during infection is mediated by ubiquitin. *Journal of Cell Biology*, *203*(1), pp.115-128.

Fukuda, M., 2008. Regulation of secretory vesicle traffic by Rab small GTPases. *Cell Mol Life Sci*, *65*(18), pp.2801-2813.

Fukuda, M., 2011. TBC proteins: GAPs for mammalian small GTPase Rab?. *Bioscience reports*, *31*(3), pp.159-168.

Gan, N., Zhen, X., Liu, Y., Xu, X., He, C., Qiu, J., ... & Luo, Z. Q., 2019. Regulation of phosphoribosyl ubiquitination by a calmodulin-dependent glutamylase. *Nature*, *572*(7769), 387-391.

Garg, S., Sharma, M., Ung, C., Tuli, A., Barral, D.C., Hava, D.L., Veerapen, N., Besra, G.S., Hacohen, N. and Brenner, M.B., 2011. Lysosomal trafficking, antigen presentation, and microbial killing are controlled by the Arf-like GTPase Arl8b. *Immunity*, *35*(2), pp.182-193.

Gaspar, A. H., & Machner, M. P., 2014. VipD is a Rab5-activated phospholipase A1 that protects Legionella pneumophila from endosomal fusion. *Proceedings of the National Academy of Sciences*, *111*(12), 4560-4565.

Glick, T.H., Gregg, M.B., Berman, B., Mallison, G., Rhodes, W.W. and Kassanoff, I., 1978. An epidemic of unknown etiology in a health department. I. Clinical and epidemiologic aspects. *Am J Epidemiol*, *107*(2), pp.149-160.

Gómez-Sintes, R., Ledesma, M.D. and Boya, P., 2016. Lysosomal cell death mechanisms in aging. *Ageing research reviews*, *32*, pp.150-168.

Grosshans, B.L., Ortiz, D. and Novick, P., 2006. Rabs and their effectors: achieving specificity in membrane traffic. *Proceedings of the National Academy of Sciences*, *103*(32), pp.11821-11827.

Gubas, A., & Dikic, I., 2022. A guide to the regulation of selective autophagy receptors. *The FEBS Journal*, *289*(1), 75-89.

Guo, B., Liang, Q., Li, L., Hu, Z., Wu, F., Zhang, P., Ma, Y., Zhao, B., Kovács, A.L., Zhang, Z. and Feng, D., 2014. O-GlcNAc-modification of SNAP-29 regulates autophagosome maturation. *Nature cell biology*, *16*(12), pp.1215-1226.

Gutierrez, M.G., Munafó, D.B., Berón, W. and Colombo, M.I., 2004. Rab7 is required for the normal progression of the autophagic pathway in mammalian cells. *Journal of cell science*, *117*(13), pp.2687-2697.

Haas, A.K., Fuchs, E., Kopajtich, R. and Barr, F.A., 2005. A GTPase-activating protein controls Rab5 function in endocytic trafficking. *Nature cell biology*, *7*(9), pp.887-893.

Haas, A.K., Yoshimura, S.I., Stephens, D.J., Preisinger, C., Fuchs, E. and Barr, F.A., 2007. Analysis of GTPase-activating proteins: Rab1 and Rab43 are key Rabs required to maintain a functional Golgi complex in human cells. *Journal of cell science*, *120*(17), pp.2997-3010.

Hamasaki, M., Furuta, N., Matsuda, A., Nezu, A., Yamamoto, A., Fujita, N., Oomori, H., Noda, T., Haraguchi, T., Hiraoka, Y. and Amano, A., 2013. Autophagosomes form at ER–mitochondria contact sites. *Nature*, *495*(7441), pp.389-393.

Hemesath, T.J., Steingrímsson, E., McGill, G., Hansen, M.J., Vaught, J., Hodgkinson, C.A., Arnheiter, H., Copeland, N.G., Jenkins, N.A. and Fisher, D.E., 1994. Microphthalmia, a critical factor in melanocyte development, defines a discrete transcription factor family. *Genes & development*, *8*(22), pp.2770-2780.

Hershko, A. and Ciechanover, A., 1998. The ubiquitin system. *Annual review of biochemistry*, *67*(1), pp.425-479.

Hesketh, G.G., Wartosch, L., Davis, L.J., Bright, N.A. and Luzio, J.P., 2018. The lysosome and intracellular signalling. *Endocytosis and Signaling*, pp.151-180.

Hilbi, H., Jarraud, S., Hartland, E. and Buchrieser, C., 2010. Update on Legionnaires' disease: pathogenesis, epidemiology, detection and control. *Molecular microbiology*, *76*(1), pp.1-11.

Hohenstein, A.C. and Roche, P.A., 2001. SNAP-29 is a promiscuous syntaxin-binding SNARE. *Biochemical and biophysical research communications*, *285*(2), pp.167-171.

Huang, D., Xu, B., Liu, L., Wu, L., Zhu, Y., Ghanbarpour, A., Wang, Y., Chen, F.J., Lyu, J., Hu, Y. and Kang, Y., 2021. TMEM41B acts as an ER scramblase required for lipoprotein biogenesis and lipid homeostasis. *Cell metabolism*, *33*(8), pp.1655-1670.

Huang, L., Yuan, P., Yu, P., Kong, Q., Xu, Z., Yan, X., Shen, Y., Yang, J., Wan, R., Hong, K. and Tang, Y., 2018. O-GlcNAc-modified SNAP29 inhibits autophagy-mediated degradation via the disturbed SNAP29-STX17-VAMP8 complex and exacerbates myocardial injury in type I diabetic rats. *International Journal of Molecular Medicine*, *42*(6), pp.3278-3290.

Huang, S. and Wang, Y., 2017. Golgi structure formation, function, and post-translational modifications in mammalian cells. *F1000Research*, *6*.

Hubert, V., Peschel, A., Langer, B., Gröger, M., Rees, A. and Kain, R., 2016. LAMP-2 is required for incorporating syntaxin-17 into autophagosomes and for their fusion with lysosomes. *Biology open*, *5*(10), pp.1516-1529.

Hübner, C. A., & Dikic, I., 2020. ER-phagy and human diseases. *Cell Death & Differentiation*, *27*(3), 833-842.

Huotari, J. and Helenius, A., 2011. Endosome maturation. *The EMBO journal*, *30*(17), pp.3481-3500.

Hurley, J.H. and Young, L.N., 2017. Mechanisms of autophagy initiation. *Annual review of biochemistry*, *86*, pp.225-244.

Itakura, E., Kishi-Itakura, C., & Mizushima, N., 2012. The hairpin-type tail-anchored SNARE syntaxin 17 targets to autophagosomes for fusion with endosomes/lysosomes. *Cell*, *151*(6), 1256-1269.

Itoh, T., Kanno, E., Uemura, T., Waguri, S. and Fukuda, M., 2011. OATL1, a novel autophagosome-resident Rab33B-GAP, regulates autophagosomal maturation. *Journal of Cell Biology*, *192*(5), pp.839-853.

Itoh, T., Satoh, M., Kanno, E. and Fukuda, M., 2006. Screening for target Rabs of TBC (Tre-2/Bub2/Cdc16) domain-containing proteins based on their Rab-binding activity. *Genes to cells*, *11*(9), pp.1023-1037.

Jacomin, A.C., Samavedam, S., Promponas, V. and Nezis, I.P., 2016. iLIR database: A web resource for LIR motif-containing proteins in eukaryotes. *Autophagy*, *12*(10), pp.1945-1953.

Jean, S., Cox, S., Nassari, S. and Kiger, A.A., 2015. Starvation-induced MTMR 13 and RAB 21 activity regulates VAMP 8 to promote autophagosome–lysosome fusion. *EMBO reports*, *16*(3), pp.297-311.

Jia, J., Abudu, Y.P., Claude-Taupin, A., Gu, Y., Kumar, S., Choi, S.W., Peters, R., Mudd, M.H., Allers, L., Salemi, M. and Phinney, B., 2018. Galectins control mTOR in response to endomembrane damage. *Molecular cell*, *70*(1), pp.120-135.

Jia, J., Claude-Taupin, A., Gu, Y., Choi, S.W., Peters, R., Bissa, B., Mudd, M.H., Allers, L., Pallikkuth, S., Lidke, K.A. and Salemi, M., 2020. Galectin-3 coordinates a cellular system for lysosomal repair and removal. *Developmental cell*, *52*(1), pp.69-87.

Jiang, P., Nishimura, T., Sakamaki, Y., Itakura, E., Hatta, T., Natsume, T. and Mizushima, N., 2014. The HOPS complex mediates autophagosome–lysosome fusion through interaction with syntaxin 17. *Molecular biology of the cell*, *25*(8), pp.1327-1337.

Jumper, J., Evans, R., Pritzel, A., Green, T., Figurnov, M., Ronneberger, O., Tunyasuvunakool, K., Bates, R., Žídek, A., Potapenko, A. and Bridgland, A., 2021. Highly accurate protein structure prediction with AlphaFold. *Nature*, *596*(7873), pp.583-589.

Kalayil, S., Bhogaraju, S., Bonn, F., Shin, D., Liu, Y., Gan, N., ... & Dikic, I., 2018. Insights into catalysis and function of phosphoribosyl-linked serine ubiquitination. *Nature*, *557*(7707), 734-738.

Khundadze, M., Ribaudo, F., Hussain, A., Stahlberg, H., Brocke-Ahmadinejad, N., Franzka, P., Varga, R.E., Zarkovic, M., Pungsrinont, T., Kokal, M. and Ganley, I.G., 2021. Mouse models for hereditary spastic paraplegia uncover a role of PI4K2A in autophagic lysosome reformation. *Autophagy*, *17*(11), pp.3690-3706.

Kimmelman, A.C. and White, E., 2017. Autophagy and tumor metabolism. *Cell metabolism*, *25*(5), pp.1037-1043.

Kinghorn, K.J., Grönke, S., Castillo-Quan, J.I., Woodling, N.S., Li, L., Sirka, E., Gegg, M., Mills, K., Hardy, J., Bjedov, I. and Partridge, L., 2016. A Drosophila model of neuronopathic Gaucher disease demonstrates lysosomal-autophagic defects and altered mTOR signalling and is functionally rescued by rapamycin. *Journal of Neuroscience*, *36*(46), pp.11654-11670.

Kirkegaard, T., Roth, A.G., Petersen, N.H., Mahalka, A.K., Olsen, O.D., Moilanen, I., Zylicz, A., Knudsen, J., Sandhoff, K., Arenz, C. and Kinnunen, P.K., 2010. Hsp70 stabilizes lysosomes and reverts Niemann–Pick disease-associated lysosomal pathology. *Nature*, *463*(7280), pp.549-553.

Kitao, T., Nagai, H. and Kubori, T., 2020. Divergence of Legionella effectors reversing conventional and unconventional ubiquitination. *Frontiers in Cellular and Infection Microbiology*, *10*, p.448.

Klionsky, D. J., Petroni, G., Amaravadi, R. K., Baehrecke, E. H., Ballabio, A., Boya, P., ... & Pietrocola, F., 2021. Autophagy in major human diseases. *The EMBO journal*, *40*(19), e108863.

Koerver, L., Papadopoulos, C., Liu, B., Kravic, B., Rota, G., Brecht, L., Veenendaal, T., Polajnar, M., Bluemke, A., Ehrmann, M. and Klumperman, J., 2019. The ubiquitin-conjugating enzyme

UBE 2 QL 1 coordinates lysophagy in response to endolysosomal damage. *EMBO reports*, *20*(10), p.e48014.

Kotewicz, K. M., Ramabhadran, V., Sjoblom, N., Vogel, J. P., Haenssler, E., Zhang, M., ... & Isberg, R. R., 2017. A single Legionella effector catalyzes a multistep ubiquitination pathway to rearrange tubular endoplasmic reticulum for replication. *Cell host & microbe*, *21*(2), 169-181.

Ku, B., Lee, K. H., Park, W. S., Yang, C. S., Ge, J., Lee, S. G., ... & Oh, B. H. , 2012. VipD of Legionella pneumophila targets activated Rab5 and Rab22 to interfere with endosomal trafficking in macrophages. *PLoS pathogens*, *8*(12), e1003082.

Kumar, S., Gu, Y., Abudu, Y. P., Bruun, J. A., Jain, A., Farzam, F., ... & Deretic, V., 2019. Phosphorylation of syntaxin 17 by TBK1 controls autophagy initiation. *Developmental cell*, *49*(1), 130-144.

Kumar, S., Jain, A., Farzam, F., Jia, J., Gu, Y., Choi, S.W., Mudd, M.H., Claude-Taupin, A., Wester, M.J., Lidke, K.A. and Rusten, T.E., 2018. Mechanism of Stx17 recruitment to autophagosomes via IRGM and mammalian Atg8 proteins. *Journal of Cell Biology*, *217*(3), pp.997-1013.

Kumar, S., Javed, R., Mudd, M., Pallikkuth, S., Lidke, K. A., Jain, A., ... & Deretic, V., 2021. Mammalian hybrid pre-autophagosomal structure HyPAS generates autophagosomes. *Cell*, *184*(24), 5950-5969.

Lamark, T., & Johansen, T., 2021. Mechanisms of selective autophagy. *Annual review of cell and developmental biology*, *37*, 143-169.

Lanzetti, L., Rybin, V., Malabarba, M.G., Christoforidis, S., Scita, G., Zerial, M. and Di Fiore, P.P., 2000. The Eps8 protein coordinates EGF receptor signalling through Rac and trafficking through Rab5. *Nature*, *408*(6810), pp.374-377.

Lawrence, R.E. and Zoncu, R., 2019. The lysosome as a cellular centre for signalling, metabolism and quality control. *Nature cell biology*, *21*(2), pp.133-142.

Lee, J.H., McBrayer, M.K., Wolfe, D.M., Haslett, L.J., Kumar, A., Sato, Y., Lie, P.P., Mohan, P., Coffey, E.E., Kompella, U. and Mitchell, C.H., 2015. Presenilin 1 maintains lysosomal Ca2+ homeostasis via TRPML1 by regulating vATPase-mediated lysosome acidification. *Cell reports*, *12*(9), pp.1430-1444.

Lee, J.H., Yu, W.H., Kumar, A., Lee, S., Mohan, P.S., Peterhoff, C.M., Wolfe, D.M., Martinez-Vicente, M., Massey, A.C., Sovak, G. and Uchiyama, Y., 2010. Lysosomal proteolysis and autophagy require presenilin 1 and are disrupted by Alzheimer-related PS1 mutations. *Cell*, *141*(7), pp.1146-1158.

Leidecker, O., Bonfiglio, J. J., Colby, T., Zhang, Q., Atanassov, I., Zaja, R., ... & Matic, I. , 2016. Serine is a new target residue for endogenous ADP-ribosylation on histones. *Nature chemical biology*, *12*(12), 998-1000.

Levine, B. and Kroemer, G., 2019. Biological functions of autophagy genes: a disease perspective. *Cell*, *176*(1-2), pp.11-42.

Li, H., Li, H.F., Felder, R.A., Periasamy, A. and Jose, P.A., 2008. Rab4 and Rab11 coordinately regulate the recycling of angiotensin II type I receptor as demonstrated by fluorescence resonance energy transfer microscopy. *Journal of biomedical optics*, *13*(3), pp.031206-031206.

Li, P., Gu, M. and Xu, H., 2019. Lysosomal ion channels as decoders of cellular signals. *Trends in biochemical sciences*, *44*(2), pp.110-124.

Li, Y., Cheng, X., Li, M., Wang, Y., Fu, T., Zhou, Z., ... & Pan, L., 2020. Decoding three distinct states of the Syntaxin17 SNARE motif in mediating autophagosome–lysosome fusion. *Proceedings of the National Academy of Sciences*, *117*(35), 21391-21402.

Li, Y.E., Wang, Y., Du, X., Zhang, T., Mak, H.Y., Hancock, S.E., McEwen, H., Pandzic, E., Whan, R.M., Aw, Y.C. and Lukmantara, I.E., 2021. TMEM41B and VMP1 are scramblases and regulate the distribution of cholesterol and phosphatidylserine. *Journal of Cell Biology*, *220*(6), p.e202103105.

Lim, J.A., Li, L., Shirihai, O.S., Trudeau, K.M., Puertollano, R. and Raben, N., 2017. Modulation of mTOR signaling as a strategy for the treatment of Pompe disease. *EMBO molecular medicine*, *9*(3), pp.353-370.

Liu, Y., Mukherjee, R., Bonn, F., Colby, T., Matic, I., Glogger, M., ... & Dikic, I., 2021. Serine-ubiquitination regulates Golgi morphology and the secretory pathway upon Legionella infection. *Cell Death & Differentiation*, *28*(10), 2957-2969.

Luo, J., Jiang, L., Yang, H. and Song, B.L., 2017. Routes and mechanisms of post-endosomal cholesterol trafficking: a story that never ends. *Traffic*, *18*(4), pp.209-217.

Luo, Z.Q. and Isberg, R.R., 2004. Multiple substrates of the Legionella pneumophila Dot/Icm system identified by interbacterial protein transfer. *Proceedings of the National Academy of Sciences*, *101*(3), pp.841-846.

Maeda, S., Otomo, C. and Otomo, T., 2019. The autophagic membrane tether ATG2A transfers lipids between membranes. *elife*, *8*, p.e45777.

Maeda, S., Yamamoto, H., Kinch, L.N., Garza, C.M., Takahashi, S., Otomo, C., Grishin, N.V., Forli, S., Mizushima, N. and Otomo, T., 2020. Structure, lipid scrambling activity and role in autophagosome formation of ATG9A. *Nature structural & molecular biology*, *27*(12), pp.1194-1201.

Maejima, I., Takahashi, A., Omori, H., Kimura, T., Takabatake, Y., Saitoh, T., Yamamoto, A., Hamasaki, M., Noda, T., Isaka, Y. and Yoshimori, T., 2013. Autophagy sequesters damaged lysosomes to control lysosomal biogenesis and kidney injury. *The EMBO journal*, *32*(17), pp.2336-2347.

Majer, O., Liu, B. and Barton, G.M., 2017. Nucleic acid-sensing TLRs: trafficking and regulation. *Current opinion in immunology*, *44*, pp.26-33.

Marques, A.R. and Saftig, P., 2019. Lysosomal storage disorders–challenges, concepts and avenues for therapy: beyond rare diseases. *Journal of cell science*, *132*(2), p.jcs221739.

Martina, J. A., Chen, Y., Gucek, M., & Puertollano, R. (2012). MTORC1 functions as a transcriptional regulator of autophagy by preventing nuclear transport of TFEB. *Autophagy*, *8*(6), 903-914.

Martina, J.A., Diab, H.I., Lishu, L., Jeong-A, L., Patange, S., Raben, N. and Puertollano, R., 2014. The nutrient-responsive transcription factor TFE3 promotes autophagy, lysosomal biogenesis, and clearance of cellular debris. *Science signaling*, *7*(309), pp.ra9-ra9.

Martinez, J., Malireddi, R. K., Lu, Q., Cunha, L. D., Pelletier, S., Gingras, S., ... & Green, D. R., 2015. Molecular characterization of LC3-associated phagocytosis reveals distinct roles for Rubicon, NOX2 and autophagy proteins. *Nature cell biology*, *17*(7), 893-906.

Marwaha, R., Arya, S.B., Jagga, D., Kaur, H., Tuli, A. and Sharma, M., 2017. The Rab7 effector PLEKHM1 binds Arl8b to promote cargo traffic to lysosomes. *Journal of Cell Biology*, *216*(4), pp.1051-1070.

Marzella, L., Ahlberg, J. and Glaumann, H., 1981. Autophagy, heterophagy, microautophagy and crinophagy as the means for intracellular degradation. *Virchows Archiv. B, Cell pathology including molecular pathology*, *36*(2-3), pp.219-234.

Matoba, K., Kotani, T., Tsutsumi, A., Tsuji, T., Mori, T., Noshiro, D., Sugita, Y., Nomura, N., Iwata, S., Ohsumi, Y. and Fujimoto, T., 2020. Atg9 is a lipid scramblase that mediates autophagosomal membrane expansion. *Nature structural & molecular biology*, *27*(12), pp.1185-1193.

Matsui, T., Jiang, P., Nakano, S., Sakamaki, Y., Yamamoto, H. and Mizushima, N., 2018. Autophagosomal YKT6 is required for fusion with lysosomes independently of syntaxin 17. *Journal of Cell Biology*, *217*(8), pp.2633-2645.

Matz, K.M., Guzman, R.M. and Goodman, A.G., 2019. The role of nucleic acid sensing in controlling microbial and autoimmune disorders. *International review of cell and molecular biology*, *345*, pp.35-136.

McClellan, A.J., Laugesen, S.H. and Ellgaard, L., 2019. Cellular functions and molecular mechanisms of non-lysine ubiquitination. *Open Biology*, *9*(9), p.190147.

McDade, J.E., Shepard, C.C., Fraser, D.W., Tsai, T.R., Redus, M.A., Dowdle, W.R. and Laboratory Investigation Team*, 1977. Legionnaires' disease: isolation of a bacterium and demonstration of its role in other respiratory disease. *New England Journal of Medicine*, *297*(22), pp.1197-1203.

McEwan, D.G., Popovic, D., Gubas, A., Terawaki, S., Suzuki, H., Stadel, D., Coxon, F.P., De Stegmann, D.M., Bhogaraju, S., Maddi, K. and Kirchof, A., 2015. PLEKHM1 regulates autophagosome-lysosome fusion through HOPS complex and LC3/GABARAP proteins. *Molecular cell*, *57*(1), pp.39-54.

Medina, D.L., Di Paola, S., Peluso, I., Armani, A., De Stefani, D., Venditti, R., Montefusco, S., Scotto-Rosato, A., Prezioso, C., Forrester, A. and Settembre, C., 2015. Lysosomal calcium signalling regulates autophagy through calcineurin and TFEB. *Nature cell biology*, *17*(3), pp.288-299.

Medina, D.L., Fraldi, A., Bouche, V., Annunziata, F., Mansueto, G., Spampanato, C., Puri, C., Pignata, A., Martina, J.A., Sardiello, M. and Palmieri, M., 2011. Transcriptional activation of lysosomal exocytosis promotes cellular clearance. *Developmental cell*, *21*(3), pp.421-430.

Mejlvang, J., Olsvik, H., Svenning, S., Bruun, J.A., Abudu, Y.P., Larsen, K.B., Brech, A., Hansen, T.E., Brenne, H., Hansen, T. and Stenmark, H., 2018. Starvation induces rapid degradation of

selective autophagy receptors by endosomal microautophagy. *Journal of cell biology*, *217*(10), pp.3640-3655.

Meng, B. and Lever, A.M., 2021. The interplay between ESCRT and viral factors in the enveloped virus life cycle. *Viruses*, *13*(2), p.324.

Mîinea, C.P., Sano, H., Kane, S., Sano, E., Fukuda, M., Peränen, J., Lane, W.S. and Lienhard, G.E., 2005. AS160, the Akt substrate regulating GLUT4 translocation, has a functional Rab GTPase-activating protein domain. *Biochemical Journal*, *391*(1), pp.87-93.

Mizushima, N. and Komatsu, M., 2011. Autophagy: renovation of cells and tissues. *Cell*, *147*(4), pp.728-741.

Mizushima, N., Ohsumi, Y., & Yoshimori, T., 2002. Autophagosome formation in mammalian cells. *Cell structure and function*, *27*(6), 421-429.

Morgan, A.J., Platt, F.M., Lloyd-Evans, E. and Galione, A., 2011. Molecular mechanisms of endolysosomal Ca2+ signalling in health and disease. *Biochemical Journal*, *439*(3), pp.349-378.

Mortimore, G.E., Hutson, N.J. and Surmacz, C.A., 1983. Quantitative correlation between proteolysis and macro-and microautophagy in mouse hepatocytes during starvation and refeeding. *Proceedings of the National Academy of Sciences*, *80*(8), pp.2179-2183.

Mukherjee, R. and Dikic, I., 2022. Regulation of Host-Pathogen Interactions via the Ubiquitin System. *Annual Review of Microbiology*, *76*, pp.211-233.

Muppirala, M., Gupta, V. and Swarup, G., 2011. Syntaxin 17 cycles between the ER and ERGIC and is required to maintain the architecture of ERGIC and Golgi. *Biology of the Cell*, *103*(7), pp.333-350.

Muppirala, M., Gupta, V. and Swarup, G., 2012. Tyrosine phosphorylation of a SNARE protein, syntaxin 17: implications for membrane trafficking in the early secretory pathway. *Biochimica et Biophysica Acta (BBA)-Molecular Cell Research*, *1823*(12), pp.2109-2119.

Nakamura, S., Shigeyama, S., Minami, S., Shima, T., Akayama, S., Matsuda, T., Esposito, A., Napolitano, G., Kuma, A., Namba-Hamano, T. and Nakamura, J., 2020. LC3 lipidation is essential for TFEB activation during the lysosomal damage response to kidney injury. *Nature cell biology*, *22*(10), pp.1252-1263.

Nakatogawa, H., 2020. Mechanisms governing autophagosome biogenesis. *Nature reviews Molecular cell biology*, *21*(8), pp.439-458.

Napolitano, G. and Ballabio, A., 2016. TFEB at a glance. *Journal of cell science*, *129*(13), pp.2475-2481.

Newton, H.J., Ang, D.K., Van Driel, I.R. and Hartland, E.L., 2010. Molecular pathogenesis of infections caused by Legionella pneumophila. *Clinical microbiology reviews*, *23*(2), pp.274-298.

Nixon, R.A., 2017. Amyloid precursor protein and endosomal–lysosomal dysfunction in Alzheimer's disease: inseparable partners in a multifactorial disease. *The FASEB Journal*, *31*(7), p.2729.

Ohshima, T., Yamamoto, H., Sakamaki, Y., Saito, C. and Mizushima, N., 2022. NCOA4 drives ferritin phase separation to facilitate macroferritinophagy and microferritinophagy. *Journal of Cell Biology*, *221*(10).

Omotade, T. O., & Roy, C. R., 2020. Legionella pneumophila excludes autophagy adaptors from the ubiquitin-labeled vacuole in which it resides. *Infection and immunity*, *88*(8), e00793-19.

Onoue, K., Jofuku, A., Ban-Ishihara, R., Ishihara, T., Maeda, M., Koshiba, T., Itoh, T., Fukuda, M., Otera, H., Oka, T. and Takano, H., 2013. Fis1 acts as a mitochondrial recruitment factor for TBC1D15 that is involved in regulation of mitochondrial morphology. *Journal of cell science*, *126*(1), pp.176-185.

Osawa, T., Kotani, T., Kawaoka, T., Hirata, E., Suzuki, K., Nakatogawa, H., Ohsumi, Y. and Noda, N.N., 2019. Atg2 mediates direct lipid transfer between membranes for autophagosome formation. *Nature Structural & Molecular Biology*, *26*(4), pp.281-288.

Otomo, T. and Yoshimori, T., 2017. Lysophagy: A method for monitoring lysosomal rupture followed by autophagy-dependent recovery. *Lysosomes: Methods and Protocols*, pp.141-149.

Palmieri, M., Impey, S., Kang, H., di Ronza, A., Pelz, C., Sardiello, M. and Ballabio, A., 2011. Characterization of the CLEAR network reveals an integrated control of cellular clearance pathways. *Human molecular genetics*, *20*(19), pp.3852-3866.

Papadopoulos, C. and Meyer, H., 2017. Detection and clearance of damaged lysosomes by the endo-lysosomal damage response and lysophagy. *Current Biology*, *27*(24), pp.R1330-R1341.

Papadopoulos, C., Kirchner, P., Bug, M., Grum, D., Koerver, L., Schulze, N., Poehler, R., Dressler, A., Fengler, S., Arhzaouy, K. and Lux, V., 2017. VCP/p97 cooperates with YOD 1, UBXD 1 and PLAA to drive clearance of ruptured lysosomes by autophagy. *The EMBO journal*, *36*(2), pp.135-150.

Peña-Llopis, S., Vega-Rubin-de-Celis, S., Schwartz, J.C., Wolff, N.C., Tran, T.A.T., Zou, L., Xie, X.J., Corey, D.R. and Brugarolas, J., 2011. Regulation of TFEB and V-ATPases by mTORC1. *The EMBO journal*, *30*(16), pp.3242-3258.

Peralta, E.R., Martin, B.C. and Edinger, A.L., 2010. Differential effects of TBC1D15 and mammalian Vps39 on Rab7 activation state, lysosomal morphology, and growth factor dependence. *Journal of Biological Chemistry*, *285*(22), pp.16814-16821.

Pereira-Leal, J.B. and Seabra, M.C., 2001. Evolution of the Rab family of small GTP-binding proteins. *Journal of molecular biology*, *313*(4), pp.889-901.

Perera, R.M., Di Malta, C. and Ballabio, A., 2019. MiT/TFE family of transcription factors, lysosomes, and cancer. *Annual review of cancer biology*, *3*, pp.203-222.

Perera, R.M., Stoykova, S., Nicolay, B.N., Ross, K.N., Fitamant, J., Boukhali, M., Lengrand, J., Deshpande, V., Selig, M.K., Ferrone, C.R. and Settleman, J., 2015. Transcriptional control of autophagy–lysosome function drives pancreatic cancer metabolism. *Nature*, *524*(7565), pp.361-365.

Petersen, N.H., Olsen, O.D., Groth-Pedersen, L., Ellegaard, A.M., Bilgin, M., Redmer, S., Ostenfeld, M.S., Ulanet, D., Dovmark, T.H., Lønborg, A. and Vindeløv, S.D., 2013.

Platt, F.M., 2018. Emptying the stores: lysosomal diseases and therapeutic strategies. *Nature reviews Drug discovery*, *17*(2), pp.133-150.

Platt, F.M., d'Azzo, A., Davidson, B.L., Neufeld, E.F. and Tifft, C.J., 2018. Lysosomal storage diseases. *Nature Reviews Disease Primers*, *4*(1), p.27.

Polito, V.A., Li, H., Martini-Stoica, H., Wang, B., Yang, L.I., Xu, Y., Swartzlander, D.B., Palmieri, M., Di Ronza, A., Lee, V.M.Y. and Sardiello, M., 2014. Selective clearance of aberrant tau proteins and rescue of neurotoxicity by transcription factor EB. *EMBO molecular medicine*, *6*(9), pp.1142-1160.

Popovic, D., Akutsu, M., Novak, I., Harper, J.W., Behrends, C. and Dikic, I., 2012. Rab GTPase-activating proteins in autophagy: regulation of endocytic and autophagy pathways by direct binding to human ATG8 modifiers. *Molecular and cellular biology*, *32*(9), pp.1733-1744.

Qiu, J., Sheedlo, M. J., Yu, K., Tan, Y., Nakayasu, E. S., Das, C., ... & Luo, Z. Q., 2016. Ubiquitination independent of E1 and E2 enzymes by bacterial effectors. *Nature*, *533*(7601), 120-124.

Radulovic, M., Schink, K.O., Wenzel, E.M., Nähse, V., Bongiovanni, A., Lafont, F. and Stenmark, H., 2018. ESCRT-mediated lysosome repair precedes lysophagy and promotes cell survival. *The EMBO journal*, *37*(21), p.e99753.

Rapaport, D., Fichtman, B., Weidberg, H., Sprecher, E., & Horowitz, M., 2018. NEK3-mediated SNAP29 phosphorylation modulates its membrane association and SNARE fusion dependent processes. *Biochemical and biophysical research communications*, *497*(2), 605-611.

Ravenhill, B.J., Boyle, K.B., von Muhlinen, N., Ellison, C.J., Masson, G.R., Otten, E.G., Foeglein, A., Williams, R. and Randow, F., 2019. The cargo receptor NDP52 initiates selective autophagy by recruiting the ULK complex to cytosol-invading bacteria. *Molecular cell*, *74*(2), pp.320-329.

Rega, L.R., Polishchuk, E., Montefusco, S., Napolitano, G., Tozzi, G., Zhang, J., Bellomo, F., Taranta, A., Pastore, A., Polishchuk, R. and Piemonte, F., 2016. Activation of the transcription factor EB rescues lysosomal abnormalities in cystinotic kidney cells. *Kidney international*, *89*(4), pp.862-873.

Repnik, U., Borg Distefano, M., Speth, M. T., Ng, M. Y. W., Progida, C., Hoflack, B., ... & Griffiths, G. (2017). L-leucyl-L-leucine methyl ester does not release cysteine cathepsins to the cytosol but inactivates them in transiently permeabilized lysosomes. *Journal of cell science*, *130*(18), 3124-3140.

Roberti, M.C., La Starza, R., Surace, C., Sirleto, P., Pinto, R.M., Pierini, V., Crescenzi, B., Mecucci, C. and Angioni, A., 2009. RABGAP1L gene rearrangement resulting from a der (Y) t (Y; 1)(q12; q25) in acute myeloid leukemia arising in a child with Klinefelter syndrome. *Virchows archiv*, *454*, pp.311-316.

Roczniak-Ferguson, A., Petit, C.S., Froehlich, F., Qian, S., Ky, J., Angarola, B., Walther, T.C. and Ferguson, S.M., 2012. The transcription factor TFEB links mTORC1 signaling to transcriptional control of lysosome homeostasis. *Science signaling*, *5*(228), pp.ra42-ra42.

Rolando, M., Escoll, P., Nora, T., Botti, J., Boitez, V., Bedia, C., ... & Buchrieser, C., 2016. Legionella pneumophila S1P-lyase targets host sphingolipid metabolism and restrains autophagy. *Proceedings of the National Academy of Sciences*, *113*(7), 1901-1906.

Rong, Y., Liu, M., Ma, L., Du, W., Zhang, H., Tian, Y., Cao, Z., Li, Y., Ren, H., Zhang, C. and Li, L., 2012. Clathrin and phosphatidylinositol-4, 5-bisphosphate regulate autophagic lysosome reformation. *Nature cell biology*, *14*(9), pp.924-934.

Rytkönen, A. and Holden, D.W., 2007. Bacterial interference of ubiquitination and deubiquitination. *Cell host & microbe*, *1*(1), pp.13-22.

Saftig, P. and Klumperman, J., 2009. Lysosome biogenesis and lysosomal membrane proteins: trafficking meets function. *Nature reviews Molecular cell biology*, *10*(9), pp.623-635.

Saftig, P. and Puertollano, R., 2021. How lysosomes sense, integrate, and cope with stress. *Trends in biochemical sciences*, *46*(2), pp.97-112.

Sahu, R., Kaushik, S., Clement, C.C., Cannizzo, E.S., Scharf, B., Follenzi, A., Potolicchio, I., Nieves, E., Cuervo, A.M. and Santambrogio, L., 2011. Microautophagy of cytosolic proteins by late endosomes. *Developmental cell*, *20*(1), pp.131-139.

Saleeb, R.S., Kavanagh, D.M., Dun, A.R., Dalgarno, P.A. and Duncan, R.R., 2019. A VPS33A-binding motif on syntaxin 17 controls autophagy completion in mammalian cells. *Journal of Biological Chemistry*, *294*(11), pp.4188-4201.

Sancak, Y., Bar-Peled, L., Zoncu, R., Markhard, A.L., Nada, S. and Sabatini, D.M., 2010. Ragulator-Rag complex targets mTORC1 to the lysosomal surface and is necessary for its activation by amino acids. *Cell*, *141*(2), pp.290-303.

Sardiello, M., Palmieri, M., Di Ronza, A., Medina, D.L., Valenza, M., Gennarino, V.A., Di Malta, C., Donaudy, F., Embrione, V., Polishchuk, R.S. and Banfi, S., 2009. A gene network regulating lysosomal biogenesis and function. *Science*, *325*(5939), pp.473-477.

Sawa-Makarska, J., Baumann, V., Coudevylle, N., von Bülow, S., Nogellova, V., Abert, C., Schuschnig, M., Graef, M., Hummer, G. and Martens, S., 2020. Reconstitution of autophagosome nucleation defines Atg9 vesicles as seeds for membrane formation. *Science*, *369*(6508), p.eaaz7714.

Saxton, R.A. and Sabatini, D.M., 2017. mTOR signaling in growth, metabolism, and disease. *Cell*, *168*(6), pp.960-976.

Schuck, Sebastian. "Microautophagy–distinct molecular mechanisms handle cargoes of many sizes." *Journal of Cell Science* 133, no. 17 (2020): jcs246322.

Schwartz, S.L., Cao, C., Pylypenko, O., Rak, A. and Wandinger-Ness, A., 2007. Rab GTPases at a glance. *Journal of cell science*, *120*(22), pp.3905-3910.

Seabra, M.C., Mules, E.H. and Hume, A.N., 2002. Rab GTPases, intracellular traffic and disease. *Trends in molecular medicine*, *8*(1), pp.23-30.

Seranova, E., Connolly, K.J., Zatyka, M., Rosenstock, T.R., Barrett, T., Tuxworth, R.I. and Sarkar, S., 2017. Dysregulation of autophagy as a common mechanism in lysosomal storage diseases. *Essays in biochemistry*, *61*(6), pp.733-749.

Settembre, C., Di Malta, C., Polito, V.A., Arencibia, M.G., Vetrini, F., Erdin, S., Erdin, S.U., Huynh, T., Medina, D., Colella, P. and Sardiello, M., 2011. TFEB links autophagy to lysosomal biogenesis. *science*, *332*(6036), pp.1429-1433.

Settembre, C., Fraldi, A., Medina, D.L. and Ballabio, A., 2013. Signals from the lysosome: a control centre for cellular clearance and energy metabolism. *Nature reviews Molecular cell biology*, *14*(5), pp.283-296.

Settembre, C., Zoncu, R., Medina, D.L., Vetrini, F., Erdin, S., Erdin, S., Huynh, T., Ferron, M., Karsenty, G., Vellard, M.C. and Facchinetti, V., 2012. A lysosome-to-nucleus signalling mechanism senses and regulates the lysosome via mTOR and TFEB. *The EMBO journal*, *31*(5), pp.1095-1108.

Shen, Q., Shi, Y., Liu, J., Su, H., Huang, J., Zhang, Y., Peng, C., Zhou, T., Sun, Q., Wan, W. and Liu, W., 2021. Acetylation of STX17 (syntaxin 17) controls autophagosome maturation. *Autophagy*, *17*(5), pp.1157-1169.

Shin, D., Mukherjee, R., Liu, Y., Gonzalez, A., Bonn, F., Liu, Y., ... & Dikic, I., 2020. Regulation of phosphoribosyl-linked serine ubiquitination by deubiquitinases DupA and DupB. *Molecular cell*, *77*(1), 164-179.

Sklan, E.H., Serrano, R.L., Einav, S., Pfeffer, S.R., Lambright, D.G. and Glenn, J.S., 2007. TBC1D20 is a Rab1 GTPase-activating protein that mediates hepatitis C virus replication. *Journal of Biological Chemistry*, *282*(50), pp.36354-36361.

Sklan, E.H., Staschke, K., Oakes, T.M., Elazar, M., Winters, M., Aroeti, B., Danieli, T. and Glenn, J.S., 2007. A Rab-GAP TBC domain protein binds hepatitis C virus NS5A and mediates viral replication. *Journal of virology*, *81*(20), pp.11096-11105.

Skowyra, M.L., Schlesinger, P.H., Naismith, T.V. and Hanson, P.I., 2018. Triggered recruitment of ESCRT machinery promotes endolysosomal repair. *Science*, *360*(6384), p.eaar5078.

Slot, J. W., & Geuze, H. J., 2007. Cryosectioning and immunolabeling. *Nature protocols*, *2*(10), 2480-2491.

Smeele, P. H., & Vaccari, T. ,2022. Snapshots from within the cell: Novel trafficking and non-trafficking functions of Snap29 during tissue morphogenesis. In *Seminars in Cell & Developmental Biology*. Academic Press.

Smith, M.D., Harley, M.E., Kemp, A.J., Wills, J., Lee, M., Arends, M., von Kriegsheim, A., Behrends, C. and Wilkinson, S., 2018. CCPG1 is a non-canonical autophagy cargo receptor essential for ER-phagy and pancreatic ER proteostasis. *Developmental cell*, *44*(2), pp.217-232.

Solinger, J.A. and Spang, A., 2013. Tethering complexes in the endocytic pathway: CORVET and HOPS. *The FEBS journal*, *280*(12), pp.2743-2757.

Spampanato, C., Feeney, E., Li, L., Cardone, M., Lim, J.A., Annunziata, F., Zare, H., Polishchuk, R., Puertollano, R., Parenti, G. and Ballabio, A., 2013. Transcription factor EB (TFEB) is a new therapeutic target for Pompe disease. *EMBO molecular medicine*, *5*(5), pp.691-706.

Steegmaier, M., Yang, B., Yoo, J.S., Huang, B., Shen, M., Yu, S., Luo, Y. and Scheller, R.H., 1998. Three novel proteins of the syntaxin/SNAP-25 family. *Journal of Biological Chemistry*, *273*(51), pp.34171-34179.

Steiner, B., Swart, A. L., Welin, A., Weber, S., Personnic, N., Kaech, A., ... & Hilbi, H, 2017. ER remodeling by the large GTPase atlastin promotes vacuolar growth of Legionella pneumophila. *EMBO reports*, *18*(10), 1817-1836.

Stenmark, H., 2009. Rab GTPases as coordinators of vesicle traffic. *Nature reviews Molecular cell biology*, *10*(8), pp.513-525.

Strickland, M., Nyenhuis, D., Watanabe, S.M., Tjandra, N. and Carter, C.A., 2021. Novel Tsg101 binding partners regulate viral L domain trafficking. *Viruses*, *13*(6), p.1147.

Sun, J., Deghmane, A.E., Bucci, C. and Hmama, Z., 2009. Detection of activated Rab7 GTPase with an immobilized RILP probe. In *Macrophages and Dendritic Cells* (pp. 57-69). Humana Press.

Takahashi, Y., He, H., Tang, Z., Hattori, T., Liu, Y., Young, M.M., Serfass, J.M., Chen, L., Gebru, M., Chen, C. and Wills, C.A., 2018. An autophagy assay reveals the ESCRT-III component CHMP2A as a regulator of phagophore closure. *Nature communications*, *9*(1), p.2855.

Takáts, S., Pircs, K., Nagy, P., Varga, Á., Kárpáti, M., Hegedűs, K., Kramer, H., Kovács, A.L., Sass, M. and Juhász, G., 2014. Interaction of the HOPS complex with Syntaxin 17 mediates autophagosome clearance in Drosophila. *Molecular biology of the cell*, *25*(8), pp.1338-1354.

Thelen, A.M. and Zoncu, R., 2017. Emerging roles for the lysosome in lipid metabolism. *Trends in cell biology*, *27*(11), pp.833-850.

Thiele, D.L. and Lipsky, P.E., 1990. Mechanism of L-leucyl-L-leucine methyl ester-mediated killing of cytotoxic lymphocytes: dependence on a lysosomal thiol protease, dipeptidyl peptidase I, that is enriched in these cells. *Proceedings of the National Academy of Sciences*, *87*(1), pp.83-87.

Transformation-associated changes in sphingolipid metabolism sensitize cells to lysosomal cell death induced by inhibitors of acid sphingomyelinase. *Cancer cell*, *24*(3), pp.379-393.

Tsuboyama, K., Koyama-Honda, I., Sakamaki, Y., Koike, M., Morishita, H., & Mizushima, N., 2016. The ATG conjugation systems are important for degradation of the inner autophagosomal membrane. *Science*, *354*(6315), 1036-1041.

Turco, E., Savova, A., Gere, F., Ferrari, L., Romanov, J., Schuschnig, M. and Martens, S., 2021. Reconstitution defines the roles of p62, NBR1 and TAX1BP1 in ubiquitin condensate formation and autophagy initiation. *Nature communications*, *12*(1), p.5212.

Turco, E., Witt, M., Abert, C., Bock-Bierbaum, T., Su, M.Y., Trapannone, R., Sztacho, M., Danieli, A., Shi, X., Zaffagnini, G. and Gamper, A., 2019. FIP200 claw domain binding to p62 promotes autophagosome formation at ubiquitin condensates. *Molecular Cell*, *74*(2), pp.330-346.

Tyanova, S., Temu, T., Sinitcyn, P., Carlson, A., Hein, M.Y., Geiger, T., Mann, M. and Cox, J., 2016. The Perseus computational platform for comprehensive analysis of (prote) omics data. *Nature methods*, *13*(9), pp.731-740.

Uematsu, M., Nishimura, T., Sakamaki, Y., Yamamoto, H. and Mizushima, N., 2017. Accumulation of undegraded autophagosomes by expression of dominant-negative STX17 (syntaxin 17) mutants. *Autophagy*, *13*(8), pp.1452-1464.

Van Der Kant, R., Jonker, C.T., Wijdeven, R.H., Bakker, J., Janssen, L., Klumperman, J. and Neefjes, J., 2015. Characterization of the mammalian CORVET and HOPS complexes and their modular restructuring for endosome specificity. *Journal of Biological Chemistry*, *290*(51), pp.30280-30290.

Vargas, J.N.S., Wang, C., Bunker, E., Hao, L., Maric, D., Schiavo, G., Randow, F. and Youle, R.J., 2019. Spatiotemporal control of ULK1 activation by NDP52 and TBK1 during selective autophagy. *Molecular cell*, *74*(2), pp.347-362.

Vega-Rubin-de-Celis, S., Peña-Llopis, S., Konda, M. and Brugarolas, J., 2017. Multistep regulation of TFEB by MTORC1. *Autophagy*, *13*(3), pp.464-472.

Vidya, M.K., Kumar, V.G., Sejian, V., Bagath, M., Krishnan, G. and Bhatta, R., 2018. Toll-like receptors: significance, ligands, signaling pathways, and functions in mammals. *International reviews of immunology*, *37*(1), pp.20-36.

Wandinger-Ness, A. and Zerial, M., 2014. Rab proteins and the compartmentalization of the endosomal system. *Cold Spring Harbor perspectives in biology*, *6*(11), p.a022616.

Wang, C., Wang, H., Zhang, D., Luo, W., Liu, R., Xu, D., Diao, L., Liao, L. and Liu, Z., 2018. Phosphorylation of ULK1 affects autophagosome fusion and links chaperone-mediated autophagy to macroautophagy. *Nature communications*, *9*(1), p.3492.

Wang, W., Zhang, X., Gao, Q., Lawas, M., Yu, L., Cheng, X., Gu, M., Sahoo, N., Li, X., Li, P. and Ireland, S., 2017. A voltage-dependent K+ channel in the lysosome is required for refilling lysosomal Ca2+ stores. *Journal of Cell Biology*, *216*(6), pp.1715-1730.

Ward, E.S., Martinez, C., Vaccaro, C., Zhou, J., Tang, Q. and Ober, R.J., 2005. From sorting endosomes to exocytosis: association of Rab4 and Rab11 GTPases with the Fc receptor, FcRn, during recycling. *Molecular biology of the cell*, *16*(4), pp.2028-2038.

Weber, S., Steiner, B., Welin, A. and Hilbi, H., 2018. Legionella-containing vacuoles capture PtdIns (4) P-rich vesicles derived from the Golgi apparatus. *MBio*, *9*(6), pp.e02420-18.

Weber, S., Wagner, M., & Hilbi, H., 2014. Live-cell imaging of phosphoinositide dynamics and membrane architecture during Legionella infection. *MBio*, *5*(1), e00839-13.

Willett, R., Martina, J.A., Zewe, J.P., Wills, R., Hammond, G.R. and Puertollano, R., 2017. TFEB regulates lysosomal positioning by modulating TMEM55B expression and JIP4 recruitment to lysosomes. *Nature communications*, *8*(1), p.1580.

Willforss, J., Chawade, A. and Levander, F., 2018. NormalyzerDE: online tool for improved normalization of omics expression data and high-sensitivity differential expression analysis. *Journal of proteome research*, *18*(2), pp.732-740.

Wong, Y.C., Ysselstein, D. and Krainc, D., 2018. Mitochondria–lysosome contacts regulate mitochondrial fission via RAB7 GTP hydrolysis. *Nature*, *554*(7692), pp.382-386.

Wu, H., Carvalho, P. and Voeltz, G.K., 2018. Here, there, and everywhere: The importance of ER membrane contact sites. *Science*, *361*(6401), p.eaan5835.

Xiao, Q., Yan, P., Ma, X., Liu, H., Perez, R., Zhu, A., Gonzales, E., Tripoli, D.L., Czerniewski, L., Ballabio, A. and Cirrito, J.R., 2015. Neuronal-targeted TFEB accelerates lysosomal degradation of APP, reducing Aβ generation and amyloid plaque pathogenesis. *Journal of Neuroscience*, *35*(35), pp.12137-12151.

Yamano, K., Fogel, A.I., Wang, C., van der Bliek, A.M. and Youle, R.J., 2014. Mitochondrial Rab GAPs govern autophagosome biogenesis during mitophagy. *Elife*, *3*, p.e01612.

Yamano, K., Kikuchi, R., Kojima, W., Hayashida, R., Koyano, F., Kawawaki, J., Shoda, T., Demizu, Y., Naito, M., Tanaka, K. and Matsuda, N., 2020. Critical role of mitochondrial ubiquitination and the OPTN–ATG9A axis in mitophagy. *Journal of Cell Biology*, *219*(9).

Yang, A., Pantoom, S., & Wu, Y. W., 2017. Elucidation of the anti-autophagy mechanism of the Legionella effector RavZ using semisynthetic LC3 proteins. *Elife*, *6*, e23905.

Ye, Y. and Rape, M., 2009. Building ubiquitin chains: E2 enzymes at work. *Nature reviews Molecular cell biology*, *10*(11), pp.755-764.

Yoo, S.M. and Jung, Y.K., 2018. A molecular approach to mitophagy and mitochondrial dynamics. *Molecules and cells*, *41*(1), p.18.

Yoshida, Y., Yasuda, S., Fujita, T., Hamasaki, M., Murakami, A., Kawawaki, J., Iwai, K., Saeki, Y., Yoshimori, T., Matsuda, N. and Tanaka, K., 2017. Ubiquitination of exposed glycoproteins by SCFFBXO27 directs damaged lysosomes for autophagy. *Proceedings of the National Academy of Sciences*, *114*(32), pp.8574-8579.

Yoshimura, S.I., Egerer, J., Fuchs, E., Haas, A.K. and Barr, F.A., 2007. Functional dissection of Rab GTPases involved in primary cilium formation. *The Journal of cell biology*, *178*(3), pp.363-369.

Yu, L., McPhee, C.K., Zheng, L., Mardones, G.A., Rong, Y., Peng, J., Mi, N., Zhao, Y., Liu, Z., Wan, F. and Hailey, D.W., 2010. Termination of autophagy and reformation of lysosomes regulated by mTOR. *Nature*, *465*(7300), pp.942-946.

Yuan, W. and Song, C., 2020. The emerging role of Rab5 in membrane receptor trafficking and signaling pathways. *Biochemistry Research International*, *2020*.

Zhao, M., Wang, F., Wu, J., Cheng, Y., Cao, Y., Wu, X., Ma, M., Tang, F., Liu, Z., Liu, H. and Ge, B., 2021. CGAS is a micronucleophagy receptor for the clearance of micronuclei. *Autophagy*, *17*(12), pp.3976-3991.

Zhao, Y.G. and Zhang, H., 2019. Autophagosome maturation: an epic journey from the ER to lysosomes. *Journal of Cell Biology*, *218*(3), pp.757-770.

Zhen, Y., Spangenberg, H., Munson, M.J., Brech, A., Schink, K.O., Tan, K.W., Sørensen, V., Wenzel, E.M., Radulovic, M., Engedal, N. and Simonsen, A., 2020. ESCRT-mediated phagophore sealing during mitophagy. *Autophagy*, *16*(5), pp.826-841.

Zhou, F., Wu, Z., Zhao, M., Murtazina, R., Cai, J., Zhang, A., Li, R., Sun, D., Li, W., Zhao, L. and Li, Q., 2019. Rab5-dependent autophagosome closure by ESCRT. *Journal of Cell Biology*, *218*(6), pp.1908-1927.

Zhou, Y., Zhou, B., Pache, L., Chang, M., Khodabakhshi, A.H., Tanaseichuk, O., Benner, C. and Chanda, S.K., 2019. Metascape provides a biologist-oriented resource for the analysis of systems-level datasets. *Nature communications*, *10*(1), pp.1-10.

Zhou, Z., Liu, J., Fu, T., Wu, P., Peng, C., Gong, X., Wang, Y., Zhang, M., Li, Y., Wang, Y. and Xu, X., 2021. Phosphorylation regulates the binding of autophagy receptors to FIP200 Claw domain for selective autophagy initiation. *Nature communications*, *12*(1), p.1570.

Chapter 11
Supplementary Data

Supplementary Data 1: MS spectra of PR-Ub modified STX17

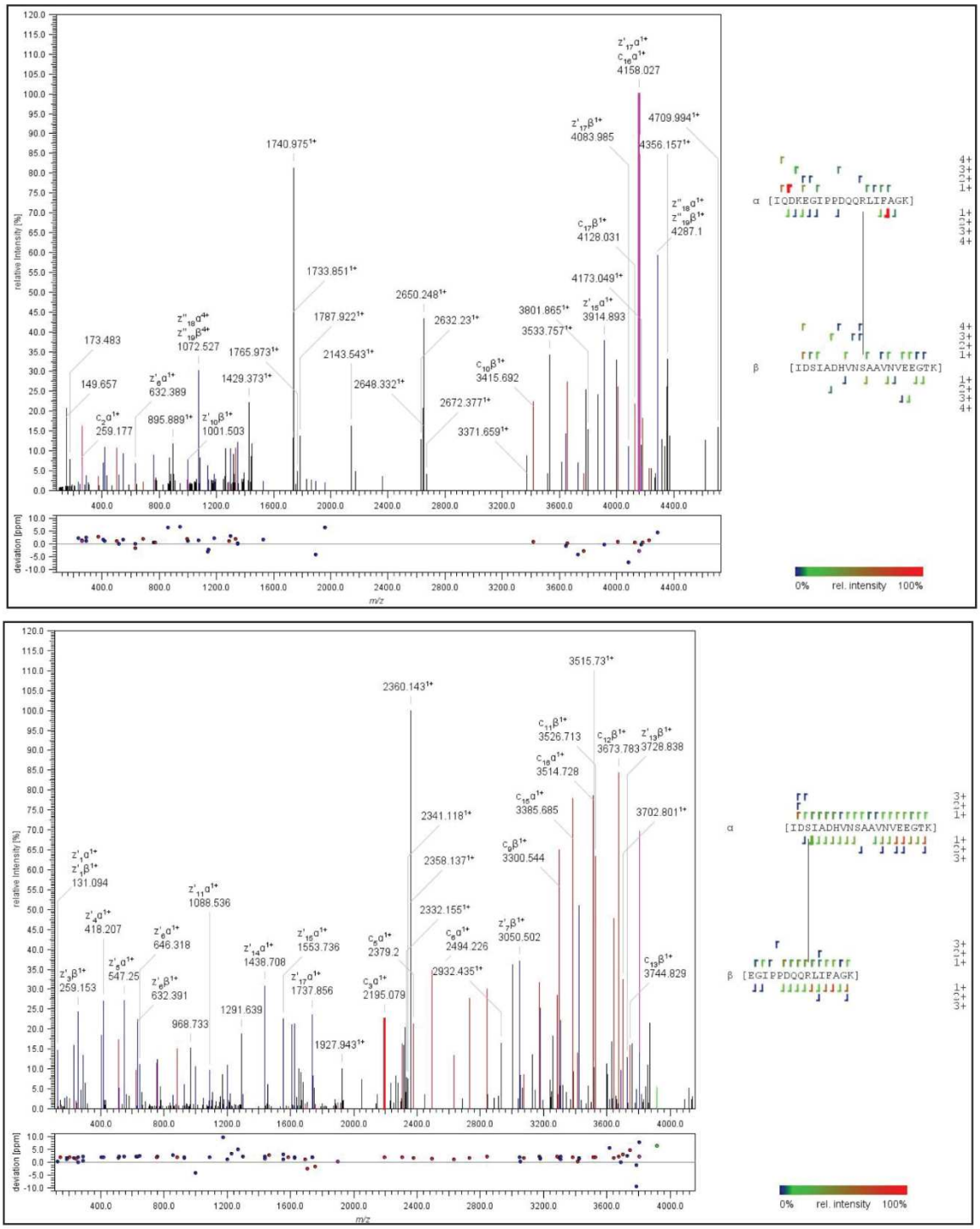

MS spectra of PR-Ub modified STX17(1-224)

Supplementary Data 2: MS spectra of PR-Ub modified SNAP29

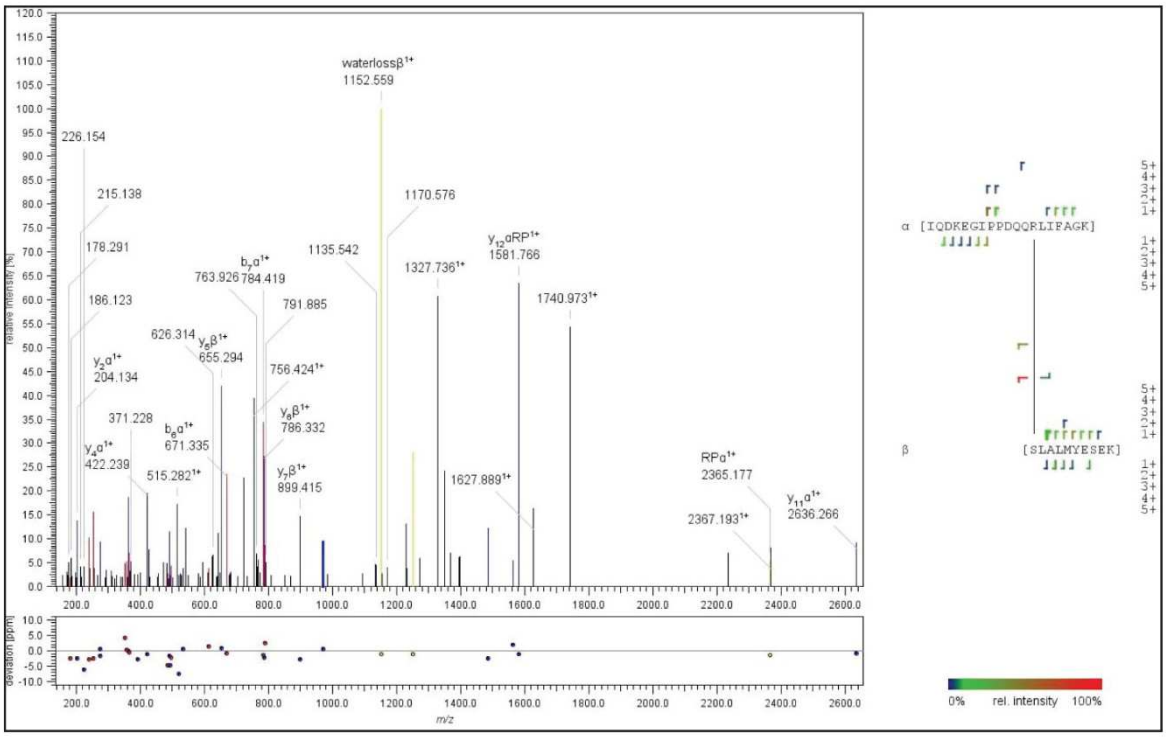

MS spectra of PR-Ub modified SNAP29

Publications

Publications

1. Bhattacharya, A., Mukherjee, R., Kuncha, S. K., Brunstein, M., Rathore, R., Junek, S., ... & Dikic, I. (2022). TBC1D15 potentiates lysosomal regeneration from damaged membranes. Nature Cell Biology (accepted for publication) (**first author**)

2. Mukherjee, R., **Bhattacharya, A**., Bojkova, D., Mehdipour, A. R., Shin, D., Khan, K. S., ... & Dikic, I. (2021). Famotidine inhibits toll-like receptor 3-mediated inflammatory signaling in SARS-CoV-2 infection. *Journal of Biological Chemistry*, *297*(2).

3. Shin, D., Mukherjee, R., Grewe, D., Bojkova, D., Baek, K., **Bhattacharya, A**., ... & Dikic, I. (2020). Papain-like protease regulates SARS-CoV-2 viral spread and innate immunity. *Nature*, *587*(7835), 657-662.

4. Shin, D., **Bhattacharya, A**., Cheng, Y. L., Alonso, M. C., Mehdipour, A. R., Ovaa, H., ... & Dikic, I. (2020). Bacterial OTU deubiquitinases regulate substrate ubiquitination upon Legionella infection. *Elife*, *9*, e58277.

5. Mukherjee, R., **Bhattacharya, A**., Sau, A., Basil, S., Chakrabarti, S., & Chakrabarti, O. (2019). Calmodulin regulates MGRN1-GP78 interaction mediated ubiquitin proteasomal degradation system. *The FASEB Journal*, *33*(2), 1927-19 (**joint first author**)